Synaptotagmin 1-triggered lipid signaling couples exo- and endocytosis

Inaugural-Dissertation

to obtain the academic degree
Doctor rerum naturalium (Dr. rer. nat.)
submitted to the Department of Biology, Chemistry, Pharmacy
of Freie Universität Berlin

by

Svenja Bolz

Berlin, October 2023

The present work of this thesis was conducted under the supervision of Prof. Dr. Volker Haucke from July 2018 to October 2023 at the Leibniz-Forschungsinstitut für Molekulare Pharmakologie, Berlin.

1st reviewer: Prof. Dr. Volker Haucke

2nd reviewer: Prof. Dr. Stephan Sigrist

Date of defense: 18.01.2024

„Wir können jeden Tag aufs Neue entscheiden, welchen Einfluss wir auf diese Welt ausüben möchten.“

Jane Goodall

Acknowledgements

First, I would like to express my deep gratitude to my supervisor **Prof. Dr. Volker Haucke**. Thank you for the excellent training, guidance and scientific inspiration during the time of my doctorate as well as my prior Master's thesis. Your continuous support, your willingness to discuss every little detail of my project and your enthusiasm for science are truly a source of motivation and were essential for the success of my project.

I owe special thanks to **Dr. Tolga Soykan** for his guidance, great experimental and scientific training and support, starting already during my undergraduate studies. Special thanks also to **Dr. Nathalie Kämpf**, who worked on sorting adaptors of Syt1 and initiated this project. I am very grateful for your trust to find answers to so many open questions.

Further, I would like to thank **Dr. Dmytro Puchkov** for his contributions in electron microscopy and thereby, insights into the ultrastructure of the synapse. Many thanks also to **Prof. Dr. Michael Krauß and Giulia Russo** for sharing your knowledge about PIPK1γ with me. I am very grateful for the help of **Dr. Wen-Ting Lo**. Your excellent expertise on structure biology made our studies on the interaction of Syt1 and PIPK1γ possible. **Dr. Martin Lehmann, Dr. Tolga Soykan and Dr. Domenico Azarnia Tehran**, you gave great experimental support that helped me answering crucial questions of my project and establishing new experiments. In this context, I would like to thank **Dr. Christopher Schmied** for automating a script with us which had been developed by **Dr. David Perrais** for the analysis of pHluorin images. Thank you, **Rainer Müller, PhD** and **Prof. Carsten Schultz, PhD,** for sharing important probes with us. I am grateful to **Prof. Dr. Oliver Daumke** for sharing his expertise in structure biology with me. I would also like to acknowledge collaborations with **Prof. Takeshi Sakaba, PhD**, **Dr. Eugenio Fornasiero**, **Dr. Rashi Goel**, **Prof. Kenneth Madsen, PhD** and **Joscha Rombach**.

I am thankful for the scientific and financial support provided by the "Deutsche Forschungsgemeinschaft" SFB 958. As a PhD representative it was a pleasure to organize scientific as well as networking events for the graduate program with **Felicitas Brüntgens**, **Dr. Sandra Maria Keiper**, **Simone Schlender** and **Jennifer Woitkuhn**.
I would further like to express my gratitude to our very skilled technicians: **Maria Mühlbauer**, thank you for supporting me in innumerous experiments and thus, allowing the

fast and comprehensive progress of the study; thank you **Claudia Bahnik** for providing help whenever needed; thank you **Delia Löwe** for all the neuronal cultures; thank you **Silke Zillmann** for organizing and helping with all important orderings. Moreover, I am very grateful for all the support from our great secretary office and the FMP-IT. I want to thank **Prof. Dr. Tanja Maritzen** for being a continuous support throughout the years and for managing the experimental administration together with **Dr. York Posor**. I would also like to thank the animal facility of the FMP: **Dr. Natali Wisbrun**, **Sina Scholz** and **Jeannette Unnasch**.

I would like to acknowledge all current and former members of the **AG Haucke**, as well as from the former **AG Maritzen** and **AG Lehmann** for their support and scientific discussions. All of you created a cheerful, collaborative, and supportive atmosphere: Kerem Can Akkaya, Irving Brugada, Gillian Leigh Dornan, Michael Ebner, Marine Gil, Hannes Gonschior, Manuel Hessenberger, Wonyul Jang, Maria Jäpel, Mudassar Khan, Philipp Alexander Koch, Gaga Kochlamazashvili, Kinga Konkel, Klaudia Kosieradzka, Marijn Kuijpers, Wen-Ting Lo, Guan-Ting Liu, Tania López Hernández, Max Lucht, Fabian Lukas, Albert Mackintosh, Mouhannad Malek, Sravanthi Nadiminti, Vini Natalia, Phuong Nguyen, Cathrine Nordgaard, Christoph Ott, York Posor, Julia Riedlberger, Filiz Sila Rizalar, Giulia Russo, Paula Samso Ferre, Linda Sawade, Tolga Soykan, Yanwei Su, Miaomiao Tian, Rozemarijn van der Veen, Dennis Vollweiter, Alexander Wallroth, Alexander Walter, Haibin Wang, Agata Witkowska, and Klaas Yperman. Special thanks to Domenico Azarnia Tehran, Claudia Bahnik, Lennart Hoffmann, Britta Kristine Oevel, Maria Mühlbauer and Dr. Tolga Soykan, who I had the privilege to work with for the entire time in the lab. Also, it was a pleasure hosting students and visiting scientists, Stephanie Himpich and Joscha Rombach.

Finally, and most importantly, I am very lucky and deeply grateful to be supported, surrounded, and loved by my family and friends, in particular my partner Marc, my parents Andrea and Gerald, my grandmother Hildegard and grandaunt Margot, Hans-Thomas, Svenja, Fibi, Michael and Iris. Special memories I will also always share with my four-pawed daily co-worker and family member, Senta.
Irrespective of two legs or four paws, without you, all that work certainly would have been impossible!

Declaration of Independence

Herewith I certify that I have prepared and written my thesis independently and that I have not used any sources and aids other than those indicated by me. This dissertation has not yet been presented to any other examination authority in the same or a similar form and has not yet been published.

Berlin, October 2023

Table of Content

Summary

Brain function relies on synaptic vesicle (SV) exocytosis and endocytosis. These cell physiological processes are crucial for neurotransmission. Ca^{2+} triggers the exocytic fusion of synaptic vesicles, which leads to the release of neurotransmitter. To sustain neurotransmission, SV exocytosis must be spatiotemporally coupled to a qualitatively and quantitatively corresponding retrieval of membrane and SV proteins via compensatory endocytosis. Yet, it is unknown how neurons balance SV exo- and endocytosis to maintain presynaptic membrane homeostasis und thereby sustain brain function.

This study identifies Synaptotagmin 1 (Syt1), the main Ca^{2+} sensor and key factor for synchronous neurotransmission, as a homeostatic, post-fusion trigger for compensatory endocytosis. Severe conserved defects in neurotransmission are caused by genetic loss, mutation, or acute inactivation of Syt1. As an SV protein, Syt1 interacts via its two C2 domains with proteins of both, the exo- and endocytic machinery, and furthermore mediates neurotransmission upon binding to charged phospholipids of the membrane.

We demonstrate that Syt1 couples SV exocytosis and compensatory endocytosis by triggering the local, activity-dependent synthesis of phosphatidylinositol 4,5-bisphosphate [$PI(4,5)P_2$] at presynaptic sites. Exocytosed Syt1 on the neuronal plasma membrane recruits phosphatidylinositol 4-phosphate [PI(4)P] 5-kinase Iγ (PIPKIγ), the main $PI(4,5)P_2$ synthesizing enzyme at the synapse. The Syt1-dependent recruitment of PIPKIγ results in elevated levels of presynaptic $PI(4,5)P_2$. As an important signaling lipid and driving force for SV endocytosis, we detect Syt1-dependent facilitation of SV endocytosis. Genetic interference with Syt1/ PIPKIγ complex formation selectively impairs $PI(4,5)P_2$-triggered SV endocytosis but not exocytic SV fusion. We show the Syt1-triggered synthesis of signaling lipids to couple SV exo- and endocytosis across a wide range of physiological stimulation paradigms. Considering Syt1 and $PI(4,5)P_2$ being associated with various physiological as well as pathophysiological processes, we predict similar mechanisms to couple fusion and retrieval in other cell types undergoing regulated secretion.

Zusammenfassung

Die Funktion des Gehirns basiert auf der Neurotransmission und den damit verbundenen physiologischen Prozessen, der Exozytose und der Endozytose. Als elementarer sekundärer Botenstoff löst Ca^{2+} die Freisetzung von Neurotransmittern durch Verschmelzung synaptischer Vesikel (SV) mit der der Plasmamembran aus. Um die Neurotransmission aufrechtzuerhalten, muss die Exozytose räumlich und zeitlich mit der entsprechenden Rückgewinnung von ebenso viel Membran und den für ein SV charakteristischen Proteinen gekoppelt sein. Dies geschieht durch kompensatorische Endozytose. Wie Neurone jedoch Exozytose von SVs und deren Rückgewinnung durch Endozytose aufeinander abstimmen, um die präsynaptische Membranhomöostase aufrechtzuerhalten und dadurch Gehirnfunktionen zu erhalten, ist weitestgehend unbekannt.

Diese Studie identifiziert Synaptotagmin 1 (Syt1), den wichtigsten Ca^{2+}-Sensor und Schlüsselfaktor der synchronen Neurotransmission, als homöostatischen Auslöser für kompensatorische Endozytose. Durch genetischen Verlust, Mutation oder akute Inaktivierung von Syt1 werden schwere evolutionär-konservierte Defekte in der Neurotransmission verursacht, die die Bedeutung Syt1's hervorheben. Als SV-Protein interagiert Syt1 über seine beiden C2-Domänen mit Proteinen, die sowohl wichtige Funktion in der Exozytose als auch in der Endozytose besitzen. Darüber hinaus reguliert Syt1 durch Bindung an geladene Membranlipide die Neurotransmission.

Wir zeigen, dass Syt1 die Exozytose von SVs mit kompensatorischer Endozytose koppelt, indem es lokale, auf die Aktivität-abgestimmte Synthese von Phosphatidylinositol 4,5-Bisphosphat [$PI(4,5)P_2$] an speziellen präsynaptischen Stellen auslöst. Exozytiertes Syt1 an der neuronalen Plasmamembran rekrutiert Phosphatidylinositol-4-Phosphat [PI(4)P] 5 Kinase Iγ (PIPKIγ), welches als wichtigstes $PI(4,5)P_2$-synthetisierende Enzym an der Synapse zu einem erhöhten Gehalt an präsynaptischem $PI(4,5)P_2$ führt. Wir weisen nach, dass die Synthese des wichtigen Signallipids als treibende Kraft für die SV-Endozytose von Syt1 abhängt und über die spezifische Rekrutierung von PIPKIγ die Endozytose von SVs erleichtert. Genetische Störung der Syt1/ PIPKIγ-Komplexbildung beeinträchtigt ausschließlich die durch $PI(4,5)P_2$ induzierte Endozytose, nicht aber die Exozytose. Über ein breites Spektrum physiologischer Stimulationsparadigmen hinweg zeigen wir, dass die Syt1-initiierte Lipidsynthese die Exo- und Endozytose von SVs koppelt. In Anbetracht zahlreicher physiologischer und pathophysiologischer Prozesse, die mit Syt1 und $PI(4,5)P_2$ assoziiert

sind, prognostizieren wir ähnliche Mechanismen zur Kopplung von Fusion und Rückgewinnung in anderen Zelltypen, die für eine regulierte Sekretion zuständig sind.

1 Introduction

Consciousness, cognition, memory, and behavior are vital functions that depend on our nervous system. The nervous system is divided into the central nervous system (CNS) composed of brain and spinal cord and the peripheral nervous system. An important component of the mammalian brain is the hippocampus. As part of the limbic system, it fulfills important roles in human learning and memory and is involved in behavioral and emotional responses (Scoville & Milner, 1957). Here, as well as in the rest of the brain, as major part of the CNS, highly specialized excitable cellular units, termed neurons, are organized in complex networks. Neurons enable the receiving, processing, and rapid transmission of electrically or chemically encoded information at specialized junctions, the synapses (Lodish et al., 2007). Being responsible for such important functions throughout the entire lifetime, the components and underlying pathways of synaptic transmission are of wide interest and their molecular mechanisms are the focus of this study.

1.1 Neurotransmission at chemical synapses

Neurotransmission relies on the generation of an electrical signal, its propagation along neuronal processes to synapses and its synaptic transmission to a downstream postsynaptic neuron. While at chemical synapses the electrical signal triggers secretion of neurotransmitters into the extracellular space, electrical synapses form gap junctions which allow direct communication via e.g., bi-directional ion flux (C. Hammond, 2015). Speed is a crucial feature of neuronal communication and requires stringent directionality. Therefore, bi-directional electrical synapses are found between glial cells of the CNS. These cells surround neurons and support their functions. In neurons, however, directionality is obtained by a highly conserved polarity and requires excitability and secretion to be strictly regulated in time and space. Each neuron contains a cell body, the soma, which is composed of the nucleus, and the perikaryon enclosing cellular organelles. This is the predominant site for protein synthesis (C. Hammond, 2015). Two types of neuronal processes extend from the soma: dendrites and axon that differ in function and structure. A neuronal soma and its dendrites form the somatodendritic compartment. The short, branched dendrites receive impulses from neighboring neurons via synapses and conduct the electrical signal towards the soma. In the soma, the incoming signal is spatio-temporally integrated, and a sodium-dependent action potential (AP) is generated at the axon initial segment upon depolarization

of the plasma membrane (C. Hammond, 2015). The AP is transmitted along the entire length of the axon passing nodes of Ranvier by a process called saltatory conduction. Because APs can only occur at the interposed nodes of Ranvier, the conductance speed of the electrical signals to reach the synaptic terminal is drastically increased (Salzer, 2015). Eventually the AP arrives at presynaptic terminals, triggers SV release and thus secretion of neurotransmitters.

1.1.1 Synaptic vesicles

The SV is the key organelle of synaptic transmission in chemical synapses and allows the propagation of a signal from one neuron to another. Its main functions are neurotransmitter uptake, relocalization to the plasma membrane and subsequent release of a quantal amount of neurotransmitters upon an AP-induced transient rise in the presynaptic Ca^{2+} concentration (Fatt & Katz, 1952). For the regulated release of neurotransmitters via a controlled interaction and subsequent fusion of SVs with the plasma membrane, a process defined as exocytosis is needed. To sustain neurotransmission, membrane and protein components of the SVs need to be retrieved in a process called endocytosis to reform fully functional SVs with precise size and tightly controlled protein composition (E. De Robertis, 1959; E. D. P. De Robertis & Bennett, 1954; Israel et al., 1968). The average SV has a diameter of 42 nm and consists of about 7000 phospholipids, 5600 cholesterol molecules and 250 membrane and membrane associated proteins (Fig. 1) (Mutch et al., 2011; Takamori et al., 2006). Most SV proteins are classified into either transport proteins, such as different integral membrane proteins mediating neurotransmitter uptake, or trafficking proteins, involved in SV membrane traffic (Fernández-Chacón & Südhof, 1999). Using mass spectrometry, specific proteins were found to be present with a relatively low copy number, such as the integral membrane protein vesicular glutamate transporter 1 (vGLUT1), which transports glutamate into the SV and is characteristic for excitatory neurons (Bellocchio et al., 2000). Glutamate transport happens in exchange for luminal H^+ whose electrochemical gradient is produced by the vacuolar H^+-ATPase (V-ATPase), another transport protein with only one to two copies per SV. Other SV proteins are much more abundant such as Synaptobrevin 2 [Syb2, also known as vesicle-associated membrane protein 2 (VAMP2)] with about 69.8 molecules per vesicle or Synaptophysin (Syp) with an average copy number per vesicle of 32 (Takamori et al., 2006; Wilhelm et al., 2014). Syb2 as a soluble NSF (N-ethylmaleimide-sensitive factor) attachment protein receptor (SNARE) protein has a crucial function for SV docking and

fusion. By forming a tight four-helical trans-SNARE complex with two plasma membrane proteins, the synaptosomal associated protein 25 (SNAP-25) and syntaxin1, it promotes the fusion of SVs with the plasma membrane (Jahn & Fasshauer, 2012; Schoch et al., 2001). Syb2 has been described to form a heteromer with Syp promoting Syb2 endocytic sorting (Calakos & Scheller, 1994; Edelmann et al., 1995; Gordon et al., 2012) while Syp itself also forms homomultimers in SV membranes (Thomas et al., 1988). In contrast to Syb2 and Syp, Synaptotagmin 1 (Syt1), the most important Ca^{2+} sensor that triggers Ca^{2+}-dependent neurotransmitter release (Fernández-Chacón et al., 2001) shows very little intervesicle variation and much less abundance with 15 molecules per vesicle. This is a similarity Syt1 shares with its sorting adaptor, the synaptic vesicle protein 2 (SV2) (Kaempf et al., 2015; Lazzell et al., 2004; Schivell et al., 1996, 2005). Binding of Ca^{2+} to the cytoplasmic C2A domain of Syt1 enables the protein to interact with the negatively charged phospholipids on the plasma membrane and thus, supports the SNARE-dependent vesicle fusion (Edelmann et al., 1995; Martens & McMahon, 2008; Pang et al., 2006; Schiavo et al., 1996).

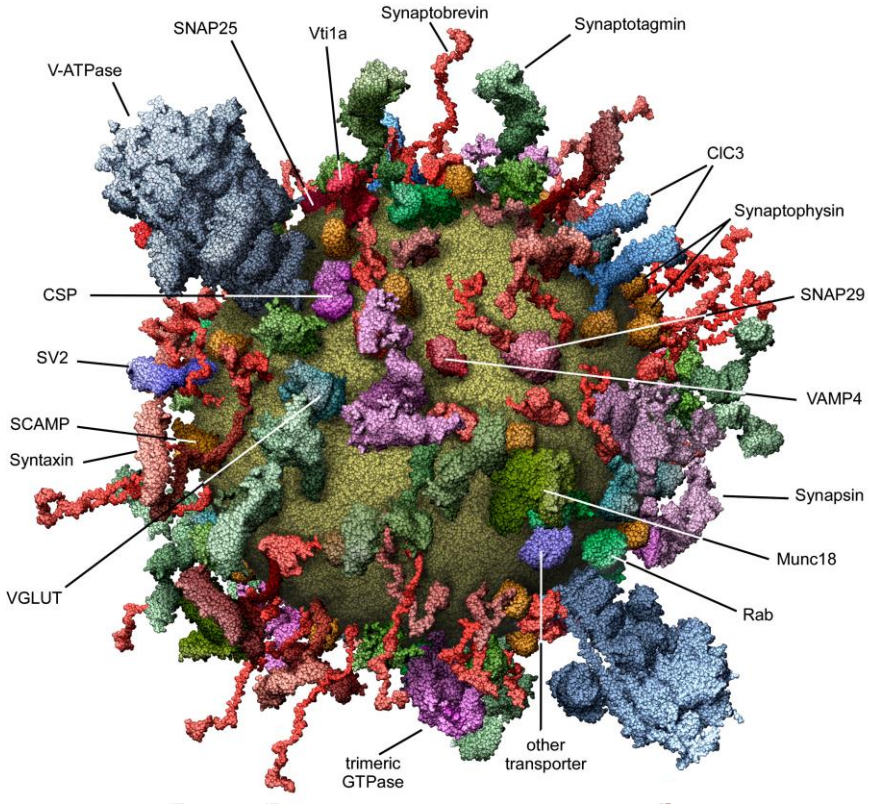

Figure 1: A synaptic vesicle
Molecular model of the outside of an average SV based on a space-filling model depicting all macromolecules at near atomic resolution. Taken from (Takamori et al., 2006).

Syb2, Syp and Syt1 are anchored to the SV via their transmembrane domain. This is different for SV-associated proteins such as synapsin which localize to the SV by interacting with SV membrane lipids or SV proteins. Synapsin is required for synapse formation, maturation as well as SV clustering (Cesca, F.; Baldelli, P.; Valtorta, F., and Benfenati, 2010).

1.1.2 Synaptic vesicle cycle

Sustained neurotransmission via continued SV exocytosis would progressively lead to an increase of the presynaptic plasma membrane and would require a constant supply of newly formed SVs and its components. Yet, presynaptic terminals are distant from the soma where de novo synthesis of SV proteins mainly takes place. In addition, the comparatively slow axonal transport necessitates recycling of SVs locally in the presynapse. This cycle includes vesicle translocation, docking and Ca^{2+} triggered fusion via exocytosis, release-site clearance, compensatory endocytosis, reformation of SVs and SV clustering (Fig. 2).

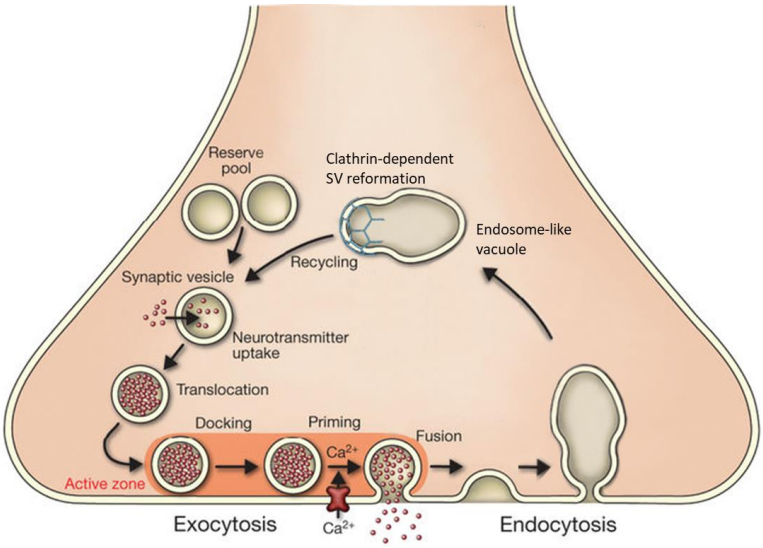

Figure 2: Synaptic vesicle cycle
Model for the cycle of synaptic vesicles. Neurotransmitter-filled vesicles translocate to release sites at the active zone, dock, prime and fuse with the plasma membrane upon AP-triggered Ca^{2+} influx to release neurotransmitters via exocytosis. While the released neurotransmitters diffuse through the synaptic cleft to propagate the signal to the postsynapse, SV material is retrieved via compensatory endocytosis and SVs are reformed and reclustered. Modified and taken from (Jahn & Fasshauer, 2012).

1.1.2.1 Synaptic vesicle pools

Depending on their functional state, SVs can be mainly classified into three categories: the recycling pool, the readily-releasable pool and the reserve pool (Rizzoli & Betz, 2005). The

recycling pool comprises all SVs continuously undergoing exo- and endocytosis and accounts for 5 – 20 % of the total pool size under physiological conditions (de Lange et al., 2003; Richards et al., 2000). Only in exceptional conditions, such as during high-frequency stimulation or upon inhibition of endocytosis, the reserve pool is released. This pool contains 80 – 95 % of the total pool (de Lange et al., 2003; Richards et al., 2000).

As a subpopulation of the recycling pool, the readily-releasable pool (RRP) consists of SVs that are tethered or docked to the plasma membrane and hence can immediately fuse in response to an AP. Constituting only ~ 2 % of the total pool size, the RRP is rapidly depleted if the stimulus proceeds and needs to be replenished by the recycling pool. Only high-frequency stimulation triggers the recruitment of SVs from the reserve pool because under physiological conditions the SV-associated phosphoprotein synapsin sequesters the SVs belonging to the reserve pool by binding to actin. Thereby, the formation of a liquid phase has been suggested which results in its separation from the rest of the cytosol (Milovanovic et al., 2018). Thus, replenishment of SVs from the reserve pool may happen upon stimulation dependent affinity-loss of synapsin to actin (Bykhovskaia, 2011). In addition, also the existence of SVs that never undergo fusion (Fernandez-Alfonso & Ryan, 2008) as well as specific, highly mobile SVs that can re-localize to other terminals have been reported (Staras et al., 2010).

1.1.3 Molecular mechanisms of the synaptic vesicle cycle

1.1.3.1 Exocytosis

Chemical synapses consist of the presynaptic terminal, the synaptic cleft and the postsynaptic compartment and are generally characterized by a unidirectional transmission (C. Hammond & Esclapez, 2015). In the presynapse, the axonal electrical signal is converted into a chemical signal to bridge the gap between presynaptic axon and postsynaptic dendrite. This is achieved via membrane depolarization at the synaptic terminal, which triggers N- or P/Q-type voltage-gated Ca^{2+} channels ($Ca_v2.1$ and $Ca_v2.2$) to open. Due to their clustering close to docked and release-ready SVs the resulting presynaptic Ca^{2+} influx is locally restricted to a region within the presynapse, termed active zone (AZ). The quick opening and closing of the voltage-gated Ca^{2+} channels, diffusion of Ca^{2+} from the AZ and removal by Ca^{2+}-ATPases or Na^{+}/ Ca^{2+} exchangers into e.g., mitochondria and endoplasmic reticulum (ER), results in a transient increase in the presynaptic Ca^{2+} concentration (C.

Hammond & Esclapez, 2015). This transient rise leads to the fusion of tethered, neurotransmitter-filled SVs with the plasma membrane at the AZ (Dittman & Ryan, 2009; Haucke et al., 2011a; Jahn & Fasshauer, 2012; Katz & Miledi, 1967; Saheki & De Camilli, 2012).

The AZ contains special release sites that are located close to the voltage-gated Ca^{2+} channels (Kittel et al., 2006) and enables SVs to tether, dock, prime and eventually fuse with the plasma membrane. These processes are supported via the cytomatrix of the active zone (CAZ) comprising membrane-associated proteins including Munc13 which regulates SNARE formation, Rab3 interacting molecules (RIMs), GIT family proteins, liprin, Rab6 interacting proteins, piccolo and bassoon (Haucke et al., 2011a).

Neurotransmitter-filled SVs dock and prime at defined sites within the AZ, a process which generates the RRP (Andrews-Zwilling et al., 2006; Imig et al., 2014; Malsam et al., 2008). This is mediated by the SV-localized Rab3a, a small GTPase binding to RIM and Munc13. Munc13 furthermore promotes the release of syntaxin 1 from Munc18 and supports correct configurations of syntaxin 1 and VAMP during the assembly of the ternary SNARE complex. The SNARE complex is subsequently formed by the SV-associated vesicular (v)-SNARE VAMP2 and the target (t)-SNAREs SNAP-25 and syntaxin-1 which are located on the presynaptic plasma membrane.

One of the main regulators of exocytosis is Ca^{2+}. In its absence molecules such as the Ca^{2+} sensors Syt1 and complexin may act as clamps to prevent fusion. Upon opening of the voltage-gated Ca^{2+} channels, the transient increase in presynaptic Ca^{2+} concentration leads to the full assembly of the SNARE complex. For activation of the SNARE complex, complexins, small soluble neuronal proteins, bind to it. This activates evoked release and suppresses spontaneous release. Formation of a full SNARE complex requires Ca^{2+}-dependent Syt1 binding of the SNARE complex, which leads to release of complexin, unlocks the SNARE complex and allows full zippering (Pang et al., 2006). This occurs especially at distinct sites at the AZ. These sites are enriched in membrane lipids like phosphatidylinositide-(4,5)-bisphosphate [$PI(4,5)P_2$] which Syt1 binds to via its C2 domain (Park et al., 2015). The assembly and resulting structural change of the SNARE complex helps to overcome electrostatic forces, pulls the SV and the plasma membrane into closer proximity (Südhof & Rothman, 2009) and thus may trigger fusion of SVs with the plasma membrane (Lin et al., 2014). The fusion pore expansion is mediated by the transmembrane domains of Syb2 and syntaxin 1 (Chiang et al., 2018; Sharma & Lindau, 2018). Upon fusion, the SNARE complex is ATP-dependently disassembled by the ATPase N-ethylmaleimide-

sensitive factor (NSF) and its cofactor, α-soluble NSF attachment protein (α-SNAP) (Ryu et al., 2016). The released neurotransmitters diffuse through the synaptic cleft and bind to cognate ligand-gated ion channels located at the electron dense postsynaptic density (PSD) (Zhai & Bellen, 2004). To ensure high efficiency of neurotransmitter recognition, active zone proteins such as trans-synaptic adhesion molecules form an alignment with their postsynaptic counterparts (Dean & Dresbach, 2006). Binding of the released neurotransmitters to postsynaptic receptors results in a conformational change in the receptor that enables ions to enter the postsynapse and to elicit a postsynaptic response (Heuser & Reese, 1973). Depending on the type of released neurotransmitters and its receptor, the response can be of excitatory or inhibitory nature regulating the state of neuronal activity. An excitatory postsynaptic potential is generated upon influx of Na^+, K^+ and Ca^{2+} ions which occurs upon binding of the excitatory neurotransmitter glutamate to ionotropic α-amino-3-hydroxy-5-methyl-4-isoxazolepropionic acid (AMPA), N-methyl-D-aspartate (NMDA), and kainate receptors (Reiner & Levitz, 2018). In contrast, binding of gamma-aminobutyric acid (GABA), an inhibitory neurotransmitter synthesized from glutamate (Modi et al., 2015), to ionotropic $GABA_A$ receptors results in an influx of Cl^- ions and thereby promotes an inhibitory postsynaptic potential.

1.1.3.2 Compensatory endocytosis

Ca^{2+}-mediated and SNARE-dependent SV fusion at the AZ requires the retrieval of SV components which fused with the AZ membrane during earlier cycles. The release sites at the AZ are limited. Therefore, release site clearance represents a rate-limiting step (Haucke et al., 2011a). Active transport or lateral diffusion is suggested to clear the release sites while cytoskeletal proteins may provide directionality (Hosoi et al., 2009; Sakaba et al., 2013). To retrieve SV components from the periphery of the AZ and from the periactive zone, a region adjacent to the AZ, different modes of compensatory endocytosis have been suggested e.g., depending on stimulation paradigm and type of synapse (Maritzen & Haucke, 2018; Soykan et al., 2016).

For decades, clathrin-mediated endocytosis (CME) was accepted to be the primary endocytic route predominantly responsible for the internalization of stranded SV proteins at the presynaptic membrane. CME is characterized by a clathrin-coat and was first observed by electron microscopy (EM) analysis of stimulated nerve-muscle preparations (Heuser & Reese, 1973) that revealed cisternal structures, coated vesicles and coated pits located

outside the AZ. Perturbation of clathrin or related cargo-specific adaptors strongly impaired the retrieval of SV membrane and thus, supported such a clathrin-based model (Augustine et al., 2006; Granseth et al., 2006; Koo et al., 2011). In CME, the endocytic adaptor protein AP2 binds to $PI(4,5)P_2$ and cargo proteins and recruits clathrin triskelia to form the characteristic clathrin coat. Accessory endocytic proteins bend the shallow clathrin-coated pit into a deep invagination, which is finally pinched-off by the GTPase dynamin. Before new neurotransmitters are taken up, SVs are uncoated and re-acidified. The existence of a readily retrievable pool consisting of pre-sorted and pre-assembled endocytic membrane and vesicle cargo bound by clathrin and adaptor complex supports the model of CME, while the low speed of CME due to the slow formation of clathrin coats (10-20 s) argues that CME can only support neurotransmission under low-frequency stimulation. Alternative modes of endocytosis may likely be required to maintain synaptic transmission at high-frequency stimulation.

Another model called “kiss-and-run” endocytosis describes a transient fusion pore of the SV with the presynaptic plasma membrane without a full SV collapse. (Alés et al., 1999; Ceccarelli et al., 1972, 1973). This model bypasses the need for endocytic sorting of SV proteins as well as the reformation of SVs from endosomal intermediates. However, this model is at odds with the finding that newly exocytosed SV proteins are mostly non-identical with those endocytosed in the same round of stimulation (Fernández-Alfonso et al., 2006; Gimber et al., 2015; Wienisch & Klingauf, 2006). Furthermore, “kiss-and-run” has been observed in endocrine cells and is debated for neurons. Therefore, clathrin-independent endocytosis (CIE) which is characterized by much faster speed (50 - 500 ms) is more likely to occur upon a wide range of stimulation paradigms. Ultrafast endocytosis (UFE) has been shown in optogenetically stimulated neurons of *C. elegans* or mice upon high pressure freezing electron microscopy (Watanabe, Liu, et al., 2013; Watanabe, Rost, et al., 2013).

After full collapse of SVs, large endocytic invaginations are formed in CIE. Similar to CME, these depend on e.g., scission by dynamin, yet they are independent of clathrin assembly and occur at the periactive zone on timescales of 50 – 100 ms (Kononenko et al., 2014; López-Hernández et al., 2022; Soykan et al., 2017). Findings of endocytic intermediates located in a stimulation dependent manner, close to the AZ upon low (Watanabe, Rost, et al., 2013) or at the periactive zone upon high frequency (Gad et al., 1998) further support such model. From the resulting endosomal-like vacuoles (ELVs) SVs are then reformed in a clathrin-dependent manner (Watanabe et al., 2014). Thereby, membrane retrieval and SV

reformation are separated from each other. Both processes were revealed to require the actin cytoskeleton (Soykan et al., 2017; Watanabe, Rost, et al., 2013; X. S. Wu et al., 2016).
Under prolonged high-frequency stimulation, activity-dependent bulk endocytosis (ADBE) outside AZs has been described to mediate internalization of large presynaptic plasma membrane invaginations (Miller & Heuser, 1984). Potentially, SV reformation happens via AP-1 and AP-3 (Cheung & Cousin, 2012) while the requirement of clathrin is under debate (Kononenko et al., 2014; Nicholson-Fish et al., 2015).

1.1.4 Coupling of exocytosis and endocytosis

Evoked neurotransmission and its activity-dependent modulation is crucial for memory storage and processing of sensory information (Vandael et al., 2020). While dysfunctions in the machinery of SV exocytosis have been linked to neurological disorders (Mullins et al., 2016; Vandael et al., 2020; Verhage & Sørensen, 2020; L. G. Wu et al., 2014), defects in compensatory endocytosis of SV membranes and SV proteins irrespective of the molecular mechanism would lead to the swelling of boutons, loss in membrane tension, impairment of pre- and postsynaptic alignment and eventually synapse death (Dittman & Ryan, 2009; Kononenko & Haucke, 2015; Maritzen & Haucke, 2018; Murthy & Stevens, 1998; Soykan et al., 2016). Therefore, SV exocytosis must immediately be followed by compensatory endocytic retrieval. Interestingly, capacitance measurements and optical recordings showed matching amounts of exocytosed and endocytosed SV membrane and SV proteins (Haucke et al., 2011a; Vandael et al., 2020; Verhage & Sørensen, 2020; L. G. Wu et al., 2014) while only under rare activity-paradigms (e.g., upon prolonged high-frequency stimulation) an endocytic overshoot has been reported (L. G. Wu et al., 2014). However, its physiological relevance remains uncertain. Various mechanisms for exo- and endocytic coupling have been suggested, including Ca^{2+} (Haucke et al., 2011a; Hosoi et al., 2009; Koch & Holt, 2012; Maritzen & Haucke, 2018; L. G. Wu et al., 2014; Xie et al., 2017). In addition to Ca^{2+}'s well established role for exocytosis during evoked neurotransmission (Katz & Miledi, 1967; Tucker & Chapman, 2002), a regulatory role for Ca^{2+} in SV endocytosis has been proposed (Dittman & Ryan, 2009; Hosoi et al., 2009; M. M. Lai et al., 1999; Maritzen & Haucke, 2018; Sankaranarayanan & Ryan, 2001; L. G. Wu et al., 2014; X. S. Wu et al., 2009; C. K. Yao et al., 2009; Zefirov et al., 2006). Interestingly, presynaptic Ca^{2+} currents correlate with endocytic rate constants at the Calyx of Held (X. S. Wu et al., 2009), and the depletion of Ca^{2+} leads to an accumulation of endocytic intermediates in lamprey (Gad et al.,

1998). Furthermore, the Ca^{2+} binding protein calmodulin and its downstream effector calcineurin were shown to regulate endocytosis (X. S. Wu et al., 2009) via dephosphorylation and hence activation of important proteins of the endocytic machinery such as the GTPase dynamin 1 (Anggono et al., 2006; Armbruster et al., 2013; M. M. Lai et al., 1999), the inositol phosphatase synaptojanin 1, the phosphatidylinositol 4-phosphate 5-kinase Iγ (PIPKIγ), the ubiquitin-binding adaptors Eps15 and epsin, and the synaptobrevin-specific adaptor AP180 (Cousin & Robinson, 2001). These proteins belong to the group of dephosphins that are regulated via phosphorylation by different kinases such as cyclin-dependent kinase 5 (Cdk5) (T. C. Tan et al., 2003). However, upon interference with the exocytic release machinery AP-triggered Ca^{2+} influx does not generally induce endocytic retrieval of SV membranes on its own. This has been shown upon application of inhibitors like botulinum neurotoxins cleaving SNARE proteins or by other means of acute or sustained abrogation of SV fusion (Verhage et al., 2000; W. Wu et al., 2005; Yamashita et al., 2005, 2010). Thus, additional coupling mechanisms of SV exo- and endocytosis must exist to explain how the information of SV fusion is forwarded to the endocytic machinery and to couple the two processes qualitatively and quantitatively.

1.1.4.1 Exo-endocytic coupling via the signaling lipid $PI(4,5)P_2$

A very straightforward model is SV exo-endocytic coupling via the induced synthesis of membrane lipids (Haucke et al., 2011a; Koch & Holt, 2012; Lauwers et al., 2016; Puchkov & Haucke, 2013) such as $PI(4,5)P_2$ (Fig. 3).

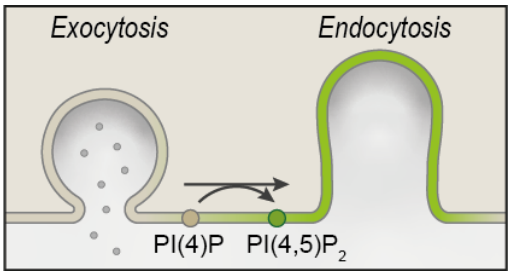

Figure 3: Lipid signaling couples SV exo- and endocytosis.
Model for SV exo- and endocytic coupling. Synthesis of the signaling lipid $PI(4,5)P_2$ from PI(4)P in neurons is activity-dependent and couples SV exocytosis with SV endocytosis. Taken from (Bolz et al., 2023).

$PI(4,5)P_2$ is a membrane signaling phospholipid whose impairment has been linked to endocytic defects, synapse dysfunction and neurodegeneration (Cao et al., 2017; Pan et al., 2020; Schechter et al., 2020). It belongs to the family of phosphoinositides (PI) which are

derived from phosphatidylinositols (PtdIns). Characterized by a diacylglycerol backbone which is esterified to the *myo*-inositol headgroup at its 1' position, seven different PI species can be formed by different metabolizing enzymes. These PI kinases and phosphatases are stereoselectively recruited to subcellular membranes and generate the different PI species by altering the phosphorylation state of hydroxylgroups of the *myo*-inositol ring at position 3', 4' and 5' (Balla, 2013). By binding to and recruiting various proteins to cellular membranes, PIs regulate various cell-physiological processes including vesicle trafficking, signal transduction, regulation of ion channels and remodeling of the actin cytoskeleton (De Matteis & Godi, 2004; Di Paolo & De Camilli, 2006; Krauß & Haucke, 2007; Posor et al., 2022). Despite accounting for less than 1 % of the total brain lipids (Wenk et al., 2003), $PI(4,5)P_2$ is one of the most abundant PIs and can be generated from phosphatidylinositol-4-phosphate [PI(4)P] and phosphatidylinositol-5-phosphate [PI(5)P]. However, PI(4)P is more abundant at the plasma membrane (Guo et al., 2003) and thus the major substrate for type I phosphatidylinositol phosphate kinases (PIP-kinases) in the brain to generate $PI(4,5)P_2$ (Di Paolo et al., 2004; Di Paolo & De Camilli, 2006; Guo et al., 2003). In return, conversion of $PI(4,5)P_2$ happens via phospholipase C (PLC) into diacylglycerol (DAG) and inositoltrisphosphate (IP_3) or via phosphorylation into phosphatidylinositol-(3,4,5)-trisphosphate [$PI(3,4,5)P_3$] (Di Paolo & De Camilli, 2006). The fact that $PI(4,5)P_2$ depletion leads to impaired exocytosis (Di Paolo et al., 2004) and increased levels of $PI(4,5)P_2$ result in the accumulation of SVs (Cremona et al., 1999; W. T. Kim et al., 2002) illustrates how fundamental regulated $PI(4,5)P_2$ turnover is to synaptic homeostasis (G. R. V. Hammond & Schiavo, 2007).

The major $PI(4,5)P_2$ synthesizing enzyme in the brain is PIPKIγ. Among several splice variants, the predominant form is PIPK1γ661, alternatively named PIPK1γ90/v2 (Ishihara et al., 1996, 1998; Nakano-Kobayashi et al., 2007; Wenk et al., 2001). It belongs to the type I kinases which share a conserved catalytic core domain with type II and type III PIP-kinases from yeast to human. Although its other isoforms, PIPKIα and PIPKIβ, could potentially compensate for the loss of PIPKIγ, neurons from PIPKIγ KO mice revealed impaired neurotransmission (Balla, 2013; Di Paolo et al., 2004; Giudici et al., 2004). In line with this, mice lacking PIPKIα and β can survive until adulthood (Volpicelli-Daley et al., 2010) while loss of PIPKIγ leads to early postnatal death (Di Paolo et al., 2004) indicating vital functions of PIPKIγ in the synapse.

As a cytoplasmic enzyme, PIPKIγ localizes to the plasma membrane via the C-terminus of its conserved kinase core domain that harbors the activation loop. This loop confers substrate

specificity for PI(4)P (Arioka et al., 2004; Doughman et al., 2003; Kunz et al., 2000). Phosphorylation regulates localization and kinase activity. Cyclin dependent kinase 5 (CdK5) phosphorylates PIPKIγ at serine 650 under resting conditions, while AP-induced Ca^{2+} influx activates the phosphatase calcineurin. Calcineurin then dephosphorylates and thus, activates PIPKIγ (Cousin & Robinson, 2001; Nakano-Kobayashi et al., 2007) which allows association with the F-actin binding protein talin and relocalization to the plasma membrane (Di Paolo et al., 2002; Sang et al., 2005). Furthermore, small GTPases like RhoA, Rac1 and Cdc42 or ADP-ribosylation factors, such as ARF6, potentiate PIPKIγ recruitment and allow for regulated $PI(4,5)P_2$ synthesis and thus may trigger endocytosis (Krauss et al., 2003; Morgan et al., 2004; van den Bout & Divecha, 2009).

1.1.4.1.1 $PI(4,5)P_2$ during SV exocytosis

In SV exocytosis, $PI(4,5)P_2$ is required for recruiting exocytic machinery components such as syntaxin 1, Syt1 or Munc13 (Martin, 2015; Walter et al., 2017) and for concentrating syntaxin 1 in nanoclusters at exocytic release sites (Van Den Bogaart et al., 2011).

$PI(4,5)P_2$ on the plasma membrane mediates binding to SV localized Syt1 via its C2B domain. The interaction increases Syt1's Ca^{2+} binding affinity (L. Y. Li et al., 2006; Van Bogaart et al., 2012) and thereby, facilitates SV fusion (Honigmann et al., 2013; Schiavo et al., 1996). Interestingly, also other proteins of the AZ which have been proposed to act in SV exocytosis possess C2 domains and thus, may be regulated by $PI(4,5)P_2$. Structural motifs such as C1, C2 phosphotyrosine-binding (PTB) and pleckstrin homology (PH) domains influence interaction of several proteins of the SV fusion machinery. These interactions may further be mediated by other phospholipids e.g., phosphatidylserine (PS) and DAG (Koch & Holt, 2012; Lauwers et al., 2016; Martin, 2015; Williams et al., 2009). For example, the clustering of syntaxin 1A as a required step for neurotransmission is controlled by $PI(4,5)P_2$ binding as well as binding of its downstream product $PI(3,4,5)P_3$ to its juxtamembrane region (Khuong et al., 2013; Van Den Bogaart et al., 2011).

Another, however controversially discussed role of $PI(4,5)P_2$ is its regulatory influence on the activity of voltage-dependent Ca^{2+} channels and thus on the ion influx into the synapse (Hosoi et al., 2009; Rodríguez-Menchaca et al., 2012). While the opening of voltage-dependent Ca^{2+} channels depends on $PI(4,5)P_2$, which was shown upon depletion of $PI(4,5)P_2$ by targeting the $PI(4,5)P_2$-specific PI-phosphatase synaptojanin, elevated $PI(4,5)P_2$ levels may also inhibit activity in specific scenarios (Gamper et al., 2004; Suh et al., 2010).

In contrast, uncaging of $PI(4,5)P_2$ and the resulting $PI(4,5)P_2$ increase potentiated exocytosis in adrenal chromaffin cells and lead to an increased RRP size (Walter et al., 2017). Depletion of the $PI(4,5)P_2$ synthesizing kinase PIPK1γ and consequently, reduced $PI(4,5)P_2$ levels in mice caused a smaller RRP and a strong exocytic defect under high-frequency stimulation (Di Paolo et al., 2004). Similarly, shielding of $PI(4,5)P_2$ inhibited fusion of chromaffin granules and SVs (Holz et al., 2000; Zheng et al., 2004) and reduced $PI(4,5)P_2$ levels upon overexpression of a membrane-associated variant of synaptojanin led to impaired secretion of large dense core vesicles in neuroendocrine cells (Milosevic et al., 2005).

Taken together, $PI(4,5)P_2$ marks exocytic release sites, mediates calcium influx and activates the SV fusion machinery for SV exocytosis.

1.1.4.1.2 The role of $PI(4,5)P_2$ during SV endocytosis

In the course of compensatory SV endocytosis at the periactive zone, $PI(4,5)P_2$ forms a binding platform for proteins belonging to the endocytic machinery (Di Paolo & De Camilli, 2006; Maritzen & Haucke, 2018). For example, proteins of the Bin/Amphiphysin/Rvs (BAR) - domain superfamily interact with $PI(4,5)P_2$. Having a crescent shape, they contribute to membrane remodeling during endocytosis. These proteins include e.g., Fer/Cip4 homology domain only (FCHo) 1/2 generating shallow early endocytic curvatures in CME (Henne et al., 2010) and amphiphysin, endophilin and sorting nexin 9 (SNX9) which act on membranes with higher curvature (Ferguson et al., 2009; Rao & Haucke, 2011). For SV reformation and regulation of correct SV size, clathrin adaptors (e.g., AP2, AP180 or CALM) are required (Kononenko et al., 2014; Koo et al., 2015; Soykan et al., 2016). These are also recruited by $PI(4,5)P_2$ (Collins et al., 2002; Höning et al., 2005; Rohde et al., 2002). Subsequent degradation of $PI(4,5)P_2$ then enables the disassembly of the clathrin coat while impaired turnover resulted in defective SV recycling and postnatal lethality (Cremona et al., 1999). Interestingly, endophilin recruits synaptojanin potentially to sites of high curvatures (Perera et al., 2006; Schuske et al., 2003). The resulting locally restricted hydrolysis of $PI(4,5)P_2$ at these sites coincides with recruitment of the GTPase dynamin (Chang-Ileto et al., 2011). The final vesicle scission depends on an oligomerized, helical assembly of dynamin (Kononenko et al., 2014; Mettlen et al., 2009). This oligomerization is achieved by interaction of dynamin's autoinhibitory PH domain with $PI(4,5)P_2$ on the plasma membrane (Chappie et al., 2011; Reubold et al., 2015; Takei et al.,

1995). In addition to its recruiting function for endocytic proteins, $PI(4,5)P_2$ has been proposed to indirectly influence actin dynamics. The actin cytoskeleton may be crucial for SV recycling as shown upon inhibition of formins (Soykan et al., 2017). Many actin binding proteins and small GTPases of the Rho family that are implicated in actin remodeling associate with $PI(4,5)P_2$ which could locally facilitate formation of linear actin filaments (Gorelik et al., 2011; Paul & Pollard, 2009; Saarikangas et al., 2010; Senju et al., 2017). In fact, overexpression of the $PI(4,5)P_2$ synthesizing enzyme PIPKIγ which leads to elevated $PI(4,5)P_2$ levels promoted CME in non-neuronal cells (Antonescu et al., 2011; Wenk et al., 2001) while its loss inhibited SV endocytosis (Di Paolo et al., 2004). This suggests $PI(4,5)P_2$ to be rate-limiting for SV endocytosis.

1.1.4.2 Exo-endocytic coupling via SV proteins

As another mechanism to couple SV exocytosis with SV endocytosis, surface stranded SV proteins may act as a control gear. After being exocytosed to the plasma membrane, these SV proteins could operate as recruiting hubs to initiate SV endocytosis until the steady-state distribution at rest is recovered (Fig. 4) (Haucke et al., 2011a; Koch & Holt, 2012; Maritzen & Haucke, 2018).

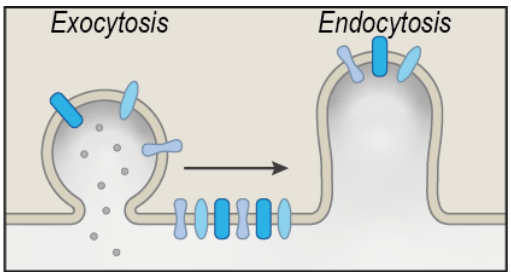

Figure 4: Plasma membrane localized SV proteins might couple SV exo- and endocytosis.
Model for SV exo- and endocytic coupling. Neuronal activity dependent exocytosis leads to the surface accumulation of SV proteins that act as endocytic substrates or recruiting hubs for proteins of the endocytic machinery. SV endocytosis is thereby directly coupled to exocytosis and operates until the steady-state distribution of SV proteins at rest is restored. Taken from (Bolz et al., 2023).

In line with such a model, loss or inhibition of proteins implicated in SV endocytosis such as dynamin or AP2 caused impaired SV fusion (Hosoi et al., 2009; Hua et al., 2013; Kawasaki et al., 2000; Shupliakov et al., 1997; Wadel et al., 2007). Sustained as well as acute abrogation of SV exocytosis and AP-induced Ca^{2+} influx impaired compensatory SV endocytosis (Verhage et al., 2000; Yamashita et al., 2010). Appearance of endocytic intermediates located in a stimulation dependent manner, close to the AZ upon low

frequency (Watanabe, Rost, et al., 2013) or at the periactive zone upon high frequency (Gad et al., 1998), further indicate the need for regulated SV protein turnover (Mutch et al., 2011). In this context, two processes targeting freshly exocytosed SV proteins are proposed. First, the stimulation-dependent release site clearance and secondly, SV protein sorting to enable efficient retrieval (Haucke et al., 2011a). Following SV fusion, the specialized release sites must be kept available for sustained neurotransmission. Interactions of AZ scaffolds e.g., of piccolo binding to the actin- and dynamin-binding protein Abp1 (Fenster et al., 2003) and the peripheral AZ scaffold GIT (Podufall et al., 2014), may provide a link to endocytosis. The exocytosed and rapidly diffusing SV proteins may then associate with sorting adaptors e.g., Syt1 with its specific endocytic adaptor Stonin2 [Stn2, stoned B in Drosophila; (Phillips et al., 2000)] or Syb2 with the sorting adaptor AP180 (Koo et al., 2015). This enables the confinement, reclustering and final sorting of SV proteins (Gimber et al., 2015). The confined SV proteins could subsequently act as recruiting platform for further sorting adaptors like AP2 which binds to cargo proteins and orchestrates clathrin coat assembly (Wieffer et al., 2009). Similarly, assembly with internal sorting adaptors like the SV protein vGLUT1, which itself can be sorted via AP-2 and endophilin (S. H. Kim & Ryan, 2009; P. K. Tan et al., 1998; Voglmaier et al., 2006), may control Syp and Syb1 retrieval (Pan et al., 2015).

Furthermore, the self-assembly of SV proteins could potentiate their clustering (Bennett et al., 1992) and hence their efficient retrieval as described for Syb2 and Syp (Calakos & Scheller, 1994; Chanaday & Kavalali, 2021; Edelmann et al., 1995; Siddiqui et al., 2007; Xu et al., 2013; Z. Zhang et al., 2013) as well as for Syt1 and SV2 (Lazzell et al., 2004; Schivell et al., 1996, 2005). These mechanisms can further be promoted by Ca^{2+}/calcineurin (Cousin & Robinson, 2001; Hosoi et al., 2009; M. M. Lai et al., 1999; Sankaranarayanan & Ryan, 2001; X. S. Wu et al., 2009; C. K. Yao et al., 2009).

However, sorting of SV proteins only partially occurs on the plasma membrane, but rather proceeds in a clathrin- and AP-2 dependent manner at later stages of the SV cycle at ELVs (Kononenko et al., 2014; Soykan et al., 2017; Watanabe, Trimbuch, Camacho-Pérez, Rost, Brokowski, Söhl-Kielczynski, et al., 2014) (Fig. 5) (Mutch et al., 2011; Takamori et al., 2006). The depletion of selective endocytic sorting adaptors leads to the partial redistribution of synaptic proteins to the presynaptic plasma membrane and to defects in SV endocytosis (Kaempf et al., 2015; Kononenko et al., 2013; Koo et al., 2015). Therefore, the amount of SV proteins present at the plasma membrane may intrinsically regulate the coupling of SV exocytosis and SV endocytosis.

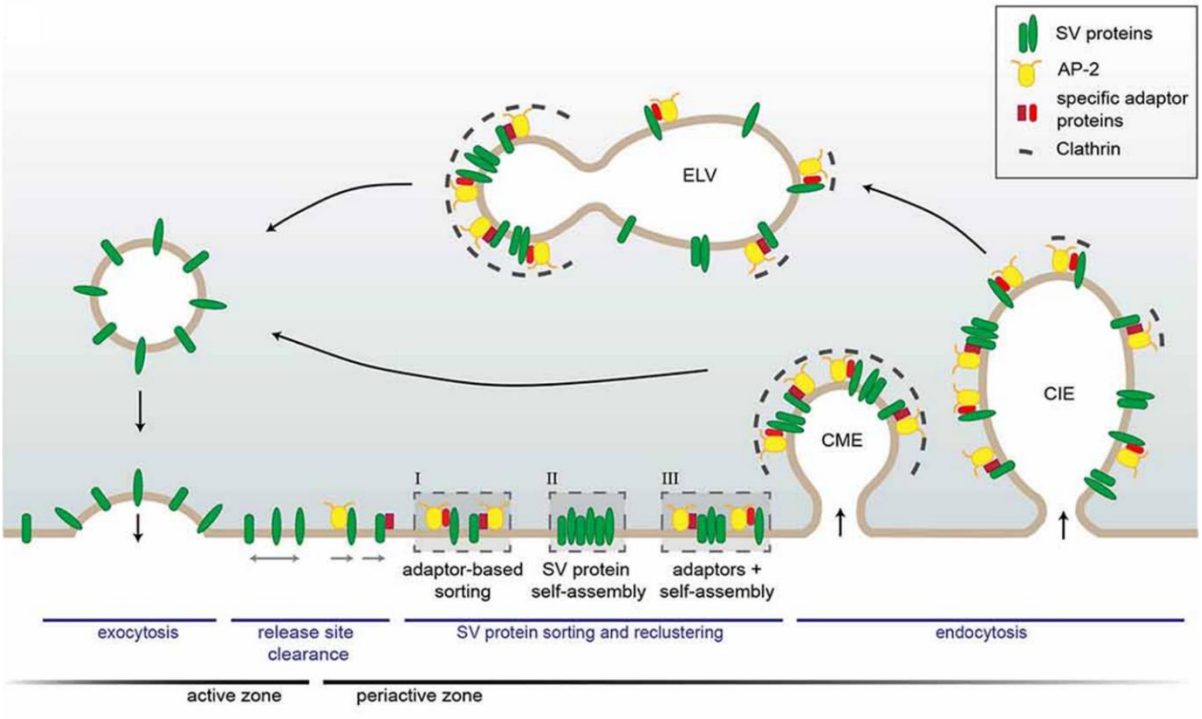

Figure 5: Clustering and sorting of SV proteins throughout the SV cycle
Following exocytosis at the AZ, SV proteins are confined by specific endocytic sorting adaptors (I), upon self-assembly (II) or a combination of both (III) to allow precise and efficient retrieval. Depending on the mechanism of endocytosis at the periactive zone, SVs are directly reformed via clathrin-mediated endocytosis (CME) or later reformed from endosomal-like vacuoles (ELVs) after clathrin-independent endocytosis (CIE). Taken from (Kaempf & Maritzen, 2017).

1.2 The SV protein Synaptotagmin 1

A candidate for an SV protein that may act as a post-fusion trigger for endocytosis is Syt1. Syt1 is thought to be the major Ca^{2+} sensor for fast SV exocytosis and was shown in numerous studies to be a key factor for neurotransmission (Chapman, 2008; Geppert et al., 1994). In mice, Syt1 absence resulted in early postnatal death while neurons lacking Syt1 displayed impaired synchronous neurotransmitter release that shifted towards asynchronicity (Fernández-Chacón et al., 2001; Geppert et al., 1994; Perin et al., 1991).

Syt1 belongs to a family of membrane-trafficking proteins. The mammalian synaptotagmin family includes 17 genes, while in *Drosophila melanogaster* or in *Caenorhabditis elegans* only seven or eight genes are encoded. Despite their high evolutionary conservation (Craxton, 2010), its members reveal different expression and subcellular localization patterns, vary in their biochemical properties, particularly their calcium affinity, and show distinct kinetics (Chen & Jonas, 2017; Südhof, 2002). The expression of most *Drosophila*

and mammalian isoforms is restricted to the nervous system, and four isoforms of the mouse genome, Syt1, -2, -9 (also stated as -5) and -12, specifically localize to SVs (Chen & Jonas, 2017; Glavan et al., 2009; Mittelsteadt et al., 2009). Syt1 is highly expressed in the rostral brain, and Syt2 exists predominantly in the caudal brain. Functional studies identified Syt1, -2 and -9 as fast Ca^{2+} sensors for SV exocytosis (Xu et al., 2007). Yet, they displayed fundamental differences in their kinetics and Ca^{2+} dependence suggesting that they mediate distinct release probabilities of different subsets of neurons (Maximov, 2009). In contrast, Syt7, which is located abundantly at the plasma membrane, was characterized as a slow Ca^{2+} sensor with high affinity to Ca^{2+} (Y. C. Li et al., 2017). Similarly, most other Ca^{2+} binding proteins in the nerve terminal display higher affinities for Ca^{2+} than Syt1. This supports Syt1 to act as the main calcium sensor specifically for synchronous neurotransmitter release.

1.2.1 Structure

Syt1 is a 65 kDa SV protein and composed of a short, glycosylated luminal N-terminus, a single transmembrane domain spanning the SV membrane once, a variable linker region and two large cytoplasmic domains containing Ca^{2+} binding motifs (C2 domains), the carboxy-terminal C2A and C2B domain (Fernandez et al., 2001; Perin et al., 1991). Syt1 binds a total of five Ca^{2+} ions, three by C2A and two by C2B (Brose et al., 1992). These C2 domains also mediate interactions with binding partners such as the SNARE complex and negatively charged residues of the lipid bilayers in a Ca^{2+} dependent manner (Kiessling et al., 2018; Littleton et al., 2001; Schiavo et al., 1996). Furthermore, penetration of phosphatidylserine containing membranes by Syt1 was suggested to occur via hydrophobic residues within the Ca^{2+} binding loops of the C2A and C2B domain (Chapman & Davis, 1998; Fernandez et al., 2001) (Fig. 6). Interestingly, the intrinsic Ca^{2+} binding affinity of Syt1 is non-physiologically low and increases upon phospholipid binding by 40 - 1000-fold resulting in its apparent Ca^{2+}-affinity (Radhakrishnan et al., 2009; Van Bogaart et al., 2012). This suggests that Ca^{2+} binding most likely occurs in combination with electrostatic interactions of negatively charged residues with phospholipids and ultimately, in close proximity to voltage gated Ca^{2+} channels (Brewer et al., 2015; Brose et al., 1992; L. Y. Li et al., 2006; Perin et al., 1991).

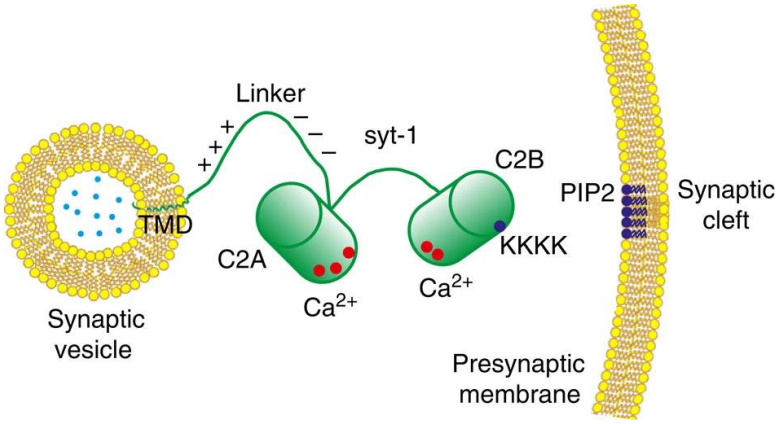

Figure 6: Schematic illustration of the domain structure of Synaptotagmin 1
Synaptotagmin 1 is composed of a short luminal N-terminus followed by a transmembrane domain (TMD) anchoring it to the SV, a charged linker region and two C2 domains. The C2 domains, C2A and C2B, harbor five calcium ion binding sites (red dots). The poly-lysine patch (KKKK) (blue dot) of the C2B domain binds negatively charged PI(4,5)P_2 (PIP2) at the presynaptic plasma membrane (blue lipids). The SV is filled with neurotransmitters (cyan dots). Taken from (Lin et al., 2014).

A closer look at the C2B domain reveals its importance for many processes. Syt1-C2B has been implicated in membrane bending and membrane fusion (Gruget et al., 2020; S. Wang et al., 2016) and in fusion pore opening (Y. Lai et al., 2015), stabilization (Caparotta et al., 2020) and expansion (Nyenhuis et al., 2021). Specifically the polybasic patch KRLKKKTTIKK at position 321-332 in the rat Syt1-C2B domain (PDB ID: 1k5w) mediates several interactions e.g. with AP2, Stn2, and PI(4,5)P_2 (Bai et al., 2004; L. Y. Li et al., 2006).

1.2.2 Syt1 function in endo- and exocytosis

1.2.2.1 Syt1's role in exocytosis

Based on Syt1's membrane-binding affinity and importance as a Ca^{2+} sensor, Syt1 has been extensively studied over decades and several molecular mechanisms suggest how Syt1 mediates the Ca^{2+} dependent SV fusion. Syt1 has been discussed to oligomerize into a circular conformation prior to SV fusion (J. Wang et al., 2017; Zanetti et al., 2016) and may act as a SV-plasma membrane distance regulator via basic residues within the C2B domain that directly bind PI(4,5)P_2 at the plasma membrane prior to influx of Ca^{2+} (Bai et al., 2004; Brose et al., 1992; Park et al., 2015). This would allow SV tethering and subsequently SNARE-mediated SV docking (Imig et al., 2014; Walter et al., 2010). Furthermore, Syt1 may trigger SNARE unclamping by displacing complexin (Maximov et al., 2009), yet direct

evidence displaying full SNARE zippering upon displacement of complexin is missing. In contrast, Syt1 has been discussed to clamp SNARE zippering itself as loss of Syt1 lead to an increase of spontaneous release (Chicka et al., 2008; Diantonio & Schwarz, 1994; Littleton et al., 1994; Xu et al., 2009). Full length Syt1, however, slightly increased the efficiency of Ca^{2+} independent fusion (Y. Lai & Shin, 2012; Z. Wang et al., 2011). Although Syt1-SNARE association has been widely discussed and a crystal structure has been solved showing the interaction with the primed pre-fusion SNARE complex (Brewer et al., 2015; Chicka et al., 2008; C. Li et al., 1995; Zhou et al., 2015), its impact on Ca^{2+} dependent SV fusion under physiological conditions remains controversial (Jahn & Fasshauer, 2012; Park et al., 2015). Ca^{2+} binding by the C2 domains may unlock the SNARE complex and thus promote full SV fusion (Zhou et al., 2017) allowing synchronous release and calcium cooperativity (Guan et al., 2017). Furthermore, Ca^{2+} binding to Syt1 may directly assist SV fusion. Upon Ca^{2+}-induced shielding of negative charges, Syt1 may be able to penetrate the lipid bilayers with its C2 domains and thus may destabilize the membrane (Bai et al., 2002; Fernandez et al., 2001). Binding to both, the SV and plasma membrane, Syt1 may bridge the membranes and contribute to fusion (Hui et al., 2009; Martens et al., 2007). Despite some controversial results, these findings underline Syt1's significance for a multitude of stages of SV fusion (Jahn & Fasshauer, 2012; Koh & Bellen, 2003).

1.2.2.2 Syt1's role in endocytosis

Syt1 does not only interact with a variety of proteins involved in SV exocytosis but additionally binds to key players of the endocytic machinery and charged membrane lipids (Brewer et al., 2015; Chapman, 2008; Fernandez et al., 2001; Jahn & Fasshauer, 2012; Zhou et al., 2017). It has been described as a key factor for synchronous neurotransmission. However, Syt1 loss did not only diminish synchronous neurotransmitter release but also impaired compensatory endocytosis (Y. C. Li et al., 2017) indicating a possible role as a post-fusion trigger for endocytosis. Furthermore, the calcium binding ability of Syt1 may not only be important for SV fusion but also for SV fission shown by capacitance measurements in chromaffin cells and rescue experiments with Ca^{2+} binding deficient mutants (Poskanzer et al., 2006; Van Den Bogaart et al., 2012; J. Yao et al., 2012).

Genetic loss, acute photoinactivation and loss of function mutations of Syt1 at neuromuscular junctions in *C. elegans* (Jorgensen et al., 1995) and *D. melanogaster* (Littleton et al., 2001; Poskanzer et al., 2003, 2006) lead to vast impairments including delay

of endocytosis and depletion of SVs at synaptic terminals while hippocampal Syt1-depleted neurons similarly showed delayed SV endocytosis (Y. C. Li et al., 2017; Nicholson-Tomishima & Ryan, 2004). Interestingly, genetic inactivation of stoned B in *D. melanogaster*, Syt1's evolutionary conserved endocytic sorting adaptor, resulted in severely paralyzed larvae with early embryonic lethality and impaired neurotransmission (Andrews et al., 1996; Diril et al., 2006; Jung et al., 2007; Maritzen et al., 2010). As Syt1 was able to rescue the phenotype, this was directly linked to mislocalized or degraded Syt1 and SV depletion (Fergestad et al., 1999; Fergestad & Broadie, 2001). Furthermore, the ectopic overexpression of Syt1 and Stn2 resulted in an enrichment of Stn2 at the plasma membrane and in Syt1 internalization in fibroblasts (Diril et al., 2006). This is likely due to Stn2's interaction with Syt1 as a specific endocytic sorting adaptor which links Syt1 to the endocytic machinery. Stn2 consists of an N-terminal WxxF motif interacting with AP2, a well conserved Asn-Pro-Phe (NPF) motif binding to Eps15 homology (EH) domains present in many endocytic proteins (Haucke & De Camilli, 1999; Martina et al., 2001), a conserved stonin-homology domain (SHD) (Maritzen et al., 2010) and a C-terminal µ2-homology domain (µHD). Via a short tyrosine-based motif within the µHD, Stn2 binds to Syt1 (Fig. 7a) (Jung et al., 2007).

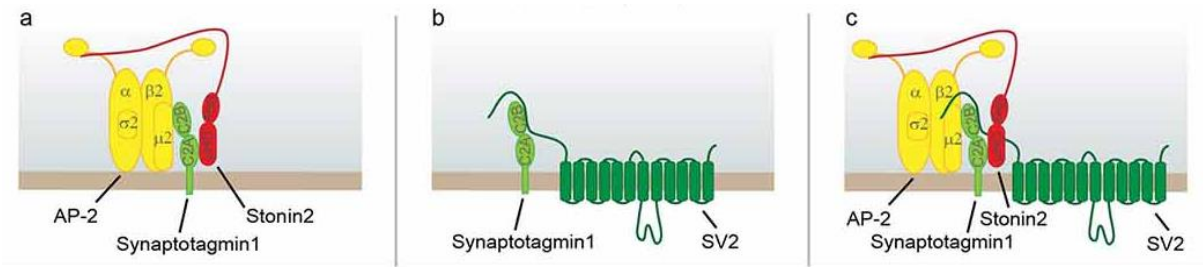

Figure 7: Schematic illustration of endocytic sorting of Synaptotagmin 1
Three possible mechanisms may sort Syt1: (a) Syt1 associates via its C2B domain with AP2 while simultaneously interacting via its C2A domain with Stn2. The Syt1-specific adaptor protein Stn2 strengthens the interaction between AP2 and Syt1 by additionally interacting with the AP2α ear. (b) Syt1 associates via its C2B domain with the N-terminus of SV2. (c) A combination of both may facilitate correct Syt1 sorting. Taken from (Kaempf & Maritzen, 2017).

Surprisingly, studies in Stn2 knockout (KO) mice did not reveal a severely impaired SV recycling or strong behavioral deficits. Only the explorative behavior of Stn2 KO mice was mildly increased. Consistent with earlier studies and Stn2's proposed sorting function for Syt1, loss of Stn2 resulted in Syt1 mislocalization to the plasma membrane. Strikingly, under these conditions accelerated SV retrieval, increased SV numbers and elevated short-term facilitation were detected (Kononenko et al., 2013). This contrasts with the severe defects

found in invertebrates and suggests a compensatory mechanism e.g., involving additional sorting adapters. In this context, SV2, a glycosylated 12-transmembrane domain protein family crucial for CNS function (Crowder et al., 1999) and implicated in epilepsy (Lynch et al., 2004), has been found to interact via a N-terminal tyrosine-based motif with the C2B domain of Syt1 in a phosphorylation-dependent manner (Haucke & De Camilli, 1999; Pyle et al., 2000; N. Zhang et al., 2015). Thereby, SV2 facilitates Syt1 internalization (Fig. 7b) (Haucke & De Camilli, 1999). This interaction is conserved for all three SV2 isoforms, A, B and C (Lazzell et al., 2004; Schivell et al., 1996, 2005) and is negatively regulated by Ca^{2+} (Schivell et al., 1996). In contrast to the evolutionary conserved Stn2, the SV2 protein family is only present in vertebrates and may therefore be implicated in a vertebrate-specific compensatory mechanism (Fig. 7c) which might explain the mild phenotype upon Stn2 loss in mice compared to the severe defects in invertebrates. Indeed, the parallel deletion of Stn2 and SV2 resulted in severe defects in mice establishing SV2 and Stn2 as redundantly acting sorters for Syt1 (Kaempf et al., 2015).

While this underlines the importance of efficient Syt1 sorting, it remains unclear how Syt1 might regulate SV endocytosis and whether and how it plays a role as a post-fusion trigger for SV endocytosis.

2 Aims of this study

Exocytosis and endocytosis are fundamental for brain function by enabling the sustained release of neurotransmitters. Neurotransmission requires tightly controlled Ca^{2+}-triggered exocytic fusion of SVs and spatiotemporally-coupled compensatory endocytic retrieval of SV lipids and proteins to avoid swelling boutons and synaptic dysfunction. The fundamental question how a presynapse "knows" how many vesicles fused and, hence, how much material needs to be retrieved by compensatory endocytosis remains unanswered. Impairment of a key factor for synchronous neurotransmission, the Ca^{2+} sensor Syt1, led to defects in both exo- and endocytosis. Therefore, Syt1 appears to be a prime candidate for mediating the spatiotemporal coupling of SV exo-/ endocytosis. Strikingly, defects in Syt1 sorting causing a surface accumulation of Syt1 did not impair but facilitate endocytic retrieval. This thesis aims at elucidating the underlying molecular mechanism, thereby advancing our molecular understanding of SV exo- and endocytic coupling. To study the role of Syt1 in presynaptic exo- and endocytic coupling, we combined mouse genetics with optical imaging. We performed live-cell microscopy to analyze the kinetics of the SV cycle, followed by confocal and super-resolution microscopy to detect presynaptic protein localization patterns and carried out electron microscopy to visualize the ultrastructure and to identify ultrastructural changes. This was combined with biochemical experiments and structural analysis to determine a unique, conserved interaction implicated in the molecular Syt1-dependent coupling mechanism.

3 Material and Methods

3.1 Materials

3.1.1 Chemicals

All chemicals were purchased from Abcam, Carl-Roth GmbH (Germany), Life Technologies (USA), Merck (Germany), Sigma-Aldrich (USA), Thermo Fisher Scientific (USA) and Tocris (UK) if not indicated differently. Consumables were obtained from B. Braun (Germany), Biozym (Germany), GE Healthcare (UK), Greiner (Germany), Millipore (USA), Sarstedt (Germany) and Schott (Germany).

3.1.2 Buffers, Media and Solutions

All buffers, media and solutions were prepared with Millipore-filtered water and were pH adjusted using NaOH or HCl. If required, solutions were autoclaved (121 °C, 1 bar) or sterile filtered. For specific protocols, buffers are specified in the corresponding methods section.

Table 1: Buffers and media used for molecular biological experiments

Buffer	**Composition**
Antibiotics stock solutions	100 mg/mL Ampicillin, sterile filtered (1000x) 50 mg/mL Kanamycin, sterile filtered (1000x)
6x DNA loading dye	0.03 % (w/v) Bromophenol blue 0.03 % (w/v) Xylene cyanol FF 60 % (v/v) Glycerol 60 mM EDTA
2 x Glycerol stock solution	50 % Glycerol 100 mM $MgSO_4$ x 7 H_2O 10 mM Tris
LB (Lysogeny broth) medium	1 % (w/v) Yeast extract 0.5 % (w/v) NaCl 0.5 % (w/v) Tryptone pH 7.4
LB plates	15 g/L Agar-agar (Roth; X965) LB medium

10x OrangeG loading dye	2 mg/mL OrangeG (Sigma, O-1625) 70 % (v/v) Glycerol
Tail lysis buffer	100 mM Tris, pH 8.5 5 mM NaEDTA 0.2 % (w/v) SDS 200 mM NaCl
50x Tris-Acetate-EDTA buffer (TAE)	200 mM Tris 100 mM Glacial acetic acid 50 mM EDTA pH 8.2 – 8.4
10x Tris-Borate-EDTA buffer (TBE)	20 mM EDTA 890 mM Tris 890 mM Boric acid
2× YT medium	1.0 % (w/v) Yeast extract 1.6 % (w/v) Tryptone 0.5 % (w/v) NaCl pH 7.4

Table 2: Buffers and solutions used for cell biological experiments and fluorescent microscopy

Buffer	**Composition**
10 x Acidic stock solution	1.2 M NaCl 35 mM KCl 40 mM KH_2PO_4 200 mM MES 50 mM $NaHCO_3$ 50 mM Glucose 12 mM Na_2SO_4 pH 5.5
Acidic imaging buffer	50 mM NaCl 1.2 mM $MgCl_2$ 1.3 mM $CaCl_2$ 1 x Acidic stock solution

Basic imaging buffer	50 mM NH_4Cl
	1.2 mM $MgCl_2$
	1.3 mM $CaCl_2$
	1 x Imaging stock solution
Basic medium for hippocampal neuron cultures	1 x MEM (Minimum Essential Media; Life Technologies)
	5 g/L Glucose
	200 mg/L $NaHCO_3$
	100 mg/L Transferrin (Merck)
Blocking buffers	10 % NGS
	0.1 % Triton X-100
	1x PBS
Digestion solution	137 mM NaCl
	5 mM KCl
	7 mM Na_2HPO
	25 mM HEPES
	pH 7.4
Dissociation solution	Hank's balanced salt solution w/o Ca^{2+} / Mg^{2+}
	50 mg/L $NaHCO_3$
	12 mM $MgSO_4$
	1 mM HEPES
	pH 7.4
Glutaraldehyde fixative	1 % (v/v) Glutaraldehyde (GA)
	2 % (w/v) Paraformaldehyde (PFA)
	2 % (w/v) Sucrose
	1 x PBS
	pH 7.4
Growth medium for hippocampal neurons	1 x Basic medium
	5 % (v/v) FCS (Biochrom)
	0.5 mM L-glutamine (Lonza)
	2 % (v/v) B27-supplement (Life Technologies)
	50 U/mL Penicillin
	50 µg/mL Streptomycin

10 x Imaging stock solution	1.2 M NaCl 35 mM KCl 40 mM KH_2PO_4 200 mM TES 50 mM $NaHCO_3$ 50 mM Glucose 12 mM Na_2SO_4 pH 7.4
Imaging buffer	50 mM NaCl 1.2 mM $MgCl_2$ 1.3 / 2 mM $CaCl_2$ 1 x Imaging stock solution 50 µM APV 10 µM CNQX
Mammalian cell culturing medium	10 % (v/v) FBS (fetal bovine serum, heat inactivated, Gibco) 1 % (v/v) P/S:100 U/mL Penicillin; 100 µg/mL Streptomycin 1 x DMEM (Dulbecco's modified Eagle medium; high glucose (4.5 g/L), + 2 mM L-glutamine)
10x Phosphate-buffered saline (PBS)	1.37 M NaCl 100 mM Na_2HPO_4 17.6 mM KH_2PO_4 26.8 mM KCl pH 7.4
PBS + $MgCl_2$	1 x PBS 10 mM $MgCl_2$
PFA fixative	4 % (w/v) Paraformaldehyde (PFA) 4 % (w/v) Sucrose 1 x PBS pH 7.4
Plating medium for hippocampal neurons	1 x Basic medium 10 % (v/v) FCS (Biochrom) 2 mM L-glutamine (Lonza) 25 mg/mL Insulin 50 U/mL Penicillin 50 µg/mL Streptomycin

Stimulation imaging buffer	50 mM NaCl 80 mM KCl 1.2 mM $MgCl_2$ 1.3 mM $CaCl_2$ 1 x Imaging stock solution

Table 3: Buffers and solutions used for biochemical experiments

Buffer	**Composition**
Antibody blocking solution	3 % BSA (bovine serum albumin) 1 x PBS
Antibody dilution solution	1 × PBS-T 3 % (w/v) BSA
Binding buffer	20 mM HEPES 100 mM KCl 2 mM $MgCl_2$ 0.1 % Triton X-100 pH 7.4
2 × Bradford reagent	200 mL 85 % H_3PO_4 100 mL Ethanol 140 g/L Coomassie G250
Brain homogenization buffer	4 mM HEPES, pH 7.4 320 mM Sucrose
Coomassie destain	10 % (v/v) Acetic acid 25 % (v/v) Methanol
Coomassie stain	1 g/L Coomassie G250 10 % (v/v) Acetic acid 25 % (v/v) Methanol
Elution buffer	50 mM Tris 300 mM NaCl 300 mM Imidazole 2 mM dithiothreitol (DTT) pH 7.2

Lysis buffer I	20 mM HEPES, pH 7.4 100 mM KCl 2 mM $MgCl_2$ 1 % (v/v) Triton X-100 1 mM PMSF 0.3 % (v/v) Protease inhibitor cocktail (Sigma)
Lysis buffer II	50 mM Tris 300 mM NaCl 10 mM Imidazole 2 mM DTT 0.5 % Triton X-100 1 tablet cOmplete, EDTA-free protease inhibitor cocktail (Pierce) pH 7.5
PBS-T	0.05 % TWEEN-20 1 x PBS
Ponceau S destain	1 % (v/v) Acetic acid
Ponceau S staining	0.4 % (w/v) Ponceau S 1 % (v/v) Acetic acid
6x SDS sample buffer	18 % (w/v) SDS 30 % (v/v) β-Mercaptoethanol 60 % (v/v) Glycerin 0.25 % (w/v) Bromophenol blue 0.325 M Tris pH 6.8
4x SDS separating gel buffer	0.4 % (w/v) SDS 1.5 M Tris pH 8.8
4x SDS stacking gel buffer	0.4 % (w/v) SDS 0.5 M Tris pH 6.8
10x SDS running buffer	250 mM Tris 10 % (w/v) SDS 1.92 M Glycine

1 x Transfer Buffer	25 mM Tris 192 mM Glycine 10 % (v/v) Methanol
Washing buffer	50 mM Tris 300 mM NaCl 20 mM Imidazole 2 mM DTT pH 7.2

3.1.3 Enzymes and kits

Enzymes regulate biological processes and often act as catalysts. All enzymes that we used for molecular biological methods were stored at -20 °C. Concentrations are indicated in the respective method sections.

Calf intestinal alkaline phosphatase (CIP) cleaving phosphoric acids and thus catalyzing substrate hydrolysis, Phusion high fidelity DNA polymerase catalyzing the synthesis of DNA molecules from nucleoside triphosphates, restriction enzymes cleaving DNA into fragments at the corresponding restriction sites and Proteinase K for inactivation of DNases and RNases were obtained from New England Biolabs (NEB).

Dream Taq DNA Polymerase and T4 DNA Ligase catalyzing the formation of a phosphodiester bond and hence, joining of two DNA strands were purchased from Thermo Fisher Scientific.

Taq DNA Polymerase (Bio & Sell) and HotStart Mouse Genotyping Kit (Sigma-Aldrich KAPA) were used to genotype tail biopsies of mice.

The NucleoSpin Plasmid kit for preparation of plasmid DNA from *Escherichia coli (E. coli)* small overnight cultures, the endotoxin-free plasmid DNA purification kit (NucleoBond®Xtra Midi EF kit) for large scale plasmid DNA isolation and the NucleoSpin®Gel and PCR Clean-up kit for purification of DNA from agarose gels and PCR reactions were purchased from Macherey-Nagel.

The calcium phosphate transfection system (ProFection Mammalian Transfection system – Calcium Phosphate E1200) were obtained from Promega for transfection of primary hippocampal cultures.

All kits were stored and used according to manufacturer’s instructions.

3.1.4 Molecular weight standards

Table 4: Molecular weight standards

Marker	Source
GeneRuler™ 1 kb DNA Ladder	Thermo Fisher Scientific (SM0311)
GeneRuler™ 100 bp DNA Ladder	Thermo Fisher Scientific (SM0241)
PageRuler Prestained Protein Ladder	Thermo Fisher Scientific (26616)

3.1.5 Oligonucleotides

3.1.5.1 DNA oligonucleotides

All synthetic oligonucleotides were obtained as lyophilized powder from BioTeZ Berlin Buch GmbH, dissolved in nuclease-free water to a concentration of 100 μM and stored at -20 °C.

Table 5: Primers used for genotyping of mouse genomic DNA. Wild type (WT). Knock out (KO)

Genotype	Primer	Sequence (5' – 3')
Stn2 WT	p22 forward	GATCCCCGGGGCCCCCTCACCTGCCTCA
	p23 reverse	GATCCTCGAGCTAGGACAGCACTGGTAAATCCA
Stn2 KO	neo forward	GGCGCGGTCCCAGGTCCAC
	neo reverse	CTTCGCCCAATAGCAGCCAGTCC
SV2A	SV2A WT forward	GAGAATATCAGGGCATCC
	SV2A KO forward	CAGTCCTCACAGTCTGTT
	SV2A combined reverse	GCCCTCTAGATACAGCTTGC
SV2B	SV2B WT forward	TGAAGGCGAGTACCAAGGCA
	SV2B KO forward	CCTGTGTGAAATTGTTATCCGCT
	SV2B combined reverse	TTCGAGAAAACAAGATTTGGGAAT
Syt1	Syt1 WT forward	GTATTCAGTGCGTCTCAGAGACAGTC
	Syt1 KO forward	GAGCGCGCGCGGCGGAGTTGTTGAC
	Syt1 combined reverse	AACTATAATTTGTCACAGGCATTGCCTTTCA

Table 6: Primers used for cloning and sequencing. Forward (fw). Reverse (rv).

Primer	**Sequence (5' – 3')**
pCAG _fw	GCAACGTGCTGGTTATTGTG
GFP/YFP/CFP_fw	GCAGAAAGCCCAGTTCAACTG
GFP/YFP/CFP_rv	TGAAGAAGTCGTGCTGCTTC
mRFP_rv	GAGGAGTCCTGGGTCACG
Syp-pH sense XbaI_fw	GCGCTCTAGAGCCACCATGGACGTGGTGAATCAG
Syp-pH antisense SalI_rv	GCGCGTCGACTCACTACCTCCCTTTAAAC
CMV_fw	CGCAAATGGGCGGTAGGCGTG
pGEX seq_fw	GGGCTGGCAAGCCACGTTTGGTG
pHlourin_fw	AAGATGACGGGAACTACAAG
pHlourin_rv	GCCTCCATCTTCAATGTTGTG
Syt1C2B_beg_fw	AAACTGGGTGACATCTGC
Syt1C2B_R322E_fw	GAGCTGAAGAAGAAAAAGACGACGATTAAGAAG
Syt1C2B_R322E_rv	CTTACCGTTCTGCATCAGGTGAATCTT
Syt1C2B-(K)A321E_fw	GAGAGGCTGAAGAAGAAAAAGACG
Syt1C2B-(K)A321E_rv	ACCGTTCTGCATCAGGTGAATC
Syt1C2B-(K)A354E_fw	GAAGTGCAAGTGGTGGTAACTG
Syt1C2B-(K)A354E_rv	CTGGATTTGCTCGAACGGAAC
Age1_vGLUT1pH_fw	GCGCACCGGTGCCACCATGGAGTTCC
Xba1_vGLUT1pH_rv	GCGCTCTAGATCAGTAGTCCCGGACAG
PIPKIγ_fw	CTTGTTGTTCGGCGGCGG
PIPKIγ_rv	AAGGAGGCCGAGTTCCTGC
vGLUT1_fw	GCAGAAAGCCCAGTTCAACTG
vGLUT1_rv	GCCACAATGGCAAAGCCAAAG
FBP17_fw	TTGAGAAAATGGACGCTG
FBP17 K33E_fw	GAGGAAAGGACAGAGATTGAACTCAGCTATG
FBP17 K33E_rv	CACAAACTTGATATATTTCTCAAGAATATCAATTCCC

3.1.5.2 Small hairpin RNA oligonucleotides

pLKO.1-plasmids encoding for different small hairpin RNA (shRNA) oligonucleotides were obtained from Sigma-Aldrich. For neuronal specificity, each shRNA was then inserted into an FUGW expression vector for dual expression of shRNA under the control of a U6-promotor and expression of nuclear localized RFP controlled by a human

synapsin 1-promotor. A non-targeting sequence was used as negative control (Watanabe et al., 2014).

Table 7: shRNA sequences

shRNA	Target organism	Sequence (5' – 3')	ID
Syt1	Mus musculus, CDS	GAGCAAATCCAGAAAGTGCAA	TRCN0000093258
Syt1	Mus musculus, 3'UTR	CGGCCATGCATTCCTGATACAATC	TRCN0000380868
FBP17	Mus musculus, 3'UTR	GTTAGTGTGCTGCGTTCAATT	TRCN0000350892
vGLUT1	Mus musculus, 3'UTR	TGAACTGTCCCTCCAAATAAA	NM_182993.2_2125

3.1.6 Plasmid vectors

All bacterial and mammalian expression vectors used in this study were either obtained by cloning or received as indicated. Based on the cell type used in a specific experiment a vector was chosen. For expression of proteins in mammalian cell lines pcDNA3.1-based vectors (Thermo Fisher Scientific) were used. Due to their cytomegalovirus (CMV) promoter, these vectors ensure constitutive expression of the inserted genes (Xia et al., 2006). Derivatives of pcDNA3.1 carrying fluorescent tags or promotors providing exclusively neuronal expression [pcDNA3.1 modified (Wienisch & Klingauf, 2006), pmCherry-C (Clontech (France)] were chosen for specific needs. For expression of N-terminally tagged GST recombinant proteins carrying a thrombin cleavage site in *E. coli*, the pGEX-4T-1 vector was chosen. Based on a T7 promoter, the expression is IPTG inducible and resistant to ampicillin allowing for selection. For long-term storage, all plasmids were stored at -20 °C in nuclease- and endotoxin-free water at a concentration of 1 µg/µL.

Table 8: Vectors used for recombinant protein expression

Construct	Insert species	Vector	Source
vGLUT1-pHluorin	rat	FUGW	Voglmaier, UCSF, San Francisco, CA

Syp-pHluorin	rat	pcDNA3.1, modified	L. Lagnado
GST-Syt1 C2A	rat	pGEX4T-1	(Jung et al., 2007)
GST-Syt1 C2B	rat	pGEX4T-1	(Jung et al., 2007)
GST-Syt2 C2B	rat	pGEX4T-1	E.R. Chapman, University of Wisconsin
GST-Syt7 C2B	rat	pGEX4T-1	E.R. Chapman, University of Wisconsin
GST-Syt9 C2B	rat	pGEX4T-1	E.R. Chapman, University of Wisconsin
GST-Syt1 C2B K321A	rat	pGEX4T-1	Cloned by Natalie Kämpf
GST-Syt1 C2B K321A K354A	rat	pGEX4T-1	Cloned by Natalie Kämpf
GST-Syt1 C2B R322E	rat	pGEX4T-1	This study
His_{10}-PIPKIγ	human	pFL-10his	Cloned by Wen-Ting Lo
mCherry-PIPKIγ	human	pmCherry-C	Cloned by Michael Krauss
mCherry-PIPKIγ K188A D316E	human	pmCherry-C	This study
mCherry-Synaptotagmin1	rat	pmCherry-C	Cloned by Natalie Kämpf
mCherry-Synaptotagmin1 R322E	rat	pmCherry-C	This study
eGFP-PH-PLCδ1	human	pET28a	(Milosevic et al., 2005)
eGFP-PH-PLCδ1 K30A K32A W36N	human	pET28a	(Milosevic et al., 2005)
vGLUT1	mouse	pmCherry-C	(Kwon et al., 2016)
vGLUT1ΔAH	mouse	pmCherry-C	Cloned by Svenja Bolz
vGLUT1ΔAH + AH($vGAT_{CT}$)	mouse	pmCherry-C	Cloned by Svenja Bolz
vGLUT1ΔAH + AH(Hecate)	mouse	pmCherry-C	Cloned by Svenja Bolz
mCherry	Discosoma sp.	pmCherry-N1	Cloned by Svenja Bolz
mCherry-FBP17	human	pmCherry-N1	This study
mCherry-FBP17K33E	human	pmCherry-N1	This study

3.1.7 Antibodies

To detect and image discrete components appropriately labeled antibodies are used that bind specifically to their target antigen.

3.1.7.1 Primary antibodies

Primary antibodies used for immunoblotting and immunocytochemistry were stored at -20 °C and were diluted with 50 % (v/v) glycerol for protection during freeze-thaw cycles. The depicted dilutions refer to the glycerol-diluted stock concentration.

Table 9: Primary antibodies used in this study. Cat # - catalog number; IB - immunoblotting; ICC - immunocytochemistry; gp - guinea pig; ms - mouse; rb - rabbit; ^{S} and ^{F} and ^{L} indicate dilution for STED staining and fixation including GA or used in live-imaging.

Antigen	**Host species**	**Dilutions**		**Source**	**Cat #**
		IB	**ICC**		
AP2-α	ms		1:200 ^{S}	Abcam	ab2730
AP2-µ	ms	1:500		BD Biosciences	611351
Bassoon	gp		1:100 ^{S}	Synaptic Systems	141 004
Clathrin heavy chain	ms	1:500		CHC TD1	homemade
Dynamin	ms		1:100 ^{S}	Upstate	05-319
FBP17	rb		1:200	Thermo Fisher	PA5-28626
GFP	rb		1:1000 ^{F}	Abcam	ab6556
Homer-1	rb		1:200 ^{S}	Synaptic Systems	160 003
MAP2	gp		1:300	Synaptic Systems	188 004
PIPKIγ	ms	1:70	1:300 ^{S}	BD Biosciences	611148
PI(4)P	ms		1:70 ^{F}	Echelon Biosciences	Z-P004
$PI(4,5)P_2$	ms		1:400 ^{F}	Echelon Biosciences	Z-A045
Polyhistidin (HRP conjugated)	ms	1:2000		Sigma-Aldrich	A7058
RFP	rb		1:400	MBL	PM005
SNAP-25	ms	1:500		Synaptic Systems	111 011
Stonin2	rb	1:800		Sigma-Aldrich	HPA003086

Synaptophysin	ms		1:500	Synaptic Systems	101 011
Synaptotagmin1	ms	1:500	1:100	Synaptic Systems	105 011
Synapsin 1/2	gp		1:200	Synaptic Systems	106 004
vGAT	rb		1:200[L]	Synaptic Systems	131 103CpH
vGLUT1	gp		1:500	Synaptic Systems	135 304

3.1.7.2 Secondary antibodies

For immunocytochemistry, secondary antibodies used in this study were Alexa Fluor (AF)-conjugated. Secondary antibodies applied in immunoblotting experiments were horseradish peroxidase (HRP)-conjugated.

Table 10: Secondary antibodies used in this study. Cat # - catalog number; IB - immunoblotting; ICC - immunocytochemistry; d - donkey; gp - guinea pig; gt - goat; ms - mouse; rb - rabbit; AF - Alexa Fluor; HPR - horseradish peroxidase

Antigen	**Host species**	**Conjugate**	**Dilution**		**Source**	**Cat #**
			IB	**ICC**		
Ms IgG	goat	AF488		1:400	Life technologies	A-11001
Ms IgG	goat	AF568		1:400	Life technologies	A-11031
Ms IgG	goat	AF594		1:200	Life technologies	A-11032
Ms IgG	goat	AF647		1:400	Life technologies	A-21235
Ms IgG	goat	Atto 647N		1:200	Active Motif	15038
Ms IgM	goat	AF568		1:400	Life technologies	A-21043
Rb IgG	goat	AF488		1:400	Life technologies	A-11008
Rb IgG	goat	AF488		1:200	Life technologies	A-11034
Rb IgG	goat	AF568		1:400	Life technologies	A-11011
Rb IgG	goat	AF647		1:400	Life technologies	A-21244
Rb IgG	goat	Atto 647N		1:200	Active Motif	15048
Gp IgG	donkey	AF488		1:200	Jackson Immuno Research	706-545-148
Gp IgG	goat	AF568		1:200	Life technologies	A-11075
Ms IgG	goat	HRP	1:10,000		Jackson Immuno Research	106-035-003
Rb IgG	goat	HRP	1:10,000		Jackson Immuno Research	111-035-003

3.1.8 Probes

For specific staining of $PI(4,5)P_2$ as described before (Milosevic et al., 2005), fusion proteins consisting of eGFP and the $PI(4,5)P_2$ binding PH domain of PLCδ1 (PH-PLCδ1-eGFP) or the binding mutant eGFP-PH-PLCδ1 K30A K32A W36N were used. They were recombinantly expressed in *E. coli*, purified, and stored in 50 % glycerol at -80 °C (courtesy of Uwe Fink, FMP, Berlin) until use in immunocytochemistry at a final concentration of 0.25 µg/ mL.

To increase $PI(4,5)P_2$ levels in a temporally controllable manner as described before (Walter et al., 2017), a membrane-permeant, photoactivatable $PI(4,5)P_2$-compound, a kind gift from Martin Schultz (EMBL, Heidelberg) was used. Immediately prior to application, the trifunctional $PI(4,5)P_2$ carrying a coumarin cage, clickable alkyne and cross-linkable diazirine (TF-$PI(4,5)P_2$/AM) was dissolved in 50 mM DMSO and 10 % pluronic F127 and applied at a final concentration of 20 µM.

3.1.9 Bacteria strains

For cloning, amplification and storage of plasmid DNA, the chemically competent *E. coli* TOP10 strain (Life Technologies) was used. Expression of recombinant proteins was carried out in *E. coli* BL21 CodonPlus (DE3)-RP strain (Stratagene) which carries extra copies of rare tRNA genes. The lac UV5 promotor controlling the T7 RNA polymerase enables the IPTG-induced expression of heterologous proteins at high levels.

3.1.10 Eukaryotic cell lines

Based on its high replication rates, transfection efficiency and high protein expression levels (Wurm, 2004) the human embryonic kidney cell line 293T (HEK) from the American Type Culture Collection (ATCC) was used for biochemical experiments. In addition, due to a temperature-sensitive mutant version of the SV40 large T antigen HEK 293T were also used for virus amplification. The epithelial cervical cancer cell line HeLa from ATCC was used for experiments visualizing changes in the plasma membrane due to its higher adherence properties compared to HEK cells (Potthoff et al., 2012). The cells were cultured in Mammalian cell culturing medium in a humidified incubator at 37 °C and 5 % CO_2 and were routinely tested for mycoplasma with a PCR-based Mycoplasma test kit (PromoKine).

3.1.11 Mouse strains

All animal experiments were reviewed and approved by the ethics committee of the "Landesamt für Gesundheit und Soziales" (LAGeSo) Berlin and were conducted according to the committee's guidelines under the corresponding animal experimentation permits. The LAGeSo and the institute's animal care officer monitored compliance with all regulations. Professional caretakers checked all mice daily for their health status which was documented in the corresponding health reports. Standard pathogens were monitored at regular intervals. Mice were group-housed under 12/ 12 h light/ dark cycle in standard individually ventilated cages (IVCs) containing bedding and nesting material with access to food and water ad libitum. All mice used for experiments were naive and no drug tests were performed. Mice from both sexes were used and multiple independent experiments using several biological replicates were performed. Neuronal cultures were prepared from postnatal mice immediately after birth (for Syt1) or at day one to day three (for WT, Stn2) according to the corresponding animal experimentation permits. Sample sizes for animal experiments were estimated by biometrical calculations where possible and multiple independent experiments were carried out using several biological replicates specified in the legends to figures.

Table 11: Mouse strains used in this study. Wild type (WT). Knock out (KO). Heterozygous (HET)

Mouse strain	**Source**	**Breeding**
C57BL/ 6J	Charles River	Interbreeding of C57BL/6J mice preserving stock of wild type mice.
Syt1 (B6;129S-Syt1^{tm1Sud})	(Geppert et al., 1994)	Breeding of Syt1 heterozygous mice to obtain Syt1 WT and KO mice
Stn2 (B6;Ston2^{tm1Vha})	(Kononenko et al., 2013)	Breeding of Stn2 heterozygous mice to obtain Stn2 WT and KO mice
SV2A/ SV2B	Kind gift from S. Bajjalieh (Custer et al., 2006) [SV2A described in (Crowder et al., 1999) and SV2B KO in (Morgans et al., 2009)]	Interbreeding of SV2A HET/ SV2B KO mice to obtain SV2A/B double KO (DKO) mice

3.1.12 Software and internet resources

Table 12: Software and internet tools used in this study.

Software/Website	Source	Application
BLAST (Basic local alignment search tool)	https://www.ebi.ac.uk/Tools/msa/clustalo	DNA and protein sequences alignment
Fiji (ImageJ)	NIH, Open Source Software	Image analysis and quantification
Illustrator CS6	Adobe Systems, USA	Illustrations and figures
Image Lab Software	BIO-RAD	Immunoblot acquisition and analysis
Jalview	https://www.jalview.org	Visualization of sequence alignments
Micromanager	https://www.micro-manager.org/	Epifluorescent image acquisition (ImageJ based)
Microsoft Office 365	Microsoft	Text, analysis, and visualization
NCBI Homepage	www.ncbi.nlm.nih.gov/	Database for DNA and protein sequences and scientific literature
Prism v.8	Graphpad	Statistical analysis, graphs
PyMOL	Schrödinger	Visualization of 3D structures of proteins
PyRAT (Python Based Relational Animal Tracking)	Scionics Computer Innovation	Organization and coordination of mice, breedings and experiments used by animal facility
SnapGene	GSL Biotech	Cloning strategy design, DNA analysis
Uniprot	https://www.uniprot.org/	Research on genes and proteins; determination of homology of proteins

3.2 Methods

3.2.1 Molecular biology methods

3.2.1.1 Cloning strategies

Cloning strategies for site directed mutagenesis or insertion of a gene and genetically encoded polypeptide tag of interest into a specific vector were designed with the software SnapGene from GSL Biotech. All primers used for the specific amplification of a target sequence were purchased from BioTez (Germany). These primers were designed to have a 15 – 18 bp overlap with the target sequence, a GC content of 40 – 60 %, a melting temperature between 50 and 70 °C within a range of 5 °C for primer pairs, 4 additional nucleotides at the 5' end and no tendency to form secondary structures. For insertion of the target sequence into a specific vector, the corresponding restriction enzyme binding site sequence was included flanked by the 4 additional nucleotides at each non-binding end ensuring efficient cleavage. Using these primers, the DNA of interest was amplified by polymerase chain reaction (PCR). The target vector and the PCR product were then digested using the required restriction enzymes, purified, ligated, and finally transformed into chemically competent *E. coli*. To screen for positive clones, colony PCR and subsequently sequencing were performed to exclude frame shifts, additional stop codons and compatible restriction sites.

3.2.1.2 Polymerase chain reaction and site directed mutagenesis

For the exponential amplification of a target DNA sequence, the polymerase chain reaction was developed by Kary Mullis. In a repeated cycle of denaturation of a template DNA, priming of DNA synthesis by annealing of characteristic oligonucleotides and elongation of the DNA strands, the PCR allows an exponential amplification of a specific DNA sequence. Distinct primers that are complementary to the template DNA defined the start and end of the newly synthesized DNA, which subsequently serves as a new template in a following PCR cycle. For PCR the high fidelity (HF) Phusion polymerase (New England Biolabs, NEB) characterized by a high proofreading activity was used. In contrast, PCR based screens to identify positive clones were carried out with the more error prone and hence cheaper DreamTaq Polymerase (Fermentas). Performed with a total volume of 50 µL, PCRs contained 1 x HF Phusion buffer, 25 mM dNTPs, 20 µM of each primer, 50 ng plasmid DNA and 1 Unit Phusion polymerase and were run with the following protocol in a

thermocycler (peqSTAR, Peqlab). Furthermore, colony PCR were subsequently carried out to identify the successful integration of the DNA insert into the desired vector backbone. For this screening, 500 µL of LB media (with the corresponding antibiotic) were inoculated with prior transformed colonies and incubated at 37 °C and 200 rpm for 1 h. Afterwards, 1 µL of media was used as template for the colony PCR. As positive control the original template DNA was added to the PCR mix having a total volume of 50 µL (1 x DreamTaq buffer, 50 µM of each dNTP, 20 µM of each primer, 2 µl of bacteria suspension and 1 Unit of DreamTaq Polymerase). A sample lacking the primers was included as a negative control. Denaturation, annealing, and elongation formed one cycle of the PCR. This cycle was repeated for 25 - 35 times. The annealing temperature was adjusted to the individual melting temperatures of the used primers.

Table 13: PCR cycle program for Phusion and DreamTaq Polymerase

Step	**Phusion polymerase**		**Dream taq polymerase**	
Initial Denaturation	94 °C	4 min	95 °C	5 min
Denaturation	94 °C	40 s	95 °C	30 s
Annealing	50 - 70 °C	40 s	50 - 70 °C	40 s
Elongation	72 °C	15 – 30 s/kbp	72 °C	60 s/kbp
Final elongation	72 °C	10 min	72 °C	5 min
Storage	8 °C	∞	8 °C	∞

For the insertion of a specific mutation into a target DNA sequence, site-directed mutagenesis was performed. Here, two primers were designed with no overlapping sequences. While the reverse primer covered the target DNA sequence, the forward primer carried the mutated nucleotides of interest in addition to 15 – 18 bp of the DNA target sequence. The PCR was directly followed by a DpnI digest to eliminate the template DNA, subsequent phosphorylation of newly synthesized fragments and finally ligation of the phosphorylated PCR product.

3.2.1.3 Analytical agarose gel electrophoresis and DNA isolation

For size separation of DNA fragments, 1 % (w/v) agarose was dissolved in 1 x TAE buffer and supplemented with 100 ng/µl ethidiumbromide (EtBr) (Roth) for DNA detection by UV light. The cast gel was covered with 1 x TAE in a horizontal chamber (Perfect Blue,

PeqLab), DNA samples containing 1 x DNA loading buffer were loaded and separated for 20 min at 120 V.

The gel was placed on a UV table (UVT-28 LV, Herolab), DNA fragments of interest were visualized by UV light, documented with the G-Box gel documenting system (Syngene) and cut out of the agarose gel under minimized UV-exposure. According to manufacturer's instructions, the DNA fragments were gel extracted with the NucleoSpin Gel and PCR cleanup kit from Macherey-Nagel.

3.2.1.4 DNA restriction digest

For integration of the target DNA into an expression vector, DNA restriction digest was carried out. After PCR amplification of the DNA sequence carrying enzyme restriction sites compatible with the expression vector, gel electrophoresis and purification, the PCR product as well as 2 µg of the expression vector were digested with FastDigest restriction enzymes (NEB, 10 Units). 10 x FastDigest Green Buffer (2 µL) was added and the final volume of 20 µL was incubated for 1 – 2 h at 37 °C. Following heat inactivation of the restriction enzymes, the products were purified by agarose gel electrophoresis and DNA isolation (3.2.1.3.).

3.2.1.5 Ligation of DNA fragments into linearized vectors

After the DNA restriction digest, the DNA fragment of interest was integrated into the linearized vector with the T4-DNA ligase. 50 – 100 ng of linearized vector as determined by NanoDrop ND-1000 (Peqlab) were mixed with a two - to four-fold molar excess of the DNA fragment. As negative control, the linearized vector was used without adding the DNA fragment. The ligation reaction was supplied with T4 ligase (5 Units), 4 µL 5 x T4 ligase buffer, at a final total volume of 20 µL, properly mixed and incubated at 22 °C for 2 h. The product was directly used for 3.2.1.6.

3.2.1.6 Transformation of chemically competent *E. coli*

Following a heat shock protocol, 50 µL aliquots of chemically ($CaCl_2$) competent *E.coli* of the TOP10 strain were thawed on ice, up to 1 µg of purified plasmid DNA added and left on ice for 30 minutes. The heat shock was applied by incubation at 42 °C for 50 s followed by a period of 5 minutes on ice. In the case of ampicillin, the bacteria were directly plated on a LB-agar plate supplemented with ampicillin for selection. For all other resistances, prior to plating bacterial cultures were incubated with 500 µL LB without antibiotics at 37 °C for

30 min and 200 rpm. The plates were incubated at 37 °C overnight. For colony PCR, positive clones were picked on the next day and grown in 5 mL LB at 37 °C and 200 rpm overnight.

3.2.1.7 Purification of plasmid DNA from *E. coli* cultures

For DNA Mini-preparations, plasmid DNA was isolated from small scale *E.coli* overnight-cultures using the NucleoSpin®Gel and PCR Clean-up kit from Macherey-Nagel according to the manufacturer's instructions. After alkaline lysis of cells, cell debris, proteins and precipitated genomic DNA were removed by centrifugation. To eliminate contaminants, the plasmid DNA of interest was bound to a silica membrane, subsequently washed, and finally eluted. Plasmid DNA preparations for e.g., plasmid transfection of neuronal cultures, from large scale *E. coli* overnight-cultures were carried out using the NucleoBond® Xtra endotoxin free (EF) plasmid purification kit from Macherey-Nagel. Following the manufacturer's instructions cultures were centrifuged at 4 °C, 4000 g for 30 min and lysed with a NaOH/ SDS containing buffer. Contaminants of the cell lysate were removed via column filters. To eliminate all endotoxins, plasmid DNA was bound to a high binding capacitance silica resin. The plasmid DNA was eluted, precipitated with isopropanol, and reconstituted to 1 µg/ µL with nuclease- and endotoxin-free water.

3.2.1.8 Spectrophotometric determination of DNA concentrations

Due to the specific absorption of nucleic acids of UV light at 260 nm, the resulting extinction at this wavelength can be measured in photometric plastic cuvettes with a photometer (BioPhotometer, Eppendorf). Using the Lambert Beer Law (I), the DNA concentration was determined.

(I) $$c = \frac{E_{260\,nm}}{\mathrm{d} \times \varepsilon_{dsDNA}} \times dilution$$

The photometric plastic cuvettes have a cross section of 1 cm (d). The molar extinction coefficient of double stranded DNA is 50 mL/ µg*cm (ε_{dsDNA}). Further, the dilution of the DNA used in every experiment needs to be considered for the calculation. To control the quality of DNA, the ratio between extinction at 260 nm and at 280 nm must be in the range of 1.8 – 2.1. Higher ratios are indicative of contaminations with larger amounts of proteins with absorption maxima of 280 nm.

3.2.1.9 Sequencing of DNA

Sequencing of the purified plasmid DNA was performed with LGC Genomics, using the chain termination method (Sanger et al., 1977). 4 µL of 5 µM primer dilution and 10 µL 100 ng/µL plasmid DNA of interest were sent to LGC in separate tubes. Sequencing results were analyzed with SnapGene.

3.2.1.10 Storage of bacterial clones

For long-term storage, a small volume of a respective *E.coli* overnight culture was mixed 1:1 with 50 % (v/v) Glycerol stock solution and stored in cryotubes at -80 °C.

3.2.1.11 Isolation and genotyping of genomic DNA from mouse tissue

Genomic DNA was isolated from ear biopsies of adult mice or tail biopsies from newborn pubs (p0 to p3) provided by the animal facility. For fast and reliable genotyping results, the KAPA HotStart Mouse Genotyping Kit (Sigma-Aldrich) was used. According to manufacturer's instructions, the genomic DNA was extracted from the biopsies in a 50 µL lysis-reaction containing 1 Unit of the KAPA Express Extract enzyme and 1 x KAPA Extract buffer at 75 °C for 30 min. Based on a thermostable protease, this enzyme is finally heat inactivated at 90 °C for 5 min and the supernatant used for genotyping PCR.
To genotype the genetically modified genomic DNA from the different mouse strains (listed in 3.1.11), primers (listed in 3.1.5.1., Table 5) were used in a reaction mix containing a 2 x KAPA2G Fast (HotStart) Genotyping Mix including 1.5 mM $MgCl_2$, dNTPs, an engineered DNA polymerase and loading dye.

3.2.2 Cell biological methods

3.2.2.1 Cell culture of HEK 293T and HeLa cells

Human embryonic kidney 293T (HEK293T) and HeLa cells were obtained from ATCC and cultured in Mammalian cell culturing medium at 37 °C and 5 % CO_2. Cells were routinely tested for mycoplasma to exclude any contamination. For passaging every 3 - 5 days, a quick washing step with 1 x PBS was followed by incubation with 0.05 % (v/v) trypsin/ EDTA (Gibco) for 5 min at 37 °C. Trypsin was inactivated by application of Mammalian cell culturing medium, and the cells were then plated 1:3 to 1:10 into new dishes for further use.

3.2.2.2 Transfection of HeLa cells for ICC

For immunocytochemistry (ICC), HeLa cells were seeded on glass coverslips which were coated for 1 h with an extracellular matrix protein solution [5 % (v/v) Matrigel (Corning, 356231) in serum-reduced Opti-MEM^{TM} (Thermo Fisher, 51985-042)] to ensure proper cell attachment. Subsequently, HeLa cells with a confluency of ~ 60 % were transfected with DNA plasmids using JetPrime (VWR, 114-75) according to the manufacturer's instructions. The transfection method is based on cationic polymer-based reagents forming complexes with the negatively charged DNA. Due to excess of the reagent's positive charge these complexes bind to the heparan sulfate proteoglycans on negatively charged plasma membranes of the cell. Upon endocytosis the DNA-consisting complexes are taken up, reside in early endosomes and are subsequently released upon osmotic swelling caused by the high pH-buffering capacity (Boussif et al., 1995; Medina-Kauwe et al., 2005; Sandbichler et al., 2013).

3.2.2.3 Transfection of HEK 293T cells for virus production

For virus production, one day prior to transfection HEK293T cells were seeded at a density of 1 x 10^7 cells/ 15 cm dish (Gibco) in Mammalian cell culturing medium. For introduction of DNA plasmids into HEK cells, calcium phosphate transfection at a confluency of 50 - 60 % was performed on the next day. This method is based on spontaneous precipitation and subsequent endocytic uptake of calcium complexes incorporating the DNA (F. L. Graham & Van Der Eb, 1973) and was used to produce lentiviruses of the 2nd generation of lentiviral packaging. Here, three plasmids, each containing one component of the virus, need to be expressed to enable virus production. The first plasmid is the transfer plasmid carrying the shRNA under a U6-promoter for its transcription by the RNA Polymerase III, a fluorescent tag under a CMV promoter for infection control as well as the psi packaging sequence for recognition to be incorporated into the virus. The second is psPAX2 being the lentiviral packaging plasmid encoding for the viral genes pol, gag, rev, and tat as well as the rev-response element (RRE). The third vector, pMD2.G, represents the envelope plasmid encoding for the G protein of the vesicular stomatitis virus (VSV-G) envelope enabling a wide range of host infectivity. For the transfection, appropriate amounts of DNA (30 µg transfer plasmid, 9 µg psPAX2 and 21 µg pMD2.G) were mixed with 0.24 M $CaCl_2$ and 0.1 x TE, incubated for 5 min and under constant vortexing added dropwise at a ratio of 1:1 to 2 x HBS. After 20 min incubation, the solution was added dropwise to the cells. Finally,

the plates were transferred into a humidified incubator (37 °C and 5 % CO_2). For lentivirus production, 7.45 h post transfection the culturing medium of transfected HEK 293T cells was replaced by fresh medium. At 24 h post transfection, the virus was harvested by carefully removing the supernatant from the cells. The collection media containing regular medium supplemented with 1 x NEAs (non-essential amino acids) and 1 mM sodium pyruvate was given to the cells for further virus production. Virus harvesting was repeated 36 h and 48 h post transfection when virus production reached its limit. After discarding the cells, the supernatants were pooled and filtered with a 0.45 µm filter to remove cell debris. The virus was concentrated by centrifugation in an Amicon Ultra-15 100 kDa filter column to a final volume of 500 µL at 5000 g at 4 °C for 20 min. The virus could then be directly used for primary hippocampal neuron transduction or stored at -80 °C for later use. Transduction was carried out by addition of 2 - 4 µL of virus depending on the density of plated neurons and the desired transduction rate.

3.2.2.4 Preparation of primary hippocampal neurons

Neuronal hippocampal cell cultures were prepared by surgical isolation of both hippocampi from postnatal mice at p1 - 3 (for WT, Stn2, SV2A/B) or p0 (for Syt1) pooled from one to two genotypically identical littermates. The hippocampi were rapidly dissected under a binocular microscope and placed into ice-cold Hanks' balanced salt solution (HBSS; Thermo Fisher Scientific) containing 10 % FBS, followed by further dissection into ~1 mm^3 sized parts and four brief washes with 5 mL HBSS with and without 10 % FBS. To dissociate individual neurons, first trypsin digestion was performed by application of 2.5 mL Digestion solution supplemented with 5 mg/ mL trypsin, 750 U DNase (sterile filtered through a 0.22 µm pore filter) and incubation for 15 min at 37 °C. Four brief HBSS washes with each 5 mL with and without 10 % FBS were used to stop the digest. Finally, the tissue suspension was incubated with 2 mL Dissociation solution containing 750 U DNase (sterile filtered through a 0.22 µm pore filter) and the tissue was dissociated using a siliconized Pasteur pipette with a small opening. Dissociation was carried out by uptake and release until the solution was fully homogeneous. Before centrifugation at 400 g at 4 °C for 8 min, 2 mL HBSS containing 10 % FBS was added, and the cells were finally counted with a Neubauer chamber. 100,000 cells resuspended in plating medium were plated as 40 µL drops per 6-well poly-L-lysine coated 25 mm glass coverslip (18 mm for 12-well). Preparation of glass coverslips included cleaning with 1 M HCl for 24 h, acetone treatment overnight, a 24 h 70 % (v/v) ethanol wash and coating with 200 µL 15 µg/ mL poly-L-lysine and final

drying. 1 h after plating the cells, 2 mL plating medium for hippocampal neurons were added. At one day in vitro (DIV1) 1 mL of plating medium was exchanged with 1 mL of Growth medium for hippocampal neurons and on DIV2 1 mL of growth medium was added including 2 µM cytosine β-D-arabinofuranoside (AraC) to limit glial proliferation. In case of other drugs, information, and treatment (concentration and duration) is indicated in the corresponding method section. Cultures were grown at 37 °C and 5 % CO_2 in humidified incubators. For 12-wells, half of all volumes were taken. Lentiviral transduction for gene deletion or transient overexpression was performed at DIV2 with virus produced in HEK293T cells (ATCC) by calcium phosphate co-transfection of the individual lentiviral expression vector and its packaging plasmids, harvested after 48 h and concentrated via low-speed centrifugation. Additional transient protein expression was performed at DIV7 - 9 via calcium phosphate transfection. Hippocampal neurons were used at DIV13-16 for live-imaging, immunocytochemistry, confocal, superresolution and electron microscopy to ensure mature synapses.

3.2.2.5 Calcium phosphate transfection of primary hippocampal neurons

Primary hippocampal neuron cultures were transfected at DIV7 - 9 using a Calcium phosphate transfection kit (Promega). This kit is based on the spontaneous complex formation of calcium, phosphate, and DNA, followed by precipitation and endocytic uptake of complexes by starved cells which was induced by incubation with osmolarity adjusted Neurobasal-A medium (NBA, Gibco, Life technologies). Following the manufacturer's instructions, 6 µg plasmid DNA, nuclease-free water, and 250 mM $CaCl_2$ were mixed to a final volume of 100 µL and under constant vortexing given to an equal volume of 2 x 4-(2-hydroxyethyl)-1-piperazineethanesulfonic acid (HEPES) buffered saline. 20 min incubation was sufficient for formation of precipitates. During this time, neurons were starved at 37 °C and 5 % CO_2 in NBA that was osmolarity-adjusted with D-(+)-Mannitol prior to application. After incubation, the solution containing the precipitates was applied to the coverslips for 30 min at 37 °C and 5 % CO_2 to allow uptake of precipitates. The coverslips were washed with 2 mL osmolarity-adjusted HBSS (-Mg^{2+}/ Ca^{2+}) and finally transferred back into the original medium.

3.2.2.6 Stimulation of primary hippocampal neuron cultures

For the detection of activity-dependent changes in the generation of membrane lipids or in protein localization patterns, neuronal cultures were either electrically or chemically

stimulated on DIV14 to 15. Electrical stimulation occurred with field stimulation applying 200 action potentials (APs) at 40 Hz for 5 s. Chemically, neurons were depolarized with 80 mM potassium chloride in imaging buffer lacking NaCl for 1 min at RT. For control and hence steady-state levels, incubation occurred in absence of potassium chloride. Immediately after 1 min, the medium was aspirated, and neurons were fixed for immunocytochemistry.

3.2.2.7 Immunocytochemistry

For labeling and visualization of specific proteins, neurons were fixed on DIV13-15 with 4 % paraformaldehyde (PFA) / 4 % sucrose in phosphate buffered saline (PBS, pH 7.5) for 15 min at RT. Each coverslip was washed three times with PBS, blocked and permeabilized with 10 % NGS and 0.1 % TritonX-100 in 1 x PBS at RT and constant 200 rpm for 30 min. After blocking to avoid unspecific antibody binding, each coverslip was incubated with primary antibodies in PBS, 10 % normal goat serum (NGS) and 0.3 % Triton X-100 (Tx). For that, each coverslip was placed upside down on a 50 µL drop located on a piece of parafilm inside a dark and humid chamber and incubated for 2 h at RT. Before and after incubation with the corresponding secondary antibodies for 45 min, each coverslip was washed three times with PBS and finally mounted on glass slides in Immumount (Thermo Fisher Scientific) for confocal microscopy or in Prolong Gold Antifade (Invitrogen) for STED microscopy.

For nanobody live cell uptake at DIV14, the corresponding coverslip was incubated in 200 µL conditioned medium diluted 1:200 with GFP-tagged nanobody against Syt1 for 30 min at 37 °C and 5 % CO_2. After incubation, the coverslip was transferred into the original medium for 15 min and for labeling, neurons were three-times washed with 1x PBS and staining performed as described above.

For lipid staining, stimulation was performed with either using 80 mM KCl applied for 1 min or 200 APs at 40 Hz, followed by fixation with 2 % PFA/ 2 % sucrose/ 1 % glutaraldehyde in 1 x PBS for 20 min at RT and three washes with PBS containing 50 mM NH_4Cl to additionally quench free aldehyde groups. This was followed by permeabilization with 0.5 % Saponin/ 1 % BSA in 1 x PBS for 30 min at RT after which each coverslip was incubated with the indicated antibodies or purified probe diluted in 1 % BSA/ 10 % NGS in 1 x PBS. For detecting $PI(4,5)P_2$, an alternative and hence direct comparison to antibody labeling was carried out. The eGFP-labeled PH domain of PLCδ1 (PH-PLCδ1-eGFP) or its binding-deficient mutant used for negative control was added at a concentration of 0.25 µg/mL during permeabilization and additionally applied in 1 % BSA

in 1 x PBS for another 30 min. These coverslips were then stained with primary antibody to further enhance the GFP signal. Prior to mounting, each coverslip was again thoroughly washed with 1 x PBS and incubated with the corresponding secondary antibody for 45 min.
For live cell imaging of endogenous vGAT, each coverslip was incubated with CypHer5E-conjugated antibodies directed against the luminal domain of vGAT (1:200 from 1 mg/ mL stock) for 1 h at 37 °C and 5 % CO_2 in the conditioned culture medium and washed with conditioned imaging buffer before imaging.

3.2.3 Microscopy and quantitative image analysis

3.2.3.1 Fluorescence microscopy

To detect and localize fluorescently labeled biomolecules such as proteins, DNA, and membrane lipids in fixed as well as in living cells, fluorescence microscopy was used. The fluorescent labeling of proteins was either achieved via genetically encoded protein-tags that allow detection both in fixed and in living cells, or via antibodies directed against specific epitopes of a target protein which are coupled with fluorescent dyes.
For detection and localization, light of a specific wavelength excites electrons of the labelling fluorophore to a higher energy state. Immediate relaxation to the ground state results in emission of light with a longer wavelength. Using dichroic mirrors and spectral emission filters, excitation and emission wavelengths can be separated and detected. In addition, multi-color images detecting differently labeled fluorescent molecules is possible if each fluorophore is characterized by a unique excitation- and emission-wavelength profile. For quantitative analysis of different conditions within independent experiments, microscopic settings were kept constant. Analysis was performed with ImageJ, Excel, and Prism (Graphpad).

3.2.3.2 Live-cell imaging

In epifluorescence microscopy as a form of widefield microscopy the whole sample is illuminated to allow for fast acquisition in live cells.
To study the exo- and endocytic cycle of SVs, pHlourin fused to the luminal domain of an SV protein was used. As a variant of the green fluorescent protein (GFP), pHluorin is genetically modified to reach a higher pH sensitivity (pKa = 7.1). At low pH it is found in a protonated state that results in a quenched fluorescence while at neutral pH it can efficiently be excited with a wavelength of 488 nm (Miesenböck et al., 1998). In neurons, pHluorin-

tagged SV proteins residing on SVs are present in an acidic environment (pH ~ 5.5) and hence are quenched. Upon depolarization, SVs fuse with the plasma membrane leading to exposure of the luminal pHluorin-tag to the extracellular, neutral environment (pH ~ 7.4). This shift in pH unquenches the fluorophore and leads to an increase in fluorescence intensity. Following endocytosis of SV proteins tagged with pHluorin, SVs are re-acidified resulting in a protonated, quenched state of pHluorin (Sankaranarayanan et al., 2000). Following transfection of cultured primary hippocampal neurons with a pHluorin construct (described in 3.2.2.4) on DIV13-15, neurons were imaged in an equilibrated and osmolarity-adjusted physiological imaging buffer. Each coverslip was placed in a stimulation chamber attached with two lateral electrodes (RC-47FSLP, Warner instruments). For electrical field stimulations with 200 APs at 100 mA, 40 Hz and 5 s the chamber was connected to the stimulator (MultiStim SYSTEM-D330, Harvard Apparatus). Image acquisition was performed with the Nikon Eclipse Ti microscope under the control of the MicroManager 4.11 and supplied with an eGFP filter set (F36-526) and TRITC filter set (F36-503), a 40 x oil-immersion objective with 1.3 numerical aperture (NA) and a sCMOS camera (Neo, Andor) attached to a 200 Watt mercury lamp (Lumen 200, Prior Scientific). An incubator (Okolab) around the microscope ensured physiological conditions if required and the PerfectFocus Autofocus system from Nikon further supports stable imaging. The neutral density filter 4 and 50 ms exposure were applied to avoid bleaching of fluorophores during acquisition time. To exclude postsynaptic responses upon stimulation, NMDA and AMPA receptors were inhibited by APV (50 μM) and CNQX (10 μM).

For identification of stimulation-induced responding synapses, 20 boutons were chosen as regions of interest (ROI) and each fluorescence intensity trace (F) was analyzed using custom-written macros (https://github.com/DennisVoll/pHluorin_ROI_selector/) or alternatively analyzed via automated analysis (Schmied et al., 2021). Responding boutons were corrected for photobleaching if needed. To eliminate biological variation in intensities, the fluorescence intensities of each trace derived from one image were background-corrected and a mean of all traces of one condition was computed (F). To calculate the apparent release of SVs, the mean fluorescent intensities (F) were normalized to the initial fluorescence (F_0) prior to stimulation. Further normalizing the fluorescent intensity changes over time by subtraction of F_0 from the maximum peak fluorescence revealed the endocytic retrieval ($\Delta F/F$). A monoexponential decay fit for the $\Delta F/ F$ curves generated by Prism (Graphpad) software yielded the endocytic time constant τ. The monoexponential fit of the decay curve is given by:

(I) $$I(t) = y_0 + A * e^{\frac{-t}{\tau}}$$

I(t) reflects the fluorescence intensity at time t and y_0 depicts the intensity plateau at t_{max}. A is the initial intensity measured at I(0) subtracted by y_0. With these parameters τ, the endocytic decay time constant, can be calculated.

To exclude variabilities in expression levels or increased surface retention of pHluorin-tagged SV proteins caused by defective endocytosis or reacidification defects of the synaptic vesicle, ammonium or acid quench assays were carried out. This was done by either applying ammonium buffer (50 mM NaCl replaced by NH_4Cl) at the end of each trace to unquench the total pool of pHluorin and thereby, calculate the surface-to-total ratio. To exclude for potential reacidification defects, local perfusion with acidic buffer [2-(N-morpholino) ethane-sulfonic acid replaced TES, adjusted to pH 5.5] quenching pHluorins located on the plasma membrane for 20 s before and after electrical stimulation using the perfusion Fast-Step System were performed. In both tests neurons responded to electrical stimuli which ensured neuronal health.

To further control for potential overexpression artefacts and study endocytosis of endogenous SV proteins, cypHer-based antibody uptake assays were performed with the same settings as pHluorin based assays at physiological conditions. However, having opposite characteristics to pHlourin, CypHer fused to an antibody detecting SV proteins is quenched upon exposure to a neutral environment and unquenched in acidic conditions such as after endocytosis of the antibody detected SV protein.

To artificially increase levels of $PI(4,5)P_2$, TF-$PI(4,5)P_2$/AM was used. This probe is cell permeable and photo activatable at 405 nm which leads to release of the coumarin cage and allows uptake of the cell-permeable form of the acetoxy methyl ester (AM)-protected phosphatidylinositol derivate. Endogenous lipases and esterases remove the AM protection group so that the biologically active lipids integrate into membranes (Subramanian et al., 2010). Neurons were incubated with/ without 20 µM TF-$PI(4,5)P_2$/AM (dissolved in 50 mM DMSO and 10 % pluronic F127) for 20 min before imaging as described in 3.1.8.. One image acquisition cycle was monitored before activation of the probe. Before the second image acquisition with 488 nm, neurons were exposed to one uncaging frame at 405 nm (200 ms exposure) for photo activation of $PI(4,5)P_2$.

3.2.3.3 Confocal microscopy

While widefield microscopy allows for fast acquisition, confocal microscopy provides much better z-resolution and hence yields a more precise localization of fluorescently labeled molecules. This is due to reduced out-of-focus light through implementation of a pinhole to the light-path. The shorter acquisition time furthermore reduces the possibility of photobleaching of fluorophores. Imaging of fixed samples was performed on a Zeiss laser scanning confocal microscope (LSM710) with the Digital microscope camera AxioCam (Zeiss), controlled by the Imaging-Software ZEN (Zeiss) with a scanning format of 1,024 x 1,024 pixels using a 63 x oil-immersion objective with 1.3 NA equipped with an Argon laser at 488 nm, a DPSS laser at 561 nm and a Helium Neon laser at 633 nm for excitation. Images were acquired with equal acquisition settings within each immunostaining. Quantitative and qualitative image analyses were carried out with ImageJ. Co-staining of control synaptic proteins was used to create non-biased region of interest (ROI) selection masks. The presynaptic masks were obtained by applying median filter, background subtraction with a sliding paraboloid and auto-thresholding and the resulting mask was used to measure the mean fluorescence intensity of the protein of interest or a lipid. Finally, background subtraction or for quantifications, normalization of fluorescent intensities were performed to enable comparison of independent experiments.

3.2.3.4 TIRF microscopy

Total internal reflection fluorescence (TIRF) microscopy is used to exclusively illuminate fluorophores near the cell surface, its plasma membrane. With a laser beam set to a variable angle in the TIRF objective the specimen is illuminated. For total internal reflection, this angle is set to a critical degree resulting in laser beam reflection at the interface of the two media (glass-coverslip and aqueous specimen medium). The resulting evanescent field decays exponentially to vertical distance. Depending on wavelength, entrance angle, and refraction indices of the laser beam, 60 – 100 nm from the phase boundary, here the plasma membrane, can be excited (Axelrod, 2001). TIRF microscopy was performed with a Nikon Eclipse Ti microscope operated by open-source ImageJ-based micromanager software and equipped with 60 x TIRF objective (oil-immersion, Nikon), sCMOS camera (Neo, Andor), 200-Watt mercury lamp (Lumen 200, Prior), a triple-color TIRF setup (laser lines: 488 nm, 568 nm, 647 nm) and an incubation chamber (37 °C).

3.2.3.5 Stimulated emission depletion (STED) microscopy and analysis

To improve resolution even further, time-gated stimulated emission depletion (gSTED) super-resolution microscopy was performed which is based on confocal laser scanning microscopy but overcomes the diffraction limit. This is achieved through a combination of excitation and depletion with a doughnut-shaped, red-shifted depletion laser. The resulting detected fluorescence is based on a point-spread function and is hence much more precise. Imaging of all fixed samples stained with the STED corresponding antibodies was performed on a Leica SP8 TCS 3xSTED microscope (Leica Microsystems) equipped with two STED lasers for depletion at wavelengths of 592 nm and 775 nm and a pulsed white-light excitation laser at ~80 ps pulse width and 80 MHz repetition rate (WLL, NKT Photonics) triggered the pulsed 775 nm STED laser. Three-color STED imaging was performed by sequentially exciting ATTO 647N at 646 nm, Alexa Fluor 594 at 598 nm and Alexa Fluor 488 at 488 nm while emission of Alexa Fluor 488 was depleted with the 592 nm laser and emission of ATTO 647N and Alexa Fluor 594 were depleted by the 775 nm laser. Fluorescence signals were detected sequentially at appropriate spectral regions distinct from STED lasers by hybrid detectors within 0.3 – 6 ns after the excitation laser pulse and images were taken with an HC PL APO CS2 100×/ 1.40 NA oil objective (Leica Microsystems), a scanning format of 1024 × 1024 pixels, 8-bit sampling and six-fold zoom acquiring three z-stacks resulting in voxel dimensions of 18.9 nm^2. Synapses characterized by a clear apposition of pre- and postsynaptic staining oriented parallel to the focal plane were chosen for analysis and the intensities of the acquired z-stacks with a total distance of 500 nm were summed. Each synapse was processed with multicolor line profiles perpendicular to the co-clusters (1 µm length, 400 nm width) using the ImageJ Macro from Kees Straatman (Marco_plot_lineprofile_multicolor, University of Leicester, UK) to determine localization patterns of proteins of interest. The resulting profiles were aligned with the bassoon maximum allowing for quantification of mean fluorescence of proteins of interest within the presynaptic region. The presynaptic region was characterized by a Bassoon profile that was clearly distinguishable from the profile of Homer1 labelling the postsynapse.

3.2.3.6 Electron microscopy

In collaboration with Dr. Dmytro Puchkov from the EM facility at Leibniz Research Institute for Molecular Pharmacology (FMP, Berlin) electron microscopy was performed. Instead of light as a source of illumination, electron microscopes use a beam of accelerated electrons.

This results in much higher resolution because electrons have much short wavelengths as photons. Thus, ultrastructural changes within i.e., the synapse, can be detected.

Hippocampal Syt1 WT and KO neurons were grown on 3 mm sapphire disks with an orientational "L" landmark at 80 nm carbon layer. At DIV14, sapphire disks were transferred one by one into imaging buffer supplemented with 15 % Ficol. After 10 min equilibration, the disks were transferred into the stimulation chamber, the timer was started and a 40 Hz, 200 AP stimulus was applied to the neurons. After stimulation, the disks were retrieved and assembled for high pressure freezing in an HMP100 instrument. If assembly lasted longer than 70 s following stimulation, the disk was discarded. Freeze substitution was performed in 1 % osmium tetroxide, 0.125 % glutaraldehyde and 0.5 % water with the following settings: 12 h at –90 °C, 17 h from -90 to –20 °C, 12 h at –20 °C, 2.5 h –20 °C to +4 °C. After a wash in acetone, neurons were incubated for 1 h in 0.1 % uranyl acetate diluted in acetone and infiltrated with epoxy resin. Following polymerization, the disks were removed, and ultrathin sections were viewed in a Zeiss 900 transmission electron microscope for subsequent morphometrical analysis of synapses.

3.2.4 Biochemical methods

3.2.4.1 Preparation of mouse brain extracts

For quantitative protein analysis, whole mouse brains of 12-days-old animals were homogenized in brain homogenization buffer supplemented with 1 mM PMSF and mammalian protease inhibitor mixture (Sigma) with a glass teflon homogenizer at 900 rpm. Large debris was removed at 900 g for 5 min and the whole brain extract finally obtained after centrifugation at 265,000 g for 15 min at 4 °C. The protein concentration was determined using the Bradford assay.

3.2.4.2 Expression of recombinant proteins in *E.coli*

E.coli BL21 bacteria transformed with pGEX4T-1 plasmids carrying the glutathione S-transferase (GST)-fusion protein of interest were grown in a 100 mL culture with the respective antibiotic at 37 °C overnight. This small-scale culture was added at a ratio of 1:10 to 500 mL 2 x yeast extract tryptone (2x YT)-medium supplemented with the respective antibiotic. The culture was grown at 30 °C at 180 rpm. Protein expression was induced with 1 mM isopropyl β-D-1-thiogalactopyranoside (IPTG) at OD_{600} 0.4 - 0.7 followed by

incubation at 20 °C and 180 rpm for 5 h. Cells were harvested with 4000 g for 20 min at 4 °C and the resulting cell pellet was resuspended in 30 mL ice-cold PBS, aliquoted and stored at -20 °C.

3.2.4.3 Expression of His_{10}-fusion proteins

His_{10}-tagged PIPKIγ was expressed in *Sf21* insect cells grown in SF900-II serum-free media (Thermo Fisher Scientific) until reaching a density of 1.5 – 2 x 10^6 cells/ mL. The culture was infected with 8 mL baculovirus which had been amplified and encoded for PIPKIγ. Collection occurred at a viability below 90 % and the cell pellets from 200 mL of culture were stored at –20 °C.

3.2.4.4 Protein quantification using Bradford assay

Protein concentrations were measured using the Bradford assay. This measurement is based on the interaction of Coomassie G-250 with proteins leading to an absorbance shift from a stable protonated form at 465 nm to a stable unprotonated form at 610 nm. The shift can be monitored at 595 nm (Bradford, 1976). For sample preparation, 500 µL millipore-filtered water was mixed with 500 µL 2 x Bradford reagent and 1 µL purified proteins or tissue extract (further diluted if needed) were added. As control, 1 µL of lysis buffer was used. Triplicates of each sample were incubated for 5 min at RT. Finally, the control was used for baseline correction and then the absorbances of each sample was measured using a photometer (BioPhotometer Plus, Eppendorf). Absorbance values in the range of 0.1 – 0.5 were considered reliable. Using a BSA standard curve with concentrations from 1 to 10 µg the measured protein concentrations were calculated.

3.2.4.5 Affinity-purification of GST- and His_{10}-fusion proteins

All GST or GST-fusion protein pellets from 3.2.4.2. were purified with the glutathione-sepharose assay. This assay is based on the specific enzyme-substrate binding reaction of GST-fusion proteins with the tripeptide Glutathione (Glutamine-Cysteine-Glycine) which is immobilized to cross-linked agarose beads using a sulfhydryl group.

For purification, the bacterial pellets were thawed in 35 mL 1 x PBS supplemented with 1 mM phenylmethylsulfonyl fluoride (PMSF), 125 U benzonase (DNase) and 1 mg/ mL lysozyme for degradation of bacterial cell walls and for removing nucleic acids. The solution was incubated for 25 min under constant rotation at 4 °C. To mechanically disrupt remaining cell walls, the solution was sonicated [1 min at 70 % power and at 4 °C, Sonoplus

(Bandelin)]. 1 % (v/v) TritonX-100 was added, and the solution incubated under constant rotation at 4 °C for 15 min. All cell debris was sedimented at 35,000 g for 20 min and the supernatant incubated under constant rotation at 4 C for 2 h with 0.5 mL GST-binding resin (Novagen) that had been washed once with 1 x PBS. Three washes with 1 x ice cold PBS at 1000 g for 2 min under reduced deceleration removed all unbound material. Finally, the beads with the bound GST-fusion proteins were resuspended in 1 mL 1 x PBS.

For purification of PIPKIγ, cell pellets from 200 mL of culture were resuspended in 30 mL of lysis buffer II, sonicated for 30 s (1 s pulse on, 5 s pulse off) and finally centrifuged at 75,000 g for 20 min at 4 °C. For purification of His-tagged proteins, Histidin binding to Ni^{2+} which itself is localized to beads via the nitrilotriacetic acid (NTA)-chelator is exploited. 40 µL Nickel NTA beads (Sigma-Aldrich) were incubated with 15 mL supernatant under constant rotation for 1 h at 4 °C and collected by centrifugation at 1000 g for 2 min. The combined pellets were washed three times with washing buffer and collected by centrifugation under reduced deceleration at 1000 g for 2 min. Elution occurred with 200 µL elution buffer.

For all purified proteins, the protein concentration was measured using the Bradford assay.

3.2.4.6 GST-pulldown from rat brain extract

For GST-mediated pulldown, GST as control (30 µg) or GST-fusion protein (30 µg) was incubated with 4 mg of whole brain extract overnight under constant rotation at 4 °C. Samples were washed three times using lysis buffer I to remove non-specifically bound protein. The last wash did not contain TritonX-100. Bound proteins were eluted by boiling with 1 × SDS sample buffer, resolved by SDS-PAGE, and analyzed by immunoblotting using corresponding antibodies.

3.2.4.7 In vitro binding assays

All GST or GST-fusion proteins (expressed, purified, and coupled to Glutathione Sepharose beads as indicated previously) were incubated at equal amounts (50 µg) with 10 µg of His_{10}-fusion protein in 500 µL binding buffer under constant rotation for 2 h at 4 °C. For Ca^{2+} dependency studies, 30 µg GST-fusion proteins were used in presence of 200 µM $CaCl_2$ or 5 mM EGTA. All samples were washed three times with binding buffer and eluted in 1 × SDS sample buffer. Samples were analyzed by SDS-PAGE and immunoblotting using His-tag specific antibody.

3.2.4.8 SDS polyacrylamide gel electrophoresis (SDS-PAGE)

Sodium dodecylsulfate polyacrylamide gel electrophoresis (SDS-PAGE) was performed to separate proteins according to molecular weight (Laemmli, 1970). For that, secondary and tertiary structures were denatured by application of SDS sample buffer supplemented with ß-mercaptoethanol which reduces disulfide bonds and heat. The anionic detergent SDS further disrupts non-covalent protein interactions. In addition, unfolded polypeptide-chains are decorated with negatively charged SDS according to their molecular mass leading to a constant, characteristic mass to charge ratio. This individual charge can be used for separation in an electrical field. The discontinuous SDS-PAGE consists of a stacking and a separating gel matrix. The stacking part is characterized by wide pores and low pH of 6.8. The pH-dependent charge of glycine at the pH of 6.8 leads to its separation from faster migrating chloride ions and results in protein accumulation. Upon further current, the proteins enter the separating gel matrix defined by a pH of 8.8. At this pH, all glycine ions are recharged which results in faster migration that is defined by the proteins' individual mass to charge ratio. The running behavior can be influenced by pore size. This is based on the concentration of acrylamide which polymerizes and crosslinks with N, N'-methylenebisacrylamide due to free radicals generated by ammonium peroxodisulfate (APS) and N,N,N',N'-tetramethylethylenediamine (TEMED). SDS-PAGEs were run at a constant current of 10 – 20 mA.

Table 14: Preparation of SDS-PAGE gels

Components	**Separation gel**			**Stacking gel**
	12 %	**10 %**	**8**%	**3 %**
30 % AA/ BA mix	3 mL	2.5 mL	2 mL	0.33 mL
Millipore-filtered water	2.5 mL	3 mL	3.5 mL	1.625 mL
4x stacking or separation buffer	1.875 mL	1.875 mL	1.875 mL	0.625 mL
10 % (w/v) APS	75 µL	75 µL	75 µL	37.5 µL
TEMED	7.5 µL	7.5 µL	7.5 µL	3.75 µL

3.2.4.9 Coomassie staining of SDS-polyacrylamide gels

For visualization of proteins separated with SDS-PAGE, the gels were shortly stained with coomassie stain at 60 °C followed by an incubation for 20 min at RT. Subsequently,

unspecific background staining was removed with several washes using coomassie destain at 60 °C and incubation overnight at RT.

3.2.4.10 Immunoblotting

Detection of proteins that had been separated by SDS-PAGE was performed with immunoblotting. First, proteins that are covered with SDS and thereby carry a negative charge can quantitatively be transferred from the SDS-PAGE onto a nitrocellulose membrane (GE Healthcare, Amersham Protran 0.2. NC) by application of an electrical field. For that, stacks consisting of sponge, blotting paper, nitrocellulose membrane, gel, blotting paper, and another sponge were soaked with blotting buffer. The transfer was performed in a tank blotting chamber (BIO-RAD) at 110 V for 65 min at 4 °C. To control for comparable sample loading and quantitative transfer, proteins were reversibly visualized with Ponceau S staining for 10 min at RT followed by Ponceau S destain to remove unspecific staining. Using PBS, all Ponceau S staining was removed again, and the membrane was blocked with antibody blocking solution for 1 h at RT. Primary antibodies were diluted with antibody dilution solution and incubated overnight at 4 °C. Unbound antibody was removed by four washes in 0.05 % (v/v) Tween-20 in 1 x PBS. The membrane was incubated with the corresponding secondary antibodies conjugated with HRP and diluted with antibody dilution solution for 1h at RT and washed with 1 x PBS. Final quantitative detection was performed using chemiluminescence reagent (ECL, Amersham Biosciences). In this reaction, HRP converts luminol was part of the reagent to an oxidized, chemiluminescent form. The resulting chemiluminescence is then detected by the BIO-RAD ChemiDoc™-System run with Image Lab software (Bio-Rad).

3.2.5 Statistical analysis

All data are presented as mean ± standard error of the mean (SEM) and obtained from ≥ 3 independent experiments (e.g., independent animals or mouse cultures with identical genetic background) with > 5 individual neurons with > 20 analyzed boutons/ neuron unless otherwise stated. Normal distribution was tested using D'Agostino-Pearson or, Shapiro-Wilk test, which determined the use of parametric or non-parametric statistical tests. The statistical significance of experiments comparing two experimental groups drawn from independent experiments (N) or drawn from individual cultures (n) with normally distributed data was evaluated using a two-tailed unpaired Student's t-test. For non-normally distributed

unpaired data, two-tailed Mann-Whitney test was performed. Multiple one sample t-tests were carried out and corrected for multiple testing with false discovery rate (FDR) as indicated by grey asterisks if the significance was still met after correction for multiple testing. Comparing more than two experimental groups with normally distributed data, the statistical significance was obtained by a One-Way ANOVA, followed by a Tukey's (to compare the mean of each column with every other column) or Šidák's (to compare selected pairs of means) post hoc test in GraphPad (Prism). For more than two non-normally distributed datasets, Kruskal-Wallis test followed by two-sided Dunn's multiple comparison test was performed. The corresponding statistical tests are stated in the figure legends. Asterisks indicate significances as the following: * = $p < 0.05$, ** = $P < 0.01$, *** = < 0.001, **** = $p < 0.0001$ while $p > 0.05$ being not significant (ns) is not further stated.

4 Results

Neurotransmission relies on the action potential induced exocytosis of neurotransmitter containing synaptic vesicles (SV). This process is tightly controlled in time and space and allows propagation of the signal in postsynaptic neurons (Heuser & Reese, 1973; Katz & Miledi, 1967). To sustain this mechanism, SV proteins and lipids need to be retrieved in a timely, precise fashion via compensatory endocytosis matching the amount of newly exocytosed SV material (Dittman & Ryan, 2009; Soykan et al., 2016). This functional and physical link to couple SV exocytosis and endocytosis requires a strict regulation because changes in membrane composition and tension as well as the availability of proteins to reform SVs influence the speed of the SV cycle and defects would lead to synapse dysfunction. Evidence from optical recordings, electrophysiological capacitance measurements and electron microscopy assign important coupling functions to the membrane lipid $PI(4,5)P_2$ as well as to surface stranded SV proteins (Haucke et al., 2011; Hosoi et al., 2009; Koch & Holt, 2012; Maritzen & Haucke, 2017; L. G. Wu et al., 2014) (Fig. 3,4). Despite all efforts, the fundamental question of how exocytosis and endocytosis are balanced for maintaining membrane homeostasis remains unsolved. A qualitative and at the same time quantitative intrinsic surrogate measure would allow such precise coupling mechanism and therefore was the primary focus of this work.

4.1 Acceleration of SV endocytosis by exocytosed Synaptotagmin 1

Among all synaptic key players, Synaptotagmin1 (Syt1) as the main calcium sensor (Geppert et al., 1994) has been found indispensable for both, exocytosis (Mutch et al., 2011) and endocytosis (Jorgensen et al., 1995; Littleton et al., 2001; Poskanzer et al., 2003). Being crucial for synchronous release in hippocampal neurons (Chapman, 2008; Geppert et al., 1994; Zhou et al., 2015, 2017), loss of its Ca^{2+} binding ability leads to exo- and endocytic defects (Poskanzer et al., 2003; J. Yao et al., 2012; L. H. Yao et al., 2012). During SV recycling, Syt1 is sorted via its endocytic adaptors, Stonin2 (Stn2) (Diril et al., 2006; Jung et al., 2007) and Synaptic Vesicle Protein 2 (SV2) (J. Yao et al., 2010). Surprisingly, missorting of Syt1 leading to accumulation on the plasma membrane does not result in impairment but in fact facilitation of the SV cycle (Kaempf et al., 2015; Kononenko et al., 2013). In this context, Syt1 is proposed to have functions in major potential coupling pathways including surface protein stranding which in turn influences the rate of retrieval of

synaptic vesicle proteins. Therefore, this study aimed to unravel Syt1's molecular function in coupling exocytic fusion with compensatory endocytic retrieval in hippocampal neurons to understand the fundamental question of how neurons qualitatively and quantitatively control the amount of synaptic vesicle retrieval.

4.1.1 Synaptotagmin 1 loss leads to impaired SV kinetics associated with fundamental changes in synapse ultrastructure.

4.1.1.1 Synaptotagmin 1 loss of function leads to SV recycling defects.

To address Syt1's function in the SV cycle, we made use of hippocampal neuronal cultures derived from Syt1 KO mice (Fig. 8a) (B6;129S-Syt1^{tm1Sud}, RRID: IMSR_JAX:002478) (Geppert et al., 1994) and studied the kinetics of SVs by monitoring overexpressed vesicular glutamate transporter 1 (vGLUT1) fused to a pH-sensitive GFP variant (pHluorin).

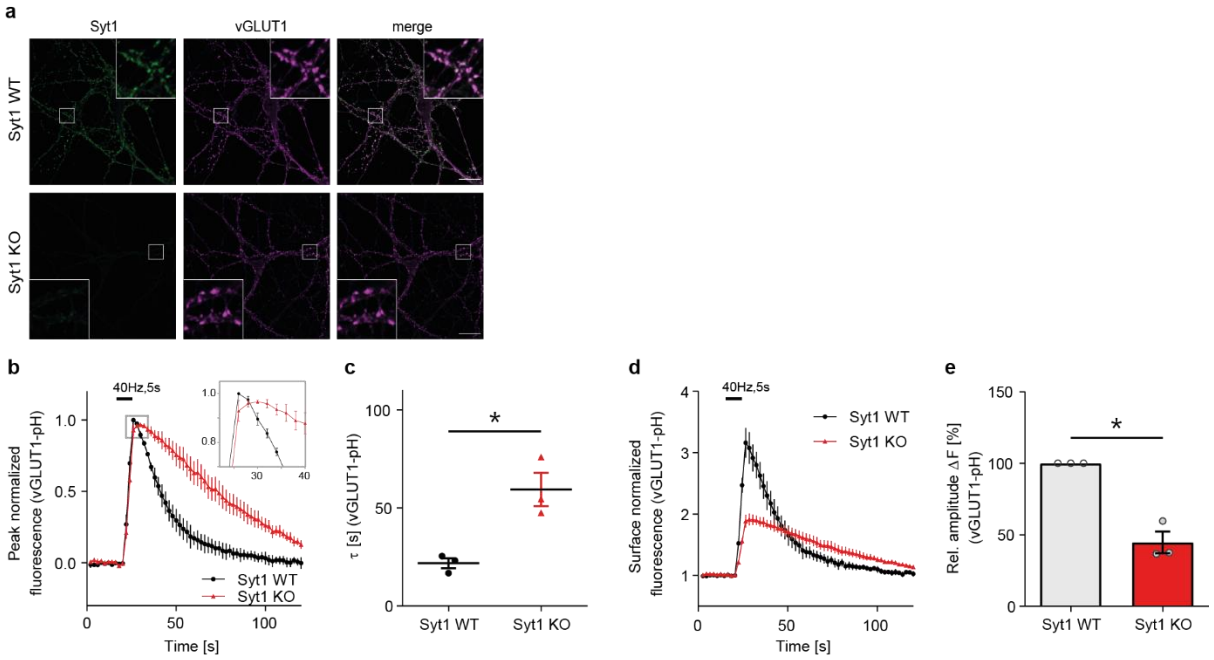

Figure 8: Syt1 loss leads to delayed vGLUT1-pH endocytosis and impaired exocytosis.
(a) Representative confocal images of Syt1 WT/KO hippocampal neurons (DIV15) stained for Syt1 and for vGLUT1; Scale bar: 20 µm. **(b)** Average normalized vGLUT1-pH fluorescence traces of hippocampal neurons from wild-type (WT) or Syt1 knockout (KO) mice stimulated with 200 APs at 40 Hz. vGLUT1-pH release is asynchronous (zoom, top right) and endocytosis is slowed in Syt1 KO neurons. Data represent mean ± SEM from N = 3 independent experiments with > 300 analyzed boutons per condition. **(c)** Endocytic decay time constants (τ) of data shown in (b) reveal defects in neurons from Syt1 KO mice. τ_{WT} = 22 ± 2 s, τ_{Syt1KO} = 59 ± 9 s; unpaired two-tailed t-test. **(d)** Average normalized vGLUT1-pH fluorescence traces of hippocampal neurons from WT or Syt1 KO mice stimulated with 200 APs at 40 Hz. Exocytic events of vGLUT1-pH depicted by the fluorescence amplitude are impaired in Syt1 KO neurons. Data represent mean ± SEM from N = 3 independent experiments with > 300 analyzed boutons per condition. **(e)** Normalized vGLUT1-pH peak florescence amplitude (ΔF) of control (WT) and Syt1 KO neurons following stimulation with 200 APs at 40 Hz as shown in (d). Syt1 KO: 45 ± 8 %; one sample t-test.

Loss of Syt1 lead to significantly delayed endocytic retrieval times of vGLUT1-pHluorin (pH) in response to train stimulations with 200 APs (Fig. 8b,c) [consistent with (Y. C. Li et al., 2017; Nicholson-Tomishima & Ryan, 2004)]. Furthermore, Syt1 KO neurons displayed a reduced exocytic response (Fig. 8d,e) visible in the fluorescence increase upon stimulation (ΔF) in addition to an increase of asynchronous release represented by delayed release in response to stimulation (Fig. 8b, zoom top right).

All defects in SV kinetics were also present, yet slightly less prominent, when monitoring the much more abundant synaptic vesicle protein Synaptophysin instead of vGLUT1. This suggests a general SV kinetic defect caused by loss of Syt1 (Fig. 9a-d).

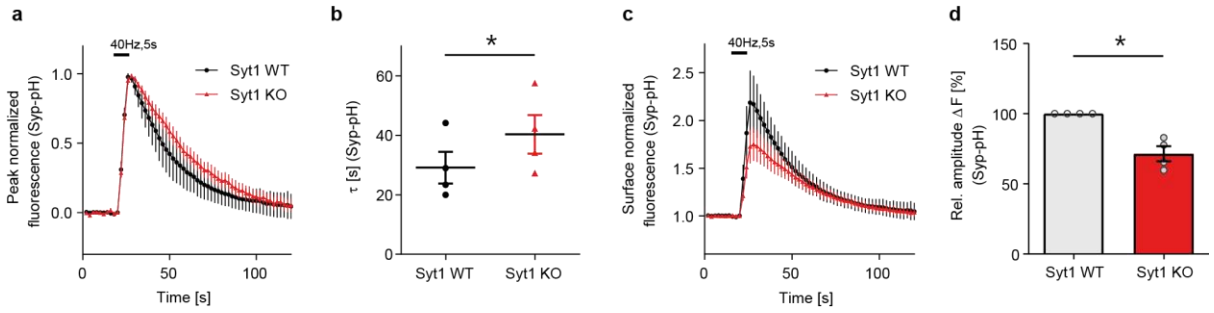

Figure 9: Loss of Syt1 impairs SV kinetics unspecific of SV protein.
(a) Average normalized Syp-pH fluorescence traces of hippocampal neurons from WT or Syt1 KO mice stimulated with 200 APs at 40 Hz. Synaptophysin-pH endocytosis is delayed in Syt1 KO neurons. Data represent mean ± SEM from N = 4 independent experiments with > 400 analyzed boutons per condition. **(b)** Endocytic decay time constants (τ) of data shown in (a). τ_{WT} = 29 ± 5 s, τ_{Syt1KO} = 40 ± 7 s; unpaired two-tailed t-test. **(c)** Average normalized Synaptophysin-pH fluorescence traces of hippocampal neurons from WT or Syt1 KO mice stimulated with 200 APs at 40 Hz. Exocytic events of Synaptophysin-pH depicted by the fluorescence amplitude are impaired in Syt1 KO neurons. Data represent mean ± SEM from N = 4 independent experiments with > 400 analyzed boutons per condition. **(d)** Normalized Synaptophysin-pH peak florescence amplitude (ΔF) of control (WT) and Syt1 KO neurons following stimulation with 200 APs at 40 Hz as shown in (c). Syt1 KO: 71 ± 5 %; one sample t-test.

Furthermore, depletion of Syt1 via acute lentiviral knockdown (KD) (Fig. 10a) and monitoring the kinetics of vGLUT1-pH confirmed all defects depicted in Syt1 KO neurons (Fig. 10b-d). The exocytic defect (Fig. 10d) was further verified by application of low pH buffer before and after stimulation resulting in quenching of surface-stranded vGLUT1-pH (Fig. 10e). The ratio metric analysis of the two quenching steps thereby confirmed that the exocytic defect (Fig. 10d) was not caused by defective SV reacidification upon loss of Syt1 (Fig. 10f). To address, whether loss of Syt1 causes changes in protein levels and thereby result in defects in the SV cycle, whole brain lysates of Syt1 WT and KO were analyzed. However, unchanged levels of Syt1-associated endocytic adaptors such as Stn2, AP2 or clathrin (Fig. 10g) were detected.

Results

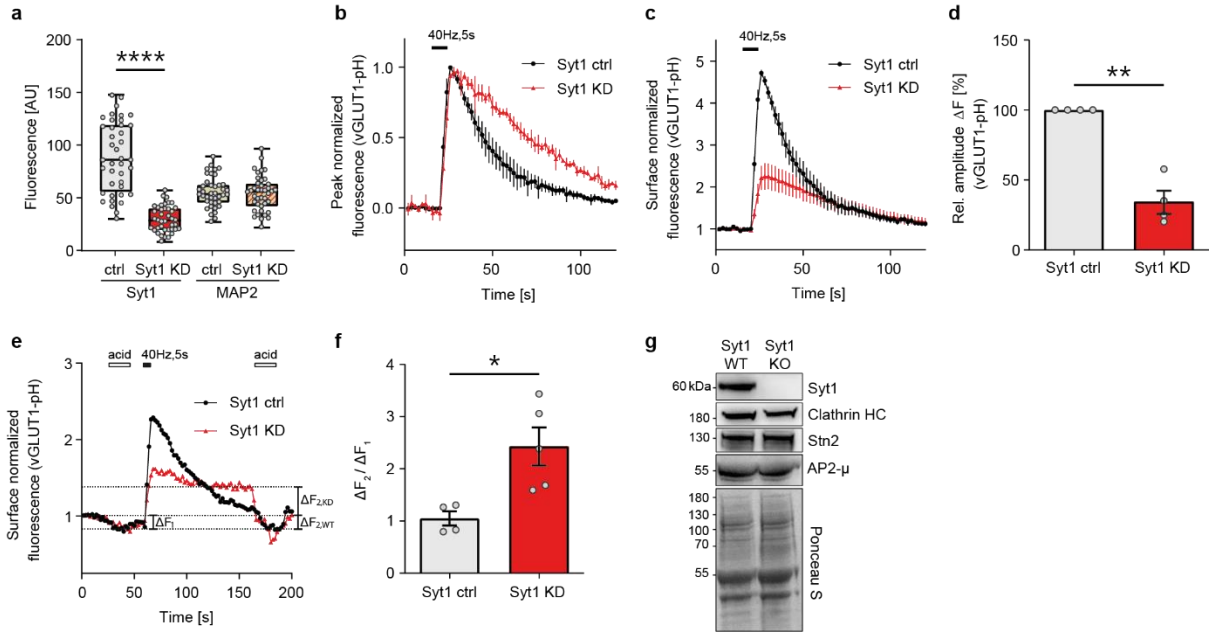

Figure 10: Loss of Syt1 widely impairs SV kinetics.
(a) Fluorescence intensities of Syt1- and of MAP2-labeled hippocampal neurons transduced with non-specific shRNA (Syt1 ctrl) or shRNA targeting Syt1 (Syt1 KD). Neurons transduced with shRNA targeting Syt1 reveal specific depletion of Syt1 within MAP2-positive areas. Boxplot depicts min to max intensities of n = 40 images from 5-6 independent cultures per condition; One-way ANOVA with Šidák's post-test. **(b)** Average normalized vGLUT1-pH fluorescence traces of hippocampal neurons lentivirally transduced with non-specific control (Syt1 ctrl) or Syt1 shRNA (Syt1 KD) and stimulated with 200 APs at 40 Hz reveal defect upon loss of Syt1. Data represent mean ± SEM from N = 4 independent experiments with > 400 analyzed boutons per condition. **(c)** Average normalized vGLUT1-pH fluorescence traces of hippocampal neurons lentivirally transduced with non-specific control (Syt1 ctrl) or Syt1 shRNA (Syt1 KD) and stimulated with 200 APs at 40 Hz. Exocytic events of vGLUT1-pH depicted by the fluorescence amplitude are impaired in Syt1 KD neurons. Data represent mean ± SEM from N = 4 independent experiments with > 400 analyzed boutons per condition. **(d)** Normalized vGLUT1-pH peak florescence amplitude (ΔF) of control (WT) and Syt1 KD neurons following stimulation with 200 APs at 40 Hz as shown in (c). Syt1 KD: 34.55 ± 8.34 %; one sample t-test. **(e,f)** Representative average normalized vGLUT1-pH fluorescence traces of hippocampal neurons lentivirally transduced with control (Syt1 ctrl) or Syt1 shRNA (Syt1 KD) and stimulated with 200 APs at 40 Hz and exposed to low pH imaging buffer before and after stimulation. Delayed endocytic retrieval of vGLUT1-pH in the Syt1 depleted hippocampal neurons [shown in (b) and Fig. 8c] is not caused by defects in re-acidification of endocytosed synaptic vesicles (e). Ratios of differences in surface-normalized fluorescence of vGLUT1-pH upon application of low pH imaging buffer post- (ΔF2) vs. pre-stimulus (ΔF1) in Syt1 ctrl (Syt1 ctrl: 1.05 ± 0.14) compared to Syt1 KD neurons (Syt1 KD: 2.43 ± 0.36) (f). Data represents mean/ independent culture ± SEM from $n_{Syt1\ ctrl}$ = 4, $n_{Syt1\ KD}$ = 5 independent cultures/ condition with > 100 – 150 boutons per condition, unpaired two-tailed t-test. **(g)** Unchanged total levels of clathrin heavy chain (HC), Stn2 and AP2-μ in total brain lysates from Syt1 vs. Syt1 KO mice. Ponceau S staining is shown as loading control. Input: 30 µg of total brain extract used as starting material. Molecular weight markers (in kDa) are indicated on the left. A representative example of n = 3 independent experiment is shown.

To eliminate potential overexpression artefacts of vGLUT1-pH in hippocampal neurons and to test a general function of Syt1 in SV recycling, we further monitored endogenously tagged vesicular GABA transporter (vGAT) during the SV cycle. For that, antibodies conjugated with the low pH-activated fluorophore CypHer (López-Hernández et al., 2022) were used. Consistently, Syt1 depleted hippocampal neurons displayed significant defects in kinetics of SV endocytosis in response to stimulation with 200 APs (Fig. 11a,b). To further

scrutinize the hypothesis of Syt1 possessing an indispensable and hence general function in the SV cycle independent of the level of neuronal activity, we applied a stimulus known to only release the readily-releasable SV pool. In response to such a stimulus of 50 APs, Syt1 depleted neurons also showed SV endocytosis defects (Fig. 11c,d) suggesting a fundamental importance of Syt1 in the SV cycle independent of stimulation strength.

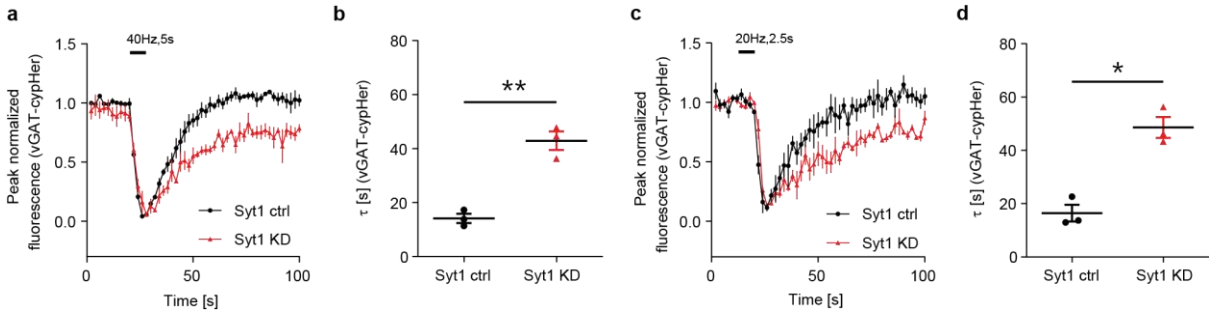

Figure 11: Loss of Syt1 leads to a fundamental impairment of the SV cycle.
(a) Average normalized fluorescence traces of hippocampal neurons transduced with control (Syt1 ctrl) or Syt1-shRNA-encoding lentivirus and incubated with anti-vGAT CypHer5E-coupled antibodies reveal defects in the endocytosis of endogenous vGAT upon loss of Syt1. Neurons were stimulated with 200 APs at 40 Hz and recorded at 37°C. Data represent mean ± SEM from N = 3 independent experiments with > 300 analyzed boutons per condition. **(b)** Endocytic decay time constants (τ) of data shown in (a). τ_{WT} = 14 ± 2 s, $\tau_{Syt1\ KD}$ = 43 ± 3 s; unpaired two-tailed t-test. **(c)** Average normalized fluorescence traces of hippocampal neurons transduced with control (Syt1 ctrl) or Syt1-shRNA-encoding lentivirus (Syt1 KD) and incubated with anti-vGAT CypHer5E-coupled antibodies. Neurons were stimulated with 50 APs at 20 Hz and recorded at 37 °C. The defect in the uptake of endogenous vGAT upon loss of Syt1 is independent of stimulation strength. Data represent mean ± SEM from N = 3 independent experiments with > 300 analyzed boutons per condition. **(d)** Endocytic decay time constants (τ) of data shown in (c). τ_{ctrl} = 16 ± 3 s, $\tau_{Syt1\ KD}$ = 49 ± 4 s; unpaired two-tailed t-test.

4.1.1.2 Ultrastructural changes rationalize functional defects upon Syt1 loss

To assess whether the SV recycling defects revealed by optical imaging experiments were also visible at the ultrastructural level, we performed high pressure freezing (HPF) electron microscopy. We analyzed synapses from WT and Syt1 KO hippocampal neurons either unstimulated or in response to 200 APs (Fig. 12a,b). Thus, we aimed to investigate Syt1's impact on plasma membrane invaginations, on the formation of internal endosome-like vacuoles (ELVs) characterized by a morphologically discernible coat as well as on the number of SVs within the presynapse in presence of synaptic activity. Interestingly, all structural findings reflect the functional defects we had found in Syt1 hippocampal neurons. While upon stimulation WT neurons (Fig. 12a) displayed higher numbers of ELVs that have undergone fission from the plasma membrane, this number was significantly decreased in synapses from Syt1 KO hippocampal neurons (Fig. 12c,f). In line with this observation, non-coated plasma membrane invaginations were instead increased in number (Fig. 12d,g) yet

similar in size (depth: WT = 68 ± 9 nm, KO = 58 ± 4 nm; width: WT = 38 ± 6 nm, KO = 45 ± 10 nm) whereas the overall number of SVs was partially reduced (Fig. 12e,h). These results further endorse Syt1's fundamental role in SV endocytosis by suggesting Syt1 to promote the formation of ELVs and thereby SV replenishment.

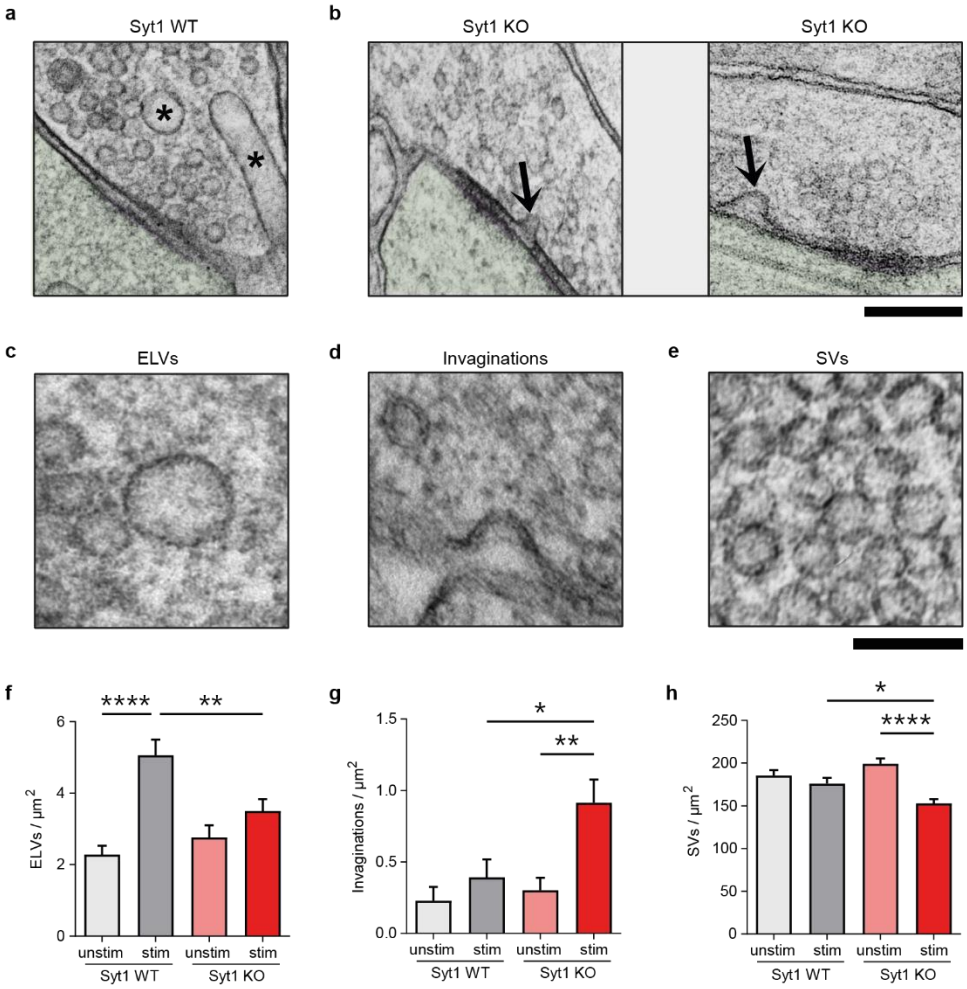

Figure 12: Structural changes upon loss of Syt1 reflect impaired SV kinetics.
(a,b) Representative electron micrographs of synapses from stimulated (200 APs, 40 Hz) WT (a) and Syt1 KO (two examples in b) hippocampal neurons. Note the accumulation of post-fission endosome-like vesicles (ELVs) in WT synapses (stars) and membrane invaginations in Syt1 KO synapses (arrows). Purple: postsynaptic density (PSD); green: postsynaptic element. Scale bar: 200 nm. **(c-e)** Representative examples of ELVs (c), membrane invaginations (d), and synaptic vesicles (SVs) (e). Scale bar: 100 nm. **(f-h)** Quantitative morphometric analysis of ELVs (f), membrane invaginations (g), and SVs (h) normalized per bouton area (µm^2). ELVs and SVs are reduced, whereas membrane invaginations are increased in Syt1 KO boutons post stimulation. Data represent n = synapses ± SEM from 3 - 4 individual cultures per condition with $n_{Syt1\ WT,\ unstim}$ = 184, $n_{Syt1\ WT,\ stim}$ = 165, $n_{Syt1\ KO,\ unstim}$ = 169, $n_{Syt1\ KO,\ stim}$ = 191, Kruskal-Wallis test followed by two-sided Dunn's multiple comparison test. Courtesy of Dmytro Puchkov (FMP)

4.1.2 Surface stranded Synaptotagmin 1 leads to facilitated SV kinetics.

While loss of Syt1 lead to impairment of endocytosis, we wanted to test the hypothesis of exocytosed Syt1 actively promoting SV endocytosis. During the SV cycle Syt1 is selectively

sorted by its adapter Stonin 2 (Diril et al., 2006; Jung et al., 2007; Kaempf et al., 2015; Kononenko et al., 2013). In case of Stn2 loss, activity-dependent surface accumulation of Syt1 has been reported in Stn2 KO neurons (Diril et al., 2006; Jung et al., 2007; Kaempf et al., 2015; Kononenko et al., 2013). Interestingly, hippocampal neurons lacking Stn2 (Fig. 13a) revealed accelerated endocytic kinetics monitored by either vGLUT1-pH or Synaptophysin-pH (Fig. 13b,c) [consistent with (Kaempf et al., 2015; Kononenko et al., 2013)] which is coherent with the hypothesis of Syt1's fundamental role in SV recycling.

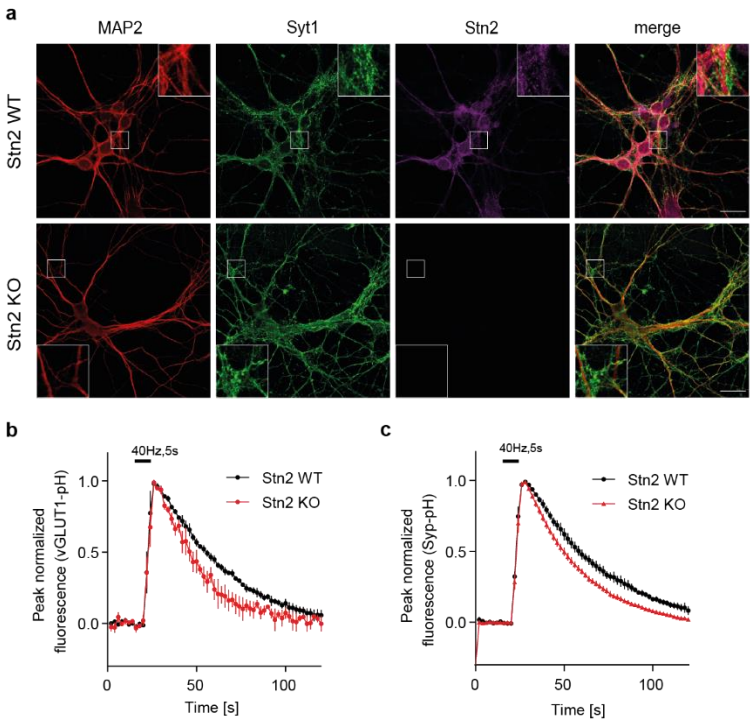

Figure 13: Exocytosed Synaptotagmin 1 drives SV endocytosis.
(a) Representative confocal images of Stn2 WT/KO hippocampal neurons (DIV15) stained for MAP2, Syt1 and for Stn2. Scale bar: 20 µm. **(b)** Average normalized vGLUT1-pH fluorescence traces of hippocampal neurons from WT or Stn2 KO mice stimulated with 200 APs at 40 Hz. The kinetics of vGLUT1-pH endocytosis are accelerated in Stn2 KO neurons. Data represent mean ± SEM from N = 3 independent experiments with > 300 analyzed boutons per condition. **(c)** Average normalized Synaptophysin-pH fluorescence traces of hippocampal neurons from WT or Stn2 KO mice stimulated with 200 APs at 40 Hz. Upon loss of Stn2 endocytosis of Synaptophysin-pH is accelerated. Data represent mean ± SEM from N = 3 independent experiments with > 300 analyzed boutons per condition.

Additionally, in contrast to loss of Syt1, Stn2 KO neurons possessing plasma membrane stranded Syt1 showed an increase in exocytic events monitored by either vGLUT1-pH (Fig. 14a,b) or Synaptophysin-pH (Fig. 14c,d) whereas presynaptic calcium influx was unaltered (Bolz et al., 2023).

These opposite findings of SV kinetics seem to depend on the presence of Syt1. Upon loss of Syt1, exocytosis is reduced while endocytosis is delayed. Instead, surface accumulation of

Syt1 leads to increased exocytosis and facilitation of endocytosis. Overall, this indicates that Syt1 may be an intrinsic surrogate measure for the speed of the SV cycle.

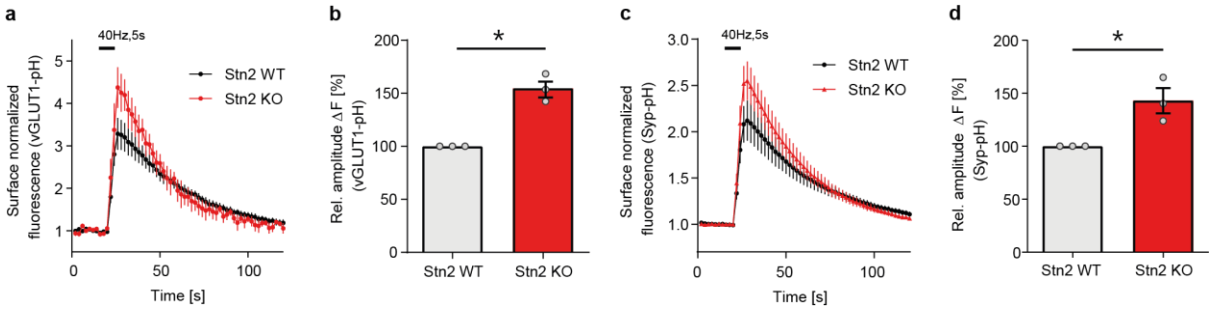

Figure 14: Exocytosed Synaptotagmin 1 facilitates SV exocytosis.
(a) Average normalized vGLUT1-pH fluorescence traces of hippocampal neurons from WT or Stn2 KO mice stimulated with 200 APs at 40 Hz. Exocytic vGLUT1-pH events depicted by the fluorescence amplitude are increased in Stn2 KO neurons. Data represent mean ± SEM from N = 3 independent experiments with > 300 analyzed boutons per condition. **(b)** Normalized vGLUT1-pH peak florescence amplitude (ΔF) of control (WT) and Stn2 KO neurons following stimulation with 200 APs at 40 Hz. Stn2 KO: 155 ± 8 %; one sample t-test. **(c)** Average normalized Synaptophysin-pH fluorescence traces of WT or Stn2 KO derived hippocampal neurons stimulated with 200 APs at 40 Hz. The increase of fluorescence amplitude depicts a facilitation of exocytic events of Synaptophysin-pH upon loss of Stn2. Data represent mean ± SEM from N = 3 independent experiments with > 300 analyzed boutons per condition. **(d)** Normalized Synaptophysin-pH peak florescence amplitude (ΔF) of control (WT) and Stn2 KO neurons following stimulation with 200 APs at 40 Hz. Stn2 KO: 143 ± 11 %; one sample t-test.

4.1.3 Exocytosed Synaptotagmin 1 actively regulates SV endocytosis.

To further challenge the hypothesis of Syt1 tuning the rate of SV endocytosis, we depleted Syt1 in Stn2 KO neurons via acute lentiviral KD (as in Fig. 10a). Indeed, loss of Syt1 in Stn2 KO hippocampal neurons lead to a significant decrease of endocytosis monitored by vGLUT1-pH (Fig. 15a,b).

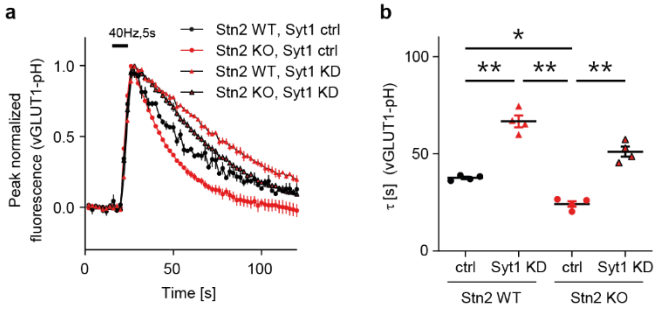

Figure 15: Exocytosed Synaptotagmin 1 tunes the rate of SV endocytosis.
(a) Average normalized vGLUT1-pH fluorescence traces of hippocampal neurons from WT or Stn2 KO mice transduced with control (Syt1 ctrl) or Syt1-shRNA-encoding lentivirus (Syt1 KD) and stimulated with 200 APs at 40 Hz. Data represents mean ± SEM from N = 4 independent experiments with > 350 analyzed boutons per condition. **(b)** Endocytic decay time constants (τ) of vGLUT1-pH-expressing hippocampal neurons from WT or Stn2 KO mice and transduced with control (Syt1 ctrl) or Syt1-shRNA-encoding lentivirus (Syt1 KD) as shown in (a). Loss of Syt1 in neurons derived from Stn2 KO mice reverts facilitated SV endocytic rates. $\tau_{WT\ ctrl}$ = 38 ± 1 s, $\tau_{Stn2\ KO\ ctrl}$ = 24 ± 3 s; $\tau_{WT,\ Syt1\ KD}$ = 67 ± 6 s, $\tau_{Stn2\ KO,\ Syt1\ KD}$ = 51 ± 5 s. Data represent mean ± SEM from N = 4 independent experiments with > 350 analyzed boutons per condition. One-way ANOVA with Tukey's post-test.

Consistent with our hypothesis, this Syt1-dependent reversal from accelerated to impaired SV endocytosis assigns Syt1 an active role as a gating pulse for SV endocytosis.

4.2 Exocytosed Synaptotagmin 1 promotes the synthesis of signaling lipids.

Facilitation of endocytosis could be promoted by the accumulation of Syt1 via an enhanced recruitment of endocytic proteins e.g., Stn2 (L. G. Wu et al., 2014). However, our findings of unchanged levels of Stn2 upon loss of Syt1 (Fig. 10g) and facilitated endocytosis in the absence of Stn2 (Fig. 13b,c) makes this theory unlikely. Therefore, we focused on the membrane lipid, $PI(4,5)P_2$, whose synthesis has directly been linked to SV kinetics (Di Paolo et al., 2004; Di Paolo & De Camilli, 2006; Posor et al., 2022). In various models it has been shown that depletion of $PI(4,5)P_2$ leads to impaired exocytosis (Di Paolo et al., 2004; Milosevic et al., 2005) as well as delayed SV endocytosis (Di Paolo et al., 2004; Di Paolo & De Camilli, 2006; Posor et al., 2022). Therefore, we hypothesized that exocytosed Syt1 actively tunes the rate of SV endocytosis by promoting local synthesis of $PI(4,5)P_2$.

4.2.1 Syt1 promotes a stimulation-dependent increase of $PI(4,5)P_2$.

To test this, we investigated the stimulation dependence of $PI(4,5)P_2$ levels in presynaptic boutons of hippocampal neurons. For $PI(4,5)P_2$ specific labelling we used the recombinant $PI(4,5)P_2$ binding PH domain of phospholipase Cδ (eGFP-PH-PLCδ1) as a specific probe. To control the specificity, staining with the mutant eGFP-PH-PLCδ1 K30A K32A W36N which is incapable of binding $PI(4,5)P_2$ resulted in background fluorescence (Fig. 16a).

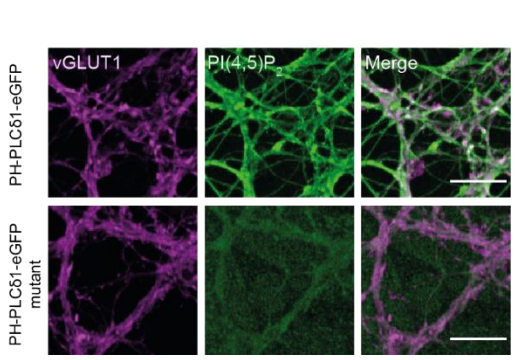

Figure 16: Specificity of eGFP-PH-PLCδ1 as $PI(4,5)P_2$ binder
(a) Representative confocal images of hippocampal neurons from WT mice labeled for $PI(4,5)P_2$ using recombinant eGFP-PH-PLCδ1 (top, green) or eGFP-PH-PLCδ1 K30A K32A W36N, the $PI(4,5)P_2$-binding mutant of eGFP-PH-PLCδ1 (bottom, green), and vGLUT1 (magenta) indicating $PI(4,5)P_2$ specificity of eGFP-PH-PLCδ1. Scale bar: 10 µm.

Results

Using the recombinant PI(4,5)P_2 binding PH domain as a specific probe (Fig. 16a) chemical (Fig. 17a,b) as well as electrical train stimulation of 200 APs at 40 Hz (Fig. 17e) resulted in a specific presynaptic increase of PI(4,5)P_2 levels.

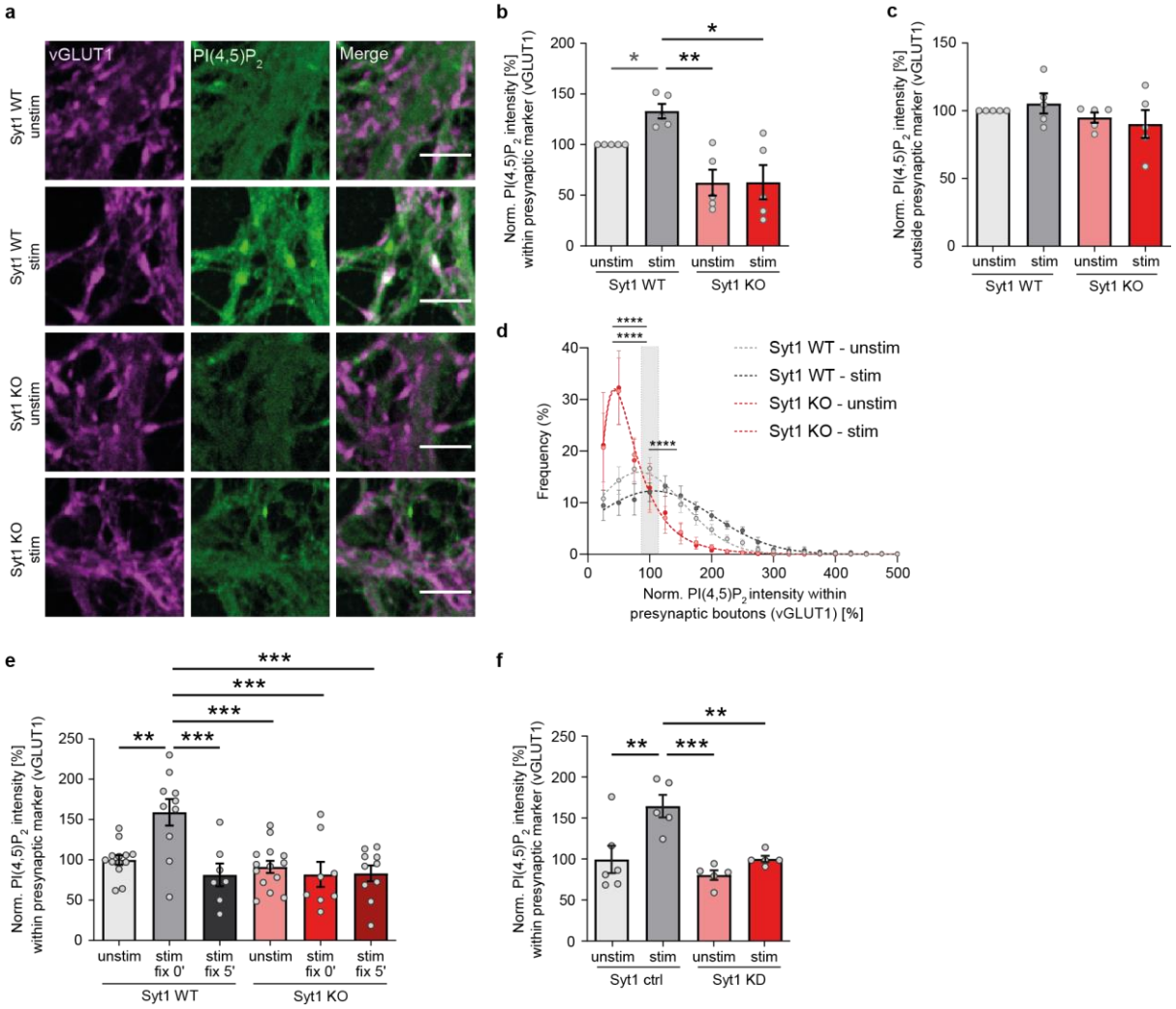

Figure 17: Syt1 promotes synthesis of presynaptic PI(4,5)P_2.
(a) Representative confocal images of non-stimulated or stimulated hippocampal neurons from WT or Syt1 KO mice and labeled for PI(4,5)P_2 using recombinant eGFP-PH-PLCδ1 (green) and the presynaptic marker vGLUT1 (magenta). Scale bar: 5 µm. **(b)** Quantification of presynaptic PI(4,5)P_2 levels in vGLUT1-positive presynaptic boutons of non-stimulated or stimulated (80 mM KCl for 60 s) WT vs Syt1 KO neurons. The levels of PI(4,5)P_2 in non-stimulated WT neurons were set to 100 %. Stimulation induced increase of PI(4,5)P_2 is lost in Syt1 KO neurons. Data are mean ± SEM from N = 5 independent experiments with > 20 analyzed images per condition. One sample t-test followed by correction for multiple testing (grey). One-way ANOVA with Tukey's post-test (black). **(c)** Quantification of PI(4,5)P_2 levels outside vGLUT1-positive presynaptic boutons of non-stimulated or stimulated WT vs. Syt1 KO neurons. The levels of PI(4,5)P_2 in non-stimulated WT neurons were set to 100 %. Data are mean ± SEM from N = 5 independent experiments with > 20 analyzed images per condition. One sample t-test followed by correction for multiple testing (grey). One-way ANOVA with Tukey's post-test (black). **(d)** Quantification of presynaptic PI(4,5)P_2 levels per individual vGLUT1-positive presynaptic bouton of non-stimulated or stimulated (80 mM KCl for 60 s) WT vs Syt1 KO neurons (a,b) reveals increased PI(4,5)P_2 levels positive puncta upon stimulation. Loss of Syt1 leads to decreased PI(4,5)P_2 levels of vGLUT1-positive puncta. Levels of PI(4,5)P_2 were normalized to the mean of PI(4,5)P_2 in non-stimulated WT neurons (set to 100 %, grey box) and statistically compared with non-stimulated WT neurons. Data are mean ± SEM from N = 5 independent experiments with > 20 analyzed images per condition. **(e)** Hippocampal neurons from WT or Syt1 KO mice were left unstimulated or stimulated (200 APs, 40 Hz) and fixed immediately (fix 0') or after a 5 min recovery period (fix 5'). PI(4,5)P_2 within presynaptic boutons

marked by vGLUT1 was detected using specific antibodies. Data represent mean/ image ± SEM with $n_{Syt1\ WT,\ unstim}$ = 13, $n_{Syt1\ WT,\ stim,\ fix\ 0'}$ = 10, $n_{Syt1\ WT,\ stim,\ fix\ 5'}$ = 7, $n_{Syt1\ KO,\ unstim}$ = 14, $n_{Syt1\ KO,\ stim,\ fix\ 0'}$ = 8, $n_{Syt1\ KO,\ stim,\ fix\ 5'}$ = 10 images from 4 independent cultures per condition. One-way ANOVA with Tukey's post-test. **(f)** Quantification of presynaptic PI(4,5)P_2 levels in vGLUT1-positive presynaptic boutons of non-stimulated or stimulated (200 APs, 40 Hz) hippocampal neurons lentivirally transduced with control (Syt1 ctrl) or Syt1 shRNA (Syt1 KD). The levels of the mean intensity of PI(4,5)P_2 in non-stimulated WT neurons were set to 100 %. Data are mean/ image ± SEM from $n_{Syt1\ ctrl,\ unstim}$ = 6, $n_{Syt1\ ctrl,\ stim}$ = 5, $n_{Syt1\ KD,\ unstim}$ = 5, $n_{Syt1\ KD,\ stim}$ = 5 images per condition from 4 individual cultures per condition. One-way ANOVA with Tukey's post-test.

This rise was absent in the surrounding axon (Fig. 17c) and was an immediate response to stimulation as the increase of PI(4,5)P_2 vanished after termination of the stimulus and returned to baseline (Fig. 17e). The analysis of PI(4,5)P_2 levels of individual boutons revealed a gaussian-like probability distribution that was shifted towards elevated presynaptic PI(4,5)P_2 levels in a stimulation-dependent manner when normalized to steady-state (100 %, Fig. 17d).

Remarkably, loss of Syt1 resulted in abrogation of the stimulation-induced increase of PI(4,5)P_2 in hippocampal neurons either using Syt1 KO mice (Fig. 17a-e) or hippocampal neurons acutely depleted of Syt1 via lentiviral shRNA (Fig. 17f). To control all findings, we verified the results depicted upon labelling with the recombinant PI(4,5)P_2 binding PH domain instead with PI(4,5)P_2 specific antibodies (Fig. 17e,f).

To test whether the elevated Syt1-dependent presynaptic PI(4,5)P_2 levels are a unique phenotype under strong stimulation or depict a general activity-dependent mechanism, we analyzed the PI(4,5)P_2 levels in a stimulation dependent manner. Strikingly, the increase of PI(4,5)P_2 levels correlated well with stimulation strength. In contrast to an increase upon stimulation with 100, 50 or only 20 APs, silenced neuronal activity in the presence of tetrodotoxin (TTX) showed reduced PI(4,5)P_2 levels when compared to basal activity (Fig. 18a,b). Using multicolor time-gated stimulated emission-depletion (gSTED) microscopy, we visualized distinct stimulation-induced PI(4,5)P_2 nanoclusters within vGLUT1-positive boutons (Fig. 18c).

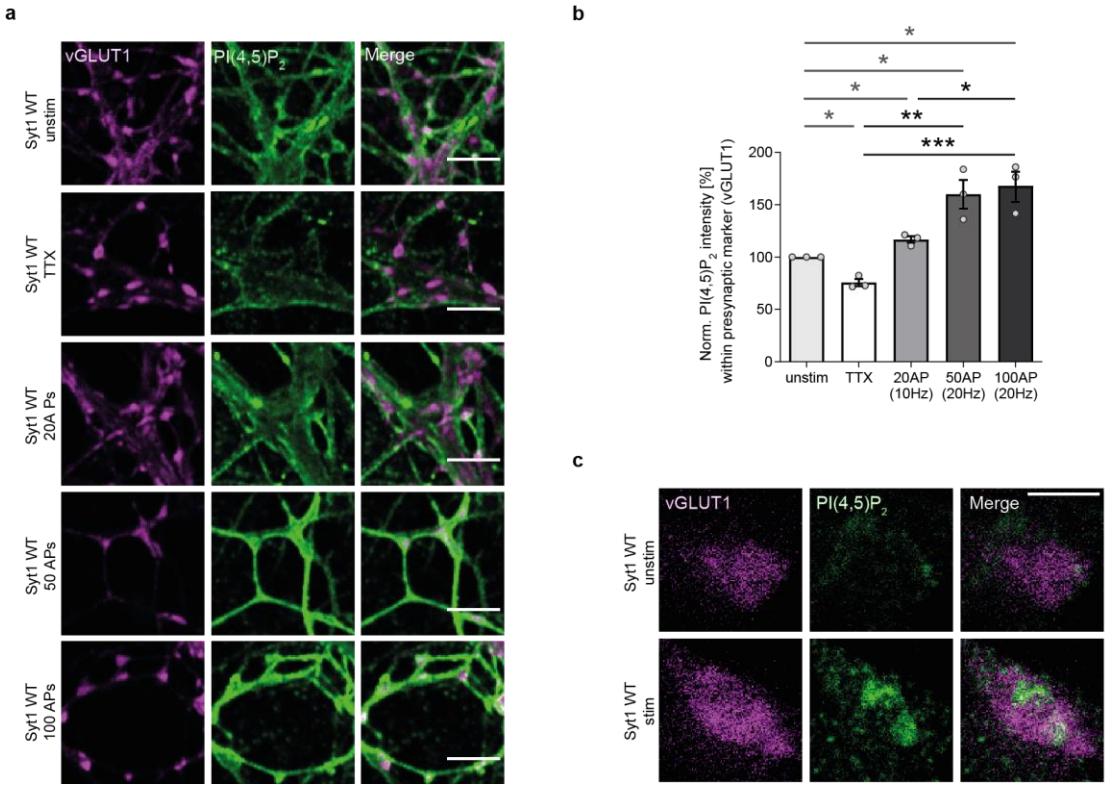

Figure 18: Rate of presynaptic PI(4,5)P_2 synthesis correlates with activity and organizes into nanoclusters.
(a) Representative confocal images of non-stimulated, silenced (TTX) or stimulated (20, 50 or 100 APs) hippocampal neurons from WT mice and labeled for PI(4,5)P_2 using recombinant eGFP-PH-PLCδ1 (green) and the presynaptic marker vGLUT1 (magenta). Scale bar: 5 µm. **(b)** Quantification of presynaptic PI(4,5)P_2 levels in vGLUT1-positive presynaptic boutons of non-stimulated vs. silenced (TTX), or stimulated (20, 50 or 100 APs) WT neurons. The levels of PI(4,5)P_2 in non-stimulated WT neurons were set to 100 %. Data are mean ± SEM from N = 3 independent experiments with > 15 analyzed images per condition. One sample t-test followed by correction for multiple testing (grey). One-way ANOVA with Tukey‘s post-test (black). **(c)** Representative STED images of non-stimulated, or stimulated (80 mM KCl for 60 s) hippocampal neurons from WT mice and labeled for PI(4,5)P_2 using recombinant eGFP-PH-PLCδ1 (green) and the presynaptic marker vGLUT1 (magenta). Scale bar: 0.5 µm.

These results suggest exocytosed Syt1 to be required for the stimulation-induced presynaptic synthesis of PI(4,5)P_2.

4.2.2 Accumulation of Synatotagmin 1 enhances the synthesis of PI(4,5)P_2 in a stimulation-dependent manner.

The activity-dependent increase of PI(4,5)P_2 could in principle be caused by surface-stranded or by vesicular Syt1. To test this, PI(4,5)P_2 levels were monitored in hippocampal Stn2 KO neurons having increased Syt1 surface levels (Diril et al., 2006; Jung et al., 2007; Kaempf et al., 2015; Kononenko et al., 2013). At steady-state, levels of

$PI(4,5)P_2$ were significantly elevated in Stn2 KO neurons (Fig. 19a). Upon stimulation, this increase was further amplified.

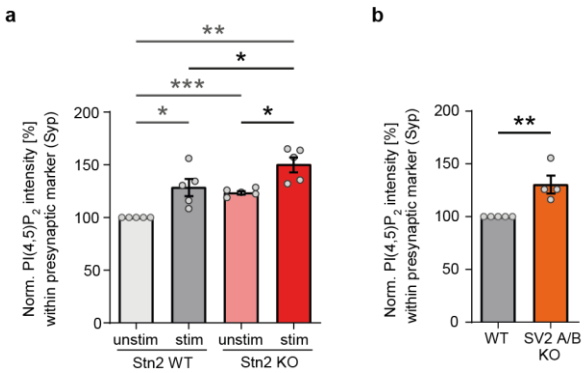

Figure 19: Surface stranded Syt1 is responsible for activity-induced increase of $PI(4,5)P_2$.
(a) Quantification of presynaptic $PI(4,5)P_2$ levels in Syp-positive presynaptic boutons of non-stimulated or stimulated WT vs. Stn2 KO neurons. The levels of $PI(4,5)P_2$ in non-stimulated WT neurons were set to 100 %. Data represent mean ± SEM from N = 5 independent experiments with > 25 images/ condition. One sample t-test followed by correction for multiple testing (grey). One-way ANOVA with Tukey's post-test (black). **(b)** Quantification of presynaptic $PI(4,5)P_2$ levels in Syp-positive presynaptic boutons of stimulated WT vs. SV2A/B double KO neurons. The levels of $PI(4,5)P_2$ in stimulated WT neurons were set to 100 %. Data represent mean ± SEM from N = 4 independent experiments with > 20 images/ condition. One sample t-test Courtesy of Natalie Kaempf (FMP)

A similar scenario had been found when monitoring $PI(4,5)P_2$ levels in hippocampal neurons from SV2A and SV2B KO mice in which Syt1 is similarly redistributed from SVs to the neuronal plasma membrane [Fig. 19b, consistent with (Kaempf et al., 2015)].

This suggests that exocytosed Syt1 on the plasma membrane promotes the synthesis of $PI(4,5)P_2$ and thereby, facilitates SV endocytosis.

4.2.3 Re-supplying $PI(4,5)P_2$ rescues endocytic defect upon loss of Synaptotagmin 1.

If our model is correct, re-supplying $PI(4,5)P_2$ should rescue the impaired SV endocytosis in hippocampal neurons depleted of Syt1. We therefore used exogenous membrane-permeant $PI(4,5)P_2$ that upon uncaging was inserted into the neuronal membrane acting endogenously and hence increased $PI(4,5)P_2$ levels. Application of this compound fully restored the impaired endocytic retrieval upon loss of Syt1 (Fig. 20a,b). In line with Syt1's well-known role in calcium-triggered neurotransmission (Chapman, 2008; Geppert et al., 1994; Jahn & Fasshauer, 2012; Zhou et al., 2017), this rescue was endocytosis specific as it failed to restore the defective exocytic vesicle fusion of Syt1 depleted neurons (Fig. 20c).

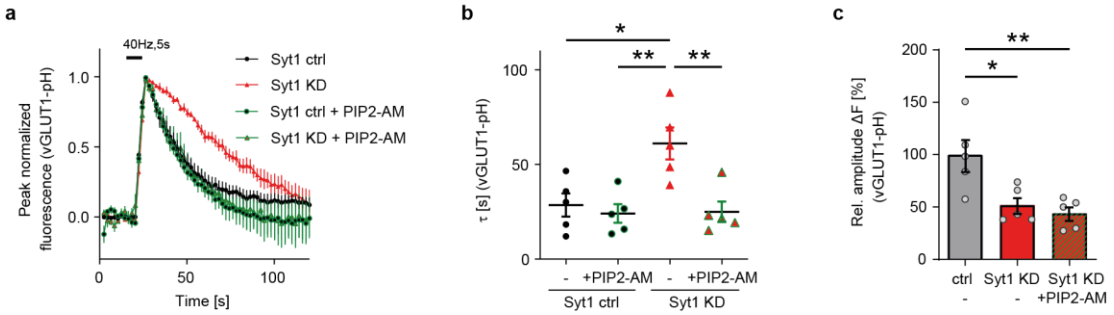

Figure 20: Re-supply of PI(4,5)P_2 exclusively rescues endocytic defect upon loss of Syt1.
(a) Average normalized vGLUT1-pHluorin fluorescence traces of hippocampal neurons lentivirally transduced with control (Syt1 ctrl) or Syt1 shRNA (Syt1 KD). Where indicated, neurons were pretreated with 20 µM membrane-permeant caged PI(4,5)P_2 [PI(4,5)P_2-AM] for 20 min. PI(4,5)P_2-AM was uncaged by UV light (405 nm for 200 ms), and neurons were stimulated with 200 APs at 40 Hz. Data represent mean/ independent culture ± SEM with n = 5 independent cultures/ condition with > 125 boutons/ condition. **(b)** Endocytic decay time constants (τ) of data shown in (a). Re-supply of PI(4,5)P_2 rescues defect in endocytic retrieval upon loss of Syt. $\tau_{Syt1\ ctrl}$ = 29 ± 6 s, $\tau_{Syt1\ ctrl\ +\ PIP2\text{-}AM}$ = 25 ± 5 s, $\tau_{Syt1\ KD}$ = 62 ± 8 s, $\tau_{Syt1\ KD\ +\ PIP2\text{-}AM}$ = 26 ± 5 s. One-way ANOVA with Tukey's post-test. **(c)** Normalized vGLUT1-pH peak florescence amplitude (ΔF) of control (WT) and Syt1 KD neurons following stimulation with 200 APs at 40 Hz. Syt1 WT = 100 ± 15 %, Syt1 KD = 52 ± 8 %, Syt1 KD + PIP2-AM = 44 ± 7 %. Data represent mean/ independent culture ± SEM with n = 5 independent cultures/ condition with > 125 boutons/ condition. One-way ANOVA with Tukey's post-test.

We therefore conclude that Syt1 may act as a counting device. Being accumulated on the plasma membrane after exocytic fusion, we propose Syt1 to promote presynaptic PI(4,5)P_2 synthesis in a quantitative and stimulation-dependent manner to facilitate SV endocytic retrieval.

4.3 Presynaptic recruitment of PIPKIγ and of other proteins of the endocytic machinery is mediated by Synaptotagmin 1.

Phosphatidylinositol-4-phosphate 5-kinase type-1γ (PIPK1γ) is the key enzyme for the generation of the majority of PI(4,5)P_2 in the hippocampus (Wenk et al., 2001). Considering the elevated PI(4,5)P_2 levels in hippocampal neurons from Stn2 KO mice which correlate with surface-stranded Syt1, we proposed Syt1 to mediate the recruitment of PIPK1γ towards the plasma membrane. This would lead to elevated PI(4,5)P_2 levels and would further promote the recruitment of other factors driving endocytosis.

4.3.1 Loss of Synaptotagmin 1 leads to inefficient recruitment of PIPKIγ and dynamin.

To test our hypothesis, we studied the effect of loss of Syt1 on the nanoscale distribution of PIPKIγ. Using multicolor time-gated stimulated emission depletion microscopy (gSTED),

hippocampal neurons from Syt1 WT or KO mice were either left untreated or were stimulated with KCl and stained for PIPKIγ, the presynaptic active zone (AZ) marker Bassoon, and Homer 1, a post-synaptic scaffold protein (Fig. 21a). For each acquired z-stack the fluorescence intensities of each marker were summed. To compare changes in distribution, synapses were chosen that show a clear apposition of pre- and postsynaptic staining and are oriented parallel to the focal plane. Each marker was quantitatively analyzed along line profiles that ran perpendicular to the labeling of Bassoon and Homer 1 (Fig. 21b).

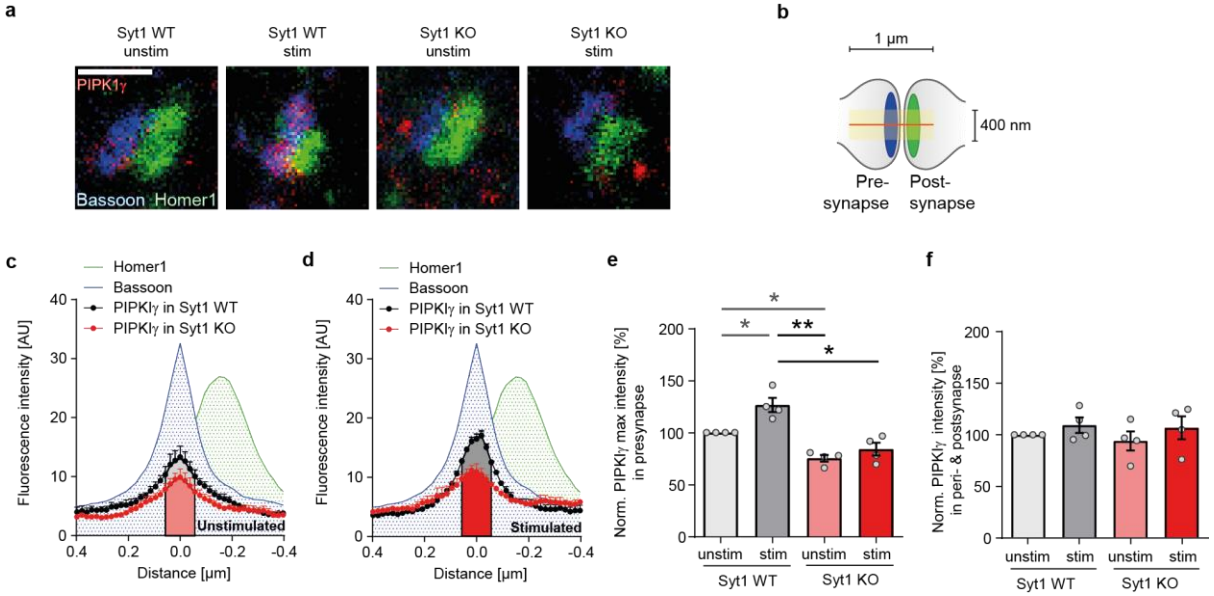

Figure 21: Loss of Syt1 abolishes stimulation-induced enrichment of PIPKIγ to the presynapse.
(a) Representative STED images of WT vs. Syt1 KO synapses of hippocampal neurons kept at rest or stimulated with 80 mM KCl for 60 s and labelled for PIPKIγ (red), Bassoon (blue) and Homer1 (green). **(b)** Scheme illustrating the analysis of the nanoscale distribution of proteins by 3-color gSTED super-resolution imaging in hippocampal neurons stained for the presynaptic AZ scaffold Bassoon (blue), the postsynaptic scaffold Homer1 (green) and the protein-of-interest (i.e., PIPKIγ, red (a)) within the indicated region (yellow). **(c,d)** Averaged line profiles of the nanoscale localization of PIPKIγ in WT vs. Syt1 KO synapses of hippocampal neurons kept a rest (c) or stimulated (d) with 80 mM KCl for 60 s. Multicolor line profiles of PIPKIγ in Syt1 WT (black) or KO (red) were aligned to the presynaptic maxima of Bassoon (blue). For the analyses in (e) the intensity of PIPKIγ in the presynapse (-0.05 - 0.05 µm) was summed (colored area under corresponding curve). **(e)** Quantification of the nanoscale presynaptic levels of PIPKIγ in synapses from WT or Syt1 KO mice as illustrated in (c,d). Presynaptic PIPKIγ intensity in non-stimulated WT synapses was set to 100 %. Loss of Syt1 abolished stimulation-induced presynaptic enrichment of PIPKIγ. Syt1 WT stim = 127 ± 7 %; Syt1 KO unstim = 75 ± 3 %, Syt1 KO stim = 84 ± 6 %. Data represent mean ± SEM from N = 3 independent experiments with > 100 analyzed synapses per condition. One sample t-test followed by correction for multiple testing (grey). One-way ANOVA with Tukey's post-test (black). **(f)** Quantification of the peri- and postsynaptic [0.4 - 0.05 and (-0.05) - (-0.4) µm] levels of PIPKIγ in synapses from WT or Syt1 KO mice as illustrated in (c,d). PIPKIγ intensity in non-stimulated WT synapses was set to 100 %. No alterations of PIPKIγ levels outside the AZ. Syt1 WT stim = 110 ± 8 %, Syt1 KO unstim = 99 ± 9 %, Syt1 KO stim = 107 ± 11 %. Data represent mean ± SEM from N = 3 independent experiments with > 100 analyzed synapses per condition. One sample t test followed by correction for multiple testing. One-way ANOVA with Tukey's post-test.

The recruitment of PIPKIγ towards the presynapse as indicated by an increase of fluorescently labelled PIPKIγ within the region of Bassoon was increased upon stimulation in WT hippocampal neurons (Fig. 21c,d). Loss of Syt1 abolished this stimulation-induced

nanoscale recruitment (Fig. 21e). To exclude other synaptic redistribution defects, we further analyzed the levels of PIPKIγ outside the AZ in peri- and postsynaptic areas [0.4 - 0.05 and (-0.05) - (-0.4) µm] and found these levels to be unaffected (Fig. 21f). The activity-induced recruitment of PIPKIγ to presynaptic sites correlates with and hence, may account for the stimulation-dependent increase of presynaptic $PI(4,5)P_2$ levels (compare Fig. 17b).

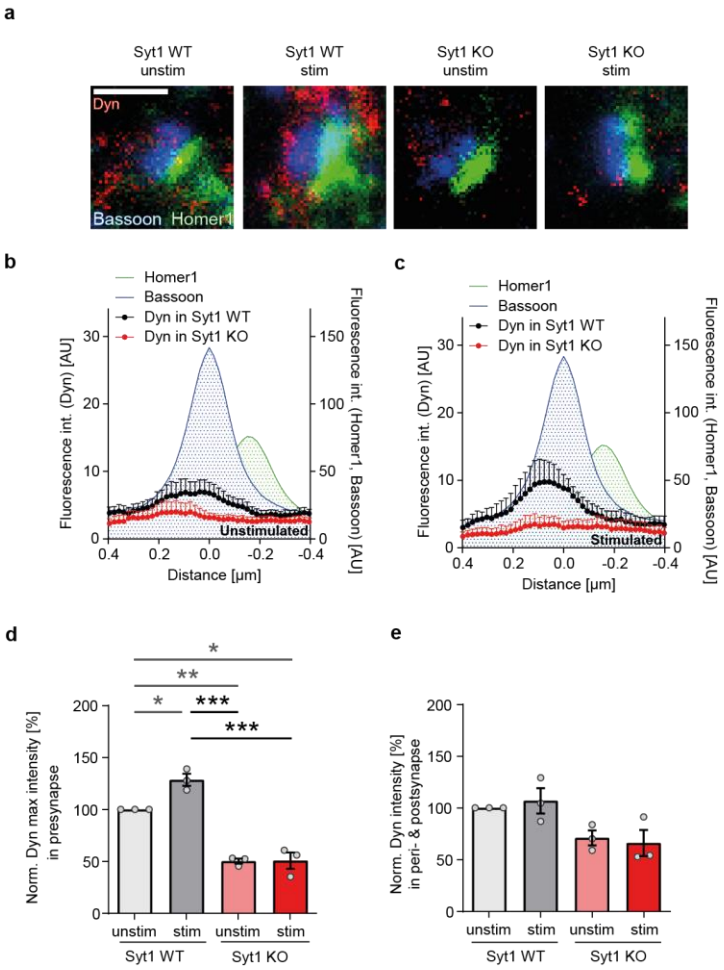

Figure 22: Stimulation-induced recruitment of dynamin 1-3 is abrogated upon loss of Syt1.
(a) Representative STED images of WT vs. Syt1 KO synapses of hippocampal neurons kept at rest or stimulated with 80 mM KCl for 60 s and labelled for dynamin 1,2,3 (red), Bassoon (blue) and Homer1 (green). **(b,c)** Averaged line profiles of the nanoscale localization of dynamin 1,2,3 in WT vs. Syt1 KO synapses of hippocampal neurons kept at rest (b) or stimulated (c) with 80 mM KCl for 60 s. Multicolor line profiles of dynamin 1,2,3 in Syt1 WT (black) or KO (red) were aligned to the presynaptic maxima of Bassoon (blue). **(d)** Quantification of the nanoscale presynaptic levels of dynamin 1-3 in synapses from WT or Syt1 KO mice as illustrated in (b,c). Presynaptic dynamin 1-3 intensity in non-stimulated WT synapses was set to 100 %. Stimulation-induced enrichment of dynamin 1-3 is abrogated upon loss of Syt1. Syt1 WT stim = 129 ± 6 %, Syt1 KO unstim = 50 ± 2 %, Syt1 KO stim = 50 ± 8 %. Data represent mean ± SEM from N = 3 independent experiments with > 100 analyzed synapses per condition. One sample t test followed by correction for multiple testing (grey). One-way ANOVA with Tukey‘s post-test (black). **(e)** Quantification of the peri- and postsynaptic levels of dynamin 1,2,3 in synapses from WT or Syt1 KO mice as illustrated in (b,c). Dynamin 1,2,3 intensity in non-stimulated WT synapses was set to 100 %. No changes in dynamin 1-3 levels outside the AZ. Syt1 WT stim = 107 ± 12 %, Syt1 KO unstim = 71 ± 8 %, Syt1 KO stim = 66 ± 13 %. Data represent mean ± SEM from N = 3 independent experiments with > 100 analyzed synapses per condition. One sample t test followed by correction for multiple testing. One-way ANOVA with Tukey‘s post-test.

To directly link the stimulation-induced and Syt1-dependent recruitment of PIPKIγ and the presynaptic increase of $PI(4,5)P_2$ with Syt1-dependent endocytosis kinetics (compare Fig. 21e,17b,15a,b), we further stained for endocytic proteins that bind $PI(4,5)P_2$. In fact, we found dynamin 1-3, a protein crucial for the scission of SV material in form of large invaginations or SVs from the plasma membrane (Mettlen et al., 2009; Reubold et al., 2015; Shupliakov et al., 1997; Yamashita et al., 2005), to be recruited to the presynapse in a similar stimulation-dependent manner in hippocampal WT neurons (Fig. 22a-e). Peri- and postsynaptic areas did not reveal any changes in redistribution (Fig. 22e). In line with our findings for PIPKIγ, also dynamin 1-3 showed no stimulation-induced recruitment upon loss of Syt1 (Fig. 22d).

Thus, we propose that Syt1 located at the presynaptic plasma membrane recruits PIPKIγ to the periactive endocytic zone, promotes local $PI(4,5)P_2$ synthesis and thereby, favors the stimulation-induced enrichment of dynamin 1-3 to finally facilitate endocytic retrieval of SV material in form of large invaginations and hence recycling of SVs.

4.3.2 Exocytosed Syt1 recruits PIPKIγ and dynamin to the presynapse.

Following this hypothesis, surface-stranded Syt1 in hippocampal neurons from Stn2 KO mice should result in additional recruitment of PIPKIγ and thus, would explain the further elevated levels of $PI(4,5)P_2$ (compare Fig. 17b). Indeed, in hippocampal neurons from Stn2 KO mice at rest or following stimulation redistribution of Syt1 to the presynapse promoted recruitment of PIPKIγ towards the presynaptic AZ and its surrounding periactive endocytic zone (Haucke et al., 2011) (Fig. 23a,c,d). Also, quantitatively analyzing the line profiles of dynamin 1-3 revealed a similarly enhanced stimulation-induced recruitment towards the presynapse upon loss of Stn2 while recruitment of the clathrin adaptor AP2 (Fig. 23b) did not display any alterations upon stimulation in hippocampal neurons from WT mice or upon loss of Stn2 (Fig. 23a,f,g,i.j). This suggests the mechanism to act either upstream or independent of AP2. In all conditions, no alterations of PIPKIγ's, dynamin 1-3's or AP2's peri- and postsynaptic levels were observed in Stn2 KO neurons (Fig. 23e,h,k).

Results

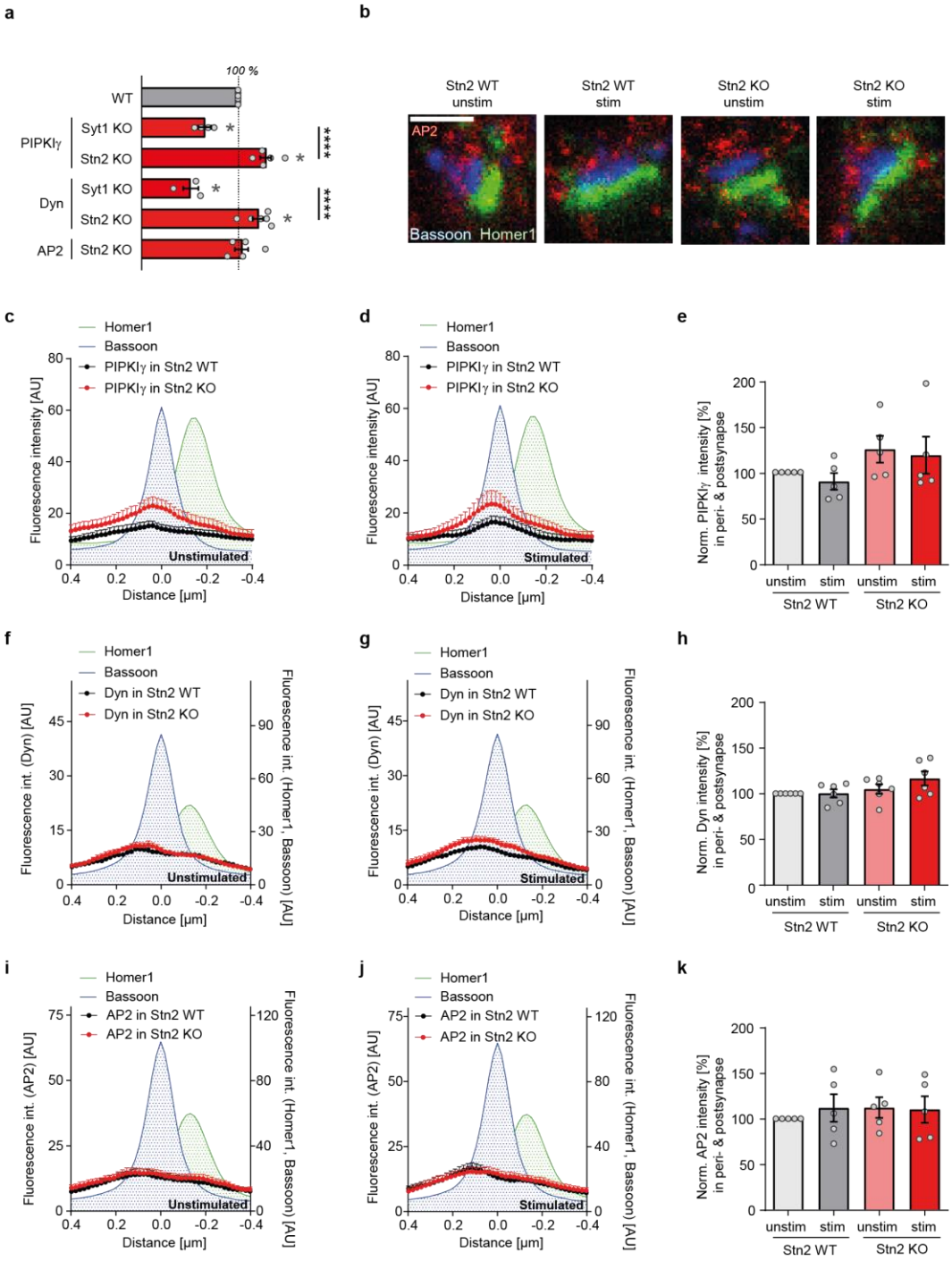

Figure 23: Exocytosed Syt1 regulates the stimulation-induced presynaptic enrichment of PIPKIγ and of dynamin 1-3.

(a) Quantification of the nanoscale presynaptic levels of PIPKIγ, dynamin 1-3 (Dyn), or AP2 in synapses post stimulation from WT, Syt1 KO, or Stn2 KO mice. Significantly reduced recruitment of PIPKIγ and dynamin 1-3 upon loss of Syt1 while surface-stranded Syt1 in Stn2 loss leads to enrichment of PIPKIγ and dynamin 1-3. AP2 recruitment is unaltered. Samples were labeled and analyzed by 3 color gSTED microscopy as described above. Data represent mean ± SEM from $N_{PIPKIγ\ in\ Syt1\ KO} = 3$, $N_{Dyn\ in\ Syt1\ KO} = 3$, $N_{PIPKIγ\ in\ Stn2\ KO} = 5$, $N_{Dyn\ in\ Stn2\ KO} = 6$, $N_{AP2\ in\ Stn2\ KO} = 5$ independent experiments with > 100 analyzed synapses per condition. One sample t test followed by correction for multiple testing (grey). One-way ANOVA with Tukey's post-test (black). **(b)** Representative STED images of WT vs. Stn2 KO synapses of hippocampal neurons kept at rest or stimulated with 80 mM KCl for 60 s and labelled for AP2 (red), Bassoon (blue) and Homer1 (green). **(c,d)** Averaged line profiles of the nanoscale localization of PIPKIγ in WT vs. Stn2 KO synapses of hippocampal neurons kept at rest (c) or stimulated (d) with 80 mM KCl for 60 s. Multicolor line profiles of PIPKIγ in Stn2 WT (black) or KO (red) were aligned to the presynaptic maxima of Bassoon (blue).

(e) Quantification of the peri- and postsynaptic levels of PIPKIγ in synapses from WT or Stn2 KO mice as illustrated in (c,d). PIPKIγ intensity in non-stimulated WT synapses was set to 100 %. Stn2 WT stim = 94 ± 10 %, Stn2 KO unstim = 118 ± 8 %, Stn2 KO stim = 112 ± 11 %. Data represent mean ± SEM from N = 5 independent experiments with > 200 analyzed synapses per condition. One sample t test followed by correction for multiple testing. One-way ANOVA with Tukey's post-test. **(f,g)** Averaged line profiles of the nanoscale localization of dynamin 1,2,3 in WT vs. Stn2 KO synapses of hippocampal neurons kept at rest (f) or stimulated (g) with 80 mM KCl for 60 s. Multicolor line profiles of dynamin 1,2,3 in Stn2 WT (black) or KO (red) were aligned to the presynaptic maxima of Bassoon (blue). **(h)** Quantification of the peri- and postsynaptic levels of dynamin 1,2,3 in synapses from WT or Stn2 KO mice as illustrated in (f,g). Dynamin 1,2,3 intensity in non-stimulated WT synapses was set to 100 %. Stn2 WT stim = 100 ± 4 %, Stn2 KO unstim = 105 ± 6 %, Stn2 KO stim = 117 ± 8 %. Data represent mean ± SEM from N = 6 independent experiments with > 250 analyzed synapses per condition. One sample t test followed by correction for multiple testing. One-way ANOVA with Tukey's post-test. **(i,j)** Averaged line profiles of the nanoscale localization of AP2 in WT vs. Stn2 KO synapses of hippocampal neurons kept at rest (i) or stimulated (j) with 80 mM KCl for 60 s. Multicolor line profiles of AP2 in Stn2 WT (black) or KO (red) were aligned to the presynaptic maxima of Bassoon (blue). **(k)** Quantification of the peri- and postsynaptic levels of AP2 in synapses from WT or Stn2 KO mice as illustrated in (i,j). AP2 intensity in non-stimulated WT synapses was set to 100 %. Stn2 WT stim = 111 ± 14 %, Stn2 KO unstim = 112 ± 12 %, Stn2 KO stim = 111 ± 15 %. Data represent mean ± SEM from N = 5 independent experiments with > 200 analyzed synapses per condition. One sample t test followed by correction for multiple testing. One-way ANOVA with Tukey's post-test. Courtesy of Natalie Kaempf (FMP)

To study whether the stimulation- and Syt1-dependent enrichment aligns with the position in relation to the presynapse, we compared each individual enrichment pattern under stimulation related to its position in hippocampal neurons of WT mice (Fig. 24a). While PIPKIγ and dynamin 1-3 localized more distantly to the AZ upon loss of Syt1, this distance was significantly reduced in conditions of Stn2 loss where Syt1 is redistributed to the presynaptic membrane yielding higher $PI(4,5)P_2$ levels (Fig. 24a).

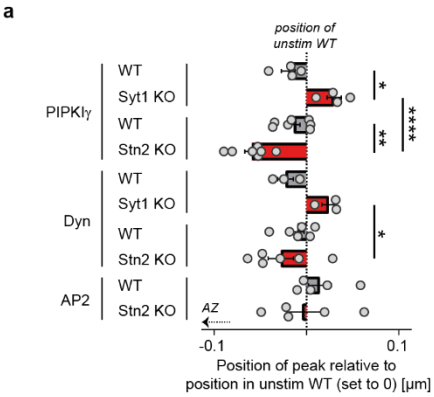

Figure 24: Relative position of PIPKIγ and Dyn towards the AZ depends on exocytosed Syt1.
(a) Localization of the max. intensity of a protein of interest post stimulation in synapses of WT or Syt1 KO or Stn2 KO hippocampal neurons in relation to its position in synapses of WT hippocampal neurons kept at rest revealing a position closer or more distant to the AZ. PIPKIγ and Dyn reveal opposite locations upon loss of Syt1 or Stn2. Loss of Syt1 results in further distances of PIPKIγ and Dyn while presynaptic Syt1 upon loss of Stn2 results in reduced distances of PIPKIγ and Dyn to the AZ, AP2 distances remained unchanged. Data represent mean ± SEM from $N_{PIPKIγ\ in\ Syt1\ KO} = 3$, $N_{Dyn\ in\ Syt1\ KO} = 3$, $N_{PIPKIγ\ in\ Stn2\ KO} = 5$, $N_{Dyn\ in\ Stn2\ KO} = 6$, $N_{AP2\ in\ Stn2\ KO} = 5$ independent experiments with > 100 analyzed synapses per condition. One-way ANOVA with Tukey's post-test.

Therefore, our data suggests exocytosed Syt1 on the presynaptic plasma membrane to directly promote local synthesis of $PI(4,5)P_2$ through nanoscale enrichment of PIPKIγ at the

periactive endocytic zone. As an effector of this Syt1-triggered local $PI(4,5)P_2$ synthesis, enrichment of dynamin 1-3 is favored in a stimulation-dependent manner and thus, facilitates the kinetics of SV endocytosis.

4.3.3 PIPKIγ restores defective SV endocytosis upon loss of Syt1.

PIPK1γ is inefficiently recruited to the plasma membrane upon loss of Syt1 (compare Fig. 21c). Following this notion, we hypothesize that overexpression of catalytically active PIPKIγ should recover delayed endocytic retrieval in Syt1-depleted neurons. Indeed, impaired kinetics of SV endocytosis in Syt1-depleted neurons were fully restored upon overexpression of active but not catalytically inactive PIPKIγ (Krauss et al., 2006) (Fig. 25a-c).

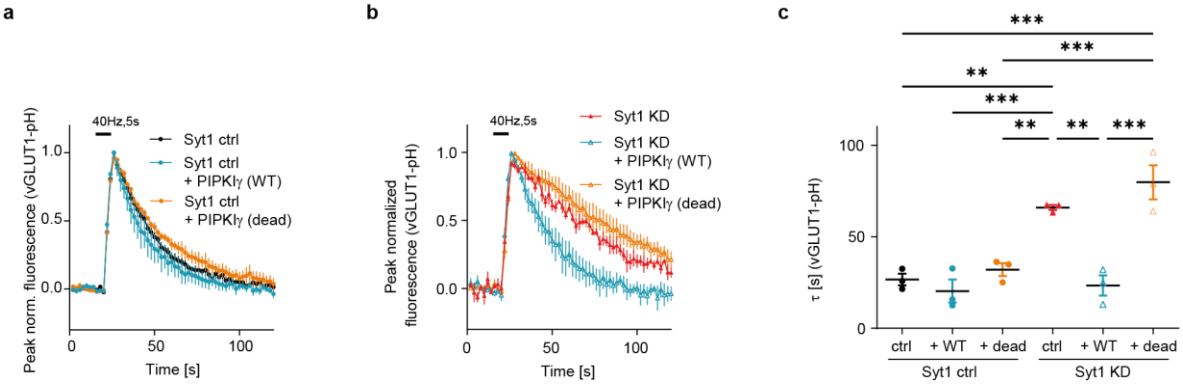

Figure 25: Catalytically active PIPKIγ restores defective SV endocytosis in Syt1 depleted neurons.
(a) Average normalized vGLUT1-pHluorin fluorescence traces of stimulated (200 APs, 40 Hz) hippocampal neurons lentivirally transduced with control (Syt1 ctrl) and subsequently transfected with empty vector or vector encoding PIPKIγ or catalytically inactive mutant PIPKIγ (dead). Data represent mean ± SEM from N = 3 independent experiments with > 250 analyzed boutons per condition. **(b)** Overexpression of active PIPKIγ rescues defective SV endocytosis in Syt1-depleted neurons. Average normalized vGLUT1-pH fluorescence traces of stimulated (200 APs, 40 Hz) Syt1-depleted (Syt1 KD) hippocampal neurons transfected with empty vector or vector encoding active PIPKIγ or inactive mutant PIPKIγ (dead). Data represent mean ± SEM from N = 3 independent experiments with > 250 analyzed boutons per condition. **(c)** Endocytic decay time constants (τ) of data shown in (a,b). $\tau_{Syt\ ctrl}$ = 27 ± 3 s, $\tau_{Syt1\ ctrl\ +\ PIPKI\gamma\ (WT)}$ = 20 ± 6 s, $\tau_{Syt1\ ctrl\ +\ PIPKI\gamma\ (dead)}$ = 32 ± 4 s, $\tau_{Syt1\ KD}$ = 66 ± 1 s, $\tau_{Syt1\ KD\ +\ PIPKI\gamma\ (WT)}$ = 23± 6 s, $\tau_{Syt1\ KD\ +\ PIPKI\gamma\ (dead)}$ = 80 ± 9 s. One-way ANOVA with Tukey's post-test. * $p < 0.05$, ** $p < 0.01$, *** $p < 0.001$.

These data further support the idea that exocytosed Syt1 triggers local $PI(4,5)P_2$ synthesis at the periactive endocytic zone via PIPKIγ recruitment and thereby, facilitates dynamin-mediated SV endocytosis.

4.4 Syt1 interacts with PIPKIγ to drive endocytosis.

While PIPKIγ is less efficiently recruited to endocytic sites in absence of plasma membrane-localized Syt1, Syt1 surface stranded due to loss of its sorting adapter Stn2 lead to increased recruitment of PIPKIγ. This provokes the question whether Syt1 associates with PIPKIγ and thus, acts as an intrinsic surrogate measure of SV exocytosis to regulate PIPKIγ recruitment.

4.4.1 Syt1 interacts with PIPKIγ through its C2B domain in a calcium-independent conserved manner.

To test this hypothesis, we performed co-immunoprecipitation of native endogenous Syt1 with PIPKIγ from synaptosomes, which were obtained from rat brain by detergent-based lysis and purification. In the presence of calcium, we found Syt1 and PIPKIγ to co-immunoprecipitate (Fig. 26a). To narrow down the interaction site within Syt1 and to evaluate any conservation of the association, we performed pull-down assays with either GST, GST-bound Syt1 C2A, its C2B domain or alternative C2B domains of Syt2, 7 or 9. The different Syts were chosen for their range in characteristics and function. Syt2 was selected due to its Syt1 related function as a low affinity Ca^{2+} sensor, Syt7 as a high affinity Ca^{2+} sensor with role in asynchronous release and Syt9 as a brain-expressed Syt-family member for which a function has so far only been found in neuroendocrine cells. Interestingly, the cytoplasmic C2B domain of Syt1 but not its C2A domain was able to affinity-capture PIPKIγ from brain lysates. Binding of the C2B domains of Syt2, 7 and 9 indicated that the binding mode is conserved across the Syt-family members (Fig. 26b).
Testing the affinity of closely related C2 domains of Synaptotagmin-related proteins such as Extended Synaptotagmin (ESyt) 2 C2C (Fig. 26c) to PIPKIγ confirmed a rather conserved interaction potential.
However, the interaction might still be mediated by other proteins present in brain lysates. To probe a direct association and test its dependence on calcium, we purified recombinant his_{10}-tagged PIPKIγ from insect cells with which we repeated the pull-down assay with either GST, GST-bound Syt1 C2A or its C2B domain in presence of calcium or EGTA. The observed interaction of Syt1 and PIPKIγ confirms our hypothesis of a direct association of the two proteins. Interestingly, the C2B domain of Syt1 captured recombinant PIPKIγ irrespective of the presence or absence of calcium (Fig. 26d). This suggests that the calcium dependence of the interaction observed upon co-immunoprecipitation of Syt1 and PIPKIγ *in*

situ (compare Fig. 26a) may rather be caused by regulatory pathways than directly impacting the complex formation of Syt1 and PIPKIγ.

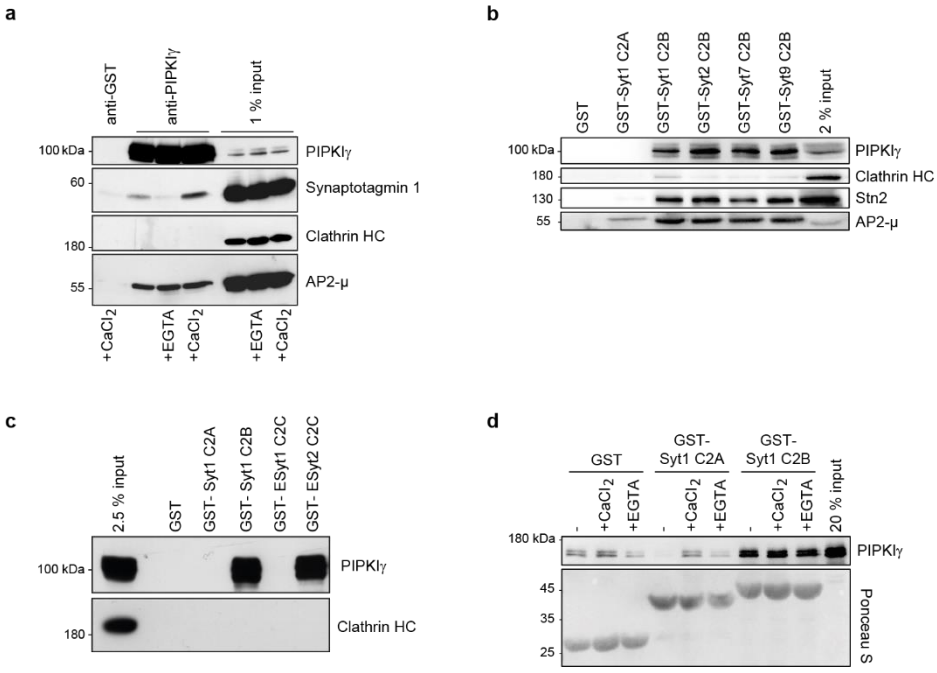

Figure 26: Conserved interaction of Syt C2B to PIPKIγ
(a) PIPKIγ co-immunoprecipitates with Syt1 from rat brain synaptosomes. Detergent-lysed rat brain synaptosomes were subjected to immunoprecipitation using rabbit antibodies against PIPKIγ. Anti-glutathione-S-transferase (GST) antibodies were used as control. Lysates were left untreated or supplemented with 5 mM EGTA or 200 µM $CaCl_2$. The affinity-purified material was analyzed by immunoblotting for the indicated proteins. Clathrin HC (clathrin heavy chain) and AP2-µ serve as negative and positive controls. Input: 1 % of rat brain synaptosomal extract used as starting material. Molecular weight markers (in kDa) are indicated on the left. Courtesy of Michael Krauss (FMP) **(b)** Conserved Syt/ PIPKIγ complex formation. Immunoblot analysis of material affinity-purified from mouse brain extracts using immobilized GST, GST-fused Syt1 C2A domain (Syt1 C2A), Syt1 C2B, Syt2 C2B, Syt7 C2B, or Syt9 C2B as baits. Clathrin heavy chain (HC) was used as negative control. PI(4)P 5-kinase type Iγ (PIPKIγ) and Stonin 2 (Stn2) were detected. Input: 2 % of mouse brain extract used as starting material. Molecular weight markers (in kDa) are indicated on the left. **(c)** Conserved C2 domain/ PIPKIγ complex formation. Immunoblot analysis of material affinity-purified from mouse brain extracts using immobilized GST, GST-fused Syt1 C2A domain (Syt1 C2A), Syt1 C2B, Extended-Syt1 (ESyt1) C2C or ESyt2 C2C as baits. Clathrin heavy chain (HC) was used as negative control. PIPKIγ was detected. Input: 2.5 % of mouse brain extract used as starting material. Molecular weight markers (in kDa) are indicated on the left. Courtesy of Michael Krauss (FMP)**. (d)** Direct Syt1/ PIPKIγ complex formation is not Ca^{2+} dependent in vitro. Immunoblot analysis of affinity purified His_{10}-PIPKIγ and immobilized GST, GST-fused Syt1 C2A domain (C2A) or C2B domain (C2B) as baits in presence of $CaCl_2$ (200 µM) or EGTA (5 mM). PIPKIγ interactions were detected. Ponceau S staining is shown as a loading control. Input: 20 % of purified His_{10}-PIPKIγ used as starting material. Molecular weight markers (in kDa) are indicated on the left.

4.4.2 Syt1/ PIPKIγ complex formation is required for SV endocytosis.

The association of Syt1 with PIPKIγ may be of fundamental importance for the SV cycle. Following this idea, Syt1 lacking its ability to bind to PIPKIγ should lead to impaired SV kinetics. Therefore, we replaced Syt1 with its mutant lacking the C2B domain. To check whether loss of PIPKIγ binding influences the kinetics of vGLUT1-pHluorin retrieval we

performed the pHluorin-based functional analysis with the Syt1 mutant lacking the C2B domain. The Syt1 mutant lacking its C2B domain exerted a mild dominant-negative effect on the rate of SV retrieval (Fig. 27a) and completely lost its ability to restore defective SV endocytosis of vGLUT1-pHluorin in Syt1-depleted neurons (Fig. 27b,c).

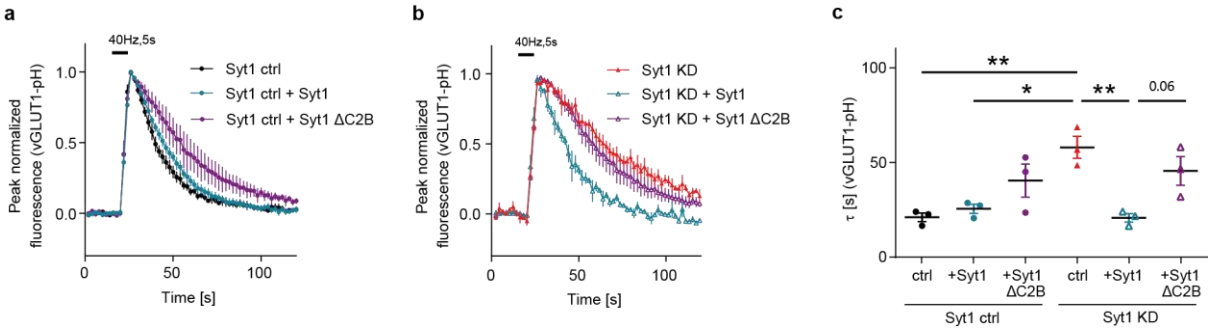

Figure 27: Syt1/ PIPKIγ complex formation is indispensable for endocytosis.
(a,b) C2B-mediated Syt1/ PIPKIγ complex formation is required for SV endocytosis. Average normalized vGLUT1-pHluorin fluorescence traces of stimulated (200 APs, 40 Hz) control (Syt1 ctrl) (a) or Syt1-depleted (Syt1 KD) (b) lentivirally vGLUT1-pH transduced hippocampal neurons transfected with empty vector (ctrl) or vectors encoding WT Syt1 or Syt1 mutant lacking its C2B domain (Syt1 ΔC2B). Data represent mean ± SEM from N = 3 independent experiments with > 250 analyzed boutons per condition. **(c)** Endocytic decay time constants (τ) of data shown in (a,b). Data represent mean ± SEM from N = 3 independent experiments with > 250 analyzed boutons per condition, One-way ANOVA with Tukey's post-test.

This suggests that the physical association of Syt1 and PIPKIγ is crucial for initiating SV retrieval.

4.4.3 Alignment of C2 binding and non-binding domains reveal potential interaction site.

The C2B domain of Syt1 possesses general interaction sites for many proteins belonging to the endocytic machinery. Loss of the entire domain may therefore impair other functions and hence can only partially verify the importance of Syt1/ PIPKIγ interaction. Therefore, our aim was to unravel Syt1's precise binding site for PIPKIγ. Using our knowledge on PIPKIγ binding and non-binding C2 domains, we aligned their sequences according to their binding ability (Fig. 28a). The alignment of the core of PIPKIγ-binding C2 domains of Syt1, 2, 7, and 9 compared to the core of non-PIPKIγ-binding Syt1-C2A and ESyt1-C2C domains identified two potential interaction sites for PIPKIγ within the C2B domain of Syt1. Since K326 (green) had already been identified as important for the process of calcium-independent lipid binding, we focused on the arginine (magenta) at the position 322 for our further studies. Besides the conservation, R322's exposed orientation makes it a promising candidate (Fig. 28b).

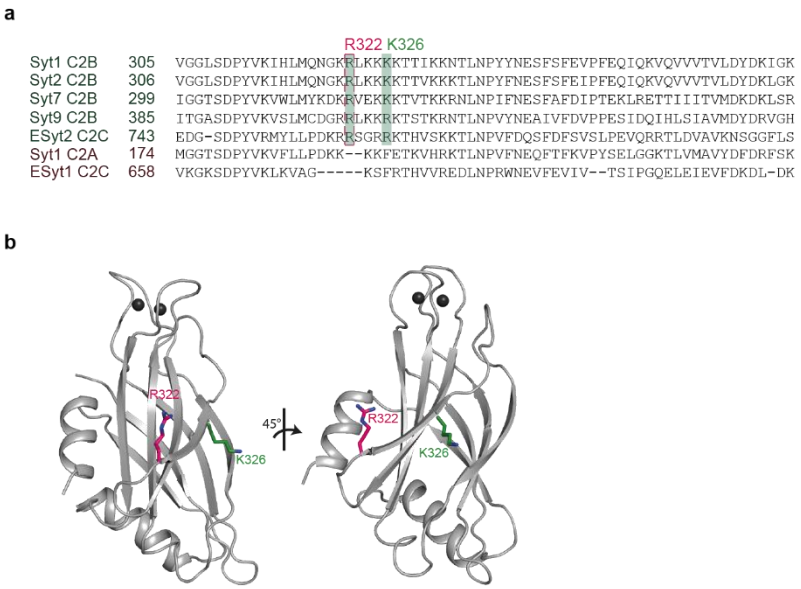

Figure 28: Putative interaction site of Syt1 to bind to PIPKIγ
(a) Primary sequence alignment of PIPKIγ binding vs. non-binding C2 domains reveal putative interaction sites (magenta: R322; green: K326). Binders: Syt1 C2B, Syt2 C2B, Syt7 C2B, Syt9 C2B (Fig. 26b), and ESyt2 C2C (Fig. 26c) (dark green) vs. non-binders: Syt1 C2A and ESyt1 C2C (Fig. 26b,c) (dark red). **(b)** Ribbon diagram of the structure of the Syt1 C2B domain in its Ca^{2+} (black)-bound state (PDB: 1K5W). Conserved putative interaction sites for PIPKIγ (magenta: R322; green: K326) are highlighted.

4.4.4 Direct interaction of Syt1 C2B R322 to PIPKIγ

To test whether Syt1 C2B R322 is exclusively involved in the association and hence recruitment of PIPKIγ, we performed mutagenesis of R322E. To probe binding of Syt1 via R322 to PIPKIγ, we purified recombinant his_{10}-tagged PIPKIγ from insect cells with which we repeated the pull-down assay with either GST, GST-bound Syt1 C2A or its WT or mutated C2B domain. Mutagenesis of R322E within the C2B domain of Syt1 completely abrogated its ability to bind to PIPKIγ (Fig. 29a).

Mutagenesis of R322E within the C2B domain of Syt1 similarly failed to affinity-capture PIPKIγ from brain lysates whereas its interaction with Syt1's endocytic adaptor, Stn2, or the association with the plasma membrane SNARE protein, SNAP-25 were unaffected (Fig. 29b). This suggests R322 to be part of a specific interaction site for PIPKIγ while folding and function of the domain seems unaffected.

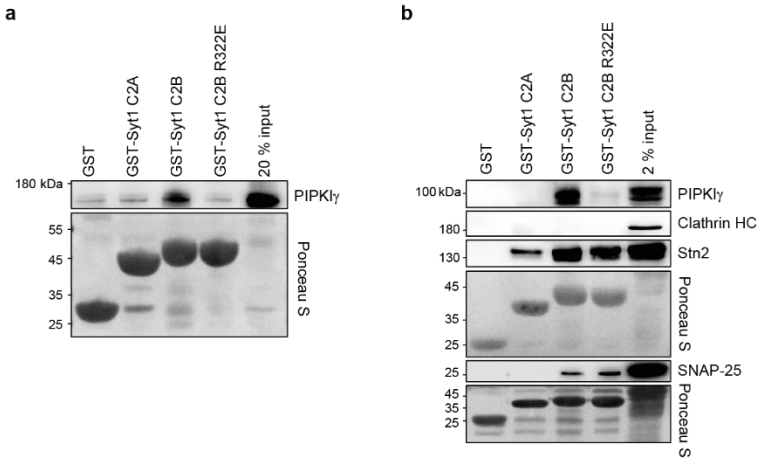

Figure 29: Complex formation of Syt1/ PIPKIγ via Syt1 C2B R322
(a) Direct Syt1/ PIPKIγ complex formation is selectively impaired by mutation of R322E in vitro. Immunoblot analysis of affinity purified His_{10}-PIPKIγ and immobilized GST, GST-fused Syt1 C2A domain (C2A), C2B domain (C2B), or R322E mutant C2B as baits. PIPKIγ interactions were detected. Ponceau S staining is shown as loading control. Input: 20 % of purified His_{10}-PIPKIγ used as starting material. Molecular weight markers (in kDa) are indicated on the left. **(b)** Mutation of R322E selectively impairs Syt1 complex formation with PIPKIγ. Immunoblot analysis of material affinity-purified from mouse brain extracts using immobilized GST, GST-fused Syt1 C2A domain (C2A), C2B domain (C2B), or R322E mutant C2B as baits. Clathrin heavy chain (HC) was used as negative control. PIPKIγ, Stonin 2 (Stn2), SNAP-25 interactions were detected. Ponceau S staining is shown as loading control. Input: 2 % of mouse brain extract used as starting material. Molecular weight markers (in kDa) are indicated on the left.

4.4.5 Loss of interaction between Syt1 and PIPKIγ leads to exclusive endocytic defect.

The biochemical data suggests Syt1 to directly associate with PIPKIγ via R322 and to recruit PIPKIγ to the periactive endocytic zone which results in generation of a local pool of $PI(4,5)P_2$ that facilitates dynamin-mediated endocytic retrieval of SV membranes post-fusion. Following this hypothesis, abrogation of the association of Syt1 and PIPKIγ should fail to restore any defect in SV kinetics observed upon loss of Syt1. Therefore, we tested the ability of Syt1 R322E, the PIPKIγ-binding-deficient mutant Syt1, to rescue impaired SV retrieval in hippocampal neurons depleted of Syt1. Monitoring vGLUT1-pHluorin, re-expression of WT Syt1 restored defective SV endocytosis under depletion of Syt1 while the PIPKIγ binding-deficient mutant Syt1, Syt1 R322E, did not rescue (Fig. 30b,c). The rate of vGLUT1-pHluorin endocytosis was unaffected upon overexpression in control hippocampal neurons (Fig. 30a).

Results

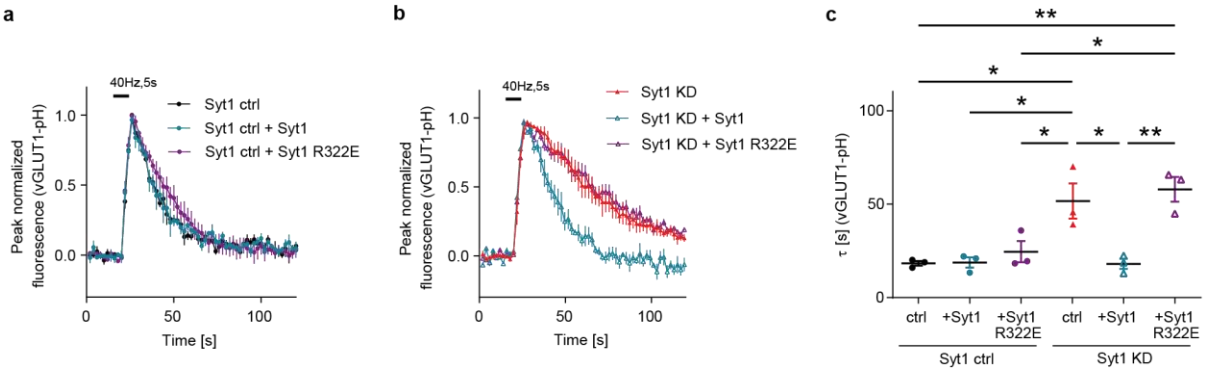

Figure 30: Complex formation of Syt1 with PIPKIγ is required for SV endocytosis.
(a) Average normalized vGLUT1-pHluorin fluorescence traces of stimulated (200 APs, 40 Hz) control (Syt1 ctrl) lentivirally vGLUT1-pH transduced hippocampal neurons transfected with empty vector (ctrl) or vectors encoding WT Syt1 or PIPKIγ-binding defective mutant Syt1 (R322E). Data represent mean ± SEM from N = 3 independent experiments with > 250 analyzed boutons per condition. **(b)** Complex formation of Syt1 with PIPKIγ is required for SV endocytosis. Average normalized vGLUT1-pH fluorescence traces of stimulated (200 APs, 40 Hz) Syt1-depleted (Syt1 KD) lentivirally vGLUT1-pH transduced hippocampal neurons transfected with empty vector (ctrl) or vectors encoding WT Syt1 or PIPKIγ-binding defective mutant Syt1 (R322E). Data represent mean ± SEM from N = 3 independent experiments with > 250 analyzed boutons per condition. **(c)** Endocytic decay time constants (τ) of data shown in (a,b). Data represent mean ± SEM from N = 3 independent experiments with > 250 analyzed boutons per condition, One-way ANOVA with Tukey's post-test. * $p < 0.05$, ** $p < 0.01$, *** $p < 0.001$.

While loss of Syt1 lead to impaired synchronous exocytic vesicle fusion, surface-stranded Syt1 in Stn2 KO neurons increased SV exocytosis. This may indicate a general defect of the entire SV cycle. Therefore, we tested whether association of Syt1 and PIPKIγ globally affects the SV cycle or rather possesses a fundamental role in coupling exocytosis with equal rates of endocytosis. Taking advantage of the pH dependency of vGLUT1-pHlourin, we calculated the surface-to-total ratio by stimulation (depicted as physiological) and final application of ammonium buffer at the end of each trace revealing the entire pool of pHluorin molecules (depicted as NH_4Cl) (Fig. 31a). We compared each surface-to-total ratio in WT or in Syt1-depleted neurons under re-expression of WT or mutant Syt1-R322E. Syt1 loss caused a significant exocytic defect. Interestingly, PIPKIγ-binding-deficient mutant Syt1 fully restored defects in synchronous SV exocytosis in neurons depleted of Syt1 (Fig. 31b). This is in line with its ability to interact with SNAP-25 (compare Fig. 29b) and indicates complex formation of Syt1 and PIPKIγ to be fundamental for SV retrieval but dispensable for SV exocytosis.

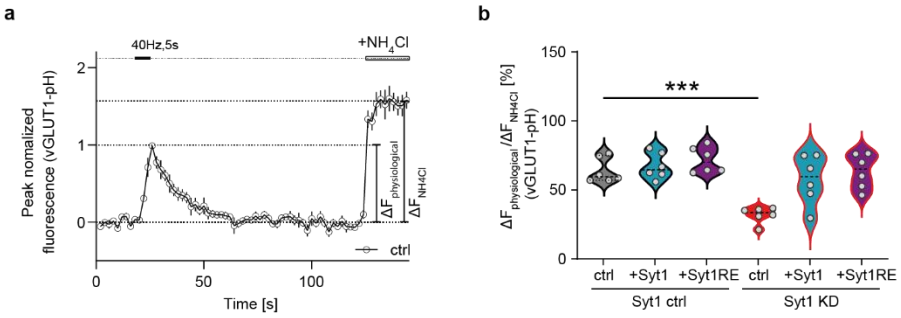

Figure 31: Syt1/PIPKIγ complex formation is dispensible for exocytosis.
(a,b) Mutant Syt1-R322E fully restored impaired synchronous exocytic vesicle fusion in Syt1 depleted neurons. Average normalized vGLUT1-pHluorin peak fluorescence traces of control (Syt1 ctrl) or Syt1-depleted (Syt1 KD) lentivirally vGLUT1-pH transduced hippocampal neurons transfected with empty vector (ctrl) or vectors encoding WT Syt1 or PIPKIγ-binding defective mutant Syt1 (R322E) upon stimulation (200 APs, 40 Hz) ($\Delta F_{physiological}$) and in response to 50 mM NH_4Cl revealing the total pool of vGLUT1-pH (ΔF_{NH4CL}). Example trace of Syt1 ctrl (a). Ratio of normalized vGLUT1-pH peak florescence amplitude following stimulation with 200 APs at 40 Hz ($\Delta F_{physiological}$) and in response to NH_4Cl (ΔF_{NH4CL}) (b). Data represent mean/ independent culture ± SEM with n = 6 independent cultures with > 125 analyzed boutons per condition, One-way ANOVA with Tukey's post-test.

Collectively, our findings identify a Syt1-based mechanism coupling SV exocytosis and SV endocytosis. Exocytosed Syt1 recruits PIPKIγ to endocytic sites which results in synthesis of a local pool of $PI(4,5)P_2$ and thus, dynamin-mediated facilitation of compensatory endocytic retrieval of SV membranes.

5 Discussion

5.1 Syt1 acts as a homeostatic measure to couple exo- and endocytosis in neurons.

SV fusion, retrieval and subsequent reformation are the basis for neuronal function and enable sustained neurotransmission (Jahn & Fasshauer, 2012; L. G. Wu et al., 2014). Multiple neurological disorders result from defects in the machinery responsible for SV exocytosis. In fact, human pathogenic mutations have been identified for all eight core components of neuronal SNAREs leading to a variety of neurodevelopmental defects. The defects range from neurodevelopmental delay manifesting in language defects or seizures to neurological motor problems such as spasms or ataxia. The severity of the disease likely correlates with functional redundancy of the affected genes (Verhage & Sørensen, 2020). Sustained neurotransmission does not only depend on SV exocytosis but also requires precisely coupled, compensatory endocytosis to maintain presynaptic homeostasis as shown by capacitance measurements and optical recordings (L. G. Wu et al., 2014). In line with this, the recycled material matches the amount of newly exocytosed SVs. Despite the finely tuned counterbalance between SV exocytosis and endocytosis, it is unlikely that the very same vesicle is exo-/ endocytosed within the same round of the SV cycle. The most compelling evidence for non-identity is that the exocytic SVs and the endocytic vesicles differ in size (Watanabe, Rost, et al., 2013) and in mildly stimulated synapses (< 50 APs) the exocytosed SV cargo tend to remain on the synaptic plasma membrane and constitute the surface pool until the next round of stimulation (Wienisch & Klingauf, 2006). It is more likely that SV material is retrieved in an activity-dependent manner via ELVs, from which SVs are subsequently clathrin-dependently reformed. Any defect in compensatory endocytosis would lead to synaptic dysfunction due to swelling of boutons and defects in SV recycling and eventually, neuronal death. Despite many proposed mechanisms coupling SV exo- and endocytosis (Haucke et al., 2011; Koch & Holt, 2012; Maritzen & Haucke, 2018; L. G. Wu et al., 2014), it remains enigmatic how the number of fused SVs is sensed at the synapse.

5.1.1 Mechanisms for coupling SV exo- and endocytosis

Plasma membrane tension is directly altered upon SV fusion and likely influences coupling of exo- and endocytosis. The lateral tension of the plasma membrane may generate an energy barrier for the endocytic machinery to overcome. In fact, increased membrane tension inhibited endocytosis (X. S. Wu et al., 2017). Tension on its own is however unlikely to account for a precise, general surrogate measure because the spatial gradient upon SV fusion equilibrates too fast to justify the spatial precision and kinetics of ultrafast endocytosis. Plasma membrane tension is likely additionally required to keep guard of the coupling process such as via recruitment of proteins implicated in membrane reformation e.g., synaptojanin, endophilin, syndapin and dynamin (Ogunmowo et al., 2023). The second messenger Ca^{2+} is another factor which is widely implicated in the processes of exo- and endocytosis but unlikely involved in precise coupling. Neuronal stimulation of Stn2 KO neurons leads to faster SV cycling kinetics but does not reveal changes in Ca^{2+} influx (Bolz et al., 2023). Similarly, the ability of Ca^{2+} influx to induce SV endocytosis is lost upon interference with acute or sustained SV exocytosis (Verhage et al., 2000; Yamashita et al., 2005). Instead, two other proposed coupling mechanisms appear more likely (Haucke et al., 2011; Koch & Holt, 2012). The fundamental components of the plasma membrane, the lipids themselves, could couple exo- and endocytosis upon triggered synthesis, e.g. of phosphatidylinositol 4,5-bisphosphate [$PI(4,5)P_2$] (Fig. 3) (Koch & Holt, 2012; Lauwers et al., 2016; Puchkov & Haucke, 2013). As a signaling lipid, $PI(4,5)P_2$ is required for SV fusion with the plasma membrane during exocytosis as well as for endocytic retrieval and likely influenced by Ca^{2+}/ calcineurin (Armbruster et al., 2013; Di Paolo & De Camilli, 2006; Hosoi et al., 2009; Posor et al., 2022; Sankaranarayanan & Ryan, 2001; Van Den Bogaart et al., 2011). Impairment of $PI(4,5)P_2$ has been linked to synapse dysfunction and neurodegeneration (Cao et al., 2017; Pan et al., 2020; Schechter et al., 2020). As an alternative coupling mechanism, exocytosed SV proteins on the plasma membrane could act as recruiting hubs for endocytic proteins and would act as rate-limiting substrates for endocytosis to operate until the conditions at steady-state have been restored (Fig. 4) (Haucke et al., 2011; Maritzen & Haucke, 2018; L. G. Wu et al., 2014).

In agreement with both coupling theories, we identify a molecular mechanism where the presynaptic SV Ca^{2+} sensor Syt1 couples SV exo- and endocytosis. Syt1 is a key factor for synchronous neurotransmission, linked to many neurodegenerative diseases (Glavan et al., 2009), and interacts with a plethora of key proteins involved in SV exo- as well as

endocytosis (Brewer et al., 2015; Chapman, 2008; Diril et al., 2006; Haucke & De Camilli, 1999; Jung et al., 2007; Zhou et al., 2015, 2017). The interaction of Syt1 with $PI(4,5)P_2$ is fundamental for SV fusion (Chapman, 2008), and loss or impairment of Syt1 results in severe and evolutionary conserved synaptic defects (Bradberry et al., 2020; Jorgensen et al., 1995; Y. C. Li et al., 2017; Nicholson-Tomishima & Ryan, 2004; Poskanzer et al., 2003, 2006) implicated in the pathophysiological mechanisms of epilepsy, Alzheimer's and Parkinson's disease (Baker et al., 2018; Glavan et al., 2009; Harper et al., 2020).

5.1.2 Molecular mechanism of Syt1-triggered synthesis of signaling lipids for coupling SV exo- and endocytosis

This work unravels the molecular mechanism of local, activity-dependent Syt1-triggered synthesis of $PI(4,5)P_2$ at the periactive zone for the nanoscale coupling of SV exo- and endocytosis. We found that in response to AP-triggered neurotransmission, exocytosed Syt1 recruits PIPKIγ to locally synthesize the signaling lipid $PI(4,5)P_2$ in an activity-dependent manner and thus promotes endocytosis (Fig. 32, left). Syt1 loss highly affects synchronous SV exocytosis and abolishes the activity-dependent recruitment of PIPKIγ and thereby, the synthesis of $PI(4,5)P_2$. Reduced $PI(4,5)P_2$ levels result in impaired recruitment of dynamin, the key endocytic protein involved in scission of SVs. Consistently, synaptic terminals reveal accumulated, stalled endocytic plasma membrane invaginations, and neurons show strongly impaired kinetics of SV endocytosis (Fig. 32, top right). Genetically elevated $PI(4,5)P_2$ via overexpression of PIPKIγ or direct supplementation of exogenous $PI(4,5)P_2$ rescues impaired SV endocytosis upon loss of Syt1. This rescue implicates that the Syt1-triggered synthesis of $PI(4,5)P_2$ is needed for the initiation of SV endocytosis. The converse situation of surface-stranded Syt1 caused by loss of Syt1's specific sorting adaptors supports the idea. Surface-stranded Syt1 lead to enhanced recruitment of PIPKIγ and hence, higher levels of $PI(4,5)P_2$, enhanced recruitment of dynamin and subsequently, facilitated SV endocytosis (Fig. 32, bottom right). Interestingly, in this situation the recruitment of AP2 is unaffected (Fig. 23a,i-k,24a). AP2 is crucial for the clathrin/ AP2 dependent budding and reformation of SVs from ELVs (Kononenko et al., 2014; Watanabe et al., 2014). The unchanged levels of AP2 indicate that AP2's action occurs downstream of initiation of SV endocytosis via Syt-triggered $PI(4,5)P_2$ synthesis. This chronology is further supported by findings with electron microscopy demonstrating a mild reduction of SV number in stimulated Syt1-depleted hippocampal synapses and more prominently, in *C. elegans*

(Jorgensen et al., 1995) as well as decreased numbers of ELVs and an increase of stalled presynaptic endocytic invaginations (Fig. 12). Correspondingly, loss of AP2 results in an accumulation of ELVs and thus represents a defect downstream of Syt1 action (Kononenko et al., 2014). Also, in light of different modes of endocytosis, in particular CME requiring AP2 at the periactive zone, unchanged, presynaptic AP2 levels independent of facilitated SV recycling argue for a predominant clathrin-independent endocytic pathway to compensate for elevated activity.

Our finding of a direct interaction between Syt1 and PIPKIγ allows us to distinguish the role of Syt1 to promote SV endocytosis from its well-established, vital role in SNARE-mediated fast synchronous neurotransmission (Jahn & Fasshauer, 2012; Kiessling et al., 2018; Xu et al., 2009; Zhou et al., 2015, 2017). We identify Syt1 to directly interact with PIPKIγ via a unique site within the C2B domain (Fig. 29). Via this specific interaction with PIPKIγ, Syt1 exclusively facilitates SV endocytosis (Fig. 30) by triggering the local synthesis of $PI(4,5)P_2$. We find the Syt1-triggered lipid synthesis of $PI(4,5)P_2$ to be directly linked to neuronal activity (Fig. 18b) and envision this molecular mechanism to sustain neurotransmission by maintaining presynaptic membrane homeostasis. Syt1 could act as a surrogate measure and the number of Syt1 molecules located on the surface would directly correlate with the number of fused SVs. By recruiting corresponding amounts of PIPKIγ, Syt1 would actively steer $PI(4,5)P_2$ synthesis for subsequent endocytosis.

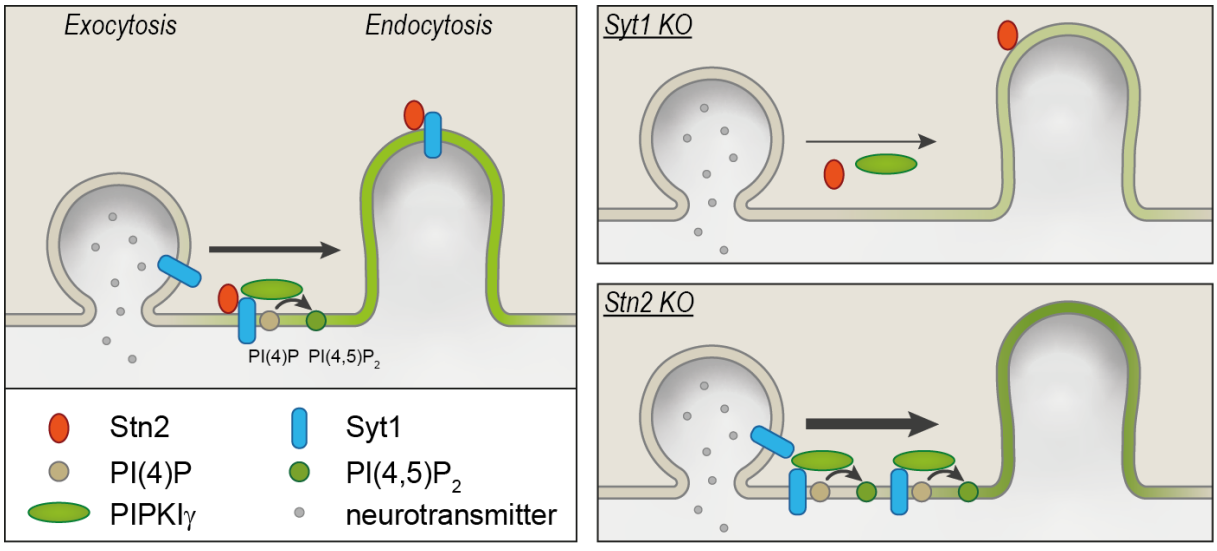

Figure 32: Syt1-triggered lipid signaling synthesis couples SV exo- and endocytosis.
Model illustrating the function of exocytosed Synaptotagmin 1 (Syt1) in the nanoscale coupling of SV exocytosis and endocytosis via complex formation with PIPKIγ and subsequent local $PI(4,5)P_2$ synthesis. Top right: In Syt1 KO synapses lack of stimulation-triggered $PI(4,5)P_2$ synthesis impairs SV endocytosis. Bottom right: Accumulation of Syt1 on the presynaptic plasma membrane facilitates SV endocytosis via exacerbated recruitment of PIPKIγ and a resulting elevation in $PI(4,5)P_2$ synthesis (Bolz et al., 2023).

Furthermore, our work finally explains the conserved SV recycling defects found upon loss of Syt1 in various studies using *C. elegans* (Watanabe, Liu, et al., 2013), *D. melanogaster* (Poskanzer et al., 2003, 2006) and mice (Nicholson-Tomishima & Ryan, 2004).

5.1.3 Syt1-triggered synthesis of signaling lipids via recruitment of PIPKIγ takes place at the periactive zone.

Our findings suggest a molecular mechanism that may help to explain how the set point of SV endocytosis is defined at the synapse. We envision Syt1 to act as a limiting resource for facilitating SV endocytosis by promoting local $PI(4,5)P_2$ synthesis at the periactive endocytic zone. At the same time it is intriguing to ask whether solely plasma membrane localized Syt1 or also vesicular Syt1 could trigger PIPKIγ recruitment and local $PI(4,5)P_2$ synthesis. The following locations for Syt1-triggered PIPKIγ recruitment are to be considered: at the SV, at the active zone of the plasma membrane or at the endocytic zone of the plasma membrane.

Our data demonstrates that it is not vesicular Syt1 as proposed by using artificial Syt1-chimeras (J. Yao et al., 2012) but surface-stranded Syt1 which facilitates SV endocytosis by promoting local $PI(4,5)P_2$ synthesis (Fig. 15, 17) (Kaempf et al., 2015). Furthermore, PIPKIγ is not enriched in the crude SV fraction upon subcellular fractionation of synapses or found on SVs via biochemical analysis (Takamori et al., 2006; Wenk et al., 2001) even though Syt1 is a prominent component of SVs. The lack of PIPKIγ recruitment to SVs could be due to the crowded environment, the high membrane curvature of SVs, missing additional recruiting factors such as the substrate itself and a potentially adverse Ca^{2+}-dependent conformational state of Syt1's C2 domains (Krauss et al., 2003; Loewen et al., 2006; Takamori et al., 2006). In line with the absence of PIPKIγ, enough product synthesized by PIPKIγ is missing on SVs. Only negligible PI levels, including $PI(4,5)P_2$, have been found on SVs (Holz et al., 2000; Takamori et al., 2006). The lack of $PI(4,5)P_2$ on SVs is in agreement with synaptojanin1-mediated dephosphorylation of $PI(4,5)P_2$ which is needed for clathrin coat disassembly during the process of SV reformation (Chang-Ileto et al., 2011; Cheung & Cousin, 2012; W. T. Kim et al., 2002; Kononenko et al., 2014; Watanabe et al., 2014). Collectively, this makes the presence and action of PIPKIγ on SVs unlikely.

Another alternative is that the Syt1-triggered PIPKIγ recruitment instead takes place on the plasma membrane. Studies indicating that soluble PIPKIγ may directly bind to plasma

membranes support a plasma membrane associated place of action. Binding may occur via direct interactions with signaling lipids as shown by substrate specificity of the activation loop. Exchanging the activation loops of type I and type II PIPK caused a switch in subcellular localization (Kunz et al., 2000). Alternatively, an intrinsic membrane-sensing mechanism by the activation loop has been proposed. Sensing may be based on a conformational change of the activation loop into an amphipathic helix (Liu et al., 2016). In either scenario, differences in the lipid composition may contribute to the preferential recruitment of PIPKIγ and promote interaction with Syt1. In addition to the interaction with Syt1, recruitment and enzymatic activity of PIPKIγ may require other plasma-membrane localized co-factors, such as small GTPases like Cdc42 or ARF6 (Di Paolo & De Camilli, 2006; Krauss et al., 2003; Posor et al., 2022). While we show a Ca^{2+}-independent, direct interaction of Syt1 and PIPKIγ in vitro (Fig. 26d,29), we demonstrate that this interaction may still be Ca^{2+}-dependently regulated (Fig. 26a). In agreement with our data, PIPKIγ is controlled in an activity-dependent manner via phosphorylation by the kinase Cdk5 and the Ca^{2+}/ calmodulin-dependent phosphatase calcineurin. Phosphorylation of PIPKIγ has been described to promote complex formation of PIPKIγ with talin, a protein linked to the presynaptic membrane (Di Paolo et al., 2002; Sang et al., 2005). As a result, PIPKIγ's ability to produce $PI(4,5)P_2$ may result from an interplay of spatially-regulated recruitment and activation at the plasma membrane.

At the plasma membrane the Syt1-triggered PIPKIγ recruitment could take place at the active zone influencing SV exocytosis or at the endocytic zone. Our data suggests that Syt1 recruits PIPKIγ to endocytic sites, to locally promote $PI(4,5)P_2$ synthesis and initiate endocytosis. We find direct evidence for this as a Syt1 mutant incapable of binding to PIPKIγ fails to restore defective SV endocytosis upon loss of Syt1 (Fig. 30) while it rescues SV exocytosis (Fig. 31). The following evidence further supports our model for Syt1-mediated PIPKIγ recruitment to endocytic sites. While $PI(4,5)P_2$ marks distinct exocytic sites (Milosevic et al., 2005), PI(4)P is enriched throughout the plasma membrane, thus represents a highly available substrate for PIPKIγ to produce $PI(4,5)P_2$ (T. Balla, 2013; Di Paolo & De Camilli, 2006; Posor et al., 2022; Wenk et al., 2001). Another argument for the recruitment of PIPKIγ to nascent endocytic sites may solely result from SV exocytosis requiring less $PI(4,5)P_2$. Compared to SV endocytosis where SV material is stimulation-dependently retrieved, the release sites at the active zone where SV dock, prime and eventually fuse in a $PI(4,5)P_2$-dependent manner are limited. They are precisely located in relation to the voltage gated Ca^{2+} channel because the action potential-induced Ca^{2+} influx

is spatially restricted to a microdomain of ~ 100nm radius around each voltage gated Ca^{2+} channel (Michel et al., 2015; Walter et al., 2018). Additionally, in contrast to endocytosis where soluble proteins are PI(4,5)P_2-dependently recruited to fulfill retrieval, minimal amounts of soluble proteins need to be recruited for SV exocytosis. This may suggest a stoichiometrically reduced need of PI(4,5)P_2 during SV exocytosis. Furthermore, a sterically unfavorable conformation of Syt1 on SVs or during SV exocytosis could potentially hinder PIPKIγ recruitment. Syt1's putative circular oligomerization may prepare SVs for fusion by acting as a calcium-dependent clamp for SV fusion and thus, locking SVs in a loose, docked state (Y. Chen et al., 2021; J. Wang et al., 2017; Zanetti et al., 2016). To initiate the subsequent fusion process, Syt1 may penetrate the plasma membrane through canonical insertion of its C2 domain into the plasma membrane and may thereby contribute to the required membrane bending for fusion (Gruget et al., 2020; Hui et al., 2009). Its consecutive binding to the SNARE machinery may then trigger fusion (Chicka et al., 2008; Guan et al., 2017; Zhou et al., 2015, 2017). After fusion, Syt1 may dissociate from the SNAREs revealing a surprisingly slow diffusion rate similar to other SV proteins e.g., Syp and Syb2 (Gimber et al., 2015). Slow diffusion may be caused by pre-assembled SV proteins which could act as diffusion barriers e.g., via clusters including transmembrane proteins (Bennett et al., 1992; Jia et al., 2006). This collectively supports our model of Syt1-triggered PIPKIγ recruitment at the periactive endocytic zone for facilitating SV endocytosis by promoting local PI(4,5)P_2 synthesis.

While we exclude the possibilities that PIPKIγ directly acts on SVs or alternatively impacts the process of exocytosis at the active zone, we can only speculate about a potential action on endosome-like vacuoles. Upon loss of Syt1, we find increased, stalled endocytic plasma membrane invaginations, correspondingly less ELVs and less similar-sized SVs (Fig. 12f-g) indicating a very early endocytic defect. Our data demonstrates that this SV endocytic defect is rescued by full length Syt1, but not by the single mutant incapable of binding PIPKIγ (Fig. 30). Yet, PI(4,5)P_2 is needed during the process of clathrin/ AP2 mediated SV reformation (Antonescu et al., 2011; Chang-Ileto et al., 2011; Rohde et al., 2002). Although we show stimulation-dependent PI(4,5)P_2 clusters within the presynaptic bouton (Fig. 18c), due to methodological limitation and the restricted spatial resolution we cannot preclude an additional role of PIPKIγ during SV reformation from ELVs.

Similarly, whether the Syt1-triggered PI(4,5)P_2 synthesis takes place prior, during or after SV protein sorting needs to be further addressed. If the proposed molecular mechanism which we believe to be highly phosphorylation-dependent takes place alongside SV protein

sorting, then phosphorylation-dependent interactions during the process of SV protein sorting might be able to act as a local finetuning tool. For example, phosphorylation of SV2 by CK1 family kinases positively controls Syt1-SV2 interaction (N. Zhang et al., 2015). Local regulation of the Syt1-triggered $PI(4,5)P_2$ synthesis via SV protein sorting is further supported by the fact that SV protein adaptors, such as Stn2 or SV2 as specific adaptors for Syt1, have no essential role in initiating SV endocytosis itself but regulate Syt1 abundance on the plasma membrane (Kaempf et al., 2015).

5.1.4 The interaction of Syt1 to PIPKIγ acts as a homeostatic trigger.

Another question is how the set point for SV endocytosis is defined. We envision that increased levels of exocytosed Syt1 on the plasma membrane recruit PIPKIγ to produce $PI(4,5)P_2$ and thus modulate SV endocytosis via dynamin. The presence of Syt1 on the plasma membrane would therefore be proportional to the amount of recruited PIPKIγ. Interestingly, intrinsic properties of the interaction site may further regulate the mechanism. Small amounts of $PI(4,5)P_2$ alongside the presence of PI(4P) could feedforward its synthesis as PIPKIγ may enhance its binding efficiency to its substrate through putative sensing of substrates via its activation loop (Kunz et al., 2000; Liu et al., 2016). The PIPKIγ binding site within the C2B domain of Syt1 (R322) is in close proximity to that of $PI(4,5)P_2$ (K326, K327). Although it is non overlapping at the amino acid level (Fig. 28a), it is conceivable that a local rise in $PI(4,5)P_2$ could eventually displace PIPKIγ from Syt1 restoring plasma membrane homeostasis. Therefore, Syt1 may act as a direct measure for the number of fused SVs as well as a homeostatic sensor coupling SV exo- and endocytosis. Local plasma membrane curvature leading to the exposure of charges may further contribute to this process.

Syt1's-specific sorting adaptors, AP2 and Stn2, similarly possess binding sites that are in close proximity to the one of PIPKIγ (Haucke et al., 2000; Haucke & De Camilli, 1999; Jarousse & Kelly, 2001; Jung et al., 2007). However, they do not directly contribute to SV endocytosis but promote the endocytic removal of Syt1 from the plasma membrane (Kaempf et al., 2015; Kononenko et al., 2013; Maritzen et al., 2010; Mullen et al., 2012). The plasma membrane retrieval seems to be primarily mediated in a clathrin-independent manner as shown by genetic manipulations of clathrin and AP2 (Kononenko et al., 2014; Soykan et al., 2017), electron microscopy (Watanabe, Liu, et al., 2013; Watanabe, Rost, et al., 2013) and

quantitative analysis of adaptor molecules (Mori & Takamori, 2018; Wilhelm et al., 2014). Absence of Syt1 results in an early endocytic defect characterized by increased presynaptic plasma membrane invaginations, and a reduced number of ELVs and SVs. Due to unchanged sizes of SVs, the defect appears to be independent and hence may be upstream of AP2 function (Fig. 23a,i-k,24a).

Nonetheless, potential downstream functions during SV reformation by clathrin/ AP2-mediated budding as well as during SV protein sorting via e.g., Stn2, could be mediated by interaction site competition (Kononenko et al., 2014; Watanabe et al., 2014). In this context, adaptor proteins such as AP2 are recruited in a $PI(4,5)P_2$-dependent manner (Collins et al., 2002; Rohde et al., 2002). AP2 has been linked to PIPKIγ recruitment and activation in the context of clathrin-dependent retrieval (Krauss et al., 2006; Nakano-Kobayashi et al., 2007). It is not unlikely that AP2 occludes PIPKIγ binding to Syt1 and instead stabilizes and facilitates endocytosis by driving $PI(4,5)P_2$-dependent budding until the clathrin-coat displaces the PIPKIγ interaction (Thieman et al., 2009).

A further question relates to the structural complexity of the interaction. Our model simplistically depicts Syt1 as an interactor of PIPKIγ. The PIPKIγ-Syt1 complex formation could promote an enzymatically beneficial orientation of the kinase in relation to the plasma membrane. Furthermore, PIPKs have been suggested to act as dimers which may regulate activity and collaboratively influence substrate binding. Although dimer arrangement and the distribution of positive charges differs between PIPKs, the orientation of its active site in relation to the associated plasma membrane seems conserved. Doubling the basic surface area upon dimerization could increase binding affinity to the membrane and kinase activity by mechanisms similar to allosteric regulation (Hansen et al., 2022; Hu et al., 2015). Along the same lines, oligomerization as well as cooperation of the two tandem C2 domains of Syt1 appear to be required for spatiotemporally-regulated SV exocytosis (Y. Chen et al., 2021; Fuson et al., 2007; Y. Lai et al., 2015; McDonald et al., 2015; J. Wang et al., 2017). For its function in SV endocytosis, the importance of structural cooperativity remains enigmatic. While we did not identify the interaction site within the sequence of PIPKIγ, we discovered PIPKIγ to bind to Syt1's C2B domain, precisely at position R322, in a conserved manner (Fig. 26b,28a,b,29). In agreement with studies demonstrating PIPKIγ dimerization, a structure of dimerized Syt1 C2AB surprisingly reveals both C2B domain-amino acid residues implicated in PIPKIγ binding to be presented in a sterically beneficial manner in the same plane (Fig. 33). This could potentially suggest that dimerized C2AB domains of Syt1

may assist in the recruitment and stabilization of dimerized PIPKIγ and hence, putatively could contribute to beneficial enzyme orientation for synthesizing $PI(4,5)P_2$.

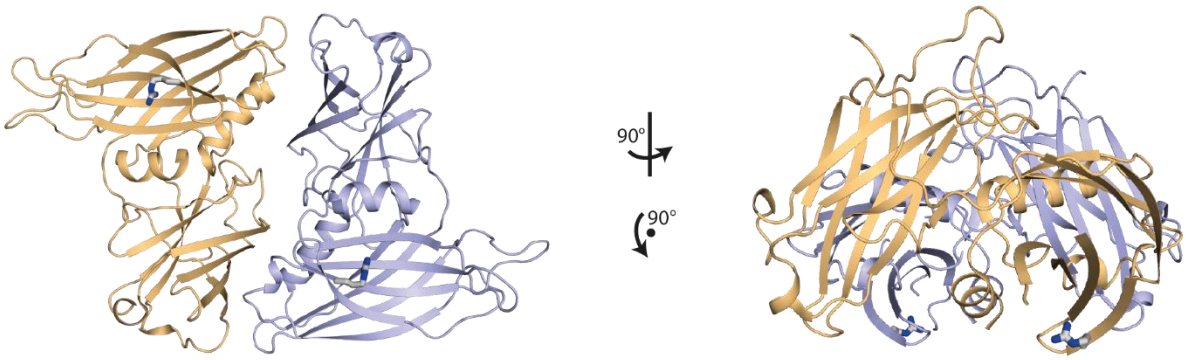

Figure 33: Structure of dimerized Syt1 C2AB potentially allosterically regulating PIPKIγ recruitment and activity
Structure of dimerized Syt1 C2AB (monomers in yellow and purple) reveals the amino acid residues implicated in PIPKIγ binding of both C2B domains in complex (R322 in grey) to be sterically beneficially presented in the same plane. Dimerized Syt1 may thus assist in the recruitment and stabilization of dimerized PIPKIγ at the plasma membrane in an allosterically regulated manner and hence, putatively contribute to enzyme activity.

5.1.5 Activation of PIPKIγ is a critical step for Syt1-triggered synthesis of signaling lipids.

For correct enzymatic function, spatiotemporally regulated subcellular recruitment and enzymatic activation must be coordinated. As an enzyme, PIPKIγ is spatiotemporally activated via different means to presumably produce local concentrations of $PI(4,5)P_2$. Most commonly, enzyme activation is achieved via modifications such as phosphorylation/ dephosphorylation or through interaction with modulators. Activity-dependent dephosphorylation of PIPKIγ and synaptojanin by Ca^{2+}/ calmodulin-dependent calcineurin regulates $PI(4,5)P_2$ turnover and thus neurotransmission in the synapse (Lee et al., 2004; Nakano-Kobayashi et al., 2007). Furthermore, Ca^{2+} binding to Syt1 may trigger conformational changes which are implicated in SNARE complex assembly, SV exocytosis as well as endocytosis (J. Yao et al., 2012; Zhou et al., 2017). Even though we show that Syt1 directly binds to PIPKIγ independent of its state of activation (Fig. 29a), we demonstrate that this interaction may be regulated in a Ca^{2+}-dependent manner (Fig. 26a). This indicates that Ca^{2+} may potentiate PIPKIγ's enzymatic activity. Although SV exo- and endocytosis are not exclusively coupled via Ca^{2+}, the second messenger Ca^{2+} regulates SV

recycling on multiple levels and could activate PIPKIγ in a stimulation-dependent manner to locally generate $PI(4,5)P_2$.

Further small GTPases, such as Rho/Rac or the ADP-ribosylation factor ARF6, may be involved in activation of PIPKIγ. Rho/Rac regulate neurite remodeling via $PI(4,5)P_2$-dependent actin polymerization and Rac1's GTP-independent interaction with PIP5K has been implicated in this process (van den Bout & Divecha, 2009). Similarly implicated in membrane trafficking, actin dynamics and SV recycling is ARF6. Activation of ARF6-GTP stimulates PIPKIγ to facilitate SV endocytosis (Krauss et al., 2003). The activation of PIPKIγ is accompanied by the presence of phosphatic acid (PA) (Moritz et al., 1992). PA itself has been shown in vitro to stimulate PIP5K activity as well as regulate its PI4P affinity (Jarquin-Pardo et al., 2007). PA is generated via $PI(4,5)P_2$-activated phospholipase D (PLD) hydrolyzing phosphatidylcholine (PC) or alternatively, via $PI(4,5)P_2$-binding diaglycerol kinase (DGK) phosphorylating diaglycerol (DAG), a product of $PI(4,5)P_2$ hydrolysis. ARF6 has thus been proposed to regulate enzymatic activity of both, PIP5K and PLD. The PLD-generated PA activates PIP5K and the PIP5K generated $PI(4,5)P_2$ again activates PLD. ARF6 may thus initiate a feedforward loop for PA and $PI(4,5)P_2$ synthesis (van den Bout & Divecha, 2009).

Furthermore, in vitro PI has been shown to stimulate autophosphorylation of PIP5K itself (Itoh et al., 2000) while phosphorylation of Src/ cyclin-dependent kinase 5 (Cdk5) positively/ negatively regulates the interaction of talin and PIP5K (Lee et al., 2005; T. C. Tan et al., 2003). Whether Cdk5 directly influences Syt1-PIPKIγ binding or indirectly upon phosphorylation and thus via protein associations is however unclear.

5.1.6 Influence of precursors or substrates on the kinetics of signaling lipid synthesis

How presence of products and substrates control the rate of local $PI(4,5)P_2$ synthesis and thus influence SV exo-endocytic coupling remains enigmatic. $PI(4,5)P_2$ and correspondingly, also PIPKIγ are predominantly localized to the plasma membrane and not enriched in the crude SV fraction (Takamori et al., 2006; Wenk et al., 2001). However, it is unclear how PI(4)P, the substrate for $PI(4,5)P_2$ synthesis by PIPKIγ, is regulated. Either the steady-state plasma membrane pool of PI(4)P or an additional supply of PI(4)P upon fusion of phosphatidylinositol 4-kinase II (PI4K) containing SVs (Guo et al., 2003) may modulate synthesis of $PI(4,5)P_2$ during SV exo- and endocytosis. PI4K is mainly implicated in cellular

traffic and Golgi functions, yet has been demonstrated to also mediate plasma membrane PI(4)P synthesis in non-neuronal cells (A. Balla & Balla, 2006; J. Tan & Brill, 2014). Accordingly, loss of PI4K depleted the plasma membrane pool of PI(4)P and $PI(4,5)P_2$ in mouse embryonic fibroblasts (MEFs) (Nakatsu et al., 2012). In contrast, acute depletion of plasma membrane localized PI(4)P did not affect $PI(4,5)P_2$ levels (G. R. V Hammond et al., 2012). The unchanged $PI(4,5)P_2$ levels suggest that either the steady-state plasma membrane pool of PI(4)P is sufficient or PI(4)P is supplied in an activity-dependent manner upon SV fusion. Our own data reveals elevated PI(4)P levels upon strong stimulation, yet unchanged PI(4)P levels upon facilitated SV recycling (Bolz et al., 2023) and indicates that it likely is an interplay of both, steady-state pool as well as PI(4)P delivered by SV fusion.

$PI(4,5)P_2$ turnover needs to be tightly spatiotemporally controlled. While substrate availability is important for generation of $PI(4,5)P_2$, its hydrolysis generating other lipid species such as DAG and PA may further influence its turnover. The turnover of $PI(4,5)P_2$ to generate DAG and inositoltrisphosphate [IP_3] is mediated by phospholipase C (Di Paolo & De Camilli, 2006). DAG can in turn be phosphorylated by DAG kinase (DGK) resulting in the production of PA. This has been linked to defects in SV exocytosis. PA affects the activity of the AZ-associated SV priming factor Munc13 and protein kinase C (PKC) which subsequently leads to phosphorylation of Munc18 and SNAP-25 (Lauwers et al., 2016). Furthermore, DAG/ PA conversion appears to facilitate SV endocytosis and hence may be implicated in SV exo-endocytic coupling. PA is a crucial co-factor for PIP5K-mediated $PI(4,5)P_2$ synthesis and facilitates SV retrieval in neurons dependent on enzymatic activity of DGK (Di Paolo & De Camilli, 2006; Goldschmidt et al., 2016). Although regulation and coordination of synaptic activity is largely unknown, the data clearly suggests an interplay of PIP metabolism and DAG/PA cycle (Maritzen & Haucke, 2018). This interplay could be mediated by Syt1. Interestingly, Syt1 has previously been shown to interact with DGK and to increase its activity by 10-fold (Barber et al., 2022). Syt1 may thus have a dual role in (I) regulating PIP metabolism upon interaction with PIPKIγ for initiating SV endocytosis and (II) modulating the DAG/PA cycle. Syt1 could be implicated in producing local pools of $PI(4,5)P_2$/ PA and thereby, generate spatially-controlled membrane curvatures. Upon Syt1-triggered $PI(4,5)P_2$ synthesis, the plasma membrane could be positively bent which is favorable for plasma membrane invaginations, or Syt1-triggered PA synthesis might lead to negative curving beneficial for SV budding. However, lateral diffusion of $PI(4,5)P_2$ or of PA within the plasma membrane is too rapid to allow the generation of local pools exclusively via enzyme activity. Instead, lateral diffusion barriers would be needed to restrict diffusion

and allow the generation of local accumulations. It is thus intriguing to think that SV protein clusters comprising transmembrane proteins e.g., Syt1's specific sorting adaptor SV2, could present such diffusion barriers (Bennett et al., 1992; Jia et al., 2006). These SV protein barriers could prevent $PI(4,5)P_2$ which is locally synthesized upon Syt1 accumulation from diffusing away counteracting a dilution of its local action. The local boundaries would result in local enrichments similar to those we visualize for $PI(4,5)P_2$ in a stimulation-dependent manner (Fig. 18c).

Additionally, local $PI(4,5)P_2$ enrichments could lead to the recruitment of important endocytic factors forming "endocytic hubs" such as proposed for vGLUT1 and Syt1 (Koch & Holt, 2012; Pan et al., 2015). As an important player of SV endocytosis, loss of vGLUT1 delayed SV endocytosis (Pan et al., 2015). Interestingly, vGLUT1's putative N-terminal amphipathic helix may be implicated in vGLUT1's endocytic function. Our preliminary data suggests that loss of the amphipathic helix similarly results in endocytic defects (Appendix Fig. 34a,b). Chimeric substitution of this helix with the amphipathic helix of vGAT, the vesicular GABA transporter and analog of vGLUT1 in inhibitory neurons, as well as with the synthetic amphipathic helix Hecate rescued this defect (Appendix Fig. 34a,b). The rescue of the chimeras indicates that the endocytic function of vGLUT1 may be due to a putative amphipathic helix sensing local $PI(4,5)P_2$ enrichments such as those Syt1-dependently generated. Future studies should verify this in vGLUT1 KD experiments (Appendix Fig. 34c,d). Despite the background of endogenous protein in our preliminary experiments, vGLUT1 may possess advantages in detecting $PI(4,5)P_2$-positive endocytic hubs aiding favorable localization and putative function in endocytosis. In the context of Syt1's function in the SV cycle, this may be able to explain the slightly more prominent SV kinetic defect we visualized with vGLUT1- over Syp-pH (Fig. 8,9,13,14).

5.2 Syt1-triggered signaling lipid synthesis beyond the scope of SV exo- and endocytosis

5.2.1 Syt1-triggered lipid signaling synthesis as a general mechanism in coupling SV exo- and endocytosis

To maintain presynaptic integrity, sustained neurotransmission requires precisely regulated SV recycling. How this occurs is despite of many years of research still controversial. Multiple modes of SV endocytosis have been proposed such as clathrin-mediated, clathrin-independent, ultra-fast, bulk-endocytosis or the highly debated mechanism of "kiss-and-run".

What all mechanisms regardless of mechanistic differences have in common is the fact that stimulation strength matters. Different stimulation strengths putatively trigger different modes of SV endocytosis. While under resting state i.e., spontaneous basal activity, fewer SVs fuse, sustained strong stimulation requires to quickly recycle large amounts of SV material. Under these conditions synaptic overshoot has been demonstrated (L. G. Wu et al., 2014) further supporting the idea of different stimulation paradigms resulting in differences in SV retrieval. This raises the question whether the coupling mechanism we propose occurs independent of neuronal activity. While the model of "kiss and run" would not require considerably larger amounts of $PI(4,5)P_2$, all other proposed endocytic retrieval mechanisms do. An increased demand for $PI(4,5)P_2$ may be because soluble proteins potentially need to be recruited to a larger region. However, "kiss and run" is highly debated and the most compelling evidence against it is that the exocytic SV and the endocytic vesicle are non-identical and differ in size (Watanabe, Rost, et al., 2013). To answer the question whether Syt-triggered $PI(4,5)P_2$ synthesis occurs independent of stimulation strength, we visualized neuronal $PI(4,5)P_2$ levels using stimulations ranging from 200 APs up to 20 APs. Our data demonstrates a stimulation-dependent increase of $PI(4,5)P_2$ (Fig. 18a,b). To test for a general activity-dependence, we silenced neuronal cultures by inhibiting basal activity. Silencing reduced plasma-membrane localized Syt1 (Kaempf et al., 2015) and significantly decreased $PI(4,5)P_2$ (Fig. 18a,b) and thus clearly indicates that the Syt1-triggered lipid signaling synthesis operates under a wide range of physiological conditions.

5.2.2 Syt1-triggered lipid signaling synthesis in the context of neurotransmission

Spatiotemporally-regulated Syt1-triggered synthesis of $PI(4,5)P_2$ likely synergizes with other possible exo-endocytic coupling mechanisms. For example, synergies may be via local or externally-caused alterations in membrane tension (Haucke et al., 2011; Maritzen & Haucke, 2018; L. G. Wu et al., 2014), recruitment of endocytic drivers such as VAMP/ Synaptobrevin (Chanaday & Kavalali, 2021; Xu et al., 2013; Z. Zhang et al., 2013) and vGLUT1 (Pan et al., 2015) or via controlled actin dynamics (Soykan et al., 2017; X. S. Wu et al., 2016).

Elevated $PI(4,5)P_2$ may enhance canonical insertion of Syt1's C2 domain into the plasma membrane and destabilize it for SV fusion (Hui et al., 2009; Martens et al., 2007). In presence of $PI(4,5)P_2$, Syt1 exhibits higher Ca^{2+} binding affinities indicating that binding of $PI(4,5)P_2$ and Ca^{2+} to Syt1 is strongly cooperative (Van Den Bogaart et al., 2012). High concentrations of Ca^{2+} even rescued the SV recycling defects caused upon partial loss of Syt1 in Drosophila (Littleton & Bellen, 1995). However, no increase in SV docking or changes in the readily releasable pool size are detected upon increased kinetics of SV recycling in Stn2 depleted synapses (Kononenko et al., 2013). The unaltered pool sizes further indicate that our mechanism of Syt1-triggered lipid signaling synthesis is Ca^{2+} mediated but does not induce SV exocytosis.

Instead, we believe Syt1-triggered lipid signaling synthesis to couple SV exo- and endocytosis. At the molecular level, locally enriched $PI(4,5)P_2$ may cause spatially restricted positive membrane deformations and increased negative charge of the plasma membrane. These sites could be sensed, stabilized, or further deformed by specific factors including BAR-domain containing proteins and proteins possessing an amphipathic helix (T. R. Graham & Kozlov, 2010; Jensen et al., 2011; McMahon & Gallop, 2005; Mim & Unger, 2012). As central regulators of membrane remodeling, the BAR domain superfamily appears crucial for a variety of cellular processes including organelle biogenesis, cell division and migration, secretion as well as endocytosis (Kamioka et al., 2004; McMahon & Gallop, 2005). For the latter, endophilin plays an important role. As a BAR-domain protein with an amphipathic helix, endophilin can associate with curved membranes by its helix sensing local lipid packing defects such as the ones triggerd by Syt1. The locally restricted deformations can then be stabilized upon association of banana-shaped BAR domain assemblies (Gallop et al., 2006; Rao & Haucke, 2011). A cascade characterized by

differently shaped BAR domains on their own associate with negatively charged phospholipids and may sequentially control curved membrane intermediates during e.g., formation of endocytic plasma membrane invaginations. Interestingly, the Ca^{2+}-dependent protein calmodulin has also been linked to enhanced membrane-sensing/ shaping activity (Myers et al., 2016). BAR-domain containing proteins often possess a PH domain which appears to confer lipid specificity and additionally, a Src homology 3 domain (SH3) domain potentially mediating protein activity. The SH3 domain interacts with other proteins of the endocytic machinery such as the GTPase dynamin mediating scission upon PH domain-dependent $PI(4,5)P_2$ binding and oligomerization (Rao & Haucke, 2011; Reubold et al., 2015). Correspondingly, our data demonstrated Syt1-dependent $PI(4,5)P_2$ lipid signaling to regulate recruitment of dynamin to presynaptic compartments in a stimulation-dependent manner (Fig. 22, 23a,f-h,24). Along the same lines, recruitment of other proteins of the endocytic machinery might be similarly regulated by Syt1-dependent $PI(4,5)P_2$ lipid signaling as our preliminary data on the BAR-domain protein formin-binding protein 17 (FBP17) suggests. FBP17 has been associated with membrane sensing/ membrane bending activity through interaction with the plasma membrane, specifically with $PI(4,5)P_2$ i.e., via the residue K33 within the BAR-domain (Tsuboi et al., 2009; Zegers & Friedl, 2015; Zhao et al., 2013). In agreement with former studies, we show FBP17's membrane tubulation activity to depend on interaction with the plasma membrane (Appendix Fig. 35a) (Echarri et al., 2019; Tsuboi et al., 2009; Zegers & Friedl, 2015; Zhao et al., 2013). FBP17 seems to be localized to synapses in hippocampal neurons and depletion of FBP17 leads to defects in SV endocytosis which can only be rescued by full length FBP17 (Appendix Fig. 35b,c,d). The mutant unable to interact with the plasma membrane does not sufficiently rescue the defect (Appendix Fig. 35c,d). Additional plasma membrane interaction sites within FBP17 i.e., via K166, may explain the partial rescue of FBP17 K33E. Collectively this indicates that FBP17 similar to vGLUT1 is an important endocytic driving factor whose localization and thus endocytic function likely depends on Syt1-triggered lipid synthesis generating $PI(4,5)P_2$ positive enrichments. FBP17's function in SV endocytosis and a dependency on local Syt1-triggered lipid synthesis should be addressed in future studies. In contrast, we do not see Syt1-triggered lipid synthesis to impair AP2 recruitment (Fig. 23a,i-k,24) which may very well be due to clathrin/ AP2 functioning in SV budding downstream of endocytic plasma membrane recruitment (Kononenko et al., 2014; Soykan et al., 2017; Watanabe et al., 2014). Whether Syt1-triggered lipid signaling synthesis may be implicated in the characteristics of individual SVs is a matter of debate. Our data suggests that correct SV

protein localization likely correlates with Syt1-triggered lipid synthesis to initiate SV endocytosis. Yet, we believe SV budding and reformation to occur downstream of the initiation of endocytic retrieval of plasma membrane invaginations by Syt1-triggered lipid synthesis. It is unclear whether SV protein sorting may act in parallel. We believe SV protein sorting is likely more important during downstream SV reformation from endosomes to ensure the generation of individual, well-defined SVs. The latter process is very well linked to $PI(4,5)P_2$ as depletion of synaptojanin and thus impaired $PI(4,5)P_2$ dephosphorylation results in accumulated clathrin-coated SVs, leads to highly impaired neurotransmission, likely autophagic defects and has been linked to Parkinson's disease (Cao et al., 2017; Cremona et al., 1999).

While SH3 domains i.e. of FBP17 modulate interactions with cytoskeletal proteins, e.g. to N-WASP for initiating actin polymerization (Rao & Haucke, 2011), $PI(4,5)P_2$-enriched membranes themselves may directly modulate actin dynamics. In the synapse, actin is highly enriched and crucial for neurotransmission (Soykan et al., 2017; X. S. Wu et al., 2016). Localization of actin binding proteins as well as Rho GTPases correlates with $PI(4,5)P_2$ abundance (Saarikangas et al., 2010). Rho GTPases are in turn connected to PIPKIγ activity and thus link actin dynamics to Syt1-dependent lipid signaling. In line with this, it is not surprising that Syt1 expression has been demonstrated to alter actin cytoskeleton and neurite outgrowth and to lead to enhanced $PI(4,5)P_2$-dependent filopodia formation (Feany & Buckley, 1993; Johnsson & Karlsson, 2012). Thus, the Syt1-triggered lipid signaling synthesis would be interesting to address in the context of actin dynamics during neurotransmission.

5.2.3 Influence of Syt1-triggered lipid signaling synthesis beyond neurotransmission

We believe that the Syt1-triggered signaling lipid synthesis is a general mechanism for neurons to couple SV fusion and retrieval. Syt1 has been demonstrated to be the primary Ca^{2+} sensor for fast, Ca^{2+}-triggered SV exocytosis. For the coupling process, our data demonstrates a non-exclusive, but likely Ca^{2+}-mediated action (Fig. 29a,26a) implying Ca^{2+} sensitivity may be of secondary importance . This is in line with our data revealing a Ca^{2+}-independent, conserved interaction of all Syts tested with PIPKIγ. Due to the high sequence similarities the interaction is likely conserved in the entire Syt-family (Fig. 28a). In the nervous system, multiple isoforms are expressed (C. Chen & Jonas, 2017; Südhof, 2002).

Eight of in total 17 Syt-expressed isoforms in mammals bind Ca^{2+} and only four are likely expressed on vesicle membranes. These may function as Ca^{2+}-sensors for Ca^{2+}-mediated transmitter release (Xu et al., 2007). In contrast, Syt7, capable of binding PIPKIγ (Fig. 26b), resides on the plasma membrane and has been described in the context of spontaneous, asynchronous neurotransmitter release and short-term plasticity (Jackman et al., 2016; Y. C. Li et al., 2017). In addition to presynaptic localization, other Syt isoforms have been linked with postsynaptic expression likely mediating receptor trafficking (D. Wu et al., 2017). Many functions of Syts have not intensively been studied. Yet our mechanism revealing Syt1 to regulate lipid synthesis could likely be conserved for all Syts across the neuron.

In agreement with this, also other Ca^{2+}-sensors could induce lipid synthesis. These sensors reveal differences in affinity like Syt1 and Syt7 and thus may increase the probability of neurotransmitter release (Sun et al., 2007). Such a candidate for a potential non-Syt interactor of PIPKIγ could be Doc2. Doc2 shares sequence similarities in its C2 domain and could thereby also mediate PIPKIγ recruitment (Groffen et al., 2010; H. Wen et al., 2010; J. Yao et al., 2011).

Despite neurons being highly specialized in rapidly regulating SV exocytosis and its compensatory endocytic retrieval, also other cell types e.g., neuroendocrine and gland cells, are capable of secreting large amounts of membrane. Therefore, comparable lipid-based mechanisms could exist in other secretory cell types and organisms that couple exocytic vesicle fusion and compensatory endocytic retrieval (Feldmann et al., 2003; Kamalesh et al., 2021; L. G. Wu et al., 2014).

Looking beyond SV exo- and endocytosis, it appears that other C2 domains can bind PIPKIγ in a similar manner as our data on extended Synaptotagmins (ESyts) reveals (Fig. 26c). While the name derives from partial structure similarities, ESyts greatly differ from conventional Syts in localizing e.g., to the ER and mediating ER-plasma membrane contact sites and lipid transport. ESyts are expressed more widely across animals, fungi, and plants which could implicate further importance of a more general C2 domain-triggered lipid synthesis in a variety of physiological processes. Accordingly, PIP5K as the essential generator of $PI(4,5)P_2$ has been widely implicated in many cellular processes including regulation of the actin cytoskeleton, cell polarity, cell-matrix as well as cell-cell adhesions, endo-, exo- and phagocytosis, cellular stress response including apoptosis, cytokinesis and nuclear functions (van den Bout & Divecha, 2009). The different isoforms of PIP5Ks have been shown to display a wide subcellular distribution including the plasma membrane, the Golgi, the nucleus (Mellman et al., 2008), vesicles, the perinuclear region (Doughman et al.,

2003), focal adhesions or adherens junctions (Di Paolo et al., 2002; Giudici et al., 2006; Ling et al., 2007) and thus can have different spatially restricted or overlapping effects on these processes. The stimulation-dependent increase of $PI(4,5)P_2$ demonstrated in this study (Fig. 18b) is therefore unique because dramatic changes have not often been observed during normal cell signaling. The local enrichment we detect in the presynapse is in line with the hypothesis of specific, locally-restricted subcellular pools of $PI(4,5)P_2$ (Honigmann et al., 2013). Like our proposed model of protein assembly putatively acting as a diffusion barrier, lateral diffusion may further be restricted by the actin cytoskeleton or other components of the SV endocytic machinery and in epithelial cells, local hubs at apical or basolateral membranes are maintained by tight junctions (Trimble & Grinstein, 2015).

In summary, we provide evidence for an activity-dependent Syt1-triggered lipid synthesis mechanism which couples SV exo- and endocytosis in neurons. Based on the outlined conservation of the underlying interactions, such a C2 domain-mediated mechanism regulating $PI(4,5)P_2$ synthesis is likely of much broader relevance and might be implicated in the context of various pathomechanisms.

5.3 Conclusions and outlook

In this study, we combined mouse genetics with optical imaging using live-cell microscopy to analyze the kinetics of the SV cycle and confocal and super-resolution microscopy to detect presynaptic protein localization patterns. In addition, we carried out electron microscopy to visualize the synaptic ultrastructure in order to identify ultrastructural changes. This was combined with biochemical experiments and structural analyses to characterize a conserved interaction between Syt1 and PIPK1γ which proved crucial for the Syt1 dependent exo-endocytic coupling mechanism we identified. In this, we show that Syt1-triggered lipid synthesis by PIPK1γ couples SV exocytosis and endocytosis. Genetic loss, mutations, and inactivation of Syt1 have been linked to severe impairments of neurotransmission, and heterogenous mutations have been associated with serious clinical pathologies and neurodegenerative diseases (Baker et al., 2018; Bradberry et al., 2020; Geppert et al., 1994; Glavan et al., 2009; Harper et al., 2020; Jorgensen et al., 1995). The results presented here strengthen Syt1's crucial function as a key factor in synchronous neurotransmission regulating the kinetics of the SV cycle, SV exocytosis (Geppert et al., 1994) as well as SV endocytosis (Y. C. Li et al., 2017; Nicholson-Tomishima & Ryan, 2004). Importantly and in line with previous findings, this mechanism gives an answer to the

long-standing question how a synapse knows how many vesicles have fused. It thus provides the synapse with an intrinsic, homeostatic, post-fusion trigger to tune SV endocytosis in an activity-dependent manner.

Our data suggests that the local Syt1-dependent $PI(4,5)P_2$ enrichments that we detect in a stimulation-dependent manner influence downstream endocytic driving factors i.e., dynamin and potentially proteins involved in membrane deformation. It is likely that local actin dynamics also rely on nanoclusters of $PI(4,5)P_2$. Further experiments focusing on $PI(4,5)P_2$ dynamics i.e., via synaptojanin KD or rescue experiments, and $PI(4,5)P_2$ downstream effects e.g., on proteins involved in membrane remodeling such BAR-domain or amphipathic helices possessing proteins, are needed. Along the same lines, further studies aiming at $PI(4,5)P_2$ hydrolysis would be interesting. We detect Syt1 to directly interact with PIPK1γ to locally synthesize $PI(4,5)P_2$. Yet, Syt1 has been shown to interact to DGK generating PA from $PI(4,5)P_2$. It is intriguing to ask whether the locally synthesized pool of $PI(4,5)P_2$ could directly be turned into local enrichments of PA and whether a spatially restricted initiation of negative curvature due to local PA aids neck formation for SV scission. Do Syt1's interaction partners rely on competitive binding and more generally, do conformational changes of Syt1's C2 domains occur upon binding of Ca^{2+} or interaction partners which have effects on interaction strength as well as enzymatic activity? Another open question persists on the place of action. While we exclude PIPKIγ to directly act on SVs/ in the exocytic process and instead propose PIPKIγ to act at the endocytic sites, we cannot precisely define the location of endocytic sites at the plasma membrane or rule out that PIPKIγ may further act on ELVs during SV reformation. Communication with the endo-lysosomal compartments that are crucial for quality control and degradation of SV compartments may be influenced by lipid dynamics and should be focus of future studies. Superresolution microscopy and lipid probes similar to those we used would provide insights to membrane identities and lipid dynamics during the SV cycle. Another open question is whether Syt1-triggered $PI(4,5)P_2$ synthesis occurs prior, during or after SV protein sorting. This is of interest because Syt1 sorting through its adaptors, Stn2 and SV2, have been associated with neurological and neurodegenerative diseases such as schizophrenia, autism spectrum disorders (Breedveld et al., 2010; Luan et al., 2011), late onset Alzheimer's disease and epilepsy (Lynch et al., 2004; Nowack et al., 2011; Rhinn et al., 2013). SV2 has even evolved to be an important antiepileptic drug target because Syt1-mislocalization may affect excitatory and inhibitory input balance and subsequently may result in epileptic seizures

(Lynch et al., 2004). Understanding the molecular detail in the context of Syt1's triggered lipid synthesis would aid the treatment of these diseases.

Beyond the scope of neurotransmission, PIP5K is the essential generator of $PI(4,5)P_2$ and has been implicated in many cellular processes (van den Bout & Divecha, 2009). In fact, perturbed $PI(4,5)P_2$ kinetics have been associated with various pathophysiological mechanisms (Cao et al., 2017; Yin & Wang, 2022). While impaired dephosphorylation of $PI(4,5)P_2$ has been linked to Parkinson's disease (Cao et al., 2017), enhanced $PI(4,5)P_2$ synthesis has been found in tumor cells(Yin & Wang, 2022). $PI(4,5)P_2$ is implicated in two upregulated signaling pathways in cancer, PI3K and PLC-based, leading to cancer hallmarks including increased cell survival, decreased apoptosis and enhanced cell migration. Identifying whether Syt1 or more generally a C2-triggered lipid synthesis is implicated in any of these pathologies would help to understand the underlying molecular mechanisms and open new possibilities for therapeutic approaches. In this context, an important question to answer is whether Syt1 can, in addition to its interaction to PIPKIγ, stimulate the catalytic activity of the kinase. This could be studied in kinase activity assays in presence of fluorescently labeled lipids.

Similarly, it would be of great interest to find the interaction site within the sequence of PIPKIγ due to strong evolutionary conservation of the kinase core domain of this protein class. PIP5Ks are not only promising molecular targets for both neurodegeneration as well as cancer but pharmacological inhibition of PIP5Ks activity i.e., via disrupting protein interactions, could result in tumor therapy as well as promote nerve regeneration (East et al., 2020; van den Bout & Divecha, 2009; Yin & Wang, 2022). Pharmacological inhibition may even hold potential for treating acquired immune deficiency syndrome (AIDS) as human immunodeficiency virus 1 (HIV-1) Gag, an important protein for viral assembly, selectively targets $PI(4,5)P_2$ enrichments at the plasma membrane similar to those we identified (Y. Wen et al., 2020). Even in plants, mutations in PIP5K indicate that production of $PI(4,5)P_2$ may be involved in development, immunity and reproduction (Doumane et al., 2021; Heilmann, 2016; Noack & Jaillais, 2017, 2020). Without any evidence of a similar mechanism to the one we propose in any of these pathologies, the need for correct localization of PIP5K to generate $PI(4,5)P_2$ enrichments and the abundance of proteins harboring C2 domains makes it intriguing to question it. Thus, elucidating potentially common mechanisms across other cell types and species would give insights into various research fields including cell survival, apoptosis, cell migration and holds promising potential for therapeutic interventions for neurodegenerative diseases and cancer.

6 Bibliography

Alés, E., Tabares, L., Poyato, J. M., Valero, V., Lindau, M., & Alvarez de Toledo, G. (1999). High calcium concentrations shift the mode of exocytosis to the kiss-and-runmechanism. *Nature Cell Biology*, *1*(1), 40–44. https://doi.org/10.1038/9012

Andrews, J., Smith, M., Merakovsky, J., Coulson, M., Hannan', F., & Kelly, L. E. (1996). The stoned Locus of Drosophila melanogaster Produces a Dicistronic Transcript and Encodes Two Distinct Polypeptides. *Genetics*, *143*, 1699–1711. https://academic.oup.com/genetics/article/143/4/1699/6016775

Andrews-Zwilling, Y. S., Kawabe, H., Reim, K., Varoqueaux, F., & Brose, N. (2006). Binding to Rab3A-interacting molecule RIM regulates the presynaptic recruitment of Munc13-1 and ubMunc13-2. *Journal of Biological Chemistry*, *281*(28), 19720–19731. https://doi.org/10.1074/jbc.M601421200

Anggono, V., Smillie, K. J., Graham, M. E., Valova, V. A., Cousin, M. A., & Robinson, P. J. (2006). Syndapin I is the phosphorylation-regulated dynamin I partner in synaptic vesicle endocytosis. *Nature Neuroscience*, *9*(6), 752–760. https://doi.org/10.1038/nn1695

Antonescu, C. N., Aguet, F., Danuser, G., & Schmid, S. L. (2011). Phosphatidylinositol-(4,5)-bisphosphate regulates clathrin-coated pit initiation, stabilization, and size. *Molecular Biology of the Cell*, *22*(14), 2588–2600. https://doi.org/10.1091/mbc.E11-04-0362

Arioka, M., Nakashima, S., Shibasaki, Y., & Kitamoto, K. (2004). Dibasic amino acid residues at the carboxy-terminal end of kinase homology domain participate in the plasma membrane localization and function of phosphatidylinositol 5-kinase γ. *Biochemical and Biophysical Research Communications*, *319*(2), 456–463. https://doi.org/10.1016/j.bbrc.2004.04.187

Armbruster, M., Messa, M., Ferguson, S. M., De Camilli, P., & Ryan, T. A. (2013). Dynamin phosphorylation controls optimization of endocytosis for brief action potential bursts. *ELife*, *2013*(2), 1–15. https://doi.org/10.7554/eLife.00845

Augustine, G. J., Morgan, J. R., Villalba-Galea, C. A., Jin, S., Prasad, K., & Lafer, E. M. (2006). Clathrin and synaptic vesicle endocytosis: studies at the squid giant synapse. *Biochem Soc Trans*, *34*(01), 68–72. https://doi.org/10.1021/acschemneuro.5b00094.Serotonin

Bibliography

Axelrod, D. (2001). Total Internal Reflection Fluorescence Microscopy in Cell Biology. *Traffic*, *2*, 764–774.

Bai, J., Tucker, W. C., & Chapman, E. R. (2004). PIP2 increases the speed of response of synaptotagmin and steers its membrane-penetration activity toward the plasma membrane. *Nature Structural and Molecular Biology*, *11*(1), 36–44. https://doi.org/10.1038/nsmb709

Bai, J., Wang, P., & Chapman, E. R. (2002). C2A activates a cryptic Ca 2-triggered membrane penetration activity within the C2B domain of synaptotagmin I. *Proceedings of the National Academy of Sciences*, *99*(3), 1665–1670. www.pnas.orgcgidoi10.1073pnas.032541099

Baker, K., Gordon, S. L., Melland, H., Bumbak, F., Scott, D. J., Jiang, T. J., Owen, D., Turner, B. J., Boyd, S. G., Rossi, M., Al-Raqad, M., Elpeleg, O., Peck, D., Mancini, G. M. S., Wilke, M., Zollino, M., Marangi, G., Weigand, H., Borggraefe, I., … Raymond, F. L. (2018). SYT1-associated neurodevelopmental disorder: A case series. *Brain*, *141*(9), 2576–2591. https://doi.org/10.1093/brain/awy209

Balla, A., & Balla, T. (2006). Phosphatidylinositol 4-kinases: old enzymes with emerging functions. In *Trends in Cell Biology* (Vol. 16, Issue 7, pp. 351–361). https://doi.org/10.1016/j.tcb.2006.05.003

Balla, T. (2013). Phosphoinositides: Tiny lipids with giant impact on cell regulation. *Physiological Reviews*, *93*(3), 1019–1137. https://doi.org/10.1152/physrev.00028.2012

Barber, C. N., Goldschmidt, H. L., Ma, Q., Devine, L. R., Cole, R. N., Huganir, R. L., & Raben, D. M. (2022). Identification of Synaptic DGKθ Interactors That Stimulate DGKθ Activity. *Frontiers in Synaptic Neuroscience*, *14*. https://doi.org/10.3389/fnsyn.2022.855673

Bellocchio, E. E., Reimer, R. J., Fremeau, J., & Edwards, R. H. (2000). Uptake of glutamate into synaptic vesicles by an inorganic phosphate transporter. *Science*, *289*(5481), 957–960. https://doi.org/10.1126/science.289.5481.957

Bennett, M. K., Calakos, N., Kreiner, T., & Scheller, R. H. (1992). Synaptic Vesicle Membrane Proteins Interact to Form a Multimeric Complex. *The Journal of Cell Biology*, *116*(3), 761–775. https://doi.org/10.1083/jcb.116.3.761.

Bolz, S., Kaempf, N., Puchkov, D., Krauss, M., Russo, G., Soykan, T., Schmied, C., Lehmann, M., Müller, R., Schultz, C., Perrais, D., Maritzen, T., & Haucke, V. (2023). Synaptotagmin 1-triggered lipid signaling facilitates coupling of exo- and endocytosis. *Neuron*, *111*. https://doi.org/10.1016/j.neuron.2023.08.016

Boussif, O., Lezoualc'h, F., Zanta, M. A., Mergny, D., Scherman, D., Demeneix, B., & Behr, J.-P. (1995). A versatile vector for gene and oligonucleotide transfer into cells in culture and in vivo: Polyethylenimine. In *Biochemistry* (Vol. 92).

Bradberry, M. M., Courtney, N. A., Dominguez, M. J., Lofquist, S. M., Knox, A. T., Sutton, R. B., & Chapman, E. R. (2020). Molecular basis for synaptotagmin-1-associated neurodevelopmental disorder. *Neuron*, *107*(1), 52-64.e7. https://doi.org/10.1016/j.neuron.2020.04.003.

Bradford, M. M. (1976). A Rapid and Sensitive Method for the Quantitation of Microgram Quantities of Protein Utilizing the Principle of Protein-Dye Binding. In *ANALYTICAL BIOCHEMISTRY* (Vol. 72). https://doi.org/10.1016/0003-2697(76)90527-3

Brewer, K. D., Bacaj, T., Cavalli, A., Camilloni, C., Swarbrick, J. D., Liu, J., Zhou, A., Zhou, P., Barlow, N., Xu, J., Seven, A. B., Prinslow, E. A., Voleti, R., Häussinger, D., Bonvin, A. M. J. J., Tomchick, D. R., Vendruscolo, M., Graham, B., Südhof, T. C., & Rizo, J. (2015). Dynamic binding mode of a Synaptotagmin-1-SNARE complex in solution. *Nature Structural and Molecular Biology*, *22*(7), 555–564. https://doi.org/10.1038/nsmb.3035

Brose, N., Petrenko, A. G., Südhof, T. C., & Jahn, R. (1992). Synaptotagmin: A Calcium Sensor on the Synaptic Vesicle Surface. *Science*, *256*, 1021–1025. https://doi.org/10.1126/science.1589771

Bykhovskaia, M. (2011). Synapsin regulation of vesicle organization and functional pools. *Seminars in Cell & Developmental Biology*, *22*(4), 387–392. https://doi.org/10.1016/j.semcdb.2011.07.003.

Calakos, N., & Scheller, R. H. (1994). Vesicle-associated membrane protein and synaptophysin are associated on the synaptic vesicle. *Journal of Biological Chemistry*, *269*(40), 24534–24537.

Cao, M., Wu, Y., Ashrafi, G., McCartney, A. J., Wheeler, H., Bushong, E. A., Boassa, D., Ellisman, M. H., Ryan, T. A., & De Camilli, P. (2017). Parkinson Sac Domain Mutation in Synaptojanin 1 Impairs Clathrin Uncoating at Synapses and Triggers Dystrophic Changes in Dopaminergic Axons. *Neuron*, *93*(4), 882-896.e5. https://doi.org/10.1016/j.neuron.2017.01.019

Caparotta, M., Tomes, C. N., Mayorga, L. S., & Masone, D. (2020). The Synaptotagmin-1 C2B Domain Is a Key Regulator in the Stabilization of the Fusion Pore. *Journal of Chemical Theory and Computation*, *16*(12), 7840–7851. https://doi.org/10.1021/acs.jctc.0c00734

Bibliography

Ceccarelli, B., Hurlbut, W. P., & Mauro, A. (1972). Depletion of vesicles from frog neuromuscular junctions by prolonged tetanic stimulation. *The Journal of Cell Biology*, *54*(1), 30–38.

Ceccarelli, B., Hurlbut, W. P., & Mauro, A. (1973). Turnover of transmitter and synaptic vesicles at the frog neuromuscular junction. *The Journal of Cell Biology*, *57*(2), 499–524. https://doi.org/10.1083/jcb.57.2.499

Cesca, F.; Baldelli, P.; Valtorta, F., and Benfenati, F. (2010). The synapsins: Key actors of synapse function and plasticity. *Progress in Neurobiology*, *91*(4), 313–348. https://doi.org/10.1016/j.pneurobio.2010.04.006.

Chanaday, N. L., & Kavalali, E. T. (2021). Synaptobrevin-2 dependent regulation of single synaptic vesicle endocytosis. *Molecular Biology of the Cell*, *32*(19), 1818–1823. https://doi.org/10.1091/mbc.E21-04-0213

Chang-Ileto, B., Frere, S. G., Chan, R. B., Voronov, S. V., Roux, A., & Di Paolo, G. (2011). Synaptojanin 1-Mediated PI(4,5)P2 Hydrolysis Is Modulated by Membrane Curvature and Facilitates Membrane Fission. *Developmental Cell*, *20*(2), 206–218. https://doi.org/10.1016/j.devcel.2010.12.008

Chapman, E. R. (2008). How does synaptotagmin trigger neurotransmitter release? *Annual Review of Biochemistry*, *77*, 615–641. https://doi.org/10.1146/annurev.biochem.77.062005.101135

Chapman, E. R., & Davis, A. F. (1998). Direct interaction of a Ca2+-binding loop of synaptotagmin with lipid bilayers. *Journal of Biological Chemistry*, *273*(22), 13995–14001. https://doi.org/10.1074/jbc.273.22.13995

Chappie, J. S., Mears, J. A., Fang, S., Leonard, M., Schmid, S. L., Milligan, R. A., Hinshaw, J. E., & Dyda, F. (2011). A pseudoatomic model of the dynamin polymer identifies a hydrolysis-dependent powerstroke. *Cell*, *147*(1), 209–222. https://doi.org/10.1016/j.cell.2011.09.003

Chen, C., & Jonas, P. (2017). Synaptotagmins: That's Why So Many. *Neuron*, *94*(4), 694–696. https://doi.org/10.1016/j.neuron.2017.05.011

Chen, Y., Wang, Y. H., Zheng, Y., Li, M., Wang, B., Wang, Q. W., Fu, C. L., Liu, Y. N., Li, X., & Yao, J. (2021). Synaptotagmin-1 interacts with PI(4,5)P2 to initiate synaptic vesicle docking in hippocampal neurons. *Cell Reports*, *34*(11). https://doi.org/10.1016/j.celrep.2021.108842

Cheung, G., & Cousin, M. A. (2012). Adaptor Protein Complexes 1 and 3 Are Essential for Generation of Synaptic Vesicles from Activity-Dependent Bulk Endosomes. *Journal of Neuroscience*, *32*(17), 6014–6023. https://doi.org/10.1523/JNEUROSCI.6305-11.2012

Chiang, C. W., Chang, C. W., & Jackson, X. B. (2018). The transmembrane domain of synaptobrevin influences neurotransmitter flux through synaptic fusion pores. *Journal of Neuroscience*, *38*(32), 7179–7191. https://doi.org/10.1523/JNEUROSCI.0721-18.2018

Chicka, M. C., Hui, E., Liu, H., & Chapman, E. R. (2008). Synaptotagmin arrests the SNARE complex before triggering fast, efficient membrane fusion in response to Ca2+. *Nature Structural and Molecular Biology*, *15*(8), 827–835. https://doi.org/10.1038/nsmb.1463

Collins, B. M., McCoy, A. J., Kent, H. M., Evans, P. R., & Owen, D. J. (2002). Molecular architecture and functional model of the endocytic AP2 complex. *Cell*, *109*(4), 523–535. https://doi.org/10.1016/S0092-8674(02)00735-3

Cousin, M. A., & Robinson, P. J. (2001). The dephosphins: Dephosphorylation by calcineurin triggers synaptic vesicle endocytosis. *Trends in Neurosciences*, *24*(11), 659–665. https://doi.org/10.1016/S0166-2236(00)01930-5

Craxton, M. (2010). A manual collection of Syt, Esyt, Rph3a, Rph3al, Doc2, and Dblc2 genes from 46 metazoan genomes - an open access resource for neuroscience and evolutionary biology. *BMC Genomics*, *11*(1), 1–21. https://doi.org/10.1186/1471-2164-11-37

Cremona, O., Paolo, G. Di, Wenk, M. R., Lüthi, A., Kim, W. T., Takei, K., Daniell, L., Nemoto, Y., Shears, S. B., Flavell, R. A., Mccormick, D. A., & De Camilli, P. (1999). Essential Role of Phosphoinositide Metabolism in Synaptic Vesicle Recycling. *Cell*, *99*, 179–188. https://doi.org/10.1016/S0092-8674(00)81649-9

Crowder, K. M., Gunther, J. M., Jones, T. A., Hale, B. D., Zhang, H. Z., Peterson, M. R., Scheller, R. H., Chavkin, C., & Bajjalieh, S. M. (1999). Abnormal neurotransmission in mice lacking synaptic vesicle protein 2A (SV2A). *PNAS*, *96*(26), 15268–15273. https://doi.org/10.1073/pnas.96.26.15268

Custer, K. L., Austin, N. S., Sullivan, J. M., & Bajjalieh, S. M. (2006). Synaptic vesicle protein 2 enhances release probability at quiescent synapses. *Journal of Neuroscience*, *26*(4), 1303–1313. https://doi.org/10.1523/JNEUROSCI.2699-05.2006

Bibliography

de Lange, R. P. J., de Roos, A. D. G., & Borst, J. G. G. (2003). Two Modes of Vesicle Recycling in the Rat Calyx of Held. *J. Neurosci.*, *23*(31), 10164–10173. https://doi.org/23/31/10164

De Matteis, M. A., & Godi, A. (2004). PI-loting membrane traffic. *Nature Cell Biology*, *6*(6), 487–492. https://doi.org/10.1038/ncb0604-487

De Robertis, E. (1959). Submicroscopic Morphology of the Synapse. In *International review of cytology* (Vol. 8, pp. 61–96). Elsevier.

De Robertis, E. D. P., & Bennett, H. S. (1954). A submicroscopic vesicular component of Schwann cells and nerve satellite cells. *Experimental Cell Research*, *6*(2), 543–545. https://doi.org/10.1016/0014-4827(54)90209-8

Dean, C., & Dresbach, T. (2006). Neuroligins and neurexins: Linking cell adhesion, synapse formation and cognitive function. *Trends in Neurosciences*, *29*(1), 21–29. https://doi.org/10.1016/j.tins.2005.11.003

Di Paolo, G., & De Camilli, P. (2006). Phosphoinositides in cell regulation and membrane dynamics. In *Nature* (Vol. 443, Issue 7112, pp. 651–657). Nature Publishing Group. https://doi.org/10.1038/nature05185

Di Paolo, G., Moskowitz, H. S., Gipson, K., Wenk, M. R., Voronov, S., Obayashi, M., Flavell, R., Fitzsimonds, R. M., Ryan, T. A., & De Camilli, P. (2004). Impaired PtdIns(4,5)P 2 synthesis in nerve terminals produces defects in synaptic vesicle trafficking. *Nature*, *421*, 415–422. www.nature.com/nature

Di Paolo, G., Pellegrini, L., Letinic, K., Cestra, G., Zoncu, R., Voronov, S., Chang, S., Guo, J., Wenk, M. R., & De Camilli, P. (2002). Recruitment and regulation of phosphatidylinositol phosphate kinase type 1g by the FERM domain of talin. *Nature*, *420*, 85–89. https://doi.org/10.1038/nature01147

Diantonio, A., & Schwarz, T. 1. (1994). The Effect on Synaptic Physiology of synapfotagmin Mutations in Drosophila. In *Neuron* (Vol. 12).

Diril, M. K., Wienisch, M., Jung, N., Klingauf, J., & Haucke, V. (2006). Stonin 2 Is an AP-2-Dependent Endocytic Sorting Adaptor for Synaptotagmin Internalization and Recycling. *Developmental Cell*, *10*, 233–244. https://doi.org/10.1016/j.devcel.2005.12.011

Dittman, J., & Ryan, T. A. (2009). Molecular Circuitry of Endocytosis at Nerve Terminals. *Annual Review of Cell and Developmental Biology*, *25*(1), 133–160. https://doi.org/10.1146/annurev.cellbio.042308.113302

Doughman, R. L., Firestone, A. J., & Anderson, R. A. (2003). Phosphatidylinositol phosphate kinases put PI4,5P2 in its place. *Journal of Membrane Biology*, *194*(2), 77–89. https://doi.org/10.1007/s00232-003-2027-7

Doumane, M., Lebecq, A., Colin, L., Fangain, A., Stevens, F. D., Bareille, J., Hamant, O., Belkhadir, Y., Munnik, T., Jaillais, Y., & Caillaud, M. C. (2021). Inducible depletion of PI(4,5)P2 by the synthetic iDePP system in Arabidopsis. *Nature Plants*, *7*(5), 587–597. https://doi.org/10.1038/s41477-021-00907-z

East, M. P., Laitinen, T., & Asquith, C. R. M. (2020). PIP5K1A: a potential target for cancers with KRAS or TP53 mutations. In *Nature reviews. Drug discovery* (Vol. 19, Issue 7, p. 436). NLM (Medline). https://doi.org/10.1038/d41573-020-00067-3

Echarri, A., Pavón, D. M., Sánchez, S., García-García, M., Calvo, E., Huerta-López, C., Velázquez-Carreras, D., Viaris de Lesegno, C., Ariotti, N., Lázaro-Carrillo, A., Strippoli, R., De Sancho, D., Alegre-Cebollada, J., Lamaze, C., Parton, R. G., & Del Pozo, M. A. (2019). An Abl-FBP17 mechanosensing system couples local plasma membrane curvature and stress fiber remodeling during mechanoadaptation. *Nature Communications*, *10*(1). https://doi.org/10.1038/s41467-019-13782-2

Edelmann, L., Hanson, P. I., Chapman, E. R., & Jahn, R. (1995). Synaptobrevin binding to synaptophysin: a potential mechanism for controlling the exocytotic fusion machine. *The EMBO Journal*, *14*(2), 224–231. https://doi.org/10.1002/j.1460-2075.1995.tb06995.x

Fatt, P., & Katz, B. (1952). Spontaneous Subthreshold Activity at Motor Nerve Endings. *Journal of Physiology*, *117*, 109–128. https://doi.org/10.1113/jphysiol.1952.sp004735

Feany, M. B., & Buckley, K. M. (1993). The synaptic vesicle protein synaptotagmin promotes formation of filopodia in fibroblasts. *Nature*, *364*, 537–540. https://doi.org/10.1038/364537a0

Feldmann, J., Callebaut, I., Raposo, G., Certain, S., Bacq, D., Dumont, C., Lambert, N., Ouachée-Chardin, M., Chedeville, G., Tamary, H., Minard-Colin, V., Vilmer, E., Blanche, S., Le Deist, F., Fischer, A., & De Saint Basile, G. (2003). Munc13-4 Is Essential for Cytolytic Granules Fusion and Is Mutated in a Form of Familial Hemophagocytic Lymphohistiocytosis (FHL3). *Cell*, *115*(4), 461–473. https://doi.org/10.1016/S0092-8674(03)00855-9

Fenster, S. D., Kessels, M. M., Qualmann, B., Chung, W. J., Nash, J., Gundelfinger, E. D., & Garner, C. C. (2003). Interactions between Piccolo and the actin/dynamin-binding

protein Abp1 link vesicle endocytosis to presynaptic active zones. *Journal of Biological Chemistry*, *278*(22), 20268–20277. https://doi.org/10.1074/jbc.M210792200

Fergestad, T., & Broadie, K. (2001). Interaction of Stoned and Synaptotagmin in Synaptic Vesicle Endocytosis. *The Journal of Neuroscience*, *21*(4), 1218–1227.

Fergestad, T., Davis, W. S., & Broadie, K. (1999). The Stoned Proteins Regulate Synaptic Vesicle Recycling in the Presynaptic Terminal. *The Journal of Neuroscience*, *19*(14), 5847–5860.

Ferguson, S., Raimondi, A., Paradise, S., Shen, H., Mesaki, K., Ferguson, A., Destaing, O., Ko, G., Takasaki, J., Cremona, O., O' Toole, E., & De Camilli, P. (2009). Coordinated Actions of Actin and BAR Proteins Upstream of Dynamin at Endocytic Clathrin-Coated Pits. *Developmental Cell*, *17*(6), 811–822. https://doi.org/10.1016/j.devcel.2009.11.005

Fernandez, I., Araç, D., Ubach, J., Gerber, S. H., Shin, O. H., Gao, Y., Anderson, R. G. W., Südhof, T. C., & Rizo, J. (2001). Three-dimensional structure of the synaptotagmin 1 C2B-domain: Synaptotagmin 1 as a phospholipid binding machine. *Neuron*, *32*(6), 1057–1069. https://doi.org/10.1016/S0896-6273(01)00548-7

Fernández-Alfonso, T., Kwan, R., & Ryan, T. A. (2006). Synaptic Vesicles Interchange Their Membrane Proteins with a Large Surface Reservoir during Recycling. *Neuron*, *51*(2), 179–186. https://doi.org/10.1016/j.neuron.2006.06.008

Fernandez-Alfonso, T., & Ryan, T. A. (2008). A heterogeneous "resting" pool of synaptic vesicles that is dynamically interchanged across boutons in mammalian CNS synapses. *Brain Cell Biol.*, *36*, 87–100. https://doi.org/10.1007/s11068-008-9030-y.A

Fernández-Chacón, R., Königstorfer, A., Gerber, S. H., García, J., Matos, M. F., Stevens, C. F., Brose, N., Rizo, J., Rosenmund, C., & Südhof, T. C. (2001). Synaptotagmin I functions as a calcium regulator of release probability. *Nature*, *410*(6824), 41–49. https://doi.org/10.1038/35065004

Fernández-Chacón, R., & Südhof, T. C. (1999). Genetics of synaptic vesicle function: Toward the complete functional anatomy of an organelle. In *Annual Review of Physiology* (Vol. 61). https://doi.org/10.1146/annurev.physiol.61.1.753

Fuson, K. L., Montes, M., Robert, J. J., & Sutton, R. B. (2007). Structure of human synaptotagmin 1 C2AB in the absence of Ca2+ reveals a novel domain association. *Biochemistry*, *46*(45), 13041–13048. https://doi.org/10.1021/bi701651k

Gad, H., Löw, P., Zotova, E., Brodin, L., & Shupliakov, O. (1998). Dissociation between Ca2+-triggered synaptic vesicle exocytosis and clathrin-mediated endocytosis at a

central synapse. *Neuron*, *21*(3), 607–616. https://doi.org/10.1016/S0896-6273(00)80570-X

Gallop, J. L., Jao, C. C., Kent, H. M., Butler, P. J. G., Evans, P. R., Langen, R., & McMahon, H. T. (2006). Mechanism of endophilin N-BAR domain-mediated membrane curvature. *EMBO Journal*, *25*(12), 2898–2910. https://doi.org/10.1038/sj.emboj.7601174

Gamper, N., Reznikov, V., Yamada, Y., Yang, J., & Shapiro, M. S. (2004). Phosphotidylinositol 4,5-bisphosphate signals underlie receptor-specific Gq/11-mediated modulation of N-type Ca2+ channels. *Journal of Neuroscience*, *24*(48), 10980–10992. https://doi.org/10.1523/JNEUROSCI.3869-04.2004

Geppert, M., Goda, Y., Hammer, R. E., Li, C., Rosahl, T. W., Stevens, C. F., & Südhof, T. C. (1994). Synaptotagmin I: A Major Ca2+ Sensor for Transmitter Release at a Central Synapse. In *Cell* (Vol. 79). https://doi.org/10.1016/0092-8674(94)90556-8

Gimber, N., Tadeus, G., Maritzen, T., Schmoranzer, J., & Haucke, V. (2015). Diffusional spread and confinement of newly exocytosed synaptic vesicle proteins. *Nature Communications*, *6*(8392), 1–11. https://doi.org/10.1038/ncomms9392

Giudici, M. L., Emson, P. C., & Irvine, R. F. (2004). A novel neuronal-specific splice variant of Type I phosphatidylinositol 4-phosphate 5-kinase isoform γ. *Biochemical Journal*, *379*(2), 489–496. https://doi.org/10.1042/BJ20031394

Giudici, M. L., Lee, K., Lim, R., & Irvine, R. F. (2006). The intracellular localisation and mobility of Type Iγ phosphatidylinositol 4P 5-kinase splice variants. *FEBS Letters*, *580*(30), 6933–6937. https://doi.org/10.1016/j.febslet.2006.11.052

Glavan, G., Schliebs, R., & Živin, M. (2009). Synaptotagmins in neurodegeneration. *Anatomical Record*, *292*(12), 1849–1862. https://doi.org/10.1002/ar.21026

Goldschmidt, H. L., Tu-Sekine, B., Volk, L., Anggono, V., Huganir, R. L., & Raben, D. M. (2016). DGKθ Catalytic Activity Is Required for Efficient Recycling of Presynaptic Vesicles at Excitatory Synapses. *Cell Reports*, *14*(2), 200–207. https://doi.org/10.1016/j.celrep.2015.12.022

Gordon, S. L., Leube, R. E., & Cousin, M. A. (2012). Synaptophysin is required for synaptobrevin retrieval during synaptic vesicle endocytosis. *Journal of Neuroscience*, *31*(39), 14032–14036. https://doi.org/10.1523/JNEUROSCI.3162-11.2011

Gorelik, R., Yang, C., Kameswaran, V., Dominguez, R., & Svitkina, T. (2011). Mechanisms of plasma membrane targeting of formin mDia2 through its amino terminal domains.

Bibliography

Molecular Biology of the Cell, *22*(2), 189–201. https://doi.org/10.1091/mbc.E10-03-0256

Graham, F. L., & Van Der Eb, A. J. (1973). A New Technique for the Assay of Infectivity of Human Adenovirus 5 DNA. In *VIROLOGY* (Vol. 52). https://doi.org/10.1016/0042-6822(73)90341-3

Graham, T. R., & Kozlov, M. M. (2010). Interplay of proteins and lipids in generating membrane curvature. *Current Opinion in Cell Biology*, *22*(4), 430–436. https://doi.org/10.1016/j.ceb.2010.05.002.Interplay

Granseth, B., Odermatt, B., Royle, S. J., & Lagnado, L. (2006). Clathrin-Mediated Endocytosis Is the Dominant Mechanism of Vesicle Retrieval at Hippocampal Synapses. *Neuron*, *51*(6), 773–786. https://doi.org/10.1016/j.neuron.2006.08.029

Groffen, A. J., Martens, S., Arazola Díez, R., Cornelisse, L. N., Lozovaya, N., De Jong, A. P. H., Goriounova, N. A., Habets, R. L. P., Takai, Y., Borst, J. G., Brose, N., Mcmahon, H. T., & Verhage, M. (2010). Doc2b Is a High-Affinity Ca 2+ Sensor for Spontaneous Neurotransmitter Release. *Science*, *327*(5973), 1614–1618. www.sciencemag.org

Gruget, C., Bello, O., Coleman, J., Krishnakumar, S. S., Perez, E., Rothman, J. E., Pincet, F., & Donaldson, S. H. (2020). Synaptotagmin-1 membrane binding is driven by the C2B domain and assisted cooperatively by the C2A domain. *Scientific Reports*, *10*(1). https://doi.org/10.1038/s41598-020-74923-y

Guan, Z., Bykhovskaia, M., Jorquera, R. A., Bryan Sutton, R., Akbergenova, Y., & Troy Littleton, J. (2017). A synaptotagmin suppressor screen indicates SNARE binding controls the timing and Ca 2+ cooperativity of vesicle fusion. *ELife*, *6*. https://doi.org/10.7554/eLife.28409.001

Guo, J., Wenk, M. R., Pellegrini, L., Onofri, F., Benfenati, F., & De Camilli, P. (2003). Phosphatidylinositol 4-kinase type IIα is responsible for the phosphatidylinositol 4-kinase activity associated with synaptic vesicles. *Proceedings of the National Academy of Sciences of the United States of America*, *100*(7), 3995–4000. https://doi.org/10.1073/pnas.0230488100

Hammond, C. (2015). Neurons. In *Cellular and Molecular Neurophysiology: Fourth Edition* (Fourth Edi). Elsevier Ltd. https://doi.org/10.1016/B978-0-12-397032-9/00001-7

Hammond, C., & Esclapez, M. (2015). The chemical synapses. In *Cellular and Molecular Neurophysiology: Fourth Edition* (Fourth Edi). Elsevier Ltd. https://doi.org/10.1016/B978-0-12-397032-9.00006-6

Hammond, G. R. V., & Schiavo, G. (2007). Polyphosphoinositol Lipids: Under-PPInning Synaptic Function in Health and Disease. *Developmental Neurobiology*, *67*, 1232–1247. https://doi.org/10.1002/dneu.20509

Hammond, G. R. V, Fischer, M. J., Anderson, K. E., Holdich, J., Koteci, A., Balla, T., & Irvine, R. F. (2012). PI4P and PI(4,5)P 2 Are Essential But Independent Lipid Determinants of Membrane Identity. *Science*, *337*(6095), 727–730. https://doi.org/10.1126/science.1222483

Hansen, S. D., Lee, A. A., Duewell, B. R., & Groves, J. T. (2022). Membrane-mediated dimerization potentiates PIP5K lipid kinase activity. *ELife*, *11*. https://doi.org/10.7554/eLife.73747

Harper, C. B., Small, C., Davenport, E. C., Low, D. W., Smillie, K. J., Martínez-Mármol, R., Meunier, F. A., & Cousin, M. A. (2020). An epilepsy-associated SV2A mutation disrupts synaptotagmin-1 expression and activity-dependent trafficking. *Journal of Neuroscience*, *40*(23), 4586–4595. https://doi.org/10.1523/JNEUROSCI.0210-20.2020

Haucke, V., & De Camilli, P. (1999). AP-2 recruitment to synaptotagmin stimulated by tyrosine-based endocytic motifs. *Science*, *285*(5431), 1268–1271. https://doi.org/10.1126/science.285.5431.1268

Haucke, V., Neher, E., & Sigrist, S. J. (2011). Protein scaffolds in the coupling of synaptic exocytosis and endocytosis. *Nature Reviews Neuroscience*, *12*(3), 127–138. https://doi.org/10.1038/nrn2948

Haucke, V., Wenk, M. R., Chapman, E. R., Farsad, K., & De Camilli, P. (2000). Dual interaction of synaptotagmin with mu2- and alpha-adaptin facilitates clathrin-coated pit nucleation. *The EMBO Journal*, *19*(22), 6011–6019. https://doi.org/10.1093/emboj/19.22.6011

Heilmann, I. (2016). Phosphoinositide signaling in plant development. *Development*, *143*(12), 2044–2055. https://doi.org/10.1242/dev.136432

Henne, W. M., Boucrot, E., Meinecke, M., Evergren, E., Vallis, Y., Mittal, R., & McMahon, H. T. (2010). FCHo proteins are nucleators of Clathrin-Mediated endocytosis. *Science*, *328*(5983), 1281–1284. https://doi.org/10.1126/science.1188462

Heuser, J. E., & Reese, T. (1973). Evidence for recycling synaptic vesicle membrane during neurotransmitter release at the frog neuromuscular junction. *J Cell Biol*, *57*, 315–344. https://doi.org/10.1083/jcb.57.2.315

Holz, R. W., Hlubek, M. D., Sorensen, S. D., Fisher, S. K., Balla, T., Ozaki, S., Prestwich, G. D., Stuenkel, E. L., & Bittner, M. A. (2000). A pleckstrin homology domain specific

for phosphatidylinositol 4,5- bisphosphate (PtdIns-4,5-P2) and fused to green fluorescent protein identifies plasma membrane PtdIns-4,5-P2 as being important in exocytosis. *Journal of Biological Chemistry*, *275*(23), 17878–17885. https://doi.org/10.1074/jbc.M000925200

Honigmann, A., Van Den Bogaart, G., Iraheta, E., Risselada, H. J., Milovanovic, D., Mueller, V., Müllar, S., Diederichsen, U., Fasshauer, D., Grubmüller, H., Hell, S. W., Eggeling, C., Kühnel, K., & Jahn, R. (2013). Phosphatidylinositol 4,5-bisphosphate clusters act as molecular beacons for vesicle recruitment. *Nature Structural and Molecular Biology*, *20*(6), 679–686. https://doi.org/10.1038/nsmb.2570

Höning, S., Ricotta, D., Krauss, M., Späte, K., Spolaore, B., Motley, A., Robinson, M., Robinson, C., Haucke, V., & Owen, D. J. (2005). Phosphatidylinositol-(4,5)-bisphosphate regulates sorting signal recognition by the clathrin-associated adaptor complex AP2. *Molecular Cell*, *18*(5), 519–531. https://doi.org/10.1016/j.molcel.2005.04.019

Hosoi, N., Holt, M., & Sakaba, T. (2009). Calcium Dependence of Exo- and Endocytotic Coupling at a Glutamatergic Synapse. *Neuron*, *63*(2), 216–229. https://doi.org/10.1016/j.neuron.2009.06.010

Hu, J., Yuan, Q., Kang, X., Qin, Y., Li, L., Ha, Y., & Wu, D. (2015). Resolution of structure of PIP5K1A reveals molecular mechanism for its regulation by dimerization and dishevelled. *Nature Communications*, *6*. https://doi.org/10.1038/ncomms9205

Hua, Y., Woehler, A., Kahms, M., Haucke, V., Neher, E., & Klingauf, J. (2013). Blocking endocytosis enhances short-term synaptic depression under conditions of normal availability of vesicles. *Neuron*, *80*(2), 343–349. https://doi.org/10.1016/j.neuron.2013.08.010

Hui, E., Johnson, C. P., Yao, J., Dunning, F. M., & Chapman, E. R. (2009). Synaptotagmin-Mediated Bending of the Target Membrane Is a Critical Step in Ca2+-Regulated Fusion. *Cell*, *138*(4), 709–721. https://doi.org/10.1016/j.cell.2009.05.049

Imig, C., Min, S. W., Krinner, S., Arancillo, M., Rosenmund, C., Südhof, T. C., Rhee, J. S., Brose, N., & Cooper, B. H. (2014). The Morphological and Molecular Nature of Synaptic Vesicle Priming at Presynaptic Active Zones. *Neuron*, *84*(2), 416–431. https://doi.org/10.1016/j.neuron.2014.10.009

Ishihara, H., Shibasaki, Y., Kizuki, N., Katagiri, H., Yazaki, Y., Asano, T., & Oka, Y. (1996). Cloning of cDNAs encoding two isoforms of 68-kDa type I

phosphatidylinositol-4-phosphate 5-kinase. *Journal of Biological Chemistry*, *271*(39), 23611–23614. https://doi.org/10.1074/jbc.271.39.23611

Ishihara, H., Shibasaki, Y., Kizuki, N., Wada, T., Yazaki, Y., Asano, T., & Oka, Y. (1998). Type I phosphatidylinositol-4-phosphate 5-kinases. Cloning of the third isoform and deletion/substitution analysis of members of this novel lipid kinase family. *Journal of Biological Chemistry*, *273*(15), 8741–8748. https://doi.org/10.1074/jbc.273.15.8741

Israel, M., Gautron, J., & Lesbats, B. (1968). Isolation of the synaptic vesicles of the electric organ of the torpedo and localization of acetylcholine at their level. *Comptes Rendus Hebdomadaires Des Seances de l'Academie Des Sciences. Serie D: Sciences Naturelles*, *266*(3), 273–275.

Itoh, T., Ishihara, H., Shibasaki, Y., Oka, Y., & Takenawa, T. (2000). Autophosphorylation of type I phosphatidylinositol phosphate kinase regulates its lipid kinase activity. *Journal of Biological Chemistry*, *275*(25), 19389–19394. https://doi.org/10.1074/jbc.M000426200

Jackman, S. L., Turecek, J., Belinsky, J. E., & Regehr, W. G. (2016). The calcium sensor synaptotagmin 7 is required for synaptic facilitation. *Nature*, *529*(7584), 88–91. https://doi.org/10.1038/nature16507

Jahn, R., & Fasshauer, D. (2012). Molecular machines governing exocytosis of synaptic vesicles. *Nature*, *490*(7419), 201–207. https://doi.org/10.1038/nature11320.Molecular

Jarousse, N., & Kelly, R. B. (2001). The AP2 binding site of synaptotagmin 1 is not an internalization signal but a regulator of endocytosis. *Journal of Cell Biology*, *154*, 857–866. https://doi.org/10.1083/jcb.200103040

Jarquin-Pardo, M., Fitzpatrick, A., Galiano, F. J., First, E. A., & Davis, J. N. (2007). Phosphatidic acid regulates the affinity of the murine phosphatidylinositol 4-phosphate 5-kinase-1β for phosphatidylinositol-4-phosphate. *Journal of Cellular Biochemistry*, *100*(1), 112–128. https://doi.org/10.1002/jcb.21027

Jensen, M. B., Bhatia, V. K., Jao, C. C., Rasmussen, J. E., Pedersen, S. L., Jensen, K. J., Langen, R., & Stamou, D. (2011). Membrane Curvature Sensing by Amphipathic Helices. *The Journal of Biological Chemistry*, *286*(49), 42603–42614. https://doi.org/10.1074/jbc.M111.271130

Jia, J. Y., Lamer, S., Schümann, M., Schmidt, M. R., Krause, E., & Haucke, V. (2006). Quantitative proteomics analysis of detergent-resistant membranes from chemical synapses: Evidence for cholesterol as spatial organizer of synaptic vesicle cycling.

Molecular and Cellular Proteomics, *5*(11), 2060–2071. https://doi.org/10.1074/mcp.M600161-MCP200

Johnsson, A. K., & Karlsson, R. (2012). Synaptotagmin 1 causes phosphatidyl inositol lipid-dependent actin remodeling in cultured non-neuronal and neuronal cells. *Experimental Cell Research*, *318*(2), 114–126. https://doi.org/10.1016/j.yexcr.2011.10.009

Jorgensen, E. M., Hartwieg, E., Schuske, K., Nonet, M. L., Jin, Y., & Horvitz, H. R. (1995). Defective recycling of synaptic vesicles in synaptotagmin mutants of Caenorhabditis elegans. *Nature*, *378*, 196–199. https://doi.org/10.1038/378196a0

Jung, N., Wienisch, M., Gu, M., Rand, J. B., Müller, S. L., Krause, G., Jorgensen, E. M., Klingauf, J., & Haucke, V. (2007). Molecular basis of synaptic vesicle cargo recognition by the endocytic sorting adaptor stonin 2. *Journal of Cell Biology*, *179*(7), 1497–1510. https://doi.org/10.1083/jcb.200708107

Kaempf, N., Kochlamazashvili, G., Puchkov, D., Maritzen, T., Bajjalieh, S. M., & Natalia L. Kononenko, and V. H. (2015). Overlapping functions of stonin 2 and SV2 in sorting of the calcium sensor synaptotagmin 1 to synaptic vesicles. *Proceedings of the National Academy of Sciences*, *112*(23), 7297–7302. https://doi.org/10.1073/pnas.1501627112

Kaempf, N., & Maritzen, T. (2017). Safeguards of neurotransmission: Endocytic adaptors as regulators of synaptic vesicle composition and function. In *Frontiers in Cellular Neuroscience* (Vol. 11). Frontiers Media S.A. https://doi.org/10.3389/fncel.2017.00320

Kamalesh, K., Scher, N., Biton, T., Schejter, E. D., Shilo, B. Z., & Avinoam, O. (2021). Exocytosis by vesicle crumpling maintains apical membrane homeostasis during exocrine secretion. *Developmental Cell*, *56*(11), 1603-1616.e6. https://doi.org/10.1016/j.devcel.2021.05.004

Kamioka, Y., Fukuhara, S., Sawa, H., Nagashima, K., Masuda, M., Matsuda, M., & Mochizuki, N. (2004). A novel dynamin-associating molecule, formin-binding protein 17, induces tubular membrane invaginations and participates in endocytosis. *Journal of Biological Chemistry*, *279*(38), 40091–40099. https://doi.org/10.1074/jbc.M404899200

Katz, B., & Miledi, R. (1967). The timing of calcium action during neuromuscular transmission. *Journal of Physiology*, *189*, 535–544.

Kawasaki, F., Hazen, M., & Ordway, R. W. (2000). Fast synaptic fatigue in shibire mutants reveals a rapid requirement for dynamin in synaptic vesicle membrane trafficking [2]. *Nature Neuroscience*, *3*(9), 859–860. https://doi.org/10.1038/78753

Khuong, T. M., Habets, R. L. P., Kuenen, S., Witkowska, A., Kasprowicz, J., Swerts, J., Jahn, R., van den Bogaart, G., & Verstreken, P. (2013). Synaptic PI(3,4,5)P3 Is

Required for Syntaxin1A Clustering and Neurotransmitter Release. *Neuron*, *77*(6), 1097–1108. https://doi.org/10.1016/j.neuron.2013.01.025

Kiessling, V., Kreutzberger, A. J. B., Liang, B., Nyenhuis, S. B., Seelheim, P., Castle, J. D., Cafiso, D. S., & Tamm, L. K. (2018). A molecular mechanism for calcium-mediated synaptotagmin-triggered exocytosis. *Nature Structural and Molecular Biology*, *25*(10), 911–917. https://doi.org/10.1038/s41594-018-0130-9

Kim, S. H., & Ryan, T. A. (2009). A distributed set of interactions controls μ2 functionality in the role of AP-2 as a sorting adaptor in synaptic vesicle endocytosis. *Journal of Biological Chemistry*, *284*(47), 32803–32812. https://doi.org/10.1074/jbc.M109.039149

Kim, W. T., Chang, S., Daniell, L., Cremona, O., Di Paolo, G., & De Camilli, P. (2002). Delayed reentry of recycling vesicles into the fusion-competent synaptic vesicle pool in synaptojanin 1 knockout mice. *Proceedings of the National Academy of Sciences of the United States of America*, *99*(26), 17143–17148. https://doi.org/10.1073/pnas.222657399

Kittel, R. J., Wichmann, C., Rasse, T. M., Fouquet, W., Schmidt, M., Schmid, A., Wagh, D. a, Pawlu, C., Kellner, R. R., Willig, K. I., Hell, S. W., Buchner, E., Heckmann, M., & Sigrist, S. J. (2006). Bruchpilot Promotes Active Zone Assembly, Ca2þ Channel Clustering, and Vesicle Release. *Science*, *312*(May), 1051–1054. https://doi.org/10.1126/science.1126308

Koch, M., & Holt, M. (2012). Coupling exo- and endocytosis: An essential role for PIP 2 at the synapse. *Biochimica et Biophysica Acta - Molecular and Cell Biology of Lipids*, *1821*(8), 1114–1132. https://doi.org/10.1016/j.bbalip.2012.02.008

Koh, T. W., & Bellen, H. J. (2003). Synaptotagmin I, a Ca2+ sensor for neurotransmitter release. *Trends in Neurosciences*, *26*(8), 413–422. https://doi.org/10.1016/S0166-2236(03)00195-4

Kononenko, N. L., Diril, M. K., Puchkov, D., Kintscher, M., Koo, S. J., Pfuhl, G., Winter, Y., Wienisch, M., Klingauf, J., Breustedt, J., Schmitz, D., Maritzen, T., & Haucke, V. (2013). Compromised fidelity of endocytic synaptic vesicle protein sorting in the absence of stonin 2. *Proceedings of the National Academy of Sciences*, *110*(6), E526–E535. https://doi.org/10.1073/pnas.1218432110

Kononenko, N. L., & Haucke, V. (2015). Molecular mechanisms of presynaptic membrane retrieval and synaptic vesicle reformation. In *Neuron* (Vol. 85, Issue 3, pp. 484–496). Cell Press. https://doi.org/10.1016/j.neuron.2014.12.016

Bibliography

Kononenko, N. L., Puchkov, D., Classen, G. A., Walter, A. M., Pechstein, A., Sawade, L., Kaempf, N., Trimbuch, T., Lorenz, D., Rosenmund, C., Maritzen, T., & Haucke, V. (2014). Clathrin/AP-2 mediate synaptic vesicle reformation from endosome-like vacuoles but are not essential for membrane retrieval at central synapses. *Neuron*, *82*(5), 981–988. https://doi.org/10.1016/j.neuron.2014.05.007

Koo, S. J., Kochlamazashvili, G., Rost, B., Puchkov, D., Gimber, N., Lehmann, M., Tadeus, G., Schmoranzer, J., Rosenmund, C., Haucke, V., & Maritzen, T. (2015). Vesicular Synaptobrevin/VAMP2 Levels Guarded by AP180 Control Efficient Neurotransmission. *Neuron*, *88*(2), 330–344. https://doi.org/10.1016/j.neuron.2015.08.034

Koo, S. J., Markovic, S., Puchkov, D., Mahrenholz, C. C., Beceren-Braun, F., Maritzen, T., Dernedde, J., Volkmer, R., Oschkinat, H., & Haucke, V. (2011). SNARE motif-mediated sorting of synaptobrevin by the endocytic adaptors clathrin assembly lymphoid myeloid leukemia (CALM) and AP180 at synapses. *Proceedings of the National Academy of Sciences of the United States of America*, *108*(33), 13540–13545. https://doi.org/10.1073/pnas.1107067108

Krauß, M., & Haucke, V. (2007). Phosphoinositide-metabolizing enzymes at the interface between membrane traffic and cell signalling. *EMBO Reports*, *8*(3), 241–246. https://doi.org/10.1038/sj.embor.7400919

Krauss, M., Kinuta, M., Wenk, M. R., De Camilli, P., Takei, K., & Haucke, V. (2003). ARF6 stimulates clathrin/AP-2 recruitment to synaptic membranes by activating phosphatidylinositol phosphate kinase type Iγ. *Journal of Cell Biology*, *162*(1), 113–124. https://doi.org/10.1083/jcb.200301006

Krauss, M., Kukhtina, V., Pechstein, A., & Haucke, V. (2006). Stimulation of phosphatidylinositol kinase type I-mediated phosphatidylinositol (4,5)-bisphosphate synthesis by AP-2μ-cargo complexes. *Proceedings of the National Academy of Sciences of the United States of America*, *103*(32), 11934–11939. https://doi.org/10.1073/pnas.0510306103

Kunz, J., Wilson, M. P., Kisseleva, M., Hurley, J. H., Majerus, P. W., & Anderson, R. A. (2000). The activation loop of phosphatidylinositol phosphate kinases determines signaling specificity. *Molecular Cell*, *5*(1), 1–11. https://doi.org/10.1016/S1097-2765(00)80398-6

Kwon, S. K., Sando, R., Lewis, T. L., Hirabayashi, Y., Maximov, A., & Polleux, F. (2016). LKB1 Regulates Mitochondria-Dependent Presynaptic Calcium Clearance and

Neurotransmitter Release Properties at Excitatory Synapses along Cortical Axons. *PLoS Biology*, *14*(7), 1–27. https://doi.org/10.1371/journal.pbio.1002516

Laemmli, U. K. (1970). Cleavage of Structural Proteins during the Assembly of the Head of Bacteriophage T4. *Nature*, *227*, 680–685. https://doi.org/10.1038/227680a0

Lai, M. M., Hong, J. J., Ruggiero, A. M., Burnett, P. E., Slepnev, V. I., De Camilli, P., & Snyder, S. H. (1999). The calcineurin-dynamin 1 complex as a calcium sensor for synaptic vesicle endocytosis. *Journal of Biological Chemistry*, *274*(37), 25963–25966. https://doi.org/10.1074/jbc.274.37.25963

Lai, Y., Lou, X., Diao, J., & Shin, Y. K. (2015). Molecular origins of synaptotagmin 1 activities on vesicle docking and fusion pore opening. *Scientific Reports*, *5*. https://doi.org/10.1038/srep09267

Lai, Y., & Shin, Y. K. (2012). The importance of an asymmetric distribution of acidic lipids for synaptotagmin 1 function as a Ca 2+ sensor. *Biochemical Journal*, *443*(1), 223–229. https://doi.org/10.1042/BJ20112044

Lauwers, E., Goodchild, R., & Verstreken, P. (2016). Membrane Lipids in Presynaptic Function and Disease. *Neuron*, *90*(1), 11–25. https://doi.org/10.1016/j.neuron.2016.02.033

Lazzell, D. R., Belizaire, R., Thakur, P., Sherry, D. M., & Janz, R. (2004). SV2B regulates synaptotagmin 1 by direct interaction. *Journal of Biological Chemistry*, *279*(50), 52124–52131. https://doi.org/10.1074/jbc.M407502200

Lee, S. Y., Voronov, S., Letinic, K., Nairn, A. C., Di Paolo, G., & De Camilli, P. (2005). Regulation of the interaction between PIPKIγ and talin by proline-directed protein kinases. *Journal of Cell Biology*, *168*(5), 789–799. https://doi.org/10.1083/jcb.200409028

Lee, S. Y., Wenk, M. R., Kim, Y., Nairn, A. C., & De Camilli, P. (2004). Regulation of synaptojanin 1 by cyclin-dependent kinase 5 at synapses. *Proc Natl Acad Sci U S A*, *101*(2), 546–551. https://doi.org/10.1073/pnas.0307813100

Li, C., Ullrich, B., Zhang, J. Z., Anderson, R. G. W., Brose, N., & Südhof, T. C. (1995). Ca(2+)-dependent and -independent activities of neural and non-neural synaptotagmins. *Nature*, *375*(6532), 594–599. https://doi.org/doi:10.1038/375594a0

Li, L. Y., Shin, O. H., Rhee, J. S., Araç, D., Rah, J. C., Rizo, J., Südhof, T., & Rosenmund, C. (2006). Phosphatidylinositol phosphates as co-activators of Ca2+ binding to C2 domains of synaptotagmin 1. *Journal of Biological Chemistry*, *281*(23), 15845–15852. https://doi.org/10.1074/jbc.M600888200

Bibliography

Li, Y. C., Chanaday, N. L., Xu, W., & Kavalali, E. T. (2017). Synaptotagmin-1- and Synaptotagmin-7-Dependent Fusion Mechanisms Target Synaptic Vesicles to Kinetically Distinct Endocytic Pathways. *Neuron*, *93*(3), 616-631.e3. https://doi.org/10.1016/j.neuron.2016.12.010

Lin, C. C., Seikowski, J., Pérez-Lara, A., Jahn, R., Höbartner, C., & Walla, P. J. (2014). Control of membrane gaps by synaptotagmin-Ca 2+ measured with a novel membrane distance ruler. *Nature Communications*, *5*, 5859. https://doi.org/10.1038/ncomms6859

Ling, K., Bairstow, S. F., Carbonara, C., Turbin, D. A., Huntsman, D. G., & Anderson, R. A. (2007). Type Iγ phosphatidylinositol phosphate kinase modulates adherens junction and E-cadherin trafficking via a direct interaction with μ 1B adaptin. *Journal of Cell Biology*, *176*(3), 343–353. https://doi.org/10.1083/jcb.200606023

Littleton, J. T., Bai, J., Vyas, B., Desai, R., Baltus, A. E., Garment, M. B., Carlson, S. D., Ganetzky, B., & Chapman, E. R. (2001). synaptotagmin Mutants Reveal Essential Functions for the C2B Domain in Ca 2-Triggered Fusion and Recycling of Synaptic Vesicles In Vivo. *Journal of Neuroscience*, *21*(5), 1421–1422. https://doi.org/10.1523/JNEUROSCI.21-05-01421.2001

Littleton, J. T., & Bellen, H. J. (1995). Synaptotagmin controls and modulates synaptic-vesicle fusion in a Ca(2+)-dependent manner. *Trends Neurosci.*, *18*(4), 177–183. https://doi.org/10.1016/0166-2236(95)93898-8

Littleton, J. T., Sternt, M., Perin, M., & Bellen, H. J. (1994). Calcium dependence of neurotransmitter release and rate of spontaneous vesicle fusions are altered in Drosophila synaptotagmin mutants. *Proc. Natd. Acad. Sci. USA*, *91*, 10888–10892.

Liu, A., Sui, D., Wu, D., & Hu, J. (2016). The activation loop of PIP5K functions as a membrane sensor essential for lipid substrate processing. *Science Advances*, *2*(11). https://doi.org/10.1126/sciadv.1600925

Lodish, H., Berk, A., Kaiser, C. A., Krieger, M., Scott, M. P., Bretscher, A., Ploegh, H., & Matsudaira, P. (2007). Cell Signaling II: Signaling Pathways that Control Gene Activity. In *Molecular Cell Biology. New York, WH Freeman and Company.: Vol. 6th ed.* (pp. P665-712).

Loewen, C. A., Royer, S. M., & Reist, N. E. (2006). Drosophila synaptotagmin I null mutants show severe alterations in vesicle populations but calcium-binding motif mutants do not. *Journal of Comparative Neurology*, *496*(1), 1–12. https://doi.org/10.1002/cne.20868

López-Hernández, T., Takenaka, K., Mori, Y., Kongpracha, P., Nagamori, S., Haucke, V., & Takamori, S. (2022). Clathrin-independent endocytic retrieval of SV proteins mediated by the clathrin adaptor AP-2 at mammalian central synapses. *ELife*, *11*, 1–33. https://doi.org/10.7554/eLife.71198

Lynch, B. A., Lambeng, N., Nocka, K., Kensel-Hammes, P., Bajjalieh, S. M., Matagne, A., Fuks, B., & Catterall, W. A. (2004). The synaptic vesicle protein SV2A is the binding site for the antiepileptic drug levetiracetam. *Proceedings of the National Academy of Sciences of the United States of America*, *101*, 9861–9866. www.pnas.orgcgidoi10.1073pnas.0308208101

Malsam, J., Kreye, S., & Söllner, T. H. (2008). Membrane traffic in the secretory pathway: Membrane fusion: SNAREs and regulation. *Cellular and Molecular Life Sciences*, *65*(18), 2814–2832. https://doi.org/10.1007/s00018-008-8352-3

Maritzen, T., & Haucke, V. (2017). Coupling of exocytosis and endocytosis at the presynaptic active zone. *Neuroscience Research*, *127*, 45–52. https://doi.org/10.1016/j.neures.2017.09.013

Maritzen, T., & Haucke, V. (2018). Coupling of exocytosis and endocytosis at the presynaptic active zone. *Neuroscience Research*, *127*, 45–52. https://doi.org/10.1016/j.neures.2017.09.013

Maritzen, T., Podufall, J., & Haucke, V. (2010). Stonins - Specialized adaptors for synaptic vesicle recycling and beyond? *Traffic*, *11*(1), 8–15. https://doi.org/10.1111/j.1600-0854.2009.00971.x

Martens, S., Kozlov, M. M., & McMahon, H. T. (2007). How Synaptotagmin Promotes Membrane Fusion. *Science*, *316*(5828), 1205–1208.

Martens, S., & McMahon, H. T. (2008). Mechanisms of membrane fusion : disparate players and common principles. *Nature Reviews Molecular Cell Biology*, *9*(7), 543. https://doi.org/10.1038/nrm2417

Martin, T. F. J. (2015). PI(4,5)P2-binding effector proteins for vesicle exocytosis. *Biochimica et Biophysica Acta - Molecular and Cell Biology of Lipids*, *1851*(6), 785–793. https://doi.org/10.1016/j.bbalip.2014.09.017

Martina, J. A., Bonangelino, C. J., Aguilar, R. C., & Bonifacino, J. S. (2001). Stonin 2: An Adaptor-like Protein that Interacts with Components of the Endocytic Machinery. *The Journal of Cell Biology*, *153*(5), 1111–1120. http://www.jcb.org/cgi/content/full/153/5/1111

Bibliography

Maximov, A. (2009). Synaptotagmins. In Larry R. Squire (Ed.), *Encyclopedia of Neuroscience* (pp. 819–821). https://doi.org/10.1016/B978-008045046-9.01358-9

Maximov, A., Tang, J., Yang, X., Pang, Z. P., & Südhof, T. C. (2009). Complexin Controls the Force Transfer from SNARE Complexes to Membranes in Fusion. *Science*, *323*, 516–521. https://doi.org/10.1126/science.1166505

McDonald, N. A., Vander Kooi, C. W., Ohi, M. D., & Gould, K. L. (2015). Oligomerization but Not Membrane Bending Underlies the Function of Certain F-BAR Proteins in Cell Motility and Cytokinesis. *Developmental Cell*, *35*(6), 725–736. https://doi.org/10.1016/j.devcel.2015.11.023

McMahon, H. T., & Gallop, J. L. (2005). Membrane curvature and mechanisms of dynamic cell membrane remodelling. *Nature*, *438*(7068), 590–596. https://doi.org/10.1038/nature04396

Medina-Kauwe, L. K., Xie, J., & Hamm-Alvarez, S. (2005). Intracellular trafficking of nonviral vectors. *Gene Therapy*, *12*(24), 1734–1751. https://doi.org/10.1038/sj.gt.3302592

Mellman, D. L., Gonzales, M. L., Song, C., Barlow, C. A., Wang, P., Kendziorski, C., & Anderson, R. A. (2008). A PtdIns4,5P2-regulated nuclear poly(A) polymerase controls expression of select mRNAs. *Nature*, *451*(7181), 1013–1017. https://doi.org/10.1038/nature06666

Mettlen, M., Pucadyil, T., Ramachandran, R., & Schmid, S. L. (2009). Dissecting dynamin's role in clathrin-mediated endocytosis. *Biochemical Society Transactions*, *37*(5), 1022–1026. https://doi.org/10.1042/BST0371022

Michel, K., Müller, J. A., Oprişoreanu, A. M., & Schoch, S. (2015). The presynaptic active zone: A dynamic scaffold that regulates synaptic efficacy. In *Experimental Cell Research* (Vol. 335, Issue 2, pp. 157–164). Academic Press Inc. https://doi.org/10.1016/j.yexcr.2015.02.011

Miesenböck, G., De Angelis, D. A., & Rothman, J. E. (1998). Visualizing secretion and synaptic transmission with pH-sensitive green fluorescent proteins. *Nature*, *394*(6689), 192–195. https://doi.org/10.1038/28190

Miller, T. M., & Heuser, J. E. (1984). Endocytosis of synaptic vesicle membrane at the frog neuromuscular junction. *Journal of Cell Biology*, *98*(2), 685–698. https://doi.org/10.1083/jcb.98.2.685

Milosevic, I., Sørensen, J. B., Lang, T., Krauss, M., Nagy, G., Haucke, V., Jahn, R., & Neher, E. (2005). Plasmalemmal phosphatidylinositol-4,5-bisphosphate level regulates

the releasable vesicle pool size in chromaffin cells. *Journal of Neuroscience*, *25*(10), 2557–2565. https://doi.org/10.1523/JNEUROSCI.3761-04.2005

Milovanovic, D., Wu, Y., Bian, X., & De Camilli, P. (2018). A liquid phase of synapsin and lipid vesicles. *Science*, *361*(6402), 604–607. https://doi.org/10.1126/science.aat5671

Mim, C., & Unger, V. M. (2012). Membrane curvature and its generation by BAR proteins. *Trends in Biochemical Sciences*, *37*(12), 526–533. https://doi.org/10.1016/j.tibs.2012.09.001.Membrane

Mittelsteadt, T., Seifert, G., Alvárez-Barón, E., Steinhäuser, C., Becker, A. J., & Schoch, S. (2009). Differential mRNA expression patterns of the synaptotagmin gene family in the rodent brain. *Journal of Comparative Neurology*, *512*(4), 514–528. https://doi.org/10.1002/cne.21908

Modi, J. P., Prentice, H., & Wu, J. Y. (2015). Regulation of GABA Neurotransmission by Glutamic Acid Decarboxylase (GAD). *Regulation of GABA Neurotransmission by Glutamic Acid Decarboxylase (GAD)*, *21*(34), 4939–4942. https://doi.org/10.2174/1381612821666150917094343

Morgan, J. R., Di Paolo, G., Werner, H., Shchedrina, V. A., Pypaert, M., Pieribone, V. A., & De Camilli, P. (2004). A role for talin in presynaptic function. *Journal of Cell Biology*, *167*(1), 43–50. https://doi.org/10.1083/jcb.200406020

Morgans, C. W., Kensel-Hammes, P., Hurley, J. B., Burton, K., Idzerdal, R., McKnight, G. S., & Bajjalieh, S. M. (2009). Loss of the synaptic vesicle protein SV2B results in reduced neurotransmission and altered synaptic vesicle protein expression in the retina. *PLoS ONE*, *4*(4). https://doi.org/10.1371/journal.pone.0005230

Mori, Y., & Takamori, S. (2018). Molecular signatures underlying synaptic vesicle cargo retrieval. In *Frontiers in Cellular Neuroscience* (Vol. 11). Frontiers Media S.A. https://doi.org/10.3389/fncel.2017.00422

Moritz, A., De Graan, P. N. E., Gispen, W. H., & Wirtz, K. W. A. (1992). Phosphatidic acid is a specific activator of phosphatidylinositol-4- phosphate kinase. *Journal of Biological Chemistry*, *267*(11), 7207–7210. https://doi.org/10.1016/s0021-9258(18)42504-5

Mullen, G. P., Grundahl, K. M., Gu, M., Watanabe, S., Hobson, R. J., Crowell, J. A., McManus, J. R., Mathews, E. A., Jorgensen, E. M., & Rand, J. B. (2012). UNC-41/stonin functions with AP2 to recycle synaptic vesicles in Caenorhabditis elegans. *PLoS ONE*, *7*(7). https://doi.org/10.1371/journal.pone.0040095

Bibliography

Mullins, C., Fishell, G., & Tsien, R. W. (2016). Unifying Views of Autism Spectrum Disorders: A Consideration of Autoregulatory Feedback Loops. *Neuron*, *89*(6), 1131–1156. https://doi.org/10.1016/j.neuron.2016.02.017

Murthy, V. N., & Stevens, C. F. (1998). Synaptic vesicles retain their identity through the endocytic cycle. *Nature*, *392*(6675), 497–501. https://doi.org/10.1038/33152

Mutch, S. A., Kensel-Hammes, P., Gadd, J. C., Fujimoto, B. S., Allen, R. W., Schiro, P. G., Lorenz, R. M., Kuyper, C. L., Kuo, J. S., M., B. S., & Chiu, D. T. (2011). Protein quantification at the single vesicle level reveals that a subset of synaptic vesicle proteins are trafficked with high precision. *Journal of Neuroscience*, *31*(4), 1461–1470. https://doi.org/10.1016/S0140-6736(02)11602-3.Association

Myers, M. D., Ryazantsev, S., Hicke, L., & Payne, G. S. (2016). Calmodulin Promotes N-BAR Domain-Mediated Membrane Constriction and Endocytosis. *Developmental Cell*, *37*(2), 162–173. https://doi.org/10.1016/j.devcel.2016.03.012

Nakano-Kobayashi, A., Yamazaki, M., Unoki, T., Hongu, T., Murata, C., Taguchi, R., Katada, T., Frohman, M. A., Yokozeki, T., & Kanaho, Y. (2007). Role of activation of PIP5Kγ661 by AP-2 complex in synaptic vesicle endocytosis. *EMBO Journal*, *26*(4), 1105–1116. https://doi.org/10.1038/sj.emboj.7601573

Nakatsu, F., Baskin, J. M., Chung, J., Tanner, L. B., Shui, G., Lee, S. Y., Pirruccello, M., Hao, M., Ingolia, N. T., Wenk, M. R., & De Camilli, P. (2012). Ptdins4P synthesis by PI4KIIIα at the plasma membrane and its impact on plasma membrane identity. *Journal of Cell Biology*, *199*(6), 1003–1016. https://doi.org/10.1083/jcb.201206095

Nicholson-Fish, J. C., Kokotos, A. C., Gillingwater, T. H., Smillie, K. J., & Cousin, M. A. (2015). VAMP4 Is an Essential Cargo Molecule for Activity-Dependent Bulk Endocytosis. *Neuron*, *88*(5), 973–984. https://doi.org/10.1016/j.neuron.2015.10.043

Nicholson-Tomishima, K., & Ryan, T. A. (2004). Kinetic efficiency of endocytosis at mammalian CNS synapses requires synaptotagmin I. *Proceedings of the National Academy of Sciences of the United States of America*, *101*(47), 16648–16652. https://doi.org/10.1073/pnas.0406968101

Noack, L. C., & Jaillais, Y. (2017). Precision targeting by phosphoinositides: how PIs direct endomembrane trafficking in plants. In *Current Opinion in Plant Biology* (Vol. 40, pp. 22–33). Elsevier Ltd. https://doi.org/10.1016/j.pbi.2017.06.017

Noack, L. C., & Jaillais, Y. (2020). Functions of Anionic Lipids in Plants. *Annual Review of Plant Biology , 71*, 71–102. https://doi.org/10.1146/annurev-arplant-081519

Nyenhuis, S. B., Karandikar, N., Kiessling, V., Kreutzberger, A. J. B., Thapa, A., Liang, B., Tamm, L. K., & Cafiso, D. S. (2021). Conserved arginine residues in synaptotagmin 1 regulate fusion pore expansion through membrane contact. *Nature Communications*, *12*(1). https://doi.org/10.1038/s41467-021-21090-x

Ogunmowo, T. H., Jing, H., Raychaudhuri, S., Kusick, G. F., Imoto, Y., Li, S., Itoh, K., Ma, Y., Jafri, H., Dalva, M. B., Chapman, E. R., Ha, T., Watanabe, S., & Liu, J. (2023). Membrane compression by synaptic vesicle exocytosis triggers ultrafast endocytosis. *Nature Communications*, *14*(1). https://doi.org/10.1038/s41467-023-38595-2

Pan, P. Y., Marrs, J., & Ryan, T. A. (2015). Vesicular glutamate transporter 1 orchestrates recruitment of other synaptic vesicle cargo proteins during synaptic vesicle recycling. *Journal of Biological Chemistry*, *290*(37), 22593–22601. https://doi.org/10.1074/jbc.M115.651711

Pan, P. Y., Sheehan, P., Wang, Q., Zhu, X., Zhang, Y., Choi, I., Li, X., Saenz, J., Zhu, J., Wang, J., Gaamouch, F. El, Zhu, L., Cai, D., & Yue, Z. (2020). Synj1 haploinsufficiency causes dopamine neuron vulnerability and alpha-synuclein accumulation in mice. *Human Molecular Genetics*, *29*(14), 2300–2312. https://doi.org/10.1093/hmg/ddaa080

Pang, Z. P., Shin, O.-H., Meyer, A. C., Rosenmund, C., & Sudhof, T. C. (2006). A Gain-of-Function Mutation in Synaptotagmin-1 Reveals a Critical Role of Ca2+-Dependent Soluble N-Ethylmaleimide-Sensitive Factor Attachment Protein Receptor Complex Binding in Synaptic Exocytosis. *Journal of Neuroscience*, *26*(48), 12556–12565. https://doi.org/10.1523/JNEUROSCI.3804-06.2006

Park, Y., Seo, J. B., Fraind, A., Pérez-Lara, A., Yavuz, H., Han, K., Jung, S. R., Kattan, I., Walla, P. J., Choi, M., Cafiso, D. S., Koh, D. S., & Jahn, R. (2015). Synaptotagmin-1 binds to PIP 2 -containing membrane but not to SNAREs at physiological ionic strength. *Nature Structural and Molecular Biology*, *22*(10), 815–823. https://doi.org/10.1038/nsmb.3097

Paul, A. S., & Pollard, T. D. (2009). Review of the mechanism of processive actin filament elongation by formins. *Cell Motility and the Cytoskeleton*, *66*(8), 606–617. https://doi.org/10.1002/cm.20379

Perera, R. M., Zoncu, R., Lucast, L., De Camilli, P., & Toomre, D. (2006). Two synaptojanin 1 isoforms are recruited to clathrin-coated pits at different stages. *Proceedings of the National Academy of Sciences of the United States of America*, *103*(51), 19332–19337. https://doi.org/10.1073/pnas.0609795104

Bibliography

Perin, M. S., Brose, N., Jahn, R., & Sudhof, T. C. (1991). Domain Structure of Synaptotagmin (p65)*. *Biochemistry*, *266*(1), 623–629.

Phillips, A. M., Smith, M., Ramaswami, M., & Kelly, L. E. (2000). The products of the Drosophila stoned locus interact with synaptic vesicles via synaptotagmin. *Journal of Neuroscience*, *20*(22), 8254–8261. https://doi.org/10.1523/jneurosci.20-22-08254.2000

Podufall, J., Tian, R., Knoche, E., Puchkov, D., Walter, A. M., Rosa, S., Quentin, C., Vukoja, A., Jung, N., Lampe, A., Wichmann, C., Böhme, M., Depner, H., Zhang, Y. Q., Schmoranzer, J., Sigrist, S. J., & Haucke, V. (2014). A presynaptic role for the cytomatrix protein GIT in synaptic vesicle recycling. *Cell Reports*, *7*(5), 1417–1425. https://doi.org/10.1016/j.celrep.2014.04.051

Poskanzer, K. E., Fetter, R. D., & Davis, G. W. (2006). Discrete Residues in the C2B Domain of Synaptotagmin I Independently Specify Endocytic Rate and Synaptic Vesicle Size. *Neuron*, *50*(1), 49–62. https://doi.org/10.1016/j.neuron.2006.02.021

Poskanzer, K. E., Marek, K. W., Sweeney, S. T., & Davis, G. W. (2003). Synaptotagmin I is necessary for compensatory synaptic vesicle endocytosis in vivo. *Nature*, *426*(6966), 559–563. https://doi.org/10.1038/nature02157

Posor, Y., Jang, W., & Haucke, V. (2022). Phosphoinositides as membrane organizers. *Nature Reviews Molecular Cell Biology*, *23*(12), 797–816. https://doi.org/10.1038/s41580-022-00490-x

Potthoff, E., Guillaume-Gentil, O., Ossola, D., Polesel-Maris, J., LeibundGut-Landmann, S., Zambelli, T., & Vorholt, J. A. (2012). Rapid and Serial Quantification of Adhesion Forces of Yeast and Mammalian Cells. *PLoS ONE*, *7*(12). https://doi.org/10.1371/journal.pone.0052712

Puchkov, D., & Haucke, V. (2013). Greasing the synaptic vesicle cycle by membrane lipids. *Trends in Cell Biology*, *23*(10), 493–503. https://doi.org/10.1016/j.tcb.2013.05.002

Pyle, R. A., Schivell, A. E., Hidaka, H., & Bajjalieh, S. M. (2000). Phosphorylation of synaptic vesicle protein 2 modulates binding to synaptotagmin. *Journal of Biological Chemistry*, *275*(22), 17195–17200. https://doi.org/10.1074/jbc.M000674200

Radhakrishnan, A., Stein, A., Jahn, R., & Fasshauer, D. (2009). The Ca2+ affinity of synaptotagmin 1 is markedly increased by a specific interaction of its C2B domain with phosphatidylinositol 4,5-bisphosphate. *Journal of Biological Chemistry*, *284*(38), 25749–25760. https://doi.org/10.1074/jbc.M109.042499

Rao, Y., & Haucke, V. (2011). Membrane shaping by the Bin/amphiphysin/Rvs (BAR) domain protein superfamily. *Cellular and Molecular Life Sciences*, *68*(24), 3983–3993. https://doi.org/10.1007/s00018-011-0768-5

Reiner, A., & Levitz, J. (2018). Glutamatergic Signaling in the Central Nervous System: Ionotropic and Metabotropic Receptors in Concert. *Neuron*, *98*(6), 1080–1098. https://doi.org/10.1016/j.neuron.2018.05.018.

Reubold, T. F., Faelber, K., Plattner, N., Posor, Y., Ketel, K., Curth, U., Schlegel, J., Anand, R., Manstein, D. J., Noé, F., Haucke, V., Daumke, O., & Eschenburg, S. (2015). Crystal structure of the dynamin tetramer. *Nature*, *525*(7569), 404–408. https://doi.org/10.1038/nature14880

Richards, D. A., Guatimosim, C., & Betz, W. J. (2000). Two Endocytic Recycling Routes Selectively Fill Two Vesicle Pools in Frog Motor Nerve Terminals. *Neuron*, *27*(3), 551–559.

Rizzoli, S. O., & Betz, W. J. (2005). Synaptic vesicle pools. *Nature Reviews Neuroscience*, *6*(1), 57–69. https://doi.org/10.1038/nrn1583

Rodríguez-Menchaca, A. A., Adney, S. K., Zhou, L., & Logothetis, D. E. (2012). Dual regulation of voltage-sensitive ion channels by PIP2. *Frontiers in Pharmacology*, *3 SEP*(September), 1–7. https://doi.org/10.3389/fphar.2012.00170

Rohde, G., Wenzel, D., & Haucke, V. (2002). A phosphatidylinositol (4,5)-bisphosphate binding site within μ-adaptin regulates clathrin-mediated endocytosis. *Journal of Cell Biology*, *158*(2), 209–214. https://doi.org/10.1083/jcb.200203103

Ryu, J. K., Jahn, R., & Yoon, T. Y. (2016). Progresses in understanding N-ethylmaleimide sensitive factor (NSF) mediated disassembly of SNARE complexes. *Biopolymers*, *105*(8), 518–531. https://doi.org/10.1002/bip.22854

Saarikangas, J., Zhao, H., & Lappalainen, P. (2010). Regulation of the actin cytoskeleton-plasma membrane interplay by phosphoinositides. *Physiological Reviews*, *90*(1), 259–289. https://doi.org/10.1152/physrev.00036.2009

Saheki, Y., & De Camilli, P. (2012). Synaptic vesicle endocytosis. *Cold Spring Harbor Perspectives in Biology*, *5*(3), 323–330.

Sakaba, T., Kononenko, N. L., Bacetic, J., Pechstein, A., Schmoranzer, J., Yao, L., Barth, H., Shupliakov, O., Kobler, O., Aktories, K., & Haucke, V. (2013). Fast neurotransmitter release regulated by the endocytic scaffold intersectin. *Proceedings of the National Academy of Sciences*, *110*(20), 8266–8271. https://doi.org/10.1073/pnas.1219234110

Bibliography

Salzer, J. L. (2015). Schwann cell myelination. *Cold Spring Harbor Perspectives in Biology*, *7*(8), 1–26. https://doi.org/10.1101/cshperspect.a020529

Sandbichler, A. M., Aschberger, T., & Pelster, B. (2013). A method to evaluate the efficiency of transfection reagents in an adherent zebrafish cell line. *BioResearch Open Access*, *2*(1), 20–27. https://doi.org/10.1089/biores.2012.0287

Sang, Y. L., Voronov, S., Letinic, K., Nairn, A. C., Di Paolo, G., & De Camilli, P. (2005). Regulation of the interaction between PIPKIγ and talin by proline-directed protein kinases. *Journal of Cell Biology*, *168*(5), 789–799. https://doi.org/10.1083/jcb.200409028

Sanger, F., Nicklen, S., & Coulson, A. R. (1977). DNA sequencing with chain-terminating inhibitors. *Proceedings of the National Academy of Sciences*, *74*(12), 5463–5467. https://doi.org/10.1073/pnas.74.12.5463

Sankaranarayanan, S., Angelis, D. De, Rothman, J. E., & Ryan, T. A. (2000). The Use of pHluorins for Optical Measurements of Presynaptic Activity. *Biophysical Journal*, *79*(4), 2199–2208. https://doi.org/10.1016/S0006-3495(00)76468-X

Sankaranarayanan, S., & Ryan, T. A. (2001). Calcium accelerates endocytosis of vSNAREs at hippocampal synapses. *Nature Neuroscience*, *4*(2), 129–136. https://doi.org/10.1038/83949

Schechter, M., Atias, M., Abd Elhadi, S., Davidi, D., Gitler, D., & Sharon, R. (2020). A-synuclein facilitates endocytosis by elevating the steady-state levels of phosphatidylinositol 4,5-bisphosphate. *Journal of Biological Chemistry*, *295*(52), 18076–18090. https://doi.org/10.1074/jbc.RA120.015319

Schiavo, G., Gu, Q.-M., Prestwich, G. D., Sollner, T. H., & Rothman, J. E. (1996). Calcium-dependent switching of the specificity of phosphoinositide binding to synaptotagmin. *Proceedings of the National Academy of Sciences*, *93*(23), 13327–13332. https://doi.org/10.1073/pnas.93.23.13327

Schivell, A. E., Batchelor, R. H., & Bajjalieh, S. M. (1996). Isoform-specific, calcium-regulated interaction of the synaptic vesicle proteins SV2 and synaptotagmin. *Journal of Biological Chemistry*, *271*(44), 27770–27775. https://doi.org/10.1074/jbc.271.44.27770

Schivell, A. E., Mochida, S., Kensel-Hammes, P., Custer, K. L., & Bajjalieh, S. M. (2005). SV2A and SV2C contain a unique synaptotagmin-binding site. *Molecular and Cellular Neuroscience*, *29*(1), 56–64. https://doi.org/10.1016/j.mcn.2004.12.011

Schmied, C., Soykan, T., Bolz, S., Haucke, V., & Lehmann, M. (2021). SynActJ: Easy-to-Use Automated Analysis of Synaptic Activity. *Frontiers in Computer Science*, *3*, 777837. https://doi.org/10.3389/fcomp.2021.777837

Schoch, S., Deak, F., Konigstorfer, A., Mozhayeva, M., Sara, Y., Sudhof, T., & Kavalali, E. (2001). SNARE Function Analyzed in Synaptobrevin / VAMP Knockout Mice. *Science*, *294*(November), 1117–1123. https://doi.org/10.1126/science.1064335

Schuske, K. R., Richmond, J. E., Matthies, D. S., Davis, W. S., Runz, S., Rube, D. A., Van Der Bliek, A. M., & Jorgensen, E. M. (2003). Endophilin is required for synaptic vesicle endocytosis by localizing synaptojanin. *Neuron*, *40*(4), 749–762. https://doi.org/10.1016/S0896-6273(03)00667-6

Scoville, W. B., & Milner, B. (1957). Loss of recent memory after bilateral hippocampal lesions. 1957. *J. Neurol. Neurosurg. Psychiatry*, *20*(11). https://doi.org/10.1136/jnnp.20.1.11

Senju, Y., Kalimeri, M., Koskela, E. V., Somerharju, P., Zhao, H., Vattulainen, I., & Lappalainen, P. (2017). Mechanistic principles underlying regulation of the actin cytoskeleton by phosphoinositides. *Proceedings of the National Academy of Sciences of the United States of America*, *114*(43), E8977–E8986. https://doi.org/10.1073/pnas.1705032114

Sharma, S., & Lindau, M. (2018). Molecular mechanism of fusion pore formation driven by the neuronal SNARE complex. *Proceedings of the National Academy of Sciences of the United States of America*, *115*(50), 12751–12756. https://doi.org/10.1073/pnas.1816495115

Shupliakov, O., Löw, P., Grabs, D., Gad, H., Chen, H., David, C., Takei, K., De Camilli, P., & Brodin, L. (1997). Synaptic vesicle endocytosis impaired by disruption of dynamin-SH3 domain interactions. *Science*, *276*(5310), 259–263. https://doi.org/10.1126/science.276.5310.259

Siddiqui, T. J., Vites, O., Stein, A., Heintzmann, R., Jahn, R., & Fasshauer, D. (2007). Determinants of Synaptobrevin Regulation in Membranes. *Molecular Biology of the Cell*, *18*(6), 2037–2046. https://doi.org/10.1091/mbc.E07-01-0049

Soykan, T., Kaempf, N., Sakaba, T., Vollweiter, D., Goerdeler, F., Puchkov, D., Kononenko, N. L., & Haucke, V. (2017). Synaptic Vesicle Endocytosis Occurs on Multiple Timescales and Is Mediated by Formin-Dependent Actin Assembly. *Neuron*, *93*(4), 854-866.e4. https://doi.org/10.1016/j.neuron.2017.02.011

Bibliography

Soykan, T., Maritzen, T., & Haucke, V. (2016). Modes and mechanisms of synaptic vesicle recycling. *Current Opinion in Neurobiology*, *39*, 17–23. https://doi.org/10.1016/j.conb.2016.03.005

Staras, K., Branco, T., Burden, J. J., Pozo, K., Darcy, K., Marra, V., Ratnayaka, A., & Goda, Y. (2010). A Vesicle Superpool Spans Multiple Presynaptic Terminals in Hippocampal Neurons. *Neuron*, *66*(1), 37–44. https://doi.org/10.1016/j.neuron.2010.03.020

Subramanian, D., Laketa, V., Müller, R., Tischer, C., Zarbakhsh, S., Pepperkok, R., & Schultz, C. (2010). Activation of membrane-permeant caged PtdIns(3)P induces endosomal fusion in cells. *Nature Chemical Biology*, *6*(5), 324–326. https://doi.org/10.1038/nchembio.348

Südhof, T. C. (2002). Synaptotagmins: Why so many? *Journal of Biological Chemistry*, *277*(10), 7629–7632. https://doi.org/10.1074/jbc.R100052200

Südhof, T. C., & Rothman, J. E. (2009). Membrane fusion: grappling with SNARE and SM proteins. *Science*, *323*(5913), 474–477. https://doi.org/10.1126/science.1161748

Suh, B. C., Leal, K., & Hille, B. (2010). Modulation of high-voltage activated Ca2+ channels by membrane phosphatidylinositol 4,5-bisphosphate. *Neuron*, *67*(2), 224–238. https://doi.org/10.1016/j.neuron.2010.07.001

Sun, J., Pang, Z. P., Qin, D., Fahim, A. T., Adachi, R., & Südhof, T. C. (2007). A dual-Ca2+-sensor model for neurotransmitter release in a central synapse. *Nature*, *450*(7170), 676–682. https://doi.org/10.1038/nature06308

Takamori, S., Holt, M., Stenius, K., Lemke, E. A., Grønborg, M., Riedel, D., Urlaub, H., Schenck, S., Brügger, B., Ringler, P., Müller, S. A., Rammner, B., Gräter, F., Hub, J. S., De Groot, B. L., Mieskes, G., Moriyama, Y., Klingauf, J., Grubmüller, H., … Jahn, R. (2006). Molecular Anatomy of a Trafficking Organelle. *Cell*, *127*(4), 831–846. https://doi.org/10.1016/j.cell.2006.10.030

Takei, K., McPherson, P. S., Schmid, S. L., & Camilli, P. De. (1995). Tubular membrane invaginations coated by dynamin rings are induced by GTP-γS in nerve terminals. In *Nature* (Vol. 374, Issue 6518, pp. 186–190). https://doi.org/10.1038/374186a0

Tan, J., & Brill, J. A. (2014). Cinderella story: PI4P goes from precursor to key signaling molecule. In *Critical Reviews in Biochemistry and Molecular Biology* (Vol. 49, Issue 1, pp. 33–58). https://doi.org/10.3109/10409238.2013.853024

Tan, P. K., Waites, C., Liu, Y., Krantz, D. E., & Edwards, R. H. (1998). A leucine-based motif mediates the endocytosis of vesicular monoamine and acetylcholine transporters.

Journal of Biological Chemistry, *273*(28), 17351–17360. https://doi.org/10.1074/jbc.273.28.17351

Tan, T. C., Valova, V. A., Malladi, C. S., Graham, M. E., Berven, L. A., Jupp, O. J., Hansra, G., McClure, S. J., Sarcevic, B., Boadle, R., Larsen, M. R., Cousin, M. A., & Robinson, P. J. (2003). Cdk5 is essential for synaptic vesicle endocytosis. *Nature Cell Biology*, *5*(8), 701–710. https://doi.org/10.1038/ncb1020

Thieman, J. R., Mishra, S. K., Ling, K., Doray, B., Anderson, R. A., & Traub, L. M. (2009). Clathrin regulates the association of PIPKIγ661 with the AP-2 adaptor β2 Appendage. *Journal of Biological Chemistry*, *284*(20), 13924–13939. https://doi.org/10.1074/jbc.M901017200

Thomas, L., Hartung, K., Langosch, D., Rehm, H., Bamberg, E., Franke, W. W., & Betz, H. (1988). Identification of synaptophysin as a hexameric channel protein of the synaptic vesicle membrane. *Science (New York, N.Y.)*, *242*(4881), 1050–1053. https://doi.org/10.1126/science.2461586

Trimble, W. S., & Grinstein, S. (2015). Barriers to the free diffusion of proteins and lipids in the plasma membrane. In *Journal of Cell Biology* (Vol. 208, Issue 3, pp. 259–271). Rockefeller University Press. https://doi.org/10.1083/jcb.201410071

Tsuboi, S., Takada, H., Hara, T., Mochizuki, N., Funyu, T., Saitoh, H., Terayama, Y., Yamaya, K., Ohyama, C., Nonoyama, S., & Ochs, H. D. (2009). FBP17 mediates a common molecular step in the formation of podosomes and phagocytic cups in macrophages. *Journal of Biological Chemistry*, *284*(13), 8548–8556. https://doi.org/10.1074/jbc.M805638200

Tucker, W. C., & Chapman, E. R. (2002). Role of synaptotagmin in Ca2+-triggered exocytosis. *Biochemical Journal*, *366*(1), 1–13. https://doi.org/10.1042/BJ20020776

Van Den Bogaart, G. Den, Meyenberg, K., Diederichsen, U., & Jahn, R. (2012). Phosphatidylinositol 4,5-bisphosphate increases Ca2+ affinity of synaptotagmin-1 by 40-fold. *Journal of Biological Chemistry*, *287*(20), 16447–16453. https://doi.org/10.1074/jbc.M112.343418

Van Den Bogaart, G., Meyenberg, K., Risselada, H. J., Amin, H., Willig, K. I., Hubrich, B. E., Dier, M., Hell, S. W., Grubmüller, H., Diederichsen, U., & Jahn, R. (2011). Membrane protein sequestering by ionic protein-lipid interactions. *Nature*, *479*(7374), 552–555. https://doi.org/10.1038/nature10545

Bibliography

van den Bout, I., & Divecha, N. (2009). PIP5K-driven PtdIns(4,5)P2 synthesis: Regulation and cellular functions. *Journal of Cell Science*, *122*(21), 3837–3850. https://doi.org/10.1242/jcs.056127

Vandael, D., Borges-Merjane, C., Zhang, X., & Jonas, P. (2020). Short-Term Plasticity at Hippocampal Mossy Fiber Synapses Is Induced by Natural Activity Patterns and Associated with Vesicle Pool Engram Formation. *Neuron*, *107*(3), 509-521.e7. https://doi.org/10.1016/j.neuron.2020.05.013

Verhage, M., Maia, A. S., Plomp, J. J., Brussaard, A. B., Heeroma, J. H., Vermeer, H., Toonen, R. F., Hammer, R. E., van den Berg, T. K., Missler, M., Geuze, H. J., & Südhof, T. C. (2000). Synaptic assembly of the brain in the absence of neurotransmitter secretion. *Science*, *287*(4), 864–869.

Verhage, M., & Sørensen, J. B. (2020). SNAREopathies: Diversity in Mechanisms and Symptoms. *Neuron*, *107*(1), 22–37. https://doi.org/10.1016/j.neuron.2020.05.036

Voglmaier, S. M., Kam, K., Yang, H., Fortin, D. L., Hua, Z., Nicoll, R. A., & Edwards, R. H. (2006). Distinct Endocytic Pathways Control the Rate and Extent of Synaptic Vesicle Protein Recycling. *Neuron*, *51*(1), 71–84. https://doi.org/10.1016/j.neuron.2006.05.027

Volpicelli-Daley, L. A., Lucast, L., Gong, L. W., Liu, L., Sasaki, J., Sasaki, T., Abrams, C. S., Kanaho, Y., & De Camilli, P. (2010). Phosphatidylinositol-4-phosphate 5-kinases and phosphatidylinositol 4,5-bisphosphate synthesis in the brain. *Journal of Biological Chemistry*, *285*(37), 28708–28714. https://doi.org/10.1074/jbc.M110.132191

Wadel, K., Neher, E., & Sakaba, T. (2007). The Coupling between Synaptic Vesicles and Ca2+ Channels Determines Fast Neurotransmitter Release. *Neuron*, *53*(4), 563–575. https://doi.org/10.1016/j.neuron.2007.01.021

Walter, A. M., Böhme, M. A., & Sigrist, S. J. (2018). Vesicle release site organization at synaptic active zones. In *Neuroscience Research* (Vol. 127, pp. 3–13). Elsevier Ireland Ltd. https://doi.org/10.1016/j.neures.2017.12.006

Walter, A. M., Müller, R., Tawfik, B., Wierda, K. D. B., Pinheiro, P. S., Nadler, A., McCarthy, A. W., Ziomkiewicz, I., Kruse, M., Reither, G., Rettig, J., Lehmann, M., Haucke, V., Hille, B., Schultz, C., & Sørensen, J. B. (2017). PIP2 optical uncaging potentiates exocytosis. *ELife*, *6*, e30203. https://doi.org/10.7554/eLife.30203

Walter, A. M., Wiederhold, K., Bruns, D., Fasshauer, D., & Sørensen, J. B. (2010). Synaptobrevin N-terminally bound to syntaxin-SNAP-25 defines the primed vesicle

state in regulated exocytosis. *Journal of Cell Biology*, *188*(3), 401–413. https://doi.org/10.1083/jcb.200907018

Wang, J., Li, F., Bello, O. D., Sindelar, C. V., Dé Ric Pincet, F., Krishnakumar, S. S., & Rothman, J. E. (2017). Circular oligomerization is an intrinsic property of synaptotagmin. *ELife*, *6*. https://doi.org/10.7554/eLife.27441.001

Wang, S., Li, Y., & Ma, C. (2016). Synaptotagmin-1 C2B domain interacts simultaneously with SNAREs and membranes to promote membrane fusion. *ELife*, *5*. https://doi.org/10.7554/eLife.14211.001

Wang, Z., Liu, H., Gu, Y., & Chapman, E. R. (2011). Reconstituted synaptotagmin I mediates vesicle docking, priming, and fusion. *Journal of Cell Biology*, *195*(7), 1159–1170. https://doi.org/10.1083/jcb.201104079

Watanabe, S., Liu, Q., Davis, M. W., Hollopeter, G., Thomas, N., Jorgensen, N. B., & Jorgensen, E. M. (2013). Ultrafast endocytosis at Caenorhabditis elegans neuromuscular junctions. *ELife*, *2013*(2), 1–24. https://doi.org/10.7554/eLife.00723

Watanabe, S., Rost, B. R., Camacho-Pérez, M., Davis, M. W., Söhl-Kielczynski, B., Rosenmund, C., & Jorgensen, E. M. (2013). Ultrafast endocytosis at mouse hippocampal synapses. *Nature*, *504*(7479), 242–247. https://doi.org/10.1038/nature12809.Ultrafast

Watanabe, S., Trimbuch, T., Camacho-Pérez, M., Rost, B. R., Brokowski, B., Söhl-Kielczynski, B., Felies, A., Davis, M. W., Rosenmund, C., & Jorgensen, E. M. (2014). Clathrin regenerates synaptic vesicles from endosomes. *Nature*, *515*(7526), 228–233. https://doi.org/10.1038/nature13846

Wen, H., Linhoff, M. W., McGinley, M. J., Li, G. L., Corson, G. M., Mandel, G., & Brehm, P. (2010). Distinct roles for two synaptotagmin isoforms in synchronous and asynchronous transmitter release at zebrafish neuromuscular junction. *Proceedings of the National Academy of Sciences of the United States of America*, *107*(31), 13906–13911. https://doi.org/10.1073/pnas.1008598107

Wen, Y., Feigenson, G. W., Vogt, V. M., & Dick, R. A. (2020). Mechanisms of PI(4,5)P2 Enrichment in HIV-1 Viral Membranes. *Journal of Molecular Biology*, *432*(19), 5343–5364. https://doi.org/10.1016/j.jmb.2020.07.018

Wenk, M. R., Lucast, L., Di Paolo, G., Romanelli, A. J., Suchy, S. F., Nussbaum, R. L., Cline, G. W., Shulman, G. I., McMurray, W., & De Camilli, P. (2003). Phosphoinositide profiling in complex lipid mixtures using electrospray ionization mass spectrometry. *Nature Biotechnology*, *21*(7), 813–817. https://doi.org/10.1038/nbt837

Bibliography

Wenk, M. R., Pellegrini, L., Klenchin, V. A., Di Paolo, G., Chang, S., Daniell, L., Arioka, M., Martin, T. F., & De Camilli, P. (2001). PIP kinase Iγ is the major PI(4,5)P2 synthesizing enzyme at the synapse. *Neuron*, *32*(1), 79–88. https://doi.org/10.1016/S0896-6273(01)00456-1

Wieffer, M., Maritzen, T., & Haucke, V. (2009). SnapShot: Endocytic Trafficking. *Cell*, *137*(2), 382.e1-382.e3. https://doi.org/10.1016/j.cell.2009.04.012

Wienisch, M., & Klingauf, J. (2006). Vesicular proteins exocytosed and subsequently retrieved by compensatory endocytosis are nonidentical. *Nature Neuroscience*, *9*(8), 1019–1027. https://doi.org/10.1038/nn1739

Wilhelm, B. G., Mandad, S., Truckenbrodt, S., Kröhnert, K., Schäfer, C., Rammner, B., Koo, S. J., Claßen, G. A., Krauss, M., Haucke, V., Urlaub, H., & Rizzoli, S. O. (2014). Vesicle Trafficking Proteins. *Science*, *344*(6187), 1023–1028. https://doi.org/10.1126/science.1252884

Williams, D., Vicôgne, J., Zaitseva, I., McLaughlin, S., & Pessin, J. E. (2009). Evidence that Electrostatic Interactions between Vesicle-associated Membrane Protein 2 and Acidic Phospholipids May Modulate the Fusion of Transport Vesicles with the Plasma Membrane. *Molecular Biology of the Cell*, *20*, 4910–4919. https://doi.org/10.1091/mbc.E09–04–0284

Wu, D., Bacaj, T., Morishita, W., Goswami, D., Arendt, K. L., Xu, W., Chen, L., Malenka, R. C., & Südhof, T. C. (2017). Postsynaptic synaptotagmins mediate AMPA receptor exocytosis during LTP. *Nature*, *544*(7650), 316–321. https://doi.org/10.1038/nature21720

Wu, L. G., Hamid, E., Shin, W., & Chiang, H. C. (2014). Exocytosis and endocytosis: Modes, functions, and coupling mechanisms. *Annual Review of Physiology*, *76*, 301–331. https://doi.org/10.1146/annurev-physiol-021113-170305

Wu, W., Xu, J., Wu, X. S., & Wu, L. G. (2005). Activity-dependent acceleration of endocytosis at a central synapse. *Journal of Neuroscience*, *25*(50), 11676–11683. https://doi.org/10.1523/JNEUROSCI.2972-05.2005

Wu, X. S., Elias, S., Liu, H., Heureaux, J., Wen, P. J., Liu, A. P., Kozlov, M. M., & Wu, L. G. (2017). Membrane Tension Inhibits Rapid and Slow Endocytosis in Secretory Cells. *Biophysical Journal*, *113*(11), 2406–2414. https://doi.org/10.1016/j.bpj.2017.09.035

Wu, X. S., Lee, S. H., Sheng, J., Zhang, Z., Zhao, W. D., Wang, D., Jin, Y., Charnay, P., Ervasti, J. M., & Wu, L. G. (2016). Actin Is Crucial for All Kinetically Distinguishable

Forms of Endocytosis at Synapses. *Neuron*, *92*(5), 1020–1035. https://doi.org/10.1016/j.neuron.2016.10.014

Wu, X. S., McNeil, B. D., Xu, J., Fan, J., Xue, L., Melicoff, E., Adachi, R., Bai, L., & Wu, L. G. (2009). Ca2+ and calmodulin initiate all forms of endocytosis during depolarization at a nerve terminal. *Nature Neuroscience*, *12*(8), 1003–1010. https://doi.org/10.1038/nn.2355

Wurm, F. M. (2004). Production of recombinant protein therapeutics in cultivated mammalian cells. In *Nature Biotechnology* (Vol. 22, Issue 11). https://doi.org/10.1038/nbt1026

Xia, W., Bringmann, P., McClary, J., Jones, P. P., Manzana, W., Zhu, Y., Wang, S., Liu, Y., Harvey, S., Madlansacay, M. R., McLean, K., Rosser, M. P., MacRobbie, J., Olsen, C. L., & Cobb, R. R. (2006). High levels of protein expression using different mammalian CMV promoters in several cell lines. *Protein Expression and Purification*, *45*(1), 115–124. https://doi.org/10.1016/j.pep.2005.07.008

Xie, Z., Long, J., Liu, J., Chai, Z., Kang, X., & Wang, C. (2017). Molecular mechanisms for the coupling of endocytosis to exocytosis in neurons. *Frontiers in Molecular Neuroscience*, *10*, 47. https://doi.org/10.3389/fnmol.2017.00047

Xu, J., Luo, F., Zhang, Z., Xue, L., Wu, X. S., Chiang, H. C., Shin, W., & Wu, L. G. (2013). SNARE Proteins Synaptobrevin, SNAP-25, and Syntaxin Are Involved in Rapid and Slow Endocytosis at Synapses. *Cell Reports*, *3*(5), 1414–1421. https://doi.org/10.1016/j.celrep.2013.03.010

Xu, J., Mashimo, T., & Südhof, T. C. (2007). Synaptotagmin-1, -2, and -9: Ca2+ Sensors for Fast Release that Specify Distinct Presynaptic Properties in Subsets of Neurons. *Neuron*, *54*(4), 567–581. https://doi.org/10.1016/j.neuron.2007.05.004

Xu, J., Pang, Z. P., Shin, O. H., & Südhof, T. C. (2009). Synaptotagmin-1 functions as a Ca2+ sensor for spontaneous release. *Nature Neuroscience*, *12*(6), 759–766. https://doi.org/10.1038/nn.2320

Yamashita, T., Eguchi, K., Saitoh, N., von Gersdorff, H., & Takahashi, T. (2010). Developmental shift to a mechanism of synaptic vesicle endocytosis requiring nanodomain Ca2+. *Nature Neuroscience*, *13*(7), 838–844. https://doi.org/10.1038/nn.2576

Yamashita, T., Hige, T., & Takahashi, T. (2005). Vesicle endocytosis requires dynamin-dependent GTP hydrolysis at a fast CNS synapse. *Science*, *307*(5706), 124–127. https://doi.org/10.1126/science.1103631

Bibliography

Yao, C. K., Lin, Y. Q., Ly, C. V., Ohyama, T., Haueter, C. M., Moiseenkova-Bell, V. Y., Wensel, T. G., & Bellen, H. J. (2009). A Synaptic Vesicle-Associated Ca2+ Channel Promotes Endocytosis and Couples Exocytosis to Endocytosis. *Cell*, *138*(5), 947–960. https://doi.org/10.1016/j.cell.2009.06.033

Yao, J., Gaffaney, J. D., Kwon, S. E., & Chapman, E. R. (2011). Doc2 is a Ca2+ sensor required for asynchronous neurotransmitter release. *Cell*, *147*(3), 666–677. https://doi.org/10.1016/j.cell.2011.09.046

Yao, J., Kwon, S. E., Gaffaney, J. D., Dunning, F. M., & Chapman, E. R. (2012). Uncoupling the roles of synaptotagmin I during endo-and exocytosis of synaptic vesicles. *Nature Neuroscience*, *15*(2), 243–249. https://doi.org/10.1038/nn.3013

Yao, J., Nowack, A., Kensel-Hammes, P., Gardner, R. G., & Bajjalieh, S. M. (2010). Cotrafficking of SV2 and synaptotagmin at the synapse. *Journal of Neuroscience*, *30*(16), 5569–5578. https://doi.org/10.1523/JNEUROSCI.4781-09.2010

Yao, L. H., Rao, Y., Varga, K., Wang, C. Y., Xiao, P., Lindau, M., & Gong, L. W. (2012). Synaptotagmin 1 is necessary for the ca 2+ dependence of clathrin-mediated endocytosis. *Journal of Neuroscience*, *32*(11), 3778–3785. https://doi.org/10.1523/JNEUROSCI.3540-11.2012

Yin, M., & Wang, Y. (2022). The role of PIP5K1A in cancer development and progression. *Med Oncol*, *39*(151).

Zanetti, M. N., Bello, O. D., Wang, J., Coleman, J., Cai, Y., Sindelar, C. V, Rothman, J. E., & Krishnakumar, S. S. (2016). *Ring-like oligomers of Synaptotagmins and related C2 domain proteins*. https://doi.org/10.7554/eLife.17262.001

Zefirov, A. L., Abdrakhmanov, M. M., Mukhamedyarov, M. A., & Grigoryev, P. N. (2006). The role of extracellular calcium in exo- and endocytosis of synaptic vesicles at the frog motor nerve terminals. *Neuroscience*, *143*(4), 905–910. https://doi.org/10.1016/j.neuroscience.2006.08.025

Zegers, M. M., & Friedl, P. (2015). Translating Membrane Tension into Cytoskeletal Action by FBP17. *Developmental Cell*, *33*(6), 628–630. https://doi.org/10.1016/j.devcel.2015.06.006

Zhai, R. G., & Bellen, H. J. (2004). The architecture of the active zone in the presynaptic nerve terminal. *Physiology*, *19*(5), 262–270. https://doi.org/10.1152/physiol.00014.2004

Zhang, N., Gordon, S. L., Fritsch, M. J., Esoof, N., Campbell, D. G., Gourlay, R., Velupillai, S., Macartney, T., Peggie, M., van Aalten, D. M. F., Cousin, M. A., & Alessi, D. R.

(2015). Phosphorylation of synaptic vesicle protein 2A at Thr84 by casein kinase 1 family kinases controls the specific retrieval of synaptotagmin-1. *Journal of Neuroscience*, *35*(6), 2492–2507. https://doi.org/10.1523/JNEUROSCI.4248-14.2015

Zhang, Z., Wang, D., Sun, T., Xu, J., Chiang, H. C., Shin, W., & Wu, L. G. (2013). The SNARE proteins SNAP25 and synaptobrevin are involved in endocytosis at hippocampal synapses. *Journal of Neuroscience*, *33*(21), 9169–9175. https://doi.org/10.1523/JNEUROSCI.0301-13.2013

Zhao, H., Michelot, A., Koskela, E. V., Tkach, V., Stamou, D., Drubin, D. G., & Lappalainen, P. (2013). Membrane-Sculpting BAR Domains Generate Stable Lipid Microdomains. *Cell Reports*, *4*(6), 1213–1223. https://doi.org/10.1016/j.celrep.2013.08.024

Zheng, Q., McFadden, S. C., & Bobich, J. A. (2004). Phosphatidylinositol 4,5-bisphosphate promotes both [3H]- noradrenaline and [14C]-glutamate exocytosis from nerve endings. *Neurochemistry International*, *44*(4), 243–250. https://doi.org/10.1016/S0197-0186(03)00149-9

Zhou, Q., Lai, Y., Bacaj, T., Zhao, M., Lyubimov, A. Y., Uervirojnangkoorn, M., Zeldin, O. B., Brewster, A. S., Sauter, N. K., Cohen, A. E., Soltis, S. M., Alonso-Mori, R., Chollet, M., Lemke, H. T., Pfuetzner, R. A., Choi, U. B., Weis, W. I., Diao, J., Südhof, T. C., & Brunger, A. T. (2015). Architecture of the synaptotagmin-SNARE machinery for neuronal exocytosis. *Nature*, *525*(7567), 62–67. https://doi.org/10.1038/nature14975

Zhou, Q., Zhou, P., Wang, A. L., Wu, D., Zhao, M., Südhof, T. C., & Brunger, A. T. (2017). The primed SNARE-complexin-synaptotagmin complex for neuronal exocytosis. *Nature*, *548*(7668), 420–425. https://doi.org/10.1038/nature23484

7 Appendix

7.1 Supplementary Figures

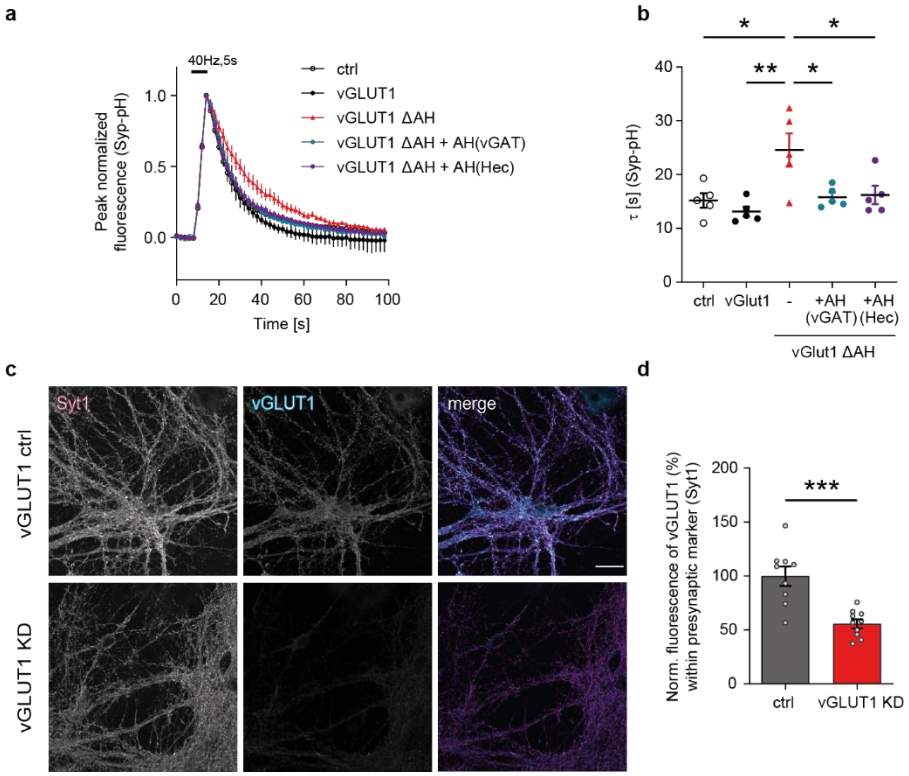

Figure 34: The endocytic function of vGLUT1 may depend on an N-terminal putative amphipathic helix. **(a)** Average normalized fluorescence traces of stimulated (200 APs, 40 Hz) hippocampal neurons transfected with Syp-pH and mCherry (ctrl) or vector encoding mCherry tagged vGLUT1, mCherry tagged vGLUT1 lacking its amphipathic helix (AH) (vGLUT1 ΔAH) or one of the vGLUT1 chimeras with AH-substitution [mCherry tagged vGLUT1 ΔAH + AH(vGAT), mCherry tagged vGLUT1 ΔAH + AH(Hec)]. Data represent mean ± SEM from N = 5 independent experiments with > 300 analyzed boutons per condition (Bolz, Master thesis). **(b)** Endocytic decay time constants (τ) of data shown in (a). τ_{ctrl} = 15 ± 1 s, τ_{VGLUT1} = 13 ± 1 s, $\tau_{vGLUT1\ \Delta AH}$ = 25 ± 3 s, $\tau_{vGLUT1\ \Delta AH + AH(vGAT)}$ = 16 ± 1 s, $\tau_{vGLUT1\ \Delta AH + AH(Hec)}$ = 16 ± 2 s. One-way ANOVA with Tukey's post-test. **(c)** Representative confocal images of hippocampal neurons transduced with non-specific shRNA (vGLUT1 ctrl) or shRNA targeting vGLUT1 (vGLUT1 KD) (DIV15) stained for vGLUT1 and for Syt1. Scale bar: 20 µm. **(d)** Norm. fluorescence intensities of vGLUT1-labeled hippocampal neurons transduced with vGLUT1 ctrl or vGLUT1 KD. Neurons transduced with shRNA targeting vGLUT1 reveal specific depletion of vGLUT1 within Syt1-positive areas. Data represents n = 9 - 10 images from 4 independent cultures per condition. Unpaired two-tailed t-test.
* $p < 0.05$, ** $p < 0.01$, *** $p < 0.001$.

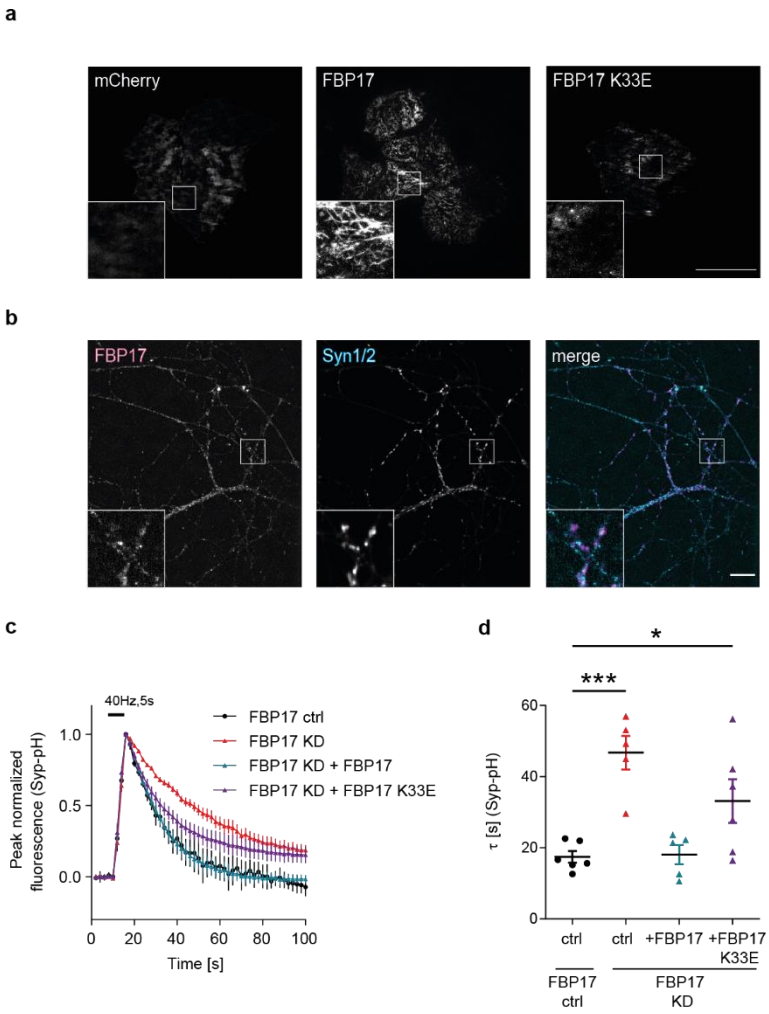

Figure 35: The synaptic protein FBP17 may drive SV endocytosis through membrane deformation via interaction with PI(4,5)P_2.
(a) Representative TIRF images of HELA M cells transfected with mCherry, mCherry tagged FBP17 or the plasma membrane binding mutant, mCherry tagged FBP17-K33E, and stained for mCherry indicate the plasma membrane tubulation activity of FBP17. Interference with plasma membrane binding (K33E) results in loss of plasma membrane tubulation. Scale bar: 50 µm. **(b)** Representative confocal images of WT hippocampal neurons (DIV15) stained for FBP17 and for Syn1/2 indicate synaptic localization of FBP17; Scale bar: 20 µm. **(c)** Interaction with the plasma membrane, likely PI(4,5)P_2-dependent, seems crucial for FBP17's endocytic function in neurons. Average normalized Syp-pH fluorescence traces of stimulated (200 APs, 40 Hz) hippocampal neurons transfected with control (FBP17 ctrl) or FBP17 KD and subsequently transfected with mCherry (ctrl) or vector encoding mCherry tagged FBP17 or the mCherry tagged plasma membrane binding mutant, FBP17 K33E. Data represent mean ± SEM from n = 4 - 5 independent cultures/ condition with > 150 analyzed boutons per condition. **(d)** Endocytic decay time constants (τ) of data shown in (c). $\tau_{FBP17\ ctrl}$ = 17 ± 2 s, $\tau_{FBP17\ KD}$ = 47 ± 5 s, $\tau_{FBP17\ KD\ +\ FBP17}$= 18 ± 3 s, $\tau_{FBP17\ KD\ +\ FBP17\ K33E}$ = 33 ± 6 s. One-way ANOVA with Tukey's post-test. * $p < 0.05$, ** $p < 0.01$, *** $p < 0.001$.

7.2 Abbreviations

α-SNAP	α soluble NSF attachment protein
AF	Alexa Fluor
AH	Amphipathic helix
AM	Acetoxymethylester
AMP	Ampicillin
AMPA	α-amino-3-hydroxy-5-methyl-4-isoxazolepropionic acid
ANOVA	Analysis of variance
AP	Action potential
APS	Ammonium peroxodisulfate
APV	(2R)-amino-5-phosphonovaleric acid
AP2/180	Adaptor protein
AraC	Cytosine β-D-arabinofuranoside
ARF	ADP-ribosylation factors
AZ	Active zone
BAR	Bin/Amphiphysin/Rvs
BLAST	Basic local alignment search tool
bp	Base pair
BSA	Bovine serum albumin
$CaCl_2$	Calcium chloride
Cav2.1/2	N- or P/Q-type voltage-gated Ca2+ channels
CAZ	Cytomatrix of the active zone
Cdc42	Cell division cycle 42
Cdk5	Cyclin dependent kinase 5
CDS	Coding sequence
C. elegans	Caenorhabditis elegans
CFP	Cyan fluorescent protein
CIE	Clathrin-independent endocytosis
CIP	Calf intestinal alkaline phosphatase
CK	Casein kinase
CME	Clathrin-mediated endocytosis
CMV	Cytomegalovirus
CNS	Central nervous system
CNQX	6-cyano-7-nitroquinoxaline-2,3-dione

ctrl	Control
DAG	Diacylglycerol
DGK	Diaglycerol kinase
DIV	Days in vitro
D. melanogaster	*Drosophila melanogaster*
DMEM	Dulbecco's modified Eagle medium
DMSO	Dimethylsulfoxid
DNA	Deoxyribonucleic acid
DNase	Deoxyribonuclease
dNTP	Deoxynucleosidtriphosphate
DTT	Dithiothreitol
Dyn	Dynamin
EDTA	Ethylene diamine tetraacetic acid
EGTA	Ethylene glycol-bis(β-aminoethyl ether)-N,N,N',N'-tetraacetic acid
EH	Eps15 homology
ELV	Endosomal-like vacuoles
EM	Electron microscopy
ER	Endoplasmic reticulum
ESyt	Extended Synaptotagmin
et al.	And others (et alii)
EtBr	Ethidiumbromide
F	Fluorescence intensity
FBP17	Formin binding protein 17
FCS	Fetal calf serum
FCHo	Fer/Cip4 homology
FDR	False discovery rate
fl	Full-length
fw	Forward
g	Acceleration of gravity
g	Gram
GA	Glutaraldehyde
GABA	Gamma-aminobutyric acid
GFP	Green fluorescent protein
GIT	G-protein-coupled receptor (GPCR)-kinase-interacting protein

Appendix

gp	Guinea pig
GST	Anti-glutathione-S-transferase
h	Hour
HBSS	Hanks' balanced salt solution
HC	Heavy chain
HD	Homology domain
HEK	Human embryonic kidney cell line
HEPES	2 x 4-(2-hydroxyethyl)-1-piperazineethanesulfonic acid
HF	High fidelity
His_6	6x Histidine tag
HPF	High pressure freezing
HRP	Horseradish peroxidase
Hz	Herz
IB	Immunoblotting
ICC	Immunocytochemistry
IgG	Immunoglobulin G
IP_3	Inositoltrisphosphate
IPTG	Isopropyl β-D-1-thiogalactopyranoside
KCl	Potassium chloride
Kan	Kanamycin
KD	Knockdown
kDa	Kilo dalton
KH_2PO_4	Monopotassium phosphate
KO	Knockout
LB	Lysogeny broth
M	Molar
m	Milli
MAP2	Microtubule-associated protein 2
mCh	mCherry
MEF	Mouse embryonic fibroblast
MEM	Minimum Essential Media
MES	2-(N-morpholino)ethansulfonic acid
$MgCl_2$	Magnesium chloride
$MgSO_4$	Magnesium sulfate

min	Minutes
mRFP	Monomeric red fluorescent protein
ms	Mouse
ms	Millisecond
NA	Numerical aperture
NaCl	Sodium chloride
$NaHCO_3$	Sodium bicarbonate
Na_2HPO_4	Disodium phosphate
Na_2SO_4	Sodium sulfate
NEA	Non-essential amino acids
NGS	Normal goat serum
NH_4Cl	Ammonium chloride
nm	Nanometer
NMDA	N-methyl-D-aspartate
NPF	Asn-Pro-Phe
n.s.	Non significant
NSF	N-ethylmaleimide-sensitive factor
NTA	Nitrilotriacetic acid
N-terminal	Amino-terminal
PA	Phosphatidic acid
PBS	Phosphate buffered saline
PBS-T	Phosphate buffered saline-Tween
PC	Phosphatidylcholine
pCAG	CMV immediate enhancer/β-actin promoter
PCR	Polymerase chain reaction
PFA	Paraformaldehyde
PH	Pleckstrin homology
pH	Preponderance of hydrogen ions
pH	pHluorin, pH-sensitive GFP variant
PI	Phosphoinositides
PIC	Mammalian protease inhibitor cocktail
PIP	Phosphatidylinositol phosphate
PIPKIγ	Phosphatidylinositol 4-phosphate [PI(4)P] 5-kinase Iγ
PI4K	Phosphatidylinositol 4-kinase

Appendix

PIP5K	Phosphatidylinositol-4-phosphate 5-kinase
$PI(3,4,5)P_3$	Phosphatidylinositol-(3,4,5)-trisphosphate
PI(4)P	Phosphatidylinositol 4-phosphate
$PI(4,5)P_2$	Phosphatidylinositol 4,5-bisphosphate
PKC	Protein kinase C
PLC	Phospholipase C
PLD	Phospholipase D
PLL	Poly-L-Lysin
PMSF	Phenylmethylsulfonyl fluoride
PS	Phosphatidylserine
PSD	Postsynaptic density
P/S	Penicillin/ Streptomycin
PTB	Phosphotyrosin-binding
PtdIns	Phosphatidylinositols
rb	Rabbit
RIM	Rab3 interacting molecule
RNA	Ribonucleic acid
ROI	Region of interest
rpm	Rounds per minute
RRP	Readily-releasable pool
RT	Room temperature
rv	Reverse
s	Seconds
SDS-PAGE	Sodium dodecylsulfate polyacrylamide gel electrophoresis
SEM	Standard error of the mean
SHD	Stonin-homology domain
SH3	Src homology 3 domain
shRNA	Small hairpin RNA
SNAP-25	Synaptosomal associated protein 25
SNARE	soluble NSF attachment protein receptor
SNX9	Sorting nexin 9
STED	Stimulated emission depletion
stim	Stimulated
Stn2	Stonin2

SV	Synaptic vesicle
SV2	Synaptic vesicle protein 2
Syb2	Synaptobrevin 2
Syp	Synaptophysin
Syt1	Synaptotagmin1
TAE	Tris-Acetate-EDTA
TBE	Tris-Borate-EDTA
TEMED	N,N,N',N'-tetramethylethylenediamine
TES	N-tris[hydroxy-methyl]-methyl-2-aminoethane-sulphonic acid
TF	Trifunctional
TIRF	Total internal reflection fluorescence
Tris	Trisaminomethane
TTX	Tetrodotoxin
UFE	Ultrafast endocytosis
unstim	Unstimulated
UTR	Untranslated region
UV	Ultraviolet
V	Voltage
V-ATPase	Vacuolar H+-ATPase
VAMP2	Vesicle-associated membrane protein 2
vGAT	Vesicular GABA transporter
vGLUT1	Vesicular glutamate transporter 1
VSV-G	Vesicular stomatits virus G protein
v/v	Volume per volume
w/v	Weight per volume
WB	Western blot
WT	Wild-type
YFP	Yellow fluorescent protein
YT	Yeast extract tryptone
µHD	µ2-homology domain
µl	Micro liters
τ	Endocytic time constant

7.3 List of Tables

7.4 List of Figures

Appendix

7.5 Publications

Bolz, S., (…), Haucke, V. (2024) *Review on phosphoinositide dynamics in the SV cycle of neurons.* Journal of Physiology (in preparation)

Bolz, S., Rombach, J., Madsen, K., Haucke, V. (2023). *The structural motif of an amphipathic helix drives SV endocytosis*. (in preparation)

(…) **Bolz, S.** (…), Haucke, V., Fornasiero, E., Rizzoli, S. (2023). *The novel Syt1 nanobody as a tool to study SV kinetics*. (in preparation)

Bolz, S., (…), Haucke, V. (2023) *STAR-protocol on phosphoinositide detection at synapses.* Cell Press (in preparation)

Bolz, S., Kaempf, N., Puchkov, D., Krauss, M., Russo, G., Soykan, T., Schmied, C., Lehmann, M., Müller, R., Schultz, C., Perrais, D., Maritzen, T., Haucke, V. (2023) *Synaptotagmin 1-triggered lipid signaling facilitates coupling of exo- and endocytosis*. Neuron; 111, 1-10, https://doi.org/10.1016/j.neuron.2023.08.016

& featured in *Nature Reviews Neuroscience*

Schmied, C., Soykan, T., **Bolz, S.**, Haucke, V., and Lehmann, M. (2021). *SynActJ: easy-to-use automated analysis of synaptic activity.* Front. Comput. Sci. 3, 777837. https://doi.org/10.3389/fcomp.2021.777837.